

**ESR Studies on the Structure of Manganese
Containing sites within Photosystem II in Higher
Plants. Evidence for a Dimer of Dimers.**

A thesis submitted for the degree of Doctor of Philosophy of
The Australian National University

by

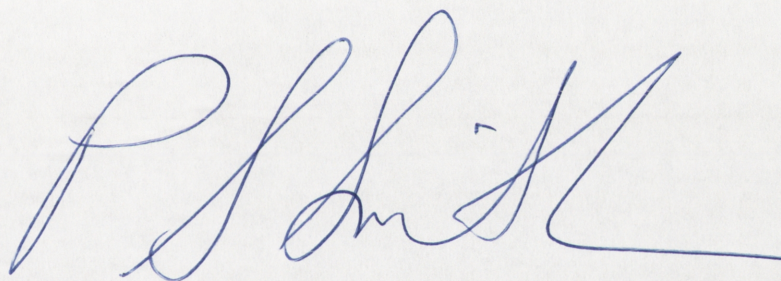


Paul James Smith

April, 1996

Declaration

This thesis is my original work, except where otherwise stated. It was completed in the Department of Chemistry at the ANU during the period March 1992 to March 1996.



Paul J. Smith

Synopsis

The oxygen evolving centre of Photosystem II requires the interaction of at least four manganese (Mn) ions for optimal functionality. In this study, Electron Spin Resonance (ESR) spectroscopy has been utilised to examine illumination induced paramagnetic states known to be associated with this Mn containing centre.

Photosystem II (PSII) is a membrane bound protein complex residing in the thylakoid membranes of chloroplasts. Two established isolation procedures were utilised to extract subchloroplast membranes containing PSII. The results obtained for the different preparations under equivalent buffer and illumination regimes were compared and found to be identical.

The oxygen evolving centre (OEC) of PSII oxidises water to dioxygen via a four step cyclic catalysis involving five redox intermediate states. These states are labelled according to the number of redox equivalents stored, and are known as S states (S_0 to S_4). S_1 is the long term stable "resting state". In this report, illumination procedures have been applied to set high proportions of the PSII centres into either the S_2 state or inhibited S_3 state. Each of these redox intermediate states contains paramagnetic centres known to involve Mn ions in the 3+ and 4+ oxidation states. The aim of this work is to examine each of the Mn derived signals to determine the spin interactions associated with each signal and develop a model structure for the Mn containing centre giving rise to the signals.

In the S_2 state, two types of signals derived from the Mn containing structures have been studied. These are the multiline signal, centred near $g \sim 2.0$ characterised by many hyperfine peaks, and the $g=4.1$ signal, a broad relatively featureless signal centred near $g=4$.

The multiline signal was observed to arise from a ground state $S=1/2$ centre under all methods of generation. Generation of the $g=4.1$ signal, its relationship to the multiline signal and its spin state were found to be determined by cryoprotectant and illumination regime effects.

Two forms of the $g=4.1$ signal were resolved and clarification of their individual spin states showed them to arise from distinct and essentially magnetically isolated Mn dimer containing structures. One form of the $g=4.1$ signal was cogenerated with the multiline signal. This form of the $g=4.1$ signal was abolished by the presence of alcohol in the pre-illumination buffer. The spin state of the centre giving rise to this $g=4.1$ signal was observed to be the first excited state, $S=3/2$, of the Mn containing centre giving rise to the multiline signal. In samples in which the multiline and this excited state $g=4.1$ signal were generated, a third spin state was observed for the first time. This third spin state gave rise to a signal at $g \approx 6.1$, named here as the $g=6$ signal. The spin state of this $g=6$ signal was determined to be the second excited state, $S=5/2$, of the multiline signal Mn centre. The temperature dependence of this correlated set of signals, the $S=1/2$ ground state multiline, $S=3/2$ first excited state $g=4.1$ signal and the second

excited state $S=5/2$ $g=6$ signals were observed to be quantitatively consistent with a Boltzmann spin state energy model for an antiferromagnetically exchange coupled Mn III-IV dimer, with a single exchange coupling constant of magnitude $J/k \sim 3.5K$.

The presence of ethylene glycol, a diol, was observed to change the temperature dependence of the multiline signal, consistent with an increase of the exchange constant to $J/k \sim 25K$, with only the ground state signal, $S=1/2$ multiline, observable in these alcohol containing samples.

The second form of the $g=4.1$ signal studied requires the presence of polyalcohols for formation in functional PSII samples. Illumination at very low temperatures generated a $g=4.1$ signal which displayed a temperature dependence consistent with it arising from a ground state centre. Line shape examination and ESR observation at different microwave frequencies indicated that at low microwave frequencies, the excited and ground state forms of the $g=4.1$ signals were almost identical, but distinguishable by their temperature dependence behaviours. At high microwave frequencies, the excited and ground state forms of the $g=4.1$ signal generated distinctly different lineshape patterns, consistent with the hypothesis that these signals arise from separate Mn containing centres. Careful examination of the $g=2$ radical region led to the observation of an excited state radical signal, intimately associated with the ground state $g=4.1$ signal. With the components believed present in PSII, to generate a ground state $g=4.1$ signal, at least three spin centres are required. Examination of the line shape of the excited state "radical" signal has led to the proposal that the ground state $g=4.1$ signal arises from the interaction of the intermediate electron transfer carrier of the donor side of PSII, a tyrosine residue YZ, with a Mn III-III dimer. The ground state of the coupled system was determined to be $S=3/2$. The structural model proposed for this centre consists of the oxidised YZ BRIDGING the Mn dimer (dimer spin $S=1$ in the ground state, $S=0$ in the first excited state). This Mn dimer containing structure is distinct from the centre giving rise to the excited state $g=4.1$ signal. The four Mn ions within PSII are shown to be located within two magnetically and spatially isolated dimer containing structures, one intimately associated with the intermediate redox donor, YZ. The second is functionally associated with water oxidation and oxygen evolution.

Examination of three different established inhibition protocols was undertaken. In Cl^- depleted samples, the S_2 state exhibited only ground state $g=4.1$ signal. Illumination to allow multiple turnovers generated a split resonance signal, associated with an altered S_3 state, called the S_3^* split signal. This signal was characterised by a peak to peak (ΔH_{p-p}) width of $\leq 10mT$, with a strictly Curie temperature dependence between 5K and 50K.

In samples treated with high levels of NaCl (1M), the S_2 state was characterised by the multiline signal. The S_3^* state was then characterised by a broader split signal, ΔH_{p-p}

width $\sim 16\text{mT}$, which followed a complex temperature dependence, indicative of effects of spin state changes and T_1 relaxation effects. Unlike the Cl^- depleted samples, the NaCl treated (effectively Ca^{++} depleted) samples displayed signals in the $g\sim 5$ region, which were observed to follow similar temperature dependence behaviour to that of the $g\sim 2$ split signal in these samples.

With functional PSII treated with either 600mM Sodium Acetate (NaAc) or 300mM Calcium Acetate (CaAc), the S_2 state was characterised by a mix of ground state $g=4.1$ and multiline signals at low (200K) illumination temperature. Higher temperatures (275K) led to generation of mainly the multiline form of the S_2 state. The S_3^* states in each of the CaAc or NaAc treated samples were characterised by a still broader form of the S_3^* split signal, $\Delta\text{Hp-p}$ width $\sim 24\text{mT}$. This form of the S_3^* state was also observed to give rise to signals in the $g\sim 4$ region. The temperature dependence of these $g\sim 4$ region signals paralleled that of the associated $g\sim 2$ split signal, similar to the results for the NaCl treated samples.

The results for the inhibited PSII are consistent with the proposal of two separate Mn containing structures. Cl^- depleted samples generate S_2 and S_3^* state signals from the Mn centre associated with YZ , the S_3^* signal arising from a spin-spin interaction between YZ^+ and an oxidised histidine moiety, most probably $\text{His } 190^+$, the Mn dimer being diamagnetic ($S=0$) in this form of the S_3^* state. Incubations with high NaCl, NaAc or CaAc, which inhibit oxygen evolving activity, still appear to lead to multiline forms of the S_2 state. The S_3^* state in these centres is proposed to arise from the oxidised, coupled multiline forming Mn dimer, and oxidised $\text{His } 332^+$. This residue is strongly suspected to be a ligand to the oxygenic functional site. From these studies, the conclusion may be drawn that each $g=4.1$ signal, excited or ground state form, arises from an $S=3/2$ state associated with a Mn dimer containing centre.

Based on these results for the S_2 state $g=4.1$ signals and S_3^* state split signals, structures and binding sites are proposed for each of the two Mn dimers within the D1 peptide of PSII. A model is presented for the structure of the oxygenic functional site and for S state turnover leading to oxidation of water and formation of dioxygen.

Acknowledgements

I wish to thank the following people for support and encouragement throughout this project:

Dr Ron Pace, my supervisor for providing a listening post and idea refinement throughout the work, and for helpful ideas during the preparation of this thesis,

Drs. Tom Wydrzynski and Jan Anderson for useful discussions throughout the project and for providing the spinach,

Karin Åhrling, who has been there with support through the tough times of this work and for providing immense help and effort in the final preparation of this Volume,

Dr Richard Bramley, for access to the Research School of Chemistry spectrometers and for very useful discussions through the project,

my fellow Pacian students, for encouragement and discussions over the experiments,

to Linda, my wife, who has helped immensely with the typing of the text and for understanding and support during the long nights,

to my family and friends, who have suffered my inattention and inability to handle the world outside during stressful times,

and my two children, Adam and Tegan, for supporting me and being patient and tolerant.

I also acknowledge the financial support of a Graduate Student Assistantship provided by the Plant Sciences Cooperative Research Centre ANU throughout my tenure as a graduate student.

This work is dedicated to Linda, Adam and Tegan,

Once a start is taken, the journey may never finish.

Table of Contents:

Synopsis	iii
Acknowledgements	vi
Table of Figures	xii
Symbols and Abbreviations	xix
Chapter 1.	1
1.1. The structure of chloroplasts.	2
1.1.1. Making Oxygen	
1.2. Photosystem II Structure	3
1.2.1. Electron Transfer Chain.	
1.2.2. The donor side components	
1.2.2.1. P680	
1.2.2.2. Cytochrome b559	
1.2.2.3. YZ and Y _D - Intermediate donors.	
1.3. Properties of Y_D and YZ.	9
1.3.1. YZ	
1.3.2. Y _D	
1.4. Manganese Oxygen Evolving Complex.	14
1.4.1. Electron Transfer and Kinetics.	
1.4.2. Mn Reduction Studies.	
1.4.3. Amino Acid Binding Sites. Mutations and Protein Modelling.	
1.4.3.1. Mutational Studies.	
1.4.3.1.1. Sites near YZ, the Secondary Donor.	
1.4.3.1.2. D1 Polypeptide Carboxyl Terminus.	
1.4.3.2. Protein Modelling Studies.	
1.5. ESR of Photosystem II.	23
1.5.1. Cryoprotectant effect.	
1.5.2. Inhibited Photosystem II	
1.5.3. Signals From Other S-States.	
1.5.3.1. S ₁ State.	
1.5.3.2. S ₃ State Signals.	
1.6. Power Saturation and Temperature Dependence Studies.	31
1.6.1. Multiline Signal.	

1.6.2. g=4.1 Signal	
1.7. Modelling.	33
1.7.1. Multiline.	
1.7.2. g=4.1 Signal.	
1.8. X Ray Studies.	38
1.9. Summary: Aim of Project.	43
Chapter 2.	42
2.1 Introduction.	42
2.2. Quantum Mechanical Analysis.	43
2.2.1. Zeeman Term $\mu_B S.g.H.$	
2.2.2. Hyperfine Interactions S.A.I.	
2.2.2.1. Isotropic Term.	
2.2.2.2. Anisotropic Term	
2.2.3. Fine Structure - Zero Field Terms S.D.S.	
2.2.4. Quadrupole Interaction I.Q.I.	
2.3. Electron Spin-Spin Interactions.	52
2.3.1. Dipolar Interaction.	
2.3.2. Heisenberg Exchange Interaction.	
2.3.1.1. Dilute - Exchange Narrowing.	
2.3.1.2. Strong Exchange.	
2.4. Transition Probability.	55
2.5. Magnetic Resonance and the Rapid Passage Condition.	55
2.6. Spin State Populations, Transitions and Saturation.	56
2.7. Relaxation Times.	57
2.7.1. Spin Lattice Relaxation.	
2.7.2. Transverse Relaxation.	
2.8. Spin Transitions and Saturation.	58
Chapter 3	66
3.1. Spinach	66
3.1.1. Spinach Harvesting.	
3.2. PSII Preparation.	67
3.2.1. PSII Preparation Protocol of Bricker et al.	
3.2.1.1. Buffers used for the Bricker Type protocol.	
3.2.2. Protocol for BBY preparation	

3.2.2.1. Buffers for the BBY Type Isolation Procedure.	
3.3. Inhibited Sample Preparation.	73
3.2.3.1. Buffers for the Cl ⁻ Depletion / F ⁻ Inhibition protocol.	
3.4. Experimental Apparatus.	75
3.4.1. Sample Illumination	
3.4.1.1. Illumination System.	
3.4.2. Electron Spin Resonance Experiments.	
3.4.2.1. Varian Spectrometer.	
3.4.2.2. Bruker Spectrometer.	
3.4.2.3. Cryogenic Temperatures.	
Chapter 4.	79
4.1. Comparison of the Two Preparations:	79
BBY- and Bricker- type PSII.	
4.1.1. Multiline Signal for Sucrose and Ethylene Glycol as Cryoprotectants.	
4.1.2. g=4.1 Signal for Ethylene Glycol as Cryoprotectant.	
4.2. Multiline Signal. PSII Illuminated at 200K	80
4.2.1. PSII Cryoprotected with 0.4M Sucrose.	
4.2.2. PSII Cryoprotected with 30% V:V Ethylene Glycol.	
4.3. g=4.1 Signals. PSII Illuminated at either 200K or 130K.	82
4.3.1. Sucrose PSII Illuminated at 200K.	
4.3.2. EG PSII Illuminated at 130K.	
4.3.3. EG PSII Illuminated at 200K.	
4.4. Relationship of g=4.1 Signals to the Multiline Signal.	83
4.4.1. EG PSII Illuminated at 130K, Annealed 200K.	
4.5. ESR Line shape Measurements Q Band (35GHz).	84
4.5.1. Multiline Signal.	
4.5.2. g=4.1 Signal.	
4.6. Temperature Dependence Studies.	86
4.6.1. Sucrose PSII Illumination at 200K.	
4.6.2. Ethylene Glycol Cryoprotected PSII.	
4.6.2.1. EG PSII Illuminated at 200K.	
4.6.2.1.1. ML Signal.	
4.6.2.1.2. g=4.1 Signal. Illumination at 200K.	
4.6.2.2. g=4.1 Signal. Illumination at 130K.	
4.6.2.2.1. Case 1: S = 3/2 Ground State.	

4.6.2.2.2. Case 2: $S = 5/2$ Ground State.	
4.6.2.2.3. Analysis of Ground and Excited States.	
4.6.3. An Excited State Signal.	
4.7. Physiological PSII - A Dimer of Dimers.	100
4.8. Studies on Inhibitory Treatments on PSII.	101
4.8.1. Cl^- / F^- exchange.	
4.8.1.1. Illumination at 200K	
4.8.1.2. Illumination at 275K.	
4.8.2. Treatment with 1M NaCl	
4.8.2.1. Illumination at 200K.	
4.8.2.2. Illumination at 273K.	
4.8.3. PSII Incubated in the Presence of 600mM Acetate.	
4.8.3.1. Illumination at 200K.	
4.8.3.1.1. Sodium Acetate .	
4.8.3.1.2. Calcium Acetate.	
4.8.3.2. Illumination at 275K.	
Chapter 5.	116
5.1. ESR signals and previous models.	116
5.1.1. Multiline spectra from SUC PSII and EG PSII	
5.1.2. One dimer or multi exchange tetramer	
5.1.3. Evidence for and against a Mn tetramer from Multiline data	
5.1.3.1. Multiline simulations	
5.1.3.2. Mn ENDOR studies on Multiline.	
5.1.3.3. Spin states	
5.2. Model for the $g=4.1$ signals.	125
5.2.1. Classification of $g=4.1$ Signals	
5.2.1.1. Excited state $g=4.1$ Signal	
5.2.1.2. Ground state $g=4.1$ Signal.	
5.2.2. Properties of the Ground State $g=4.1$ Signal	
5.2.2.1. Spin States	
5.2.2.2. Simulation Studies	
5.2.2.3. Pulsed EPR on the $g=4.1$ signal	
5.2.2.3.1. The $S=5/2$ case	
5.2.2.3.2. The $S=3/2$ Case	
5.3. The Nature of the Mn Centres	136
5.3.1. Location of the Manganese Sites	
5.3.2. Sites for binding	

5.3.2.1. <i>Inner site</i>	
5.3.2.2. <i>Outer site</i>	
5.4. Consequences of the Model	141
5.4.1. Manganese Binding and EPR	
5.4.2. Amine reduction and binding	
5.4.3. Mn Depletion, Reactivation and Photoactivation	
5.4.4. EXAFS Studies, Mn and Ca.	
5.4.5. Inhibited PSII S ₂ and Altered S ₃ States.	
5.4.5.1. S ₃ State	
5.5. Functional S state turnover	159
5.5.1. S ₁ state	
5.5.2. S ₂ state	
5.5.3. S ₃ state	
5.5.4. S ₃ to S ₄ to S ₀ transition - making Dioxygen	
5.6. Summary	162
Appendix 1	163
Appendix 2	164
Appendix 3	165
Reference List.	167

Table of Figures.

Figure	Summary
--------	---------

Figure 2.01	Block diagonal matrix format
--------------------	------------------------------

Figure 2.02	Energy level diagram for S=1 system with non zero Zero field components in the energy Hamiltonian
--------------------	---

Figure 2.03	Diagrammatic representation of nuclear charge cloud geometries for non zero quadrupole interaction
--------------------	--

Figure 2.04	Line shape function and half height width
--------------------	---

Figure 2.05	Representation of saturation curve for plot method of the Yim group (Yim, et al, 1982)
--------------------	--

Figure 4.01	Comparison of S ₂ state multiline signals generated from sucrose cryoprotected PSII from Bricker and BBY type PSII, 200K illumination
--------------------	--

Figure 4.02	Comparison of S ₂ state multiline signals generated from sucrose cryoprotected PSII from Bricker and BBY PSII, 200K illumination
--------------------	---

Figure 4.03	Comparison of S ₂ state g=4.1 signals from ethylene glycol cryoprotected PSII from Bricker and BBY PSII, 130K illumination
--------------------	---

Figure 4.04	S ₂ state multiline signal generated from sucrose cryoprotected PSII, illumination at 200K
--------------------	---

Figure 4.05	S ₂ state multiline signals generated from ethylene glycol cryoprotected PSII, 200K illumination and 130K illumination / 200K annealed
--------------------	---

Figure 4.06	S ₂ state g=4.1 signals generated in PSII, sucrose cryoprotected PSII illuminated at 200K, ethylene glycol cryoprotected PSII illuminated at 130K
--------------------	--

Figure 4.07	S ₂ state g=4.1 signal generated in ethylene glycol cryoprotected PSII 200K illumination, 130K illumination / 200K annealed
--------------------	--

Figure 4.08	S ₂ state ESR signals generated in ethylene glycol cryoprotected PSII, 130K illumination , subsequent 200K annealed
--------------------	--

Figure 4.09	S ₂ state ESR signal intensities due to cyclic 130K illumination and 200K annealing protocols
--------------------	--

Figure 4.10	S ₂ state ESR signals generated from ethylene glycol cryoprotected PSII, 130K illumination and 200K annealing, with added ethanol / no added alcohol
--------------------	---

Figure 4.11	S ₂ state multiline signals measured at Q band, sucrose cryoprotected PSII illumination at 200K, ethylene glycol cryoprotected PSII illumination at 130K
--------------------	---

Figure 4.12	S ₂ state g=4.1 signals measured at Q band, sucrose cryoprotected PSII illumination at 200K, ethylene glycol cryoprotected PSII illumination at 130K
--------------------	---

Figure 4.13	Temperature dependence of cogenerated S ₂ state multiline and g=4.1 signals from sucrose cryoprotected PSII illumination at 200K
--------------------	---

Figure 4.14 Model structures for Mn centre giving rise to cogenerated S_2 state multiline and $g=4.1$ signals, sucrose cryoprotected PSII, illumination at 200K

Figure 4.15 Temperature dependence of S_2 state $g=4.1$ line shapes generated in sucrose cryoprotected PSII, illumination at 200K

Figure 4.16 Deconvolution procedure of S_2 state ESR signal at $g=6.1$ generated in sucrose cryoprotected PSII, illumination at 200K

Figure 4.17 Temperature dependence of S_2 state $g=6.1$ signal line shape from sucrose cryoprotected PSII, illumination at 200K

Figure 4.18 Temperature dependence of S_2 state ESR signal intensities from sucrose cryoprotected PSII, illumination at 200K

Figure 4.19 Temperature dependence of S_2 state multiline signal intensity generated in ethylene glycol cryoprotected PSII, illumination at 200

Figure 4.20 Temperature dependence of S_2 state $g=4.1$ signal intensity generated in ethylene glycol cryoprotected PSII, illumination at 200K

Figure 4.21 Temperature dependence of S_2 state $g=4.1$ signal intensity from ethylene glycol cryoprotected PSII, illumination at 130K

Figure 4.22 Model structures for Mn centre giving rise to ground state S_2 state $g=4.1$ signal from ethylene glycol cryoprotected PSII

Figure 4.23 Energy level diagram for spin states for Mn structures giving rise to ground state S_2 state $g=4.1$ signal

Figure 4.24 Temperature dependence of S_2 state ESR signal line shapes from ethylene glycol PSII, illumination at 130K

Figure 4.25 Temperature dependence of ground state S_2 state $g=4.1$ signal line shape from ethylene glycol cryoprotected PSII, illumination at 130K

Figure 4.26 Temperature dependence of Signal II intensity from ethylene glycol cryoprotected PSII, 130K illumination, annealed 200K, modulation frequency 100KHz

Figure 4.27 Temperature dependence of Signal II intensity from ethylene glycol cryoprotected PSII, 130K illumination, annealed 200K, modulation frequency 400Hz

Figure 4.28 Temperature dependence of Signal II spin population from ethylene glycol cryoprotected PSII, 130K illumination, annealed 200K, mod'n frequency 400Hz

Figure 4.29 S_2 state Signal II from ethylene glycol cryoprotected PSII, 130K illumination, annealed 200K, mod frequency 400Hz

Figure 4.30 S_2 state Signal II from ethylene glycol cryoprotected PSII, 130K illumination, annealed 200K, annealed 200K left overnight prior to remeasure

Figure 4.31 Temperature dependence of S_2 state ESR signal intensities from ethylene glycol cryoprotected PSII, illumination at 130K

Figure 4.32 S_2 state Signal II spectra from ethylene glycol cryoprotected PSII, illumination at 130K, annealed 200K, difference spectra, Mod freq 400Hz, Mod Amp 0.05mT, microwave power 9.2 μ W

Figure 4.33 Model for Mn organisation within the luminal region of PSII

Figure 4.34 S_2 state ESR signals from Cl^- depleted / F^- exchange PSII, illumination at 200K

Figure 4.35 Temperature dependence S_2 state $g=4.1$ signal intensity from Cl^- depleted / F^- exchanged PSII, illumination at 200K

Figure 4.36 S_2 state Signal II line shapes from Cl^- depleted / F^- exchanged PSII 200K illumination, annealed 295K, difference spectrum illuminated minus annealed

Figure 4.37 Temperature dependence of S_2 state Signal II intensities from Cl^- depleted / F^- exchanged PSII, 200K illumination, annealed 295K

Figure 4.38 Temperature dependence of S_2 state Signal II spin population from Cl^- depleted / F^- exchanged PSII, 200K illumination, annealed 295K

Figure 4.39 Inhibited S_3 state ESR signals from Cl^- depleted / F^- exchanged PSII, illumination at 275K, split signal line shape

Figure 4.40 Temperature dependence of inhibited S_3 state split signal intensity from Cl^- depleted / F^- exchanged PSII, illumination at 275K

Figure 4.41 Comparison of S_2 state multiline signals from 1M NaCl treated PSII, untreated 200K illumination, DCMU treated 200K illumination, DCMU treated 275K illumination

Figure 4.42 Comparison of S_2 state $g=4.1$ signals from 1M NaCl treated PSII, untreated 200K illumination, DCMU treated 200K illumination, DCMU treated 275K illumination

Figure 4.43 S_2 state ESR signals from sucrose cryoprotected PSII, 1M NaCl treated illumination at 200K, untreated illumination at 200K

Figure 4.44 S_2 state ESR signals from 1M NaCl and DCMU treated PSII stored overnight before illumination at 275K

Figure 4.45 Inhibited S_3 state split signals from 1M NaCl treated PSII, illumination at 275K; PpBQ treated, EDTA treated

Figure 4.46 Inhibited S_3 state split signals from 1M NaCl treated PSII, illumination at 275K; treated with $K_2Fe(CN)_6$; overnight incubation at 273K; EDTA treated; PpBQ treated

Figure 4.47 Multiline signals from sucrose cryoprotected PSII, treated with 1M NaCl, illumination at 275K, split signal deconvoluted; untreated, illumination at 200K

Figure 4.48 Temperature dependence of inhibited S_3 state split signal from 1M NaCl treated PSII, illumination at 275K

Figure 4.49 Temperature dependence of inhibited S_3 state ESR signals region $g \sim 4$ to $g \sim 6$ line shapes from 1M NaCl treated PSII, illumination at 275K

Figure 4.50 Temperature dependence of inhibited S_3 state ESR signals region $g \sim 4$ to $g \sim 6$ intensities from 1M NaCl treated PSII, illumination at 275K

Figure 4.51 Temperature dependence of Signal II intensity from 1M NaCl treated PSII, illumination at 275K, annealed 295K

Figure 4.52 Temperature dependence Signal II line shapes from 1M NaCl treated PSII, illumination at 275K, annealed 295K

Figure 4.53 S_2 state ESR signal line shapes from NaAcetate treated PSII, illumination at 200K

Figure 4.54 S_2 state ESR signal line shapes from CaAcetate treated PSII, illumination at 200K

Figure 4.55 Temperature dependence of S_2 state $g=4.1$ signal line shapes from inhibited PSII, illumination at 200K, NaAcetate treated, CaAcetate treated

Figure 4.56 S_2 state ESR signal line shapes from NaAcetate treated PSII, DCMU treated, illumination at 275K

Figure 4.57 Inhibited S_3 state split signals from inhibited PSII illumination at 275K, NaAcetate treated, CaAcetate treated

Figure 4.58 Temperature dependence of inhibited S_3 state split signals from inhibited PSII illumination at 275K, combined for NaAcetate treated and CaAcetate treated

Figure 4.59 Inhibited S_3 state $g=4$ region signal line shapes from inhibited PSII illumination at 275K, NaAcetate treated, CaAcetate treated

Figure 4.60 Temperature dependence of inhibited S_3 state $g=4$ region signal intensities from inhibited PSII, illumination at 275K, combined for NaAcetate treated and CaAcetate treated

Figure 4.61 Inhibited S_3 state split signal line shapes for inhibited PSII, illumination at 275K, NaAcetate treated, CaAcetate treated, measured at 25K

Figure 5.01 Temperature dependence of S_2 state $g=4.1$ signal intensity from ethylene glycol cryoprotected PSII, illumination at 130K, modelled as excited state

Figure 5.02 Model arrangement of Mn binding site located near D1 polypeptide residues Y161, D170 and H190

Figure 5.03 Photographic image of model arrangement of Mn binding site located near D1 polypeptide residues H332, E333, D342 and A344

Figure 5.04 Diagrammatic image of model arrangement of Mn binding site located near D1 polypeptide residues H332, E333, D342 and A344

Figure 5.05 Model for turnover in Cl^- depleted / F^- exchanged PSII to form the ground state S_2 state $g=4.1$ signal and the inhibited S_3 state split signal

Figure 5.06 Temperature dependence of inhibited S_3 state split signal intensity from 1M NaCl treated PSII illumination at 275K, modelled as ground state with depopulation to low lying excited state

Figure 5.07 Model arrangement for Mn binding site near D1 polypeptide residues H332 to A344, arrangement and turnover for S_1 and S_2 states

Figure 5.08 Model arrangement for Mn binding site near D1 polypeptide residues H332 to A344, effect of treatment with alcohol on exchange coupling constant

Figure 5.09 Model arrangement of Mn binding site near D1 polypeptide residues H332 to A344, turnover to functional S_3 state and turnover to inhibited S_3 state

Figure 5.10 Model arrangement of Mn binding site near D1 polypeptide residues H332 to A344, turnover to S_4 state, dioxygen release, transition to S_0 state

Abbreviations and Symbols.

A	Electron Nuclear Hyperfine coupling constant
Å	Angstrom unit
ADRY	Accelerated Deactivation of Reagent Y
alc	alcohol (ethanol or methanol) added to the buffer
Ala	alanine
AR	Analytical reagent
Asp	aspartate
BBY	Berthold, Babcock and Yocum protocol
CaAcetate	Calcium Acetate $\text{Ca}(\text{OOCCH}_3)_2$
CaAc	Calcium Acetate $\text{Ca}(\text{OOCCH}_3)_2$
Chl	chlorophyll
cm^{-1}	centimeters ⁻¹ , an energy unit
Cyt	cytochrome
D	Fine structure (or Zero Field) interaction
D	axial Zero Field splitting parameter
DCMU	3,4-Dichlorophenyl-1,1-dimethylurea
DMSO	Dimethyl sulphoxide
E	rhombic Zero Field splitting parameter
EDTA	ethylene-diamine-tetra acetic acid
EG	Ethylene glycol, or ethane-1,2-diol
EG PSII	Photosystem II containing samples cryoprotected with ethylene glycol
Em	Electrochemical potential
ENDOR	Electron Nuclear Double Resonance
EPR	Electron Paramagnetic Resonance (equivalent to ESR)
ESE	Electron Spin Echo
ESEEM	Electron Spin Echo Envelop Modulation
ESR	Electron Spin Resonance
EtOH	ethanol
eV	electron Volts, an energy unit
EXAFS	Extended Xray Absorption Fine Structure
FTIR	Fourier Transform Infrared
G	Gauss
GHz	Giga Hertz
Gln	Glutamine
Glu	Glutamate

g	g-factor, a proportionality factor between the magnetic flux intensity and the frequency at which ESR resonance occurs, for a free electron, $g_e = 2.0023$
g_N	nuclear g-factor
h	Planck's Constant
H	Hamiltonian Operator
H	Magnetic Field intensity
H_0	applied magnetic field in the ESR experiment
H_1	Transverse magnetic field in the ESR experiment, due to microwave radiation
H2Q	Diprotonated, doubly reduced Quinol, typically dihydrobenzoquinol
His	Histidine
H 190	D1 polypeptide, residue Histidine 190
H 195	D1 polypeptide, residue Histidine 195
I	Nuclear Spin angular momentum
I	Nuclear spin state
IP	Intermediate potential form of the cytochrome b_{559}
IR	InfraRed
J	Exchange interaction integral
J	Total electron angular momentum
k	Boltzmann constant
K	Kelvin, measurement of Absolute Temperature
kDa	kilo Dalton
KJ	KiloJoule
L	Electron Orbital angular momentum
L	Light polypeptide for the bacterial photosynthetic complex
λ	wavelength
Leu	Leucine
LHC	Light Harvesting complex
M	Medium polypeptide for the photosynthetic bacterial complex
μ_B	Bohr magneton for an electron
μ_e	Magnetic moment for electron
μ_N	Bohr magneton for the nucleus
MA	magnetic field Modulation Amplitude
MeOH	methanol
MF	magnetic field Modulation Frequency
mT	milliTesla, measurement of magnetic flux intensity (=10Gauss)
mV	milliVolt
ν	frequency of electromagnetic radiation

NaAcetate	Sodium Acetate Na(OOCCH ₃)
NaAc	Sodium Acetate Na(OOCCH ₃)
NADP	Nicotinamide Adenine Dinucleotide Posphate
OEC	Oxygen Evolution Complex
$\Psi(0)$	wave function of the electron at the nucleus
p-p	peak to peak
P, \sqrt{P}	microwave power, square root of microwave power
P680	Primary electron donor and reaction core of PSII
P band	Microwave electromagnetic radiation band, approximately 14GHz to 16GHz
Phe	Phenylalanine
Pheo	Pheophytin
PpBQ	Phenyl-para-benzoquinone
PQ	Plastoquinone
psbA	Photosynthetic complex b gene sequence polypeptide A (D1)
psbD	Photosynthetic complex b gene sequence polypeptide D (D2)
PSI	Photosystem I
PSII	Photosystem II
p_z	p electronic orbital in the "z direction"
Q	Quadrupole interaction
Q _A	primary quinone electron acceptor of the PSII complex
Q _B	secondary quinone (and terminal) electron acceptor of the PSII complex
Q band	Microwave electromagnetic radiation band, approximately 34GHz to 36GHz
R.sphaeroides	Rhodobacter sphaeroides, a photosynthetic bacteria.
R. viridis	Rhodospseudomonas viridis, a photosynthetic bacteria
S	Electron Spin angular momentum
S	electronic spin state
SI	Signal Intensity
S ₀ , S ₁ , S ₂ , S ₃ , S ₄	Functional redox states of the oxygen evolution complex functional cycle
S ₋₁ , S ₋₂ , S ₋₃	Chemically reduced states of the oxygen evolution complex
S ₀ [*] , S ₂ [*] , S ₃ [*]	Chemically inhibited states of the oxygen evolution complex
S band	Microwave electromagnetic radiation, approximately 3GHz to 3.5GHz
Ser	Serine
Signal IIs	ESR signal derived from oxidised D2 Tyr160
	IIf, IIvf ESR signal(s) derived from redox transient for oxidised D1 Tyr161
Sucrose PSII	Photosystem II containing samples cryprotected with sucrose
T	Temperature
T1	Longitudinal or spin lattice relaxation time

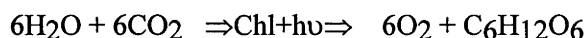
T2	Transverse or spin-spin relaxation time
TD	temperature dependence
TRIS, Tris	tris(hydroxy-methyl)aminomethane
Tx-100	Triton X-100 detergent
Tyr	Tyrosine
UV	UltraViolet
v:v	volume to volume ratio
XANES	Xray Absorbance Near Edge Spectroscopy
XAS	Xray Absorbance Spectroscopy
X band	microwave frequency band, ~ 8.5GHz to 9.8GHz
XLP	extra low potential form of cytochrome b ₅₅₉
Y _D	Tyrosine corresponding to D2 polypeptide residue 160
Y _Z	Tyrosine corresponding to D1 polypeptide residue 161
ZFS	Zero Field splitting

Chapter 1

Introduction

Molecular oxygen is essential for all heterotrophic life on earth. The major source of molecular oxygen in the atmosphere and, by convective and diffusive processes, in the oceans is as a metabolic by-product of photosynthetic carbon assimilation in plants. Photosynthesis is the use of light to provide the energy for transferring electrons from energy poor inputs to build higher energy products. The ultimate source of this energy for photosynthesis arises from the light from the sun. The evolutionary development of the biochemical components facilitating the accumulation of electrons and protons from water to be used in the fixation of CO₂ units to form basic carbohydrates has allowed the diversification of plants to nearly all parts of the planet. The major by product of this process, molecular oxygen, is essential for respiration, cycling the energy rich products of photosynthesis back to CO₂ and H₂O, powering the metabolic processes of highly developed heterotrophic life. One of the major goals of modern civilisation must be to foster the unravelling of the water splitting photosynthetic process. The quantum efficiency of this process, ie the relative number of photons of solar light used as compared to the number incident on photosynthetic surfaces approaches 90% (Ross et al., 1976, Ley and Mauzerall, 1982). The achievement of such energy returns from trapping the input of solar energy would provide a rational alternative to the burning of fossil fuels, with the added advantage of a plentiful input, water, and non polluting end products, molecular oxygen and hydrogen.

The process of photosynthesis may be described by the chemical equation



This process involves the absorption and utilisation of 24 light photons, redox chemistry involving 12 electrons and both the utilisation and production of water. This process involves the redox chemistry and interactions of many major protein complexes, water oxidation within one complex, and CO₂ fixation and water production within another. The water produced within the processes of CO₂ assimilation contains oxygen from the CO₂ fixed, and so is separable from the input water. The electrons derived from the input water are essential for the carbon fixing system.

The process by which water is split is undertaken within the thylakoid membranes of chloroplasts in higher plants and algae and chlorophyll containing membranes of photosynthetic cyanobacteria.

1.1. The structure of chloroplasts

Chloroplasts are the photosynthetic organelles which have evolved to trap light and use the energy so gained to generate the chemical building blocks of life. The inner membrane is known as the thylakoid membrane. Within the structure of the thylakoid membrane exist a number of complexes important for the conversion of solar light energy into chemical energy. Four main protein complexes have evolved, and these interact to channel electrons and H^+ ions to assimilate CO_2 into chemical energy rich compounds. Photosystem I (PSI), so called as it was the first photosystem discovered, reduces NADP using electrons photo-oxidised from plastocyanin. Photosystem II (PSII), the second photosystem discovered, reduces plastoquinone to plastoquinol using electrons photochemically derived from water. The orientation of these photosystems is vectorially equivalent, with electrons withdrawn from the lumenally located plastocyanin and water, and the electrons accepted by NADP and plastoquinone on the stromal side of the thylakoid membrane. The cytochrome b-f plastoquinol-plastocyanin oxido-reductase complex, known as the cyt b-f complex, allows the passage of electrons back across the membrane between PSII and PSI. The cyt b-f complex also pumps H^+ ions across the membrane from the stromal to lumenal sides. (For reviews on the overall electron transport chain in chloroplasts, see Mathis and Rutherford, 1987, Babcock, 1987, Anderson, 1987.)

1.1.1. Making Oxygen

The process of burning hydrogen in an oxygen containing atmosphere results in a chemical reaction which produces a very stable product, water. This makes water a very stable end product and hence a very poor choice for a starting reagent for metabolic processes. This process, which evolves a Gibbs free energy of -237KJ mol^{-1} (Aylward and Findlay, 1974), is touted as a potential alternative energy source for petroleum based fuels. However, considering alternatives, (eg H_2S , H_2O_2), H_2O is abundant, liquid over most of the earth's surface, does not seriously affect pH balance, has high specific heat and is reasonably chemically inert and, as such does not counter react with any organically based systems, eg proteins, nucleic acids etc. H_2S is gaseous at most earth surface temperatures, is not very abundant and the final product, S_2 is a solid and difficult to excrete. H_2O_2 is highly reactive with organic systems and has low abundance. Some organisms have based their metabolic processes on harvesting these as energy sources, eg Halophilic bacteria, metabolising H_2S for H^+ and electrons, excreting sulphur which accumulates as a yellow crust around thermal springs in volcanic regions. The evolution of such organisms to utilise H_2S as a source of H^+ ions and electrons arises due to the specialist niche of volcanic regions allowing a sufficiently plentiful supply of H_2S . These

organisms are based on very ancient physiology, and have been superceded by H₂O based life in all environments except the volcanic H₂S abundant sites around the world.

The abundance of water, its chemical inertness, its ability to act as a solvent for many important biological metabolic reactants and cofactors and its thermal stability make it an ideal basis of life. The evolution of mechanisms to utilise this compound as a source of H⁺ ions and electrons able to reduce and biologically assimilate CO₂ into other energy rich compounds suitable for building proteins, nucleic acids, fats etc. has enabled the development and expansion of life across this water rich planet. The development of a by-product such as molecular oxygen allows the reverse processes to generate energy and the evolution of a varied heterotrophic biosphere upon the photo autotrophic base.

The electron transfer chain in PSII has evolved to transfer electrons from water to plastoquinone. The many electron transfer components have electrochemical potentials across a wide range. On the acceptor side, pheophytin, and the iron plastoquinone centre have potentials in the range of 0 to 0.6 V. The electron donation out of the tyrosine Y_Z and from Mn²⁺ and Mn³⁺ requires a significant driving force, with ionisation enthalpies for Mn³⁺ of the order of 3 to 5 eV, though the oxidation of Mn containing compounds may be modulated by environment, protonation status and reaction chemistry.

1.2. PSII Structure

The structure of the non oxygenic bacterial photosystem reaction centre core has been elucidated by the application of X-Ray crystallography to a resolution of ~2Å (Deisenhofer, et al., 1985, Deisenhofer, et al., 1984, Michel, 1982, Zinth, et al., 1983). The bacterial photosystem core is constituted by only four polypeptides. These polypeptides consist of the L, M and H subunits, so called due to their relative molecular masses, and a c-type cytochrome complex (Deisenhofer, et al., 1985, Deisenhofer, et al., 84). The L and M subunits were observed to form a two fold symmetric dimer structure, with the reaction centre P860, bound on the symmetry axis between these subunits (Deisenhofer, et al., 1985). The crystallographic data showed the binding sites for the electron transfer components within the L and M dimer (Deisenhofer, et al., 1985, Deisenhofer, et al., 84).

Based on significant sequence homologies of the D1 and D2 polypeptides of the oxygenic PSII with the L and M subunits, respectively, of the bacterial photosystem, the electron transfer components of the higher plant PSII were proposed to be bound to the D1 and D2 polypeptides (Deisenhofer, et al., 1985, Michel and Deisenhofer, 1988, Styring, et al., 1993, Michel, et al., 1986b, Michel, et al., 1986a, Trebst, 1986). This was confirmed by experiments on PSII core complexes, where only the D1, D2, Cyt b559 polypeptides are maintained, where primary charge separation was still capable, physically identifying the D1D2 core as the

binding site of the primary components of photosynthesis (Nanbah and Satoh, 1987). The D1 and D2 polypeptides form a two fold symmetrical dimer, with the electron transfer components binding nearly symmetrically about the dimer axis. The two arms of the dimer hold a pheophytin, a redox and electron transfer active tyrosine and quinone binding site. Only one of the pheophytins and the tyrosines are functional catalytically. The Mn complex is associated with the luminal region of the D1 polypeptide (Itoh, et al., 1969, Cheniae and Martin, 1970, Cheniae, 1980). The equivalent region of the D2 polypeptide has little sequence homology to the donor side of the D1 polypeptide (Svensson, et al., 1990). The apparent duplication of the pathway from the tyrosines to the quinone binding regions is not well understood. However, it is known that the functional electron transfer follows a highly defined path through the donor side of D1, crossing to the D2 pheophytin, with the Fe Quinone complex symmetrically bound across the axis, with the Fe ion bound between the polypeptides, QA bound to D2 and QB bound to D1. (For a review of the structure of the PSII electron transfer chain, see Hansson and Wydrzynski, 1990.)

1.2.1. PSII Electron Transfer Chain

The electron transfer from water to plastoquinone is enabled by the absorption of a photon through the light harvesting complex. The energy absorbed by the LHC is transferred through a tightly exciton coupled chain of chlorophyll components into the reaction centre (for reviews see Zuber, et al., 1987, Peter, et al., 1988). The reaction centre of higher plant PSII is composed of a special pair of chlorophyll a molecules, called P680 (Montoya, et al., 1994). The capture of the photon energy into P680 excites an electron within its molecular structure. This electron is raised in electrochemical energy from the P680 base of $\sim +1.1\text{eV}$ to $\sim -0.6\text{eV}$. This excited electron is then rapidly transferred via a pheophytin molecule to an iron containing plastoquinone reductase complex.

The plastoquinone reductase complex is comprised of a non-haem iron (II) (FeII) linked to a protein bound plastoquinone QA and a mobile plastoquinone QB. The electron reaching this complex is first transferred to QA and then quickly to QB. If QB is not bound to the plastoquinone reductase complex, the electron is stabilised on the QA Fe(II) complex. The transfer of the electron from P680* to FeQA via pheophytin is very rapid, with half time in the order of a few ns - μs (Danelius, et al., 1987, Nuijs, et al., 1986, Takahashi and Asada, 1986).

P680⁺ formed by the transfer of the excited electron to the acceptor (FeQA) centre is highly unstable. P680⁺ is reduced by two sources of electrons within PSII. One source is via a recombination with the electron sited on FeQA⁻. This recombination may lead to highly reactive oxygen radical species, (Barber, 1994) see below. The second source of electrons to reduce P680⁺ is electron donation from the luminal side components of PSII, the donor side,

stabilising charge separation within PSII. This electron donation to reduce $P680^+$ occurs initially from one of three sites. Two of these sites are 'terminal' sites which act to protect $P680$ from damaging double turnover events, but which play no direct role in water oxidation. These 'side process' donors are a cytochrome b complex, cyt b559 (de Paula, et al., 1986a, Thompson and Brudvig, 1988), and a redox active tyrosine called Y_D (Vermaas, et al., 1988, Debus, et al., 1988a). The oxidised species of this tyrosine, termed Y_D^+ , is a neutral moiety due to effective deprotonation of the phenoxyl oxygen through a proton bridge H bond to another amino acid, (see later Barry and Babcock, 1988, Evelo, et al., 1989). The third path of electron donation to $P680^+$ involves functional electron transfer from the Mn containing oxygen evolving complex (OEC). On this pathway, the primary donor to $P680^+$ is another redox active tyrosine, known as Y_Z (Debus, et al., 1988b, Metz, et al., 1989). Y_D and Y_Z are located symmetrically about $P680$ on the opposite arms of the D1 D2 polypeptide core of PSII (Koulougliotis, et al., 1995). The presence of the OEC located mainly on the luminal side of the D1 polypeptide, see below, optimises the electron donation from Y_Z to $P680^+$. Electron transfer along this pathway, Y_Z to $P680^+$, is the dominant pathway for electron donation to the reaction core (Hoganson and Babcock, 1988). Y_Z^+ , formed by the electron transfer to $P680^+$, is rereduced by direct electron donation from the Mn water oxidation complex under functional conditions (reviewed in Babcock, 1987).

1.2.2. The donor side components

This work is mostly concerned with structural and functional properties of the donor side of PSII. The reader is referred to reviews of the acceptor side (Hansson and Wydrzynski, 1990, Andreasson and Vanngard, 1988) for further considerations of the pheophytin and the FeQAQB complex.

1.2.2.1. P680

$P680$ is the photoactive reaction centre and primary electron donor of PSII. This centre is the terminal pigment of the light harvesting process, absorbing the photon energy to raise the electrochemical potential of electrons to allow the electron transfer from the manganese containing water oxidation site to the FeQAQB plastoquinone reductase complex. The structure of $P680$ in higher plants and algae is somewhat similar in organisation to that of photosynthetic bacteria. Protein breakdown studies show an association of the chlorophylls of $P680$ with the D1D2 core complex (Ganago, et al., 1985, Hansson and Wydrzynski, 1990). From absorbance studies it appears likely that the $P680$ moiety is a chlorophyll dimer in higher plants, the absorbance peak arising at 680nm, while that of the reaction centre chlorophylls in highly disturbed centres is approximately 670nm, similar to Chl a monomer absorbance (Schelvis, et

al., 1994, Montoya, et al., 1994). With such breakdown of P680 intactness, forming effectively two chl a monomers, functioning at the reaction centre is lost, with absorbed photon energy dissipated by an increase in fluorescence of the accessory chlorophylls (Montoya, et al., 1994, Schelvis, et al., 1994). In functional centres, charge separation kinetic studies indicate that there are probably two distinct groups of chlorophylls associated with energy transfer to P680 (Schelvis, et al., 1994), with a time constant around 100fs (Schelvis, et al., 1994) indicating that the "terminal" accessory chl to P680 distance is approximately 30Å (Schelvis, et al., 1994). This energy is rapidly transferred through to the reaction centre complex, with charge separation forming the $P680^+Pheo^-$ couple being extremely rapid, of the order of 3ps (Schelvis, et al., 1994, Kwa, et al., 1992). This charge separated state recombines easily when the acceptor complex is dysfunctional. For stable charge transfer in functional centres, starting from transfer of the photon energy from the accessory chlorophylls to P680, through to charge stabilisation in the (FeQAQB) complex, forming $P680^+(FeQAQB)^-$, the total time is of the order of 20ps (Hansson and Wydrzynski, 1990), to 30 ps (Schelvis, et al., 1994). The structure at P680 is likely to be a chl dimer, with antiparallel orientation of the porphyrin planes, and porphyrin plane separation of $\sim 10\text{\AA}$ (Schelvis, et al., 1994, Montoya, et al., 1994, Durrant, et al., 1995). In the singlet state, the dimer has been proposed to have a strong exchange interaction, while in the $P680^+$ or the triplet state, the reaction centre is more like a pair of Chl a monomers (Hansson and Wydrzynski, 1990), and is highly reactive.

1.2.2.2. Cytochrome b559

As described before, there are three pathways of electron donation to reduce $P680^+$. Two involve tyrosine moieties, the other is Cytochrome (cyt) b559. The cyt b559 pathway is an alternative electron donation to $P680^+$ which is active under conditions in which electron donation from the water oxidation site is restricted (Thompson, et al., 1988, de Paula, et al., 1985a). There are possibly two cyt b559 per reaction centre P680 (Kaminskaya and Shuvalov, 1994, Miller and Brudvig, 1991). These cyt b559 have different redox potentials in the steady state, a high potential form with E_m of 350 - 400 mV and a low potential form with E_m of 60 - 80 mV (Kaminskaya and Shuvalov, 1994, Miller and Brudvig, 1991).

During redox transitions, changes in protein conformation change the E_m values such that the two cyt b559 centres are reclassified as IP ($E_m \sim -150$ mV) and XLP ($E_m \sim -45$ mV) (Kaminskaya and Shuvalov, 1994). Cyt b559 competes with the OEC for electron transfer to $P680^+$ (de Paula, et al., 1985a, Thompson, et al., 1988). Above 220K, the photooxidation at cyt b559 by $P680^+$ is reversible (Kaminskaya and Shuvalov, 1994). Cyt b559 can be photooxidised at temperatures to 77K (Hansson and Wydrzynski, 1990, de Paula, et al, 1985a, Thompson, et al., 1988), with electron transfer kinetics of $\sim 35\mu\text{sec}$ (Thompson, et al., 1988).

The two redox transition forms of cyt b559 are located within different regions of the PSII complex. The XLP form is located towards the stromal or acceptor side of the protein system, while the IP form is located closer to P680 (Kaminskaya and Shuvalov, 1994, Hansson and Wydrzynski, 1990). This location difference influences the electron transfer properties, and hence functionalities of the two different haems, Only the IP form appears to be photooxidisable by P680⁺, requiring bound Ca²⁺ for this process (Kaminskaya and Shuvalov, 1994, Miller and Brudvig, 1991, Thompson and Brudvig, 1988). Under conditions of strong electron donation from cyt b559, eg at 77K, one spin per PSII is shifted from P680⁺ to cyt b559 (Barber, 1994, Thompson, et al., 1988). This photooxidation at the IP cyt b559 is associated with photooxidation of another chlorophyll molecule under conditions of restricted functioning of the OEC (Barber, 1994, Thompson, et al, 1988), cycling the activity and functionality of the cyt b559 complex. In this manner of rereducing P680⁺, cyt b559 may play a role in the protection of P680 by providing the alternative electron donation site (Thompson, et al, 1988, Kaminskaya and Shuvalov, 1994, Arnon and Tang, 1988). The XLP form of cyt b559, since it has a lower negative E_m, is photoreducible, interacting with the FeQ_AQ_B site and probably plays a role in the electron/hole recombination process for this alternative donor branch (Barber, 1994, Kaminskaya and Shuvalov, 1994, Arnon and Tang, 1988). There is, however, no electron flow from XLP cyt b559 to P680⁺, possibly due to protein conformational changes during the P680 photooxidation and IP cyt b559 ⇒ P680⁺ reduction (Kaminskaya and Shuvalov, 1994).

1.2.2.3. Y_Z and Y_D - Intermediate donors

Two organic cofactors are involved in the direct electron donation from the water oxidation site to P680. One of these is the principal electron transfer component between the manganese containing OEC and P680⁺, called Y_Z (Babcock and Sauer, 1975b, Boska, et al., 1983). The other factor is labelled Y_D. Oxidation of Y_D gives rise to a stable ESR signal, with a decay time of several hours called Signal II slow or IIs (Babcock and Sauer, 1973b). Signal IIs has an isotropic g value of 2.0046, although its g tensor is anisotropic, with principle components, g_{xx} 2.0074, g_{yy} 2.0046, g_{zz} 2.0023 (Brok, et al, 1985, Brok, et al, 1986, Hogansson and Babcock, 1992). This radical centre has been shown to deprotonate via an H bonding interaction to a nearby histidine (Vass and Styring, 1991), resulting in a neutral radical being formed (Evelo, et al., 1989).

The oxidation and rereduction of Y_Z under normal oxygen evolution is very rapid. Y_Z is oxidised by P680⁺ in the range of 20 to 250 ns, the range being dependent on the charge state of the Mn containing OEC (Babcock, et al, 1983, Blankenship, et al., 1977, Warden, et al.,

1976) (see later), giving P680 Y_Z^+ , the g value of the resultant transient radical being almost identical to that of Y_D^+ . This has led to the hypothesis that YZ is a similar species as Y_D^+ (Barry and Babcock, 1987, Evelo, et al., 1989) and that it is also a neutral radical (Barry, et al, 1990, Noren and Barry, 1992). The rereduction of Y_Z^+ is on the time scale of 30 - 1300 μ s, dependent on the charge state of the Mn (see later, Dekker, et al., 1984b, Dekker, et al., 1984c, Hoganson, et al, 1989, Hoganson and Babcock, 1988, Rappaport, et al, 1994, Saygin and Witt, 1987).

In the absence of a functional Mn OEC, eg by Tris washing the PSII to remove the Mn ions, Y_Z^+ could be developed, showing very similar line shape, proton hyperfine and g value to the stable Y_D^+ (Babcock, et al, 1983, Hoganson and Babcock, 1988, Mino and Kawamori, 1994). Under these conditions, Y_Z^+ decays via recombination with $FeQA^-$, on the time scale of milliseconds (Hansson and Wydrzynski, 1990).

Early experimental data indicated that Y_Z^+ and Y_D^+ may be of plastoquinone radical nature. Both Y_Z^+ and Y_D^+ could each be developed to maximal 1:1 spin spin ratio with P680⁺ (Babcock, et al, 1983, Boska, et al, 1985, Boska, et al, 1986, Brok, et al, 1985, Brok, et al, 1986, Weiss and Renger, 1986, Warden, et al., 1976). Quantification of bound plastoquinone and ESR experiments using deuterated quinones and tyrosines, showed that PSII did not have sufficient bound PQ to account for Y_Z^+ , Y_D^+ and QA^- generation (Barry and Babcock, 1987). Deuteration of quinones did not affect the line shape at Y_Z^+ and Y_D^+ , whereas deuteration of tyrosines narrowed Y_D^+ from 20G to 7G, with no change in g value. Y_D^+ and Y_Z^+ were concluded to be tyrosine radicals (Barry and Babcock, 1987, Barry, et al, 1990, Barry and Babcock, 1988).

As both Y_Z and Y_D could donate electrons to P680⁺ and as the ESR spectra of Y_Z^+ , accumulated in Mn depleted PSII was almost identical to Y_D^+ (Babcock, et al, 1983), the tyrosines were proposed to exist in conserved positions symmetrical to P680 (Babcock, et al, 1983, Koulougliotis, et al., 1995, MacDonald, et al, 1993). From computational modelling of the PSII D1 D2 core complexes it was proposed that Y_Z was Y161 of D1 while Y_D was Y160 of D2 (Rutherford, 1989). The application of genetic sequence manipulation of the psbA and psbD genes of the chloroplast PSII polypeptides, it was found that mutating Y160 on D2 to Phe, although still allowing photoautotrophic growth, removed the capability of generating the dark stable Signal II_s (Debus, et al, 1988a, Vermaas, et al, 1988). This added weight to the speculation that the identity of YZ to be Y161 of D1. Mutation of the psb gene sequence for

* Although both Y_Z and Y_D are now known to form neutral radical species when oxidised, these forms are often referred to as Y_Z^+ and Y_D^+ , respectively.

D1, changing Y₁₆₁ to Phe, stopped the capability of photoautotrophic growth by PSII, and caused loss of Mn accumulation and rapid P680⁺ reduction (Debus, et al., 1988b, Metz, et al., 1989). This mutation determined that Y₁₆₁ on D1 was the amino acid site of YZ (Debus, et al., 1988b, Metz, et al., 1989), Y₁₆₀ of D2 was the amino acid site at Y_D (Debus, et al, 1988a, Vermaas, et al, 1988).

1.3. Properties of Y_D and YZ

The magnetic properties of tyrosine radicals have been studied by ESR, ENDOR, ESEEM and IR and indicate a general pattern of spin distribution within the tyrosine molecule. For Y_D⁺ and YZ⁺ whose ESR patterns were almost identical (Barry and Babcock, 1987), and studied under Mn depleted conditions, a hyperfine pattern typical of proton coupling to the spin was observed that was slightly different to that of other oxidisable tyrosine signals observed (Barry, et al, 1990, Bender, et al., 1989). The spin distribution about the tyrosine radical ring was very similar across oxidisable tyrosines, following an odd alternate pattern of spin distribution on the 3, 5 and 1 carbons (Barry, et al, 1990, Barry and Babcock, 1988, Hogansson and Babcock, 1992). The differences in the spectra for Y_D⁺ and YZ⁺ were proposed to arise from two geometrically influenced properties of the tyrosines (Barry, et al, 1990, Hogansson and Babcock, 1992). From analysis of ENDOR and ESEEM of YZ and Y_D, measuring the different proton hyperfine interactions, the geometry of the β methylene group was shown to be atypical compared to other tyrosines (Barry, et al, 1990, Barry and Babcock, 1988). The hyperfine coupling indicated a significant difference between the two β methylene proton interactions, with only one providing significant hyperfine (Barry, et al, 1990, Barry and Babcock, 1988, Warncke, et al, 1994). The geometry of the β methylene protons dihedral angle to the p_z orbital of the C1 carbon of the tyrosyl ring indicated proton bond angles of ~50° and ~70° (Barry, et al, 1990, Barry and Babcock, 1988). This was observed to be significantly different to other oxidisable tyrosines (see Bender, et al., 1989) and was considered a low energy configuration (Barry and Babcock, 1988, Warncke, et al, 1994). Further ENDOR studies implicated 5 sets of protons located between 3.5Å and 6.7Å from the centre of the tyrosyl ring, with their orientation normal to the ring plane, each arising from other amino acid residues (Mino, et al, 1993, Mino and Kawamori, 1994). These proton interactions with YZ and Y_D, may provide the environment to constrain the geometry of the tyrosyl ring and β methylene group conformation (Mino, et al, 1993, Mino and Kawamori, 1994). ESEEM studies of the hyperfine interaction and measurement of the g value of the oxidised Y_D ESR signal and IR vibrational studies showed that Y_D⁺ was a neutral radical, the proton being shifted off the phenoxyl oxygen within a hydrogen bonding interaction to another amino acid residue (Evelo,

et al., 1989, MacDonald, et al, 1993, Warncke, et al, 1994). Protein folding pattern modelling and psb genetic mutation showed that the amino acid hydrogen bonded to Y_D was His 189 on D2 (Svensson, et al, 1990, Svensson, et al, 1991, Svensson, et al, 1992, Styring, et al, 1993, Tommos, et al., 1993). In Mn depleted PSII, YZ was also shown to interact with the protein environment, probably through H bonding to His 190 at D1 (Svensson, et al, 1990), although an electrogenic reaction observed within the reduction of $P680^+$ by Y_Z provided some argument against the H bonding (Prokorny, et al., 1994). This provided a second geometrical difference to the other oxidisable tyrosines, as, although some have appeared as neutral tyrosine radicals, none were observed to be hydrogen bond coupled to another amino acid residue within their respective protein structures (Barry, et al, 1990, Bender, et al., 1989, MacDonald, et al, 1993).

ENDOR and FTIR studies on Y_D^+ and Y_Z^+ observed under Mn depleted conditions, showed slight differences between the geometries of the proton hyperfine and protein interactions for the YZ and Y_D varieties (MacDonald, et al, 1993, Mino, et al, 1993, Mino and Kawamori, 1994). Protein folding studies suggested a difference in the distances between YZ and His 190 on D1 and that for Y_D and His 190 on D2. These studies showed a strong hydrogen bonding between Y_D and D2 His 190 (Svensson, et al, 1990, Svensson, et al, 1991, Svensson, et al, 1992). The protein folding modelling indicated a $Y_D - D_2\text{His}190$ distance of $\sim 2.7\text{\AA}$ (Svensson, et al, 1990, Svensson, et al, 1992), while that for $Y_Z - D_1\text{His}190$ was greater than this, $\sim 4.0\text{\AA}$ (Svensson, et al, 1990, Svensson, et al, 1992, Styring, et al, 1993). This difference in Tyr - His distance and other IR, ENDOR and ESEEM studies showed that the environment at Y_D is more hydrophobic than for YZ (Svensson, et al, 1991), with the protein environment of YZ more flexible than for Y_D (Mino, et al, 1993, Mino and Kawamori, 1994), allowing YZ a greater mobility within its protein site (MacDonald, et al, 1993, Mino and Kawamori, 1994), and that the dihedral angles of the β methylene of Y_D and YZ were slightly different, (Gilchrist, et al., 1995). These factors combine to provide slightly different redox environments. These environmental variances may also be significant in allowing electron transfer properties to be different. The environments for Y_D^+ and Y_Z^+ are still very similar overall, however, and explain the unique properties of the two tyrosines, especially the stability of the Y_D^+ radical, compared to other oxidisable tyrosines and amino acids (Barry, et al, 1990, Hogansson and Babcock, 1992).

1.3.1. YZ

As noted above, the electron transfer redox carrier Y_Z has been identified as the tyrosine 161 of the D1 polypeptide (Debus, et al., 1988b, Metz, et al., 1989, Noren and Barry, 1992).

This electron carrier is the direct functional electron donor to $P680^+$, mediating the transfer of oxidising equivalents from the reaction centre to the Mn containing water oxidation complex (Boska, et al., 1983, Babcock, et al, 1983, Weiss and Renger, 1986). The kinetics of its oxidation and rereduction are quite different and these redox kinetic times vary considerably with the charge state of the manganese, (the S state), and with the presence of an active OEC (Babcock and Sauer, 1975b, Babcock and Sauer, 1975a, Boska, et al., 1983, Rappaport, et al, 1994, Weiss and Renger, 1986). In oxygen evolving PSII, the kinetics for oxidation of Y_Z by $P680^+$ are in the nanosecond range (20 - 280 ns), with rereduction of the Y_Z^+ radical by the OEC occurring on the tens to hundreds of microseconds (30 μ s - 1300 μ s) time scale (Hoganson and Babcock, 1988, Rappaport, et al, 1994), dependent on the S state and reflecting charge accumulation electrostatic effects in the OEC (Babcock, et al., 1976, Dekker, et al., 1984b, Rappaport, et al, 1994). In the absence of the Mn centre, eg by depletion of Mn by Tris washing, Y_Z still acts to reduce $P680^+$ (Babcock and Sauer, 1975a, Boska, et al., 1983, Babcock, et al, 1983). The kinetics of this oxidation are slowed to the tens of microseconds scale (Boska, et al., 1983, Hoganson and Babcock, 1989), while the rereduction of Y_Z^+ in Mn depleted PSII is slowed considerably into the millisecond and longer time range (see Hoganson and Babcock, 1988, MacDonald, et al, 1993), with decay of Y_Z^+ via recombination with acceptor side components (time scale \sim 80ms) and through oxidation of Y_D (Hoganson and Babcock, 1989). This slowing of rereduction allows a build up of YZ^+ , observable as additional signal II intensity, known as Signal II_f (Babcock and Sauer, 1975a). The accumulation of Signal II_f is dependent on the inhibition of the Mn OEC, with up to a 1:1 spin ratio of YZ^+ : $P680$ in Tris washed PSII reported (Hoganson and Babcock, 1988, Hoganson and Babcock, 1989, Babcock, et al, 1983). Optical spectra of YZ turnover in both functional O_2 evolving and in inhibited PSII, with YZ oxidation generating Signal II_v_f and Signal II_f respectively, have shown that the signal spectra are identical, with the only difference between the signals being in redox kinetics (Metz, et al., 1989). A dipolar interaction between YZ^+ and $P680^+$, developed under conditions which block the rereduction of YZ^+ while maintaining functional acceptor site turnover, manifests as a broadening of the ESR signal of $P680^+$ in the presence of YZ^+ (Hoganson and Babcock, 1989). The estimated centre-centre distance ranges from 8-12Å (Kulikov, et al, 1983) to 14-15Å (Hoganson and Babcock, 1989), while electrostatic energy and electron transfer kinetics give a distance of 11Å (Witt, 1991).

Mutation studies on the *psbA* gene of the D1 polypeptide, in which the Tyr 161 is altered to Phe, a non oxidative residue, demonstrated the importance of YZ . These mutants lost photoautotrophic capability (Debus, et al., 1988b). The mutants retained the ability to generate signal II_s (Debus, et al., 1988b, Metz, et al., 1989, Noren and Barry, 1992), but the quantum

efficiency of forming FeQA^- was decreased, with steady state charge stabilisation also lost (Debus, et al., 1988b, Metz, et al., 1989). Only ~ 0.2 Mn per PSII were accumulated in these mutants (Noren and Barry, 1992). Illumination of the D1 Tyr 161 - Phe mutants generated ESR radical signals from side pathway oxidations (Metz, et al., 1989, Noren and Barry, 1992). An ESR signal from a chlorophyll radical was observable, the signal arising probably from an accessory chlorophyll (Metz, et al., 1989). The reduction of this chlorophyll radical through charge recombination with the FeQA site was of the order of 1 ms (Metz, et al., 1989). The ESR signal from this chlorophyll radical was broader than that of P680^+ (the Chl.^+ linewidth $\Delta H \sim 11\text{G}$, while $\text{P680}^+ \Delta H \sim 7\text{G}$). The chlorophyll radical was observed to be generated in $\sim 90\%$ of centres (Metz, et al., 1989). A second ESR radical signal was observed to be generated in $\sim 60\%$ of centres, the signal having a g value of 2.004. The hyperfine pattern of this radical was typical of proton hyperfine (pattern 1:3:3:1) intensity, with a splitting of 8 to 10G (Noren and Barry, 1992). On the basis of these characteristics, the signal was proposed to arise from another oxidisable tyrosine residue, located in a different region of the protein to YD and YZ (Noren and Barry, 1992). The inability of the YZ deletion mutants to accumulate more than ~ 0.2 Mn per PSII implied that YZ plays an important role in the photoactivation, binding and stabilisation of Mn within PSII (Noren and Barry, 1992).

1.3.2. YD

The role of tyrosine 160 of the D2 polypeptide as YD has been demonstrated by genetic mutations at this site realising a loss at the Signal II_S attributed to YD^+ (Debus, et al, 1988a, Vermaas, et al, 1988). The functional role of the tyrosine, YD , is less apparent than for YZ , the direct redox carrier between P680 and the Mn OEC. The turnover kinetics of YD are complex, involving interaction with both acceptor side and donor side components of PSII. In oxygen evolving, functional PSII, the oxidation of YZ by P680^+ is so rapid (tens of ns scale) that effectively no YD oxidation occurs directly from the reaction centre (Hoganson and Babcock, 1988, Vermaas, et al, 1988). The major role of YD appears to be a stabilisation of Mn (Vass and Styring, 1991) and as a redox component in the relaxation of higher S states (see below, Styring and Rutherford, 1988). YD is efficiently oxidised by the S_2 and S_3 states on the time scale of seconds, this process being the major relaxation process for the decay of the S_2 and S_3 back to S_1 , the dark stable state (Deak, et al, 1994, Vass and Styring, 1991). The decay of oxidised YD^+ has two main pathways. YD^+ is capable of oxidising the S_0 state, forming the S_1 state (Vass, et al, 1990, Vass and Styring, 1991). This may play a role in the stabilisation of the Mn centre through all S states within the functioning of the Mn OEC. The reduction of YD^+ to YD is on the time scale of minutes, and so plays an important redox interaction role

with all the Mn S states (Vass and Styring, 1991). The interaction between S_0 and Y_D^+ accounts for a change in S state equilibrium between short and long dark adapted PSII. Illuminated, functionally active PSII has an approximate S state distribution of 25% of PSII in each redox intermediate state of the OEC (S_0 , S_1 , S_2 , S_3) (Vass and Styring, 1991). The rapid decay (in seconds) of S_2 and S_3 to S_1 leaves short dark adapted PSII in roughly 25% S_0 and 75% S_1 (Vass and Styring, 1991), longer dark time allows Y_D^+ to oxidise remnant S_0 populations to S_1 , stabilising the Mn OEC in the S_1 state (Vass and Styring, 1991).

The dark stable Y_D^+ , oxidised by relaxing S_2 and S_3 centres, decays with a half time of ~5 hours at room temperature, through recombination processes with electrons stored at the acceptor (Vass, et al, 1990), or at some other unidentified redox component (Vass and Styring, 1991). The storage of PSII containing oxidised Y_D^+ centres at 200K has been observed to result in another, more complex reduction of Y_D^+ via an interaction with cyt b559 (Vass, et al, 1990). The half time of this process is of the order of weeks. This process shifts the flash pattern of O_2 evolution in long dark adapted PSII to the fourth flash (Vass, et al, 1990).

The interaction of the S states and Y_D has been observed to be pH dependent (Deak, et al, 1994, Vass and Styring, 1991). The oxidation of Y_D by S_2 and S_3 is slowed and the reduction of Y_D^+ by S_0 is accelerated by the protonation of a nearby amino acid residue with $pK_a \sim 7.2$ (Deak, et al, 1994, Vass and Styring, 1991). Protein modelling, ENDOR, ESE and IR studies have implied that Y_D is hydrogen bonded to His 189 of D2 polypeptide (Evelo et al., 1989, Hogansson and Babcock, 1992, MacDonald, et al, 1993, Vass and Styring, 1991, Warncke, et al, 1994), with the His 189 accepting the Y_D phenoxyl proton under conditions of Y_D oxidation (Debus, et al, 1988a, Vass and Styring, 1991). It is highly likely that protonation of this Histidine while Y_D is in the reduced state is the reason for slowed oxidation of Y_D by the higher S states, and also increased rate of reduction of Y_D^+ by S_0 (Vass and Styring, 1991).

1.4. Manganese Oxygen Evolving Complex

The terminal electron donor in the electron transfer chain within PSII is water. The electron donation out of water resulting in the formation of molecular oxygen is mediated by a Mn containing prosthetic site catalysing the process of oxygen evolution, donating electrons to rereduce the oxidised intermediate donor Y_Z^+ . The mechanism of oxygen evolution proceeds via a four step process involving a cyclic electron withdrawal from the Mn site.

1.4.1. Electron Transfer and Kinetics.

The process of oxidising water to dioxygen occurs in a four step cyclic process (Joliot, et al., 1969, Kok, et al., 1970) involving five intermediate states, termed the S states (S_0 to S_4) (Kok, et al., 1970). The S states are defined as kinetically isolated steps involving the storage of oxidative equivalents within the OEC. The states S_0 to S_4 indicate the generation and storage of 0 to 4 oxidative equivalents (Kok, et al., 1970). Each step of the cycle involves the absorption of energy from a single light photon into the reaction centre, P680, stable charge separation, with P680⁺ reduced in each step by Y_Z . Rereduction of Y_Z^+ is via electron donation directly from the Mn containing oxygen evolving centre, called the OEC (Hoganson and Babcock, 1988).

Upon the turnover step from the S_3 state, the S_4 state is formed transiently as it is unstable. The resulting water oxidation chemistry, with release of dioxygen (O_2) and flow of electrons into the centre, causes rereduction of the OEC, with the complex reforming the S_0 state (Kok, et al., 1970). This transient step essentially reprimed the starting state of the oxidative cycle. The OEC appears to function by storing four oxidative holes through the cycle, rather than undertake step by step water oxidation. There is no evidence for the formation of highly reactive peroxy or hydroxy radical intermediates (Radmer and Ollinger, 1986), especially as the reagent water, although bound directly to the Mn site (Nugent, 1987, Hansson, et al., 1986), remains kinetically exchangeable throughout the S states (Messinger, et al., 1995). However, in the S_3 state, one of these reagent waters is bound more tightly than the second required for the final step (Messinger, et al., 1995, Radmer and Ollinger, 1986). Studies on ligand exchange for model metal compounds indicate that the exchange of bridging ligands is energetically unfavourable, with terminal ligands more likely to exchange with fast kinetics (Gamelin, et al., 1994). These conclusions point to reagent water being a terminal ligand through the cycle.

The kinetics of rereduction of Y_Z^+ via electron donation from the Mn OEC is dependent on the S state transition, with measurements based on UV spectroscopy for each transition indicating ranges for S_0 to S_1 ~30 μ s to 70 μ s (Dekker, et al., 1984a, Renger and Weiss, 1986, Renger, 1987, Saygin and Witt, 1987) to ~250 μ s (Rappaport, et al, 1994), S_1 to S_2 ~55 μ s (Rappaport, et al, 1994) to ~110 to 140 μ s (Dekker, et al., 1984a, Renger and Weiss, 1986, Hoganson and Babcock, 1988), S_2 to S_3 ~220 to 350 μ s (Dekker, et al., 1984a, Renger and Weiss, 1986, Renger, 1987, Hoganson and Babcock, 1988, Rappaport, et al, 1994) to ~600 μ s (Cole and Sauer, 1987) and S_3 through to S_0 ~1.0 to 1.5ms (Dekker, et al., 1984a, Cole and Sauer, 1987, Renger and Weiss, 1986, Renger, 1987, Saygin and Witt, 1987, Hoganson and Babcock, 1988, Rappaport, et al, 1994). Differences in these kinetic turnover times have been explained by differences in measurement technique and UV wavelength utilised (Rappaport, et al, 1994). The slowing of the turnover times for the higher S state transitions is consistent with

electrostatic constraints of withdrawing electrons from the Mn complex in sequentially higher oxidation states (Rappaport, et al, 1994). Proton release from the OEC during the transitions is reported to aid in counteracting the build up of charge within the centre (Renger and Weiss, 1986, Rappaport, et al, 1994, Lubbers, et al, 1993). The proton release pattern was reported to be 1, 0, 1, 2 for the initial measurements of the S state transitions (Kok, et al., 1970, Saygin and Witt, 1985, Forster and Junge, 1985), although more recent measurements have indicated proton release at each transition, the pattern following 1, 1, 1, 1 for the S state transitions (Rappaport, et al, 1994, Dekker, et al., 1984a, Lubbers, et al, 1993).

The number of Mn ions associated with PSII has been estimated via a number of techniques. Four Mn ions have been proposed to be the minimal functional number using amide reduction and Tris washing (Cheniae and Martin, 1970, Tamura and Cheniae, 1987), EDTA washing and atomic absorption (Yocum, et al, 1981), although six Mn have been proposed by atomic absorption and O₂ flash yields (Pauly and Witt, 1992). By extraction and reactivation studies, Klimov and coworkers proposed that four Mn ions are functionally associated with native PSII, with two of the four Mn ions replaceable by other divalent metal ions without significant change in centre activity (Allakhverdiyev, et al, 1993, Klimov, et al, 1982, Kulikov, et al, 1983). The two replaceable Mn ions were observed to play a structural rather than catalytic role, and not necessarily associated directly with O₂ evolution (Allakhverdiyev, et al, 1993, Allakhverdiyev, et al., 1986, Klimov, et al, 1982), although all four Mn are required for the restoration of the thermoluminescence properties of PSII (Klimov, et al, 1985).

The question of component oxidation during each transition has been approached by different techniques. X-ray absorbance studies have indicated the probable oxidation state for the four Mn in the dark S₁ state as being Mn (III)₂ Mn (IV)₂ (Guiles, et al, 1990a, Penner-Hahn, et al., 1990, MacLachlan, et al, 1992). Monitoring the changes in the Mn K edge X-ray absorption energy during S state transitions indicate oxidations within the Mn environment for each of the S₀ to S₁ (Evans, et al, 1994, Guiles, et al, 1990a, Ono, et al, 1993, Ono, et al, 1994, Sauer, et al, 1988), S₁ to S₂ (Goodin, et al, 1984, MacLachlan, et al, 1992, Yachandra, et al, 1987, Kusunoki, et al., 1993, Kusunoki, et al, 1989, Penner-Hahn, et al., 1990, Ono, et al, 1994), and S₂ to S₃ (Ono, et al, 1993, Ono, et al, 1994, Evans, et al, 1994) transitions (see later for further discussion of the X-ray data).

UV spectroscopy support an oxidation pattern for the OEC of +1, +1, +1, -3 for the transitions through the S state cycle, consistent with oxidation on each S state transition to S₃, with the S₃ to S₀ step regenerating the starting reduced state (Dekker, et al., 1984b, Dekker, et al., 1984a). The oxidation pattern has been supported by flash turnover measurements of the shifts of the K edge X-ray absorption (Flash XANES) (Ono, et al 93).

The nature of the UV absorbance changes in each step were observed not to be equivalent in terms of Mn oxidation. Differences in the UV absorption lineshape were reported

for the S_0 to S_1 , the S_1 to S_2 and S_2 to S_3 transitions (Saygin and Witt, 1987), and the S_3 to S_0 transition (Renger and Weiss, 1986) The S_0 to S_1 and S_2 to S_3 transitions were very similar, indicating the S_1 to S_2 transition did not involve direct Mn oxidation (Renger and Weiss, 1986). This oxidation pattern was not necessarily supported by proton NMR relaxation, with changes in the relaxation rates increasing for the S_1 to S_2 state, supportive of Mn III to Mn IV oxidation (Srinivasan and Sharp, 1986), with no corresponding increase for the S_2 to S_3 transition (Srinivasan and Sharp, 1986), whereby another Mn III to Mn IV oxidation is proposed by XAS (Ono, et al, 1993, Ono, et al, 1994, Evans, et al, 1994) and some UV absorbance data (Dekker, et al., 1984c, Dekker, et al., 1984b, Dekker, et al., 1984a).

The organisation of the (minimum) four Mn ions within the OEC has been explored via a number of techniques. These investigations have examined the effects of reduction and removal of Mn ions. ESR studies on paramagnetic states of the Mn centre in various S states of the catalytic cycle, under functional and inhibited conditions and X-ray absorbance studies based on the Mn K edge structure, have compared the nature of the Mn ion environment to Mn containing model complexes giving detail of the Mn location in relation to each other and ligand binding sites in the protein. For reviews on PSII functioning (see Debus, 1992, Rutherford, et al, 1991).

1.4.2. Mn Reduction and Extraction Studies

Incubation of PSII material in the presence of certain amide reagents has been reported to lead to loss of variable amounts of Mn. Using Tris-hydroxy-aminomethane (Tris), the loss of a minimum of 2 to 3 Mn per PSII was observed (Klimov, et al, 1982, Itoh, et al., 1969, Cheniae and Martin, 1970, Dolan, et al, 1990, Yocum, et al, 1981, Rickert, et al, 1991, Tamura and Cheniae, 1987), with concomitant loss of O_2 evolution (Babcock and Sauer, 1975b, Babcock and Sauer, 1975a, Boska, et al., 1983, Cheniae and Martin, 1970, Rickert, et al, 1991, Yocum, et al, 1981), photobleaching of carotenoids (Itoh, et al., 1969) and slowing rereduction of Y_Z^+ , as observed by ESR (Signal II_f) at room temperature (Astashkin, et al., 1994a, Babcock and Sauer, 1975b, Babcock and Sauer, 1975a, Boska, et al., 1983, Britt, et al., 1995, Diner, et al., 1995, Kawamori, et al., 1993, MacDonald, et al, 1993, Mino and Kawamori, 1994, Rickert, et al, 1991). This treatment of PSII membranes with Tris to remove up to 80% of the bound Mn as Mn^{2+} is observed as a direct reduction effect on the Mn without cogeneration of other ESR visible intermediates (Rickert, et al, 1991).

The treatment of PSII with hydroxylamine (NH_2OH) and hydrazine (NH_2NH_2) has been observed to result in a more differential reduction of the Mn site(s). Addition of NH_2OH leads to the reduction of Mn in single electron steps (Messinger, et al, 1991a, Messinger, et al, 1991b, Guiles, et al, 1990a) with a requirement for illumination of the NH_2OH treated S_1 state PSII, generating an oxidative equivalent before reduction to an effective S_0 state (Messinger, et al,

1991a, Beck and Brudvig, 1988b, Guiles, et al, 1990a, Forster and Junge, 1988, Kretschmann and Witt, 1993, Sivaraja and Dismukes, 1988). Further mild treatment of PSII with NH_2OH leads to loss of 2 Mn per PSII with centres reduced to formal S_{-1} state (Messinger, et al, 1991b, Messinger, et al, 1991a, Kretschmann and Witt, 1993, Sivaraja and Dismukes, 1988). This reduction of S_i states to effectively S_{i-1} states using NH_2OH has little S state dependency. In dark adapted PSII, reduction using NH_2OH leads to a common final reduced state, the S_{-1} state, independent of the ratio of S_0 and S_1 state centres, leading to loss of two Mn per centre (Messinger and Renger, 1990, Mei and Yocum, 1992). Stronger reduction with NH_2OH may lead to loss of up to 3 Mn per PSII (Sivaraja and Dismukes, 1988), with super reduced S states being formed (Messinger and Renger, 1990, Sivaraja and Dismukes, 1988, Kretschmann and Witt, 1993).

Treatment with NH_2NH_2 leads to a two electron reduction of the Mn OEC. Hydrazine reduction is observed to react in early S_i states, resulting in effective super-reduced S_{i-2} states (Messinger and Renger, 1990). This reaction between hydrazine and the OEC is strongly S state dependent, with final reduced state populations reflecting the initial S_0 to S_1 state ratios in the dark (Messinger and Renger, 1990). In this manner an effective S_{-2} state has been observed (Messinger and Renger, 1990, Kretschmann and Witt, 1993) arising from the effect of hydrazine on the S_0 state.

These treatments of PSII have been observed to be reversible by illumination. Reactivation of the functional S states was observed with O_2 evolution delayed in flash illumination experiments by the number of effective S state regressions achieved (Messinger, et al, 1991a, Kretschmann and Witt, 1993, Kebekus, et al., 1995). The most dramatic delay observed was for the generation of an effective S_{-3} state with stronger treatment with hydrazine (Messinger, et al, 1991a, Mei and Yocum, 1991b, Beck and Brudvig, 1986), although in this state Mn was observed to be highly labile (Messinger, et al, 1991a).

Ca^{++} has been observed to limit the accessibility of the reductants, and water, to the OEC (Mei and Yocum, 1991b, Mei and Yocum, 1992, Tso, et al, 1991b) and to limit the release of Mn upon reduction in the super-reduced states (Mei and Yocum, 1992, Tso, et al, 1991b). This substrate accessibility effect and maintenance of Mn upon reduction implies a structural role for Ca^{++} at the functional site (Tso, et al, 1991a, Mei and Yocum, 1991b, Mei and Yocum, 1992).

The Mn released during the treatment of PSII with hydrazine and NH_2OH is observed to be chelatable with EDTA, removing these Mn ions from a site which is reasonably accessible to the luminal solvent (Mei, et al, 1989, Riggs, et al, 1992, Takahashi and Asada, 1986).

Studies on the effect of the reductant hydroquinone have shown that two Mn ions are reducible to Mn^{2+} while OEC activity may be restored to ~80% of control activity upon

subsequent illumination (Mei, et al, 1989, Riggs, et al, 1992, Takahashi and Asada, 1986). This pool of reducible Mn is unaffected by the presence of EDTA, the Mn located within a site inaccessible to the lumen, being retained and reincorporated back into the protein restoring effectively full O₂ evolution capacity (Mei, et al, 1989, Riggs, et al, 1992). The comparison of the Mn reduction by NH₂OH and hydroquinone (H₂Q) implies the existence of two pools of bound Mn, one containing 2 Mn located in a site inaccessible to the chelators upon Mn reduction, retaining the potential to restore control O₂ evolution activity, whilst the other pool, also containing 2 Mn per PSII, is located at a site more accessible to reductants and chelators (Riggs, et al, 1992, Takahashi and Asada, 1986). Reduction at this site disrupts O₂ evolution activity leading to loss of initially 2 Mn and up to 3 Mn upon strong reduction (Kretschmann and Witt, 1993, Mei and Yocum, 1991b, Mei and Yocum, 1992, Riggs, et al, 1992, Sivaraja and Dismukes, 1988, Yocum, et al, 1981). Frasch and coworkers have observed the generation of an ESR signal arising in the g~4 region upon illumination to generate the S₂ state in PSII depleted of 2 Mn upon mild treatment with NH₂OH (Dolan, et al, 1990). The loss of the third Mn upon strong reduction at this more accessible site implies an effect on the deeper site Mn, with the loss of the outer Mn disrupting the protein organisation allowing reduction and removal of one of the deeper site Mn (Mei and Yocum, 1992).

1.4.3. Amino Acid Binding Sites.

Mutations and Protein Modelling

Of the 20 or more polypeptides that have been associated with the PSII complex (reviewed in Debus, 1992, Vermaas, et al, 1993, Anderson, 1987), studies examining the binding of Mn to the proteins have indicated that Mn binding sites exist only on the central core polypeptides, the D1 and D2 polypeptides (reviewed by Debus, 1992, Vermaas, et al, 1993). These polypeptides contain the binding site for the electron transfer pathway components of the photosystem, similar in nature to the L and M subunits of the bacterial reaction core. However, the bacterial core, although having been structurally analysed by X-ray crystallography (Deisenhofer, et al., 1985, Michel and Deisenhofer, 1988), does not possess the water splitting components of the D1/D2 core complex of higher plants.

Other polypeptides have been shown to affect the stability and functioning of the OEC although no other polypeptides have been observed to possess Mn ligand sites at this time. The identification of probable metal (Mn and Ca) ligand sites has been by examination of the effects of site specific mutants on the ability to undergo photoautotrophic growth, ability to bind and stabilise Mn, ability to evolve O₂ and effects on electron transfer through the protein based on rereduction kinetics of P680 and Y_Z. The studies have been undertaken by direct alteration of the *psb* gene sequences for each of the PSII polypeptides in the unicellular blue-green algae *Synechocystis* 6803 and *Chlamydomonas* spp. Using these studies and

crystallographic information from the non oxygenic bacterial reaction cores of the purple bacteria *Rhodospseudomonas* and *R. viridis* (Deisenhofer, et al., 1984, Deisenhofer, et al., 1985), modelling of the position of highly conserved α helices (Michel and Deisenhofer, 1988), the association of the peptides and the identity of amino acids probably involved with metal binding sites have been attempted.

1.4.3.1. Mutational Studies

The two redox components which donate electrons directly to P680, Y_D and YZ , were identified by mutational studies, as Tyr 160 of the D2 and Tyr 161 of the D1 polypeptides, respectively (Barry and Babcock, 1987, Barry and Babcock, 1988, Barry, et al, 1990, Metz, et al., 1989, Debus, et al, 1988a, Debus, et al., 1988b, Vermaas, et al, 1988, Noren and Barry, 1992). Mutational studies changing D2 Tyr 160 to Phe resulted in the loss of the dark stable ESR signal II_S and altered the activity of the centre under functional turnover and during photoactivation (Debus, et al, 1988a, Vermaas, et al, 1988). Mutation of the D1 Tyr 161 to Phe resulted in the loss of photoautotrophic growth and altered electron transfer kinetics. Disruption of electron donation to P680 (Debus, et al., 1988b, Metz, et al., 1989, Noren and Barry, 1992) occurred although the polypeptide complex was able to assemble with a functional Y_D site (Debus, et al., 1988b).

To date, mutations of carboxyl, histidyl and tyrosyl residue sites throughout the D1 and D2 polypeptides have been examined for effects on electron transport, photoautotrophy, PSII assembly, Mn binding and recombination kinetics. These mutational studies have indicated two regions of amino acid residues which affect PSII assembly and Mn photoactivation.

One of these regions is reported to be close to YZ . The other region is close to the C terminus of the D1 polypeptide, which is post translationally processed cleaving the amino acids beyond Ala 344, leaving this residue as the free carboxyl C terminus. The existence of two binding sites is supported by target size analysis, with EDTA extraction of radiation inactivated PSII. These studies reported a small binding region insensitive to EDTA washing, with the other binding site larger and more accessible the EDTA chelation of Mn which corresponded to the site of action of hydroxylamine (Takahashi and Asada, 1986).

1.4.3.1.1. Sites near YZ , the Secondary Donor

The amino acids close to the secondary donor which affect the redox properties of YZ , the binding of Mn, Mn photoactivation and the properties of the A_T thermoluminescence band, resulting from recombination, have been identified as a group of residues located at or near the luminal surface of the transmembrane D1 α helices III, IV and V. One of these, D1 Asp170, is proposed to be involved with the initial assembly of the Mn cluster (Nixon, et al, 1990, Nixon and Diner, 1992, Vermaas, et al, 1993, Styring, et al, 1993, Babcock, 1993, Chu,

et al., 1995a), possibly aiding in the binding of the first of the Mn ions during photoactivation (Nixon, et al, 1990, Nixon and Diner, 1992, Nixon and Diner, 1994). Other residues proposed to influence either Mn or Ca binding are D1 Glu189 and D1 Gln165 (Nugent, et al, 1994, Chu, et al., 1995a, Vermaas, et al, 1993, Styring, et al, 1993). Alteration of D1 Gln165 to Leu altered the ESR properties of Y_Z (Styring, et al, 1993). The role of D1 Glu189 has been shown to be important in the assembly and stabilisation of the Mn cluster (Chu, et al., 1995a, Styring, et al, 1993, Vermaas, et al, 1993) and possibly in the binding of Ca (Chu, et al., 1995a).

D1 His190 is observed to be highly important in the redox activity of Y_Z and in Mn binding. The alteration of D1 His190 hinders or blocks photoautotrophic growth (Babcock, 1993, Nixon and Diner, 1992). The ESR spectrum of Y_Z is apparently unchanged in these mutants, however, (Babcock, 1993, Nixon and Diner, 1994) which implies a significant difference between the D1 His 190- Y_Z interaction and the role of D2 His189 in stabilising Y_D by H-bonding (Tommos, et al., 1993). The loss of D2 His 189 alters the ESR spectrum of Y_D^+ significantly (Vermaas, et al, 1993, Styring, et al, 1993, Tommos, et al., 1993). The minimal effect of the loss of D1 His 190 on the ESR spectrum of Y_Z^+ was proposed to imply a lack of an H-bond between these residues (Nixon and Diner, 1994) although the influence of D1 His 190 on the redox properties of Y_Z suggested either metal binding or H-bonding (Chu, et al., 1995a). Mutation at D1 His 190 was observed to slow electron donation from Y_Z to $P680^+$ (Kramer, et al., 1994, Nixon and Diner, 1994) and inactivate the ability to oxidise water (Babcock, 1993, Roffey, et al., 1994). This led to proposals that D1 His 190 participated in the assembly, ligation and photoactivation of the Mn cluster (Roffey, et al., 1994, Chu, et al., 1995a, Babcock, 1993). In addition to these effects on the forward electron transfer, mutation of the D1 His 190 was observed to abolish the A_T thermoluminescence band (Kramer, et al., 1994, Roffey, et al., 1994). This may have been due to the loss of the D1 His 190 being a redox active amino acid, or by structural effects altering the electron transfer rates during recombination (Kramer, et al., 1994).

Mutations at D1 His 195 were observed not to affect electron donation from Y_Z to $P680$ in Mn sufficient PSII (Kramer, et al., 1994). This mutation appeared more to affect recombination pathways, with the A_T thermoluminescent bands decreasing in intensity although its temperature maximum was unchanged, implying a delay in recombination kinetics (Kramer, et al., 1994). In Mn deficient PSII in which mutations were undertaken at D1 His 195, the electron donation from Y_Z to $P680^+$ was slowed and the chl A fluorescence observed to be reduced (Roffey, et al., 1994) supporting the proposal that this amino acid was active in the recombination pathway (Kramer, et al., 1994).

1.4.3.1.2. D1 Polypeptide Carboxyl Terminus

The nature of the mutations near the Y_Z region of the D1 polypeptide affects the initial binding and photoactivation of Mn (Nixon and Diner, 1994). The mutation studies on amino acids located nearer the carboxyl terminal region of the D1 polypeptide have implicated a group of amino acids which affect the ability to evolve oxygen. These mutations appear not to influence the initial binding of Mn into the protein close to Y_Z (Nixon and Diner, 1994, Vermaas, et al, 1993).

The amino acid residues located near the C terminal region identified to affect the functioning of the OEC are D1 His332, Glu333, His337, Asp342, and the post translational cleavage C terminal residue Ala344 (Nixon and Diner, 1992, Nixon and Diner, 1994, Babcock, 1993, Vermaas, et al, 1993, Chu, et al., 1995b). The influence of D1 His332 and His337 may play a part in the nitrogen ligation to the functional Mn cluster observed by ESEEM spectroscopy in the S₁ and S₂ states (Padhye, et al., 1986, Britt, et al, 1994). Each of the side chain carboxyl ligands (D1 Glu333, Asp342) is suspected to be a monodentate ligand (one oxygen-Mn bond per residue) (Chu, et al., 1995b), with possible additional ligation to Ca (Chu, et al., 1995b, Nixon and Diner, 1994). This type of carboxyl Mn-Ca bridging is proposed in the Mn cluster model of Yachandra (Yachandra, et al, 1993) and has been observed by FTIR spectroscopy, with Ca required to be present in the S state transitions, ligated close to the functional Mn OEC site via a direct carboxyl bridge (Noguchi, et al., 1995). The role of D1 Ala344 has been shown to require a free carboxyl group at this position (Nixon and Diner, 1992). Only mutants which affect the post translational processing of the D1 polypeptide (cleavage of D1 Ser345 onwards) appear to affect the influence of this position (Nixon and Diner, 1992, Nixon and Diner, 1994).

1.4.3.2. Protein Modelling Studies

Most of the computer based protein modelling has focussed on the Y_Z and Y_D regions of the D1 and D2 polypeptides, respectively, to gain some insight into the functioning of the redox active centres involved in electron donation to P680⁺. Based on the folding patterns of the α helices of the L and M polypeptides of the bacterial photosystem (Deisenhofer, et al., 1985, Michel and Deisenhofer, 1988), the redox active and potential metal ligand residues for the homologous D1 and D2 peptides have been spliced into the sequences, followed by energy minimisation calculations.

ESR studies have indicated Y_D is H bonded to a nearby histidine, His190 on D2 (Tommos, et al., 1993, Styring, et al, 1993, Vermaas, et al, 1993). The protein modelling has supported this data, with the Y_D to His190 distance calculated to be $\sim 2.8\text{\AA}$ (Svensson, et al, 1992). Nearby Phe residues apparently fold across the luminal surface of the Y_D pocket, lifting the hydrophobicity of this residue (Svensson, et al, 1990, Svensson, et al, 1991, Styring, et al,

1993). The protein region around Y_Z in D1 was observed to be more hydrophilic (Styring, et al, 1993, Svensson, et al, 1991). The Y_D region "pocket capping" Phe residues are mostly absent in the D1 peptide, replaced by more polar carboxyl type residues, realising the hydrophilicity (Svensson, et al, 1990, Svensson, et al, 1991, Styring, et al, 1993). The opposite end of the Y_Z pocket was noted to be more hydrophilic, enhancing the charge stability on the Y_Z^+ radical, with little charge delocalisation to the protein (Svensson, et al, 1991, Styring, et al, 1993).

The nature of the Y_Z interaction with D1 His190 was predicted to be less H bonding, consistent with ESR observations of a lack of effect on Y_Z^+ by the mutation of His190 to Phe (Noren and Barry, 1992). The Protein modelling calculations placed His190 approximately 4.0Å distant from Y_Z (Styring, et al, 1993, Svensson, et al, 1990), considerably longer than expected for an H bonding interaction. The folding pattern across the phenoxyl oxygen placed two sets of potential metal ligands within $\sim 7\text{\AA}$ of the centre of the tyrosyl ring (Styring, et al, 1993, Svensson, et al, 1991). These sets of residues were Asp 170 and Gln165, and His190 and Glu189, which were also separated from each other by $\sim 7\text{\AA}$ (Styring, et al, 1993, Svensson, et al, 1991). Each of these residues is implicated in the binding and photoactivation of the Mn complex by mutational studies (see above). This evidence suggests a Mn binding site close to Y_Z (Styring, et al, 1993, Svensson, et al, 1991), although little broadening of Y_Z^+ signal in the presence of the Mn cluster has been observed (Hoganson and Babcock, 1988). However, Y_Z^+ has a much faster T1 relaxation time than Y_D^+ in the presence of the Mn cluster (Hoganson and Babcock, 1989).

By modelling an interaction between Asp170, His190, Glu333 and Asp342 on the D1 peptide, a structure 'capable' of binding a Mn tetramer was proposed (Ruffle and Nugent, 1992). This structure separated Y_Z from Asp170 and other possible metal ligand residues. This model was capable of siting the known metal liganding residues in reasonably close proximity (Ruffle and Nugent, 1992), but appeared not to satisfy the apparent proximity of Asp170 and Glu189 to Y_Z (Styring, et al, 1993, Svensson, et al, 1991). Very little is concluded about the C terminal region of the D1 peptide due to the many possible arrangements of the residues and lack of a known structural basis for modelling.

1.5. ESR of Photosystem II

A significant body of information about the structure of manganese containing sites within the OEC has been obtained from ESR studies on Photosystem II containing thylakoid membrane fractions. Nearly all of these ESR studies on Mn within the OEC have been directed at the S_2 state of the oxygen evolving cycle.

By applying a series of laser flashes to chloroplasts, followed by rapid freezing to cryogenic temperatures, Dismukes and Siderer observed an ESR signal characteristic of a trapped paramagnetic state. This signal, centred near $g=2$ featured many hyperfine peaks and was named the multiline signal. The intensity of the multiline signal showed a maximum when the ESR spectrum was recorded on the first and fifth flashes, which indicated that this signal arose in the S_2 state (Dismukes and Siderer, 1980, Dismukes and Siderer, 1981). A similar signal was generated by the freezing of broken chloroplasts under continuous illumination, trapping a paramagnetic state (Hansson and Andreasson, 1982). The signal increased in intensity upon addition of an artificial quinone acceptor, phenyl para benzoquinone (PpBQ), and an inhibitor of the Q_A site, diuron (DCMU) (Hansson and Andreasson, 1982, Andreasson, et al, 1983). Brudvig and coworkers observed the effects of intense xenon flashes and continuous illumination on the formation of the multiline signal at cryogenic temperatures. Single intense flashes were effective in inducing the multiline signal at room temperature (Brudvig, et al, 1983), confirming the proposition that the multiline arose in the S_2 state (Brudvig, et al, 1983, Dismukes and Siderer, 1981). At decreasing temperatures, the single flash was less effective in forming the multiline signal below 240K. Continuous illumination of samples frozen to low temperatures generated multiline signals down to 160K (Brudvig, et al, 1983). Above 210K, continuous illumination appeared to advance the OEC cycle beyond the S_2 state, resulting in a decrease of multiline signal intensity (Brudvig, et al, 1983).

Illumination of PSII containing samples at temperatures around 140K generated a second type of ESR signal, also attributed to manganese (Casey and Sauer, 1984). This signal was characterised by a broad, featureless resonance centred near $g=4$, and was named the $g=4.1$ signal (Casey and Sauer, 1984). Based on the line shape and g value, in comparison to $Fe\ S=5/2$ centres (Blumberg and Peisach, 1973), this $g=4.1$ signal was proposed to arise from an $S=5/2$ centre with rhombic distortion from axial symmetry (Casey and Sauer, 1984). This signal disappeared upon a short annealing at 190K, with a multiline being subsequently generated. It was proposed that the signal at $g=4.1$ was an intermediate state of electron transfer between the S_1 and S_2 states (Casey and Sauer, 1984).

Further studies using continuous illumination at 200 K showed the ability to cogenerate the multiline and the $g=4.1$ signals (Zimmermann and Rutherford, 1984). The multiline signal intensity increased upon addition of glycerol, proposed to be due to changes in the relaxation properties of the multiline signal (Zimmermann and Rutherford, 1984). The cogeneration of the multiline and $g=4.1$ signals showed a number of characteristics; the $g=4.1$ signal did not cogenerate in the presence of DCMU, and above 220K the $g=4.1$ signal decreased in intensity possibly by recombination with FeQ_A^- , while the multiline did not show an intensity loss. With short annealing periods, the rapid loss of $g=4.1$ signal corresponded with a slight increase in multiline signal intensity. Rutherford and coworkers proposed the $g=4.1$ arose from an

intermediate S state higher than the S₂ (Zimmermann and Rutherford, 1984), which differed from the observation of the g=4.1 signal generated by illumination at 140K (Casey and Sauer, 1984).

The conditions by which the multiline and g=4.1 signals could be generated were investigated as functions of pre-illumination dark adaptation time and illumination temperature (Beck, et al, 1985, de Paula, et al, 1985a, de Paula and Brudvig, 1985b). Illumination of short time dark adapted samples generated a multiline which differed from that observed for long time dark adapted samples, manifesting as slight differences in the hyperfine detail and power saturation properties (Beck, et al, 1985, de Paula and Brudvig, 1985b, de Paula, et al, 1985a). Illumination in the presence of DCMU enhanced the multiline intensities (Beck, et al, 1985). Using long time dark adapted samples, illumination in the presence of DCMU at temperatures between 77K and 235K generated a single stable charge separation (de Paula, et al, 1985a, Thompson, et al, 1988). The ESR signals observed arising from the donor side of PSII under these conditions was dependent on the illumination temperature. Only cyt b559 could be photo-oxidised below 100K (de Paula, et al, 1985a, Thompson, et al, 1988). Between 100K and 200K, the OEC S₁ state and cyt b559 competed for electron donation to P680⁺ (de Paula, et al, 1985a, Thompson, et al, 1988). This competition between the OEC and cyt b559 for electron donation to P680⁺ was also observed using FTIR and thermoluminescence (Koike and Inoue, 1987, Noguchi, et al, 1993), although the thermoluminescence properties of the S states were not affected by the oxidation state of cyt b559 (Koike and Inoue, 1987). Electron donation from the OEC due to illumination at temperatures between 100K and 160K led to a combination of g=4.1 and multiline signals being formed, the intensities of each varying with the increasing illumination temperature. Warming of the samples to 200K led to interconversion of the g=4.1 signal to the multiline signal (de Paula, et al, 1985a). Above 200K, P680⁺ was reduced by electron donation solely from the OEC, resulting in multiline signal formation (de Paula, et al, 1985a, Thompson, et al, 1988).

Under conditions allowing partial turnover into the S₃ state, no g=4.1 signal intensity was observed to develop, indicating that the g=4.1 was a property of the S₁ to S₂ turnover electron transfer (de Paula, et al, 1985a). This led to the conclusion that the g=4.1 and multiline signals arose from different illumination, electron withdrawal, ligand, and temperature dependent structural states of the Mn containing active site (de Paula, et al, 1985a). Illumination of PSII samples in the absence of PpBQ and DCMU at 200K showed the cogeneration of multiline and g=4.1 signal (Zimmermann and Rutherford, 1986). The presence of glycerol (50% v:v) or ethanol (at ~5%) inhibited this co-formation indicating that alcohols changed the properties of the Mn containing centre and affected the superhyperfine structure of the multiline signal (Zimmermann and Rutherford, 1986). They concluded from these properties and comparison of the properties of haem proteins, in which an S=3/2 intermediate

spin state gave rise to an ESR signal with $g_{\perp} \sim 4$ and $g_{\parallel} \sim 2$ (Maltempo and Moss, 1976), that the $g=4.1$ signal may arise from an $S=3/2$ state with slight rhombic distortion of the crystal field (Zimmermann and Rutherford, 1986), in contrast to the earlier assignment of the $g=4.1$ to an $S=5/2$ state (Casey and Sauer, 1984).

From these studies, two basic signal types due to Mn containing structures are observable in the S_2 state of the OEC. The nature and generation of each are influenced by the cryoprotectant and solvents added to the PSII containing sample prior to illumination.

1.5.1. Cryoprotectant effect

The discovery of the multiline and $g=4.1$ signals and the examination of their line shape properties involved the use of PSII stored under various cryoprotectant conditions. The effects of these cryoprotectants on the line shape, power saturation and temperature dependence behaviours were not examined in great detail. The line shape of the multiline signal was observed to differ slightly in terms of hyperfine spacing and superhyperfine detail when PSII was illuminated in the presence and absence of additional alcohol (Zimmermann and Rutherford, 1986, Pace, et al., 1991, Hansson, et al, 1987). These differences were observed to correlate with the absence or presence of alcohol (Pace, et al., 1991, Hansson, et al, 1987, Zimmermann and Rutherford, 1984, Zimmermann and Rutherford, 1986) or with ethylene glycol (de Paula and Brudvig, 1985b, de Paula, et al, 1986c) or glycerol (Zimmermann and Rutherford, 1984, Zimmermann and Rutherford, 1986) as cryoprotectants, or added to the sample buffer in sucrose cryoprotected PSII.

The generation of $g=4.1$ signal by continuous low temperatures (140K) illumination appeared to require the presence of glycerol or ethylene glycol as cryoprotectant, but was not affected by the presence or absence of monoalcohols under these illumination/cryoprotectant regimes (de Paula, et al, 1985a, de Paula, et al, 1986c, Thompson, et al, 1988, Casey and Sauer, 1984).

A broad comparison of the multiline signals generated in the absence or presence of alcohols showed only slight differences, with the centre giving rise to this signal assumed to be a Mn tetramer based on hyperfine interactions leading to more than 16 lines (18 - 22 in most reported multiline signals), requiring the interaction of more than 2 Mn ($I = 5/2$) to generate this number of hyperfine lines (Dismukes and Siderer, 1981, Dismukes, et al, 1982, de Paula and Brudvig, 1985b, de Paula, et al, 1986c, Haddy, et al, 1989, Kim, et al, 1992).

For most studies, the $g=4.1$ signals generated by continuous illumination at 140 K, or cogenerated in the presence of the multiline signal have been assumed to arise from the same centre and to be essentially the same signal (Haddy, et al, 1992, Kim, et al, 1992, Vänngård, et al, 1992, Zimmermann and Rutherford, 1984, Zimmermann and Rutherford, 1986). By line shape analysis at X Band, no differences are observed due to the broadness and lack of hyperfine features on the X Band signal (de Paula and Brudvig, 1985b, de Paula, et al, 1986c,

Zimmermann and Rutherford, 1984, Zimmermann and Rutherford, 1986). Line shape studies at other microwave frequencies show the $g=4.1$ signals to maintain a reasonably axial line shape. The $g=4.1$ signals indicated an axial g tensor leading to splitting at higher microwave frequencies. The g tensor components were measured, with g_{\perp} values of 4.34 and 4.14 have measured at Q Band (35GHz) for the sucrose cryoprotected PSII illuminated at 200K in the absence of alcohol (Smith, et al, 1993) and g_{\perp} values of 4.56 and 3.87 at P Band (15GHz) following illumination at 140K in glycerol or ethylene glycol cryoprotected PSII and also 200K illuminated PSII cryoprotected with sucrose (Haddy, et al, 1992, Kim, et al, 1992, Vänngård, et al, 1992). The differences in the g tensor values for these $g=4.1$ signals measured at high microwave frequency suggests that the signals may be distinct.

1.5.2. Inhibited PSII

To examine the interaction of the Mn ions within the OEC, the ligand environment and electron transfer properties, many studies have been undertaken to examine the role of cofactors such as Cl^- and Ca^{++} in stabilising the Mn site, in electron withdrawal through the protein and on the properties of ESR signals arising from illumination procedures capable of either single electron oxidation steps or continuous illumination.

Cl^- and Ca^{++} are observed to be essential cofactors for O_2 evolution. The functionality and requirements of Cl^- and Ca^{++} are reviewed by (Debus, 1992, Critchley, 1985, Homann, 1988b, Coleman, 1990, Yocum, 1991).

ESR studies on the fine structure of the S_2 state Mn multiline signal have reported no differences between Cl^- sufficient and Cl^- depleted / Br^- exchanged PSII, indicating the Cl^- anion is probably not directly liganded to the Mn cluster in the S_2 state (Yachandra, et al, 1986b, Boussac, 1995). The depletion of Cl^- from the OEC has been observed to limit the electron withdrawal through the donor side of PSII (Sinclair, 1984). In strongly Cl^- depleted PSII, the multiline signal is not generated by illumination at 200K, with the S_2 state being characterised by the generation of a $g=4.1$ signal (Baumgarten, et al, 1990, Casey and Sauer, 1984, Damoder, et al, 1986, deRose, et al., 1995, Ono, et al, 1986, Ono, et al, 1987, van Vliet and Rutherford, 1996, Yachandra, et al., 1986b). The loss of ability to generate the multiline S_2 state in Cl^- depleted PSII is paralleled by the loss of O_2 evolution (Damoder, et al, 1986, Baumgarten, et al, 1990, Boussac and Rutherford, 1994a, Casey and Sauer, 1984, Yachandra, et al., 1986b). The restoration of functional electron transfer, leading to the multiline S_2 state and the restoration of O_2 evolution, with repletion of Cl^- , is observed to follow more than one binding step; first for the restoration of capability to form the S_2 multiline state and second for the reconstitution of O_2 activity (Damoder, et al, 1986, Coleman, et al, 1987a, Coleman, et al,

1987b, Coleman and Govindjee., 1987, Beck and Brudvig, 1988a, Homann, 1988a). The binding affinity for Cl^- indicated two binding sites, with that reconstituting multiline capability being located closer to the OEC site and having an 11 fold higher affinity than the site reconstituting O_2 evolution. This latter process results in recoupling of the OEC with the reaction centre, restoring the capability to undertake the $\text{S}_3 \rightarrow \text{S}_4 \rightarrow \text{S}_0$ reaction (Damoder, et al, 1986, Baumgarten, et al, 1990, Coleman, et al, 1987b).

The influence of other anions on the ability to regenerate functional S state cycling was observed to be dependent on charge density (Damoder, et al, 1986, Ono, et al, 1987) and their influence on the redox potential of the Mn cluster (Mavankal, et al, 1986, Ono, et al, 1986, Ono, et al, 1987). With reconstitution of Cl^- depleted PSII using Br^- , both multiline and O_2 evolution capability were reconstituted in similar degree to control samples (Ono, et al, 1987, Boussac and Rutherford, 1994a, Yachandra, et al., 1986b). This restoration was observed to generate ~110% of multiline and 95% of O_2 evolution activity (Ono, et al, 1987). The higher multiline generation was observed to be correlated to a decrease of $g=4.1$ signal generation (Ono, et al, 1987). The increase of multiline capability for this anion may arise from the control PSII cogeneration of multiline and $g=4.1$ converting to a non $g=4.1$ form of multiline, in the presence of Br^- , allowing a higher spin population in the multiline state, similar to that seen for PSII in the presence of alcohols (Zimmermann and Rutherford, 1986).

The exchange of F^- for Cl^- led to a decrease in O_2 evolution capability (Ono, et al, 1986, Ono, et al, 1987, Damoder, et al, 1986, Baumgarten, et al, 1990). This inhibition was accompanied with a decrease of multiline formation to ~10 to 20% of control intensities developed by 200K illumination (Damoder, et al, 1986, Ono, et al, 1987). The multiline signal was partially generable with saturating laser flashes at 300K followed by quench cooling to 77K (Damoder, et al, 1986). The inhibition of the multiline signal was proposed to be due to an increase in the activation energy for formation of the signal (Damoder, et al, 1986), although the Cl^- depletion may not have been rigorous in these samples (Baumgarten, et al, 1990).

This reduction in multiline generation capability with increased $g=4.1$ signal generation in the S_2 state was also observed for replacement of Cl^- by acetate (CH_3COO^-), sulphate (SO_4^{2-}), iodide (I^-) and nitrate (NO_3^-) (Ono, et al, 1986, Ono, et al, 1987). Each of these inhibitions was observed to be paralleled by the an equivalent or greater generation of $g=4.1$ signal in comparison to the control sample (Ono, et al, 1986, Ono, et al, 1987). In contrast to these observations, the examination of Cl^- depleted or acetate treated particles showed no S_2 state ESR signals by illumination at 200K (Boussac and Rutherford, 1994a, MacLachlan and Nugent, 1993) and generation of the S_2 state $g=4.1$ signal in acetate treated PSII required illumination at 275K in the presence of ADRY reagents (MacLachlan and Nugent, 1993). This suggests the ESR observable S_2 state signals arise from the back reactions of double or

multiple turnovers (MacLachlan and Nugent, 1993). Illumination of Cl^- depleted PSII at 200K indicated the oxidation of components other than Mn (Boussac and Rutherford, 1994a).

1.5.3. Signals From Other S-States

ESR signals arising from Mn structures have been characterised from three S states of the OEC cycle. The S_2 state has been well characterised by the multiline and $g=4.1$ signals (see above). In non inhibited PSII samples, the S_1 state is the only other S state to have demonstrated an ESR signal. In inhibited samples, signals arising from altered S_2 state centres and from proposed double turnover states, ie. a proposed S_3^* state, have been reported.

1.5.3.1. S_1 State

The oxidation state and major structural Mn-protein motifs of the OEC have been reasonably well characterised by extended X-ray absorption fine structure (EXAFS) and X-ray absorption spectroscopy (XAS) measurements on PSII containing samples poised in the S_1 state (see above). The overall oxidation state under 'in vitro' (uninhibited) conditions has been reported to be consistent with model compounds containing Mn III and Mn IV ions, probably existing in the PSII S_1 state as $(\text{Mn III})_2(\text{Mn IV})_2$ (Cole, et al, 1987, MacLachlan, et al, 1992, Penner-Hahn, et al., 1990, Sauer, et al, 1988, Yachandra, et al, 1986a, Yachandra, et al, 1987). With the major structural Mn motif being μ -oxo-type bridged dimers, a pair of homodimers is expected for the S_1 state from oxidation turnover studies.

As model Mn dimer μ -oxo-bridged complexes have been reported to possess an antiferromagnetic exchange coupling (eg see Cooper, et al., 1978, Inoue, 1978), such a system of Mn homodimers would be expected to be diamagnetic, ie. $S=0$, in the ground state. Measurements on the S_1 state of the OEC have indeed reported that the ground state is diamagnetic (Koulougliotis, et al, 1992). This work utilised perpendicular polarisation for measurement, where the microwave field is applied perpendicular to the magnetic field, ie $H_1 \perp H_0$ with magnetic dipole transitions induced under the selection rule $\Delta m_S = \pm 1$. However, measurements utilising parallel polarisation, where the application of the microwave field parallel to the magnetic field, $H_1 \parallel H_0$, induces dipole transitions with $\Delta m_S = 0$ for partially allowed transitions (in systems with spin $> 1/2$) have shown the presence of an ESR signal in the S_1 state (Dexheimer, et al, 1990). This signal was characterised by a broad featureless resonance centred at $g \sim 4.8$ and was proposed to arise from an $S=1$ state of a Mn structure, most probably a Mn dimer. The signal was proposed to arise from the first excited state of a Mn III-III or Mn IV-IV antiferromagnetically coupled homodimer with diamagnetic $S=0$ ground state (Dexheimer, et al, 1990, Dexheimer and Klein, 1992). The S_1 $g=4.8$ signal was observed to be measurable under conditions generating the $g=4.1$ signal under illumination

at 140K (Dexheimer and Klein, 1992). The S_1 $g=4.8$ signal was observed to decrease in intensity in direct proportion to the formation of the multiline signal at 200K (Dexheimer and Klein, 1992). This correlation between the S_1 $g=4.8$ signal and the multiline signal was shown to also follow with interconversion of the $g=4.1$ signal into multiline signal upon 200K annealing of the $g=4.1$ initially generated by illumination at 140K (Dexheimer and Klein, 1992).

This correlation between the S_1 $g=4.8$ signal and the multiline signal and lack of correlation to the $g=4.1$ signal led to the proposal of two distinct magnetically isolated Mn dimers within the OEC (Dexheimer, et al, 1990, Dexheimer and Klein, 1992). One of the dimers would be involved with the formation of the $g=4.1$ signal arising from 140K illumination, the other with the S_1 $g=4.8$ signal as a thermally excited state, and the multiline signal formed in the S_2 state with illumination at 200K (Dexheimer and Klein, 1992).

This may well correlate with EXAFS data, where the formation of either the multiline or $g=4.1$ signal forms of the S_2 state results in differences in the Mn-Mn separations (Yachandra, et al, 1993, Liang, et al, 1994, deRose, et al., 1995, Dau, et al., 1995). Comparison of the EXAFS results for the S_1 state and upon the formation of the multiline S_2 state showed little difference in the Mn-Mn distance (Yachandra, et al, 1987). The comparison of the EXAFS results for the S_1 state and upon formation of the $g=4.1$ signal form of the S_2 state showed a change in the Mn-Mn peak (in the fourier transform) consistent with an increase of the Mn-Mn separation in one of the dimers with the other dimer seemingly unchanged from the S_1 state (Dau, et al., 1995, deRose, et al., 1995, Liang, et al, 1994).

1.5.3.2. S_3 State Signals

Under conditions which affect the electron transfer through the donor side of PSII, where O_2 evolution is inhibited, illumination at temperatures which permit multiple turnovers generates an ESR signal which has been assigned to a modified S_3 state (S_3^*) (Boussac, et al, 1985a, Boussac and Rutherford, 1988b, Boussac and Rutherford, 1988c, Boussac, et al, 1990a, Baumgarten, et al, 1990). This signal was characterised by a split resonance centred near $g=2$ with a variable peak to peak separation dependent on the method of inhibition. The peak to peak separation varied from ~ 10 mT for Cl^- depleted PSII samples (Boussac and Rutherford, 1994a, van Vliet, et al., 1994) to ~ 16 mT in NaCl treated (Ca^{2+} depleted) PSII (Boussac, et al, 1989, Hallahan, et al., 1992, MacLachlan, et al, 1994a, Tso, et al, 1991a, Zimmermann, et al., 1993) to 24mT for acetate (CH_3COO^-) inhibited PSII (MacLachlan and Nugent, 1993, Szalai and Brudvig, 1996, van Vliet and Rutherford, 1996). The S_3^* signal has been reported to be observable under conditions of F^- inhibition (Baumgarten, et al, 1990), high NaCl addition (Boussac, et al, 1989, van Vliet, et al., 1994), NH_4Cl addition (Andreasson and Lindberg,

1992, MacLachlan, et al, 1994a), acetate addition (MacLachlan and Nugent, 1993, Szalai and Brudvig, 1996), Cl^- depletion (Baumgarten, et al, 1990, Boussac and Rutherford, 1994a) and Ca^{++} depletion (Boussac and Rutherford, 1994b, Hallahan, et al., 1992, Andreasson and Lindberg, 1992, Tso, et al, 1991a). Under some of these conditions (high NaCl, low pH Ca^{2+} depletion), the signal has been reported to be associated with a dark stable multiline generated by an interconversion of the S_3^* signal by short term annealing, proposed to be consistent with an altered S_2 state (S_2^*) (Boussac and Rutherford, 1988c, Boussac, et al, 1990a, van Vliet, et al., 1994). This dark stable S_2^* state was also able to be directly generated from the S_1 state (Beck and Brudvig, 1986, Beck, et al, 1986, Beck and Brudvig, 1988a, Boussac, et al, 1990c). Illumination of PSII, poised in the S_1 state, inhibited by the addition of NH_4Cl at 200K to generate the S_2 state develops a $g=4.1$ signal, while short annealing at 275K of PSII samples illuminated at either 275K or 200K state results in the consequent generation of a dark stable multiline with altered hyperfine pattern (Andreasson and Lindberg, 1992, Beck and Brudvig, 1986, Beck, et al, 1986, Boussac and Rutherford, 1988b, Boussac, et al, 1990c) consistent with ligand exchange of amide nitrogens for oxygens (Britt, et al, 1989, Beck and Brudvig, 1986, Beck, et al, 1986, Beck and Brudvig, 1988a, de Paula and Brudvig, 85b, de Paula, et al 86c).

The S_3^* split signal is proposed to arise from the association of the Mn cluster and an organic radical. UV absorption, pulsed ESR and thermoluminescence measurements implicate an oxidisable histidine residue in this signal (Baumgarten, et al, 1990, Boussac, et al, 1990b, Boussac, et al, 1990a, Boussac and Rutherford, 1992b, Zimmermann, et al., 1993). The redox active electron transport chain tyrosine Y161 of the D1 protein (YZ) has also been reported to be either directly involved (Hallahan, et al., 1992, Britt, et al., 1995) or its redox properties affected such that it is less readily oxidised under some conditions generating the S_3^* split signal (Boussac and Rutherford, 1995, Tso, et al, 1991a). This inhibition of YZ oxidation may well be due to YZ^+ being trapped under the illumination conditions, restricting further electron transfer capability (Boussac, et al, 1992a, Hallahan, et al., 1992, Andreasson, et al., 1995, Britt, et al., 1995, Diner, et al., 1995). On some of the S_3^* split signals, the central peak has been reported to possess hyperfine peaks on the outer wings, consistent with the involvement of a minimal Mn dimer in the structure giving rise to these signals (MacLachlan and Nugent, 1993). EXAFS data from inhibited PSII illuminated to generate an S_2 state with reillumination generating the S_3^* , or illuminated to generate the S_3^* state directly, indicate two oxidation events within the Mn ligand environment (MacLachlan, et al, 1994b, MacLachlan, et al, 1994a, Nugent, et al, 1994, Ono, et al, 1993, Ono, et al, 1994). The Mn - radical centre signal is proposed to be spin-spin coupled in nature (Baumgarten, et al, 1990, Boussac, et al, 1990a, Boussac, et al, 1990b, Hallahan, et al., 1992, Tso, et al, 1991a, Zimmermann, et al., 1993), with

the distance over which the exchange interaction occurs calculated from the signal splitting, estimated to be less than 7.5 Å (Baumgarten, et al, 1990, Gilchrist, et al., 1995).

1.6. Power Saturation and Temperature Dependence Studies

The power saturation behaviour and temperature dependence studies undertaken on the $g=4.1$ and multiline signals have inferred that most of the differences observed in signal behaviour are due to cryoprotectant and solvent effects. These studies have provided some insight into the magnetic properties of the Mn containing structures within the OEC. A number of apparently conflicting conclusions have been forwarded, leading to extensive literature debate over the nature of the Mn centre. These conflicting results have led to different models for the spin states giving rise to the multiline and $g=4.1$ signals.

1.6.1. Multiline Signal.

The temperature dependence of the multiline signal arising from 200K illumination of PSII has been controversial. Brudvig and coworkers, using a single, presumed non-saturating, microwave power, reported that the multiline signal followed Curie type temperature dependence behaviour above $\sim 7\text{K}$ (de Paula and Brudvig, 1985b, de Paula, et al, 1986c). Below 7K, the signal intensity declined, leading to the conclusion that the multiline arises from an excited state $S=1/2$ centre lying only a few cm^{-1} above an ESR silent ground state (de Paula and Brudvig, 1985b, de Paula, et al, 1986c). The nature of this low lying ground state was not proposed nor any explanation given for the lack of any observable ESR signal from what still would be an odd electron mixed valent Mn cluster. The energy gap discussed, being only a few cm^{-1} would result in a majority of centres residing in the $S=1/2$ multiline state even at 4K, with lower temperature results not reported. Lower temperatures should have aided in the identification of any ESR signals, but even at 4K, the deviation from apparent Curie behaviour was of order 50%, for the intensity of the multiline signal (de Paula and Brudvig, 1985b, de Paula, et al, 1986c). At the lowest temperature, no additional ESR signal was observed. The power saturation plot for this specific sample, based on the Yim et al graphical method of plotting $\log_{10}(\text{signal intensity} / \sqrt{\text{Microwave power}})$ vs $\log_{10}(\text{microwave power})$ (Yim, et al., 1982) did not resolve the sub saturation region due to scatter in the data. This poor correlation to the distinct regions, where $\log_{10}(S/\sqrt{P})$ is constant (sub saturation microwave power), and $\log_{10}(S/\sqrt{P}) \propto -0.5 \times \log_{10}(P)$, leads to suspicion that, at the lowest temperatures, the Mn signals is subject to partial saturation. In other studies using either very low power Pulsed ESR techniques (Britt, et al, 1992), or by estimating the true signal intensity by extrapolating the power saturation curve to zero power (Hansson, et al, 1984, Hansson, et al, 1987, Pace, et al., 1991, Vänngård, et al, 1992), the multiline was reported to behave as if arising from a centre

exhibiting Curie behaviour down to 4.2K (Hansson, et al, 1987, Pace, et al., 1991, Vänngård, et al, 1992) or 1.2K (Britt, et al, 1992).

A second temperature dependence behaviour was reported for PSII samples not containing low molecular weight alcohols (-alc). Under these conditions, 200K illumination cogenerated the $g=4.1$ signal and the multiline (Zimmermann and Rutherford, 1984, Zimmermann and Rutherford, 1986, Hansson, et al, 1987, Pace, et al., 1991). Extrapolating the power saturation curves to zero power to obtain a true estimate of signal intensity, Pace et al reported that the multiline and $g=4.1$ signals so formed displayed complimentary deviations from Curie behaviour, consistent with the multiline and $g=4.1$ signals arising from the ground $S=1/2$ and first excited $S=3/2$ states of the same Mn containing centre (Pace, et al., 1991). The differences between the multiline species, one solely generated in the presence of alcohol at 200K, the other cogenerated in 200K illuminated samples without alcohol, manifested as differences in the observed signal intensities, hyperfine and superhyperfine structures of the multiline signals (Zimmermann and Rutherford, 1984, Zimmermann and Rutherford, 1986, Hansson, et al, 1987, Pace, et al., 1991, Smith, et al, 1993). These data appear to have been significantly overlooked as most research groups have recognised no distinctions between $g=4.1$ results (Haddy, et al, 1992, Kim, et al, 1992, Vänngård, et al, 1992, Zimmermann and Rutherford, 1984, Zimmermann and Rutherford, 1986) and worked with PSII in the presence of alcohol to maximise multiline formation with illumination at 200K (Haddy, et al, 1989, Haddy, et al, 1992, Kim, et al, 1992, Britt, et al, 1992). The difference in temperature dependence behaviour of multiline signals in the presence and absence of alcohols has been reported to be due to a change in the Heisenberg exchange coupling in PSII with added alcohol (Pace, et al., 1991), as either a solvent for PpBQ or DCMU (Pace, et al., 1991, de Paula and Brudvig, 1985b, de Paula, et al, 1986c, Vänngård, et al, 1992) or added straight to the sample (Pace, et al., 1991, Smith, et al, 1993). Calculations based on the power saturation behaviour of the multiline signal have indicated relaxation via an Orbach mechanism through a state $30-40\text{ cm}^{-1}$ above the ground (Hansson, et al, 1987, Pace, et al., 1991, de Paula, et al, 1986c) or via a Raman process (de Paula and Brudvig, 1985b, de Paula, et al, 1986c).

1.6.2. $g=4.1$ Signal

The temperature dependence of the $g=4.1$ signal generated in glycerol cryoprotected PSII illuminated at 140K has been observed to be consistent with the $g=4.1$ signal arising from a ground state centre (de Paula and Brudvig, 1985b, de Paula, et al, 1986c, Vänngård, et al, 1992, Smith and Pace, 1997). This temperature dependence behaviour of the low temperature illuminated samples is at odds with that for the $g=4.1$ signal cogenerated in sucrose cryoprotected PSII illuminated at 200K (Pace, et al., 1991, Smith and Pace, 1997). These data add to the contention that two forms of $g=4.1$ signal arise in the S_2 state of OEC turnover. This difference in temperature dependence has not been examined to any great extent, with most

studies on the $g=4.1$ signal arising in functional PSII undertaken on the ground state form formed by 140K illumination. The ability to form ESR pure states, eg with the $g=4.1$ formed by itself or with the multiline signal formed independent of any cogenerated $g=4.1$ signal has been utilised to model the signal line shapes in terms of theoretical calculations and to examine the line shapes at different microwave frequencies.

1.7. Modelling

To model the major features of the multiline and $g=4.1$ signals, simulations in terms of model Hamiltonians of the hypothesised spin systems has been applied. The approach of the modelling applied to the multiline and $g=4.1$ signals has been somewhat distinct, with the multiline modelling mostly utilising a quantum mechanical, Heisenberg exchange, hyperfine interaction approach, while the $g=4.1$ modelling has invoked Heisenberg exchange, anisotropic g tensor interaction and zero field analysis.

1.7.1. Multiline

Initial modelling of the multiline signal considered general hyperfine interactions based on an isotropic mixed valence Mn cluster. ESR measurements on Mn dimer containing model compounds (of the nature Mn III-IV, μ -oxo bridged, antiferromagnetically coupled) (Cooper, et al., 1978, Dismukes and Siderer, 1980, Dismukes and Siderer, 1981) reported 16 line hyperfine spectra. This approach noted the variance between the 16 line spectrum arising from the crystalline model compounds to the 19-22 line spectra observed from the S_2 state of PSII (Dismukes and Siderer, 1981, Dismukes, et al, 1982, Hansson and Andreasson, 1982). Measurements of the multiline signal have now been reported at four different microwave frequencies, S Band (3.5GHz), X Band (9GHz), P Band (15GHz) and Q Band (35GHz). Modelling the number of lines, width of the spectrum, hyperfine and underlying superhyperfine features on each hyperfine peak has depended on the sophistication and accuracy of the methods and Hamiltonian utilised (Dismukes and Siderer, 1981, Dismukes, et al, 1982, de Paula and Brudvig, 1985b, de Paula, et al, 1986c, Kim, et al, 1992, Haddy, et al, 1989, Kusunoki, 1992, Åhring and Pace, 1995). Using only Zeeman and isotropic hyperfine interaction terms, the Brudvig and Dismukes groups have shown that an isotropic mixed valence Mn dimer may give rise to a hyperfine pattern consisting of 16 lines, a trimer 36 lines and a tetramer with full hyperfine interaction through all four Mn ions may give rise to a hyperfine pattern with 200+ lines (Dismukes, et al, 1982, de Paula and Brudvig, 1985b, de Paula, et al, 1986c). This approach was initially used to explain the extra features in the multiline pattern above 16 lines and later invoked to explain the S Band multiline spectrum (Haddy, et al, 1989), especially as hyperfine interactions are most pronounced at this

microwave frequency. The multiline spectrum reported from S Band measurements features a highly complex hyperfine pattern with ≥ 60 peaks (Haddy, et al, 1989). With only isotropic hyperfine exchange, this pattern could only be explained by invoking a Mn tetramer centre (Dismukes, et al, 1982, de Paula, et al, 1986c, Haddy, et al, 1989). Comparison of multiline spectral measurements at X Band and Q Band (Smith, et al, 1993, Hansson, et al, 1987) indicates significant hyperfine anisotropy, and this has been proposed to be a factor in questioning the tetramer model.

Two recent modelling studies have been presented based on quantum mechanical analysis of the spin Hamiltonian systems for variable Mn clusters. Kusunoki reported a simulation with detailed anisotropic analysis of hyperfine and Zeeman terms (Kusunoki, 1992). This analysis concluded that a tetramer model best simulated the multiline spectra at each microwave frequency, with the dominance of a single dimer in the interactions within the tetramer (Kusunoki, 1992). Åhrling (Åhrling and Pace, 1995) reported a more complete analysis of the spin Hamiltonian, including Zeeman, hyperfine and quadrupole interactions, with exact, numerical diagonalisation of the energy matrix. This simulation reported the most extensive Hamiltonian so far and proposes that a single Mn dimer, with suitably anisotropic protein environment, could simulate well the multiline signals observed for S Band, X Band and Q Band data (Åhrling and Pace, 1995). It would be expected that the environment of a Mn complex within a protein would not in general be highly isotropic and comparable to that found in model compound crystals. It is of interest, however, that the Mn catalase enzyme gives rise to a 16 line ESR spectrum and is readily simulated utilising only two Mn (Haddy, et al., 1994, Ivancich, et al., 1995). The Mn water oxidising enzyme is subject to a much more severe oxidation regime for its cyclic activity, and so should exist in a much more restricted protein site. Relating the Åhrling simulation data back to the protein environment indicated the ligand structure at each Mn must be anisotropic, with the magnitude of the apparent quadrupolar interactions suggesting co-ordinate unsaturation (the Mn ions being 5 co-ordinate only). A model for the ligand geometry and substrate coordination for the Mn ions in the (probable) dimer complex, giving rise to the multiline signal in the S_2 state was presented (Åhrling and Pace, 1995).

The modelling of Åhrling proposed a ligand deficient environment for each of the Mn within the proposed exchange coupled dimer system (Åhrling and Pace, 1995). This proposed environment has some additional support with ligand ENDOR and simulation studies indicating the electron spin density about some of the Mn III ions is oblate spheroid shaped (flattened disk), which is more typical of 5 coordinate Mn environments (Dismukes, et al, 1994). The ligand ENDOR and simulation studies were claimed to support a Mn tetramer model due to the number of hyperfine peaks observed in the multiline measured at X and S Bands (Dismukes, et al, 1994), although the Åhrling and Pace simulation displayed many

hyperfine peaks (> 100) in the S Band spectrum due to quadrupolar interactions making many otherwise forbidden transitions partially allowed (Åhrling and Pace, 1995).

1.7.2. $g=4.1$ Signal

Two lines of thought have arisen with regard to the modelling of the $g=4.1$ signal. Within both, however, no segregation of the $g=4.1$ signal cogenerated with the multiline and the $g=4.1$ signal solely generated has been considered. The modelling has been approached from two directions, with models arising from $S=3/2$ or $S=5/2$ systems invoked. Initial propositions for the signal were for a rhombic $S=5/2$ system due to the crossing point being above $g=4.0$, similar to the signals for rhombic Fe^{3+} in model complexes and other protein environments (Casey and Sauer, 1984). The comparison of the $g=4.1$ to ESR signals from rhombic spin $5/2$ centres, similar to those of monomeric high spin rhombic Fe structures, led to a proposal that the $g=4.1$ signal arose from an isolated monomeric Mn IV (Hansson, et al, 1987). This was discounted by the observation of hyperfine structure on the $g=4.1$ signal generated in oriented functional PSII (Smith, et al, 1993) and NH_3 treated PSII (Kim, et al, 1990, Kim, et al, 1992). This observation demanded a Mn structure of dimeric or high nuclearity (Kim, et al, 1990, Kim, et al, 1992).

The most simple explanation for the interconversion of the $g=4.1$ signal generated by 140K illumination to the multiline signal at 200K was for the interconversion of spin states within a single Mn tetrameric structure, with ligand rearrangement upon warming to 200K. This led to the proposal by Brudvig and coworkers for a tetrameric dimer of dimers model in which illumination at 140K gave rise to an $S = 3/2$ ground state, while illumination at 200K generated a spin $1/2$ ground state (de Paula and Brudvig, 1985b, de Paula, et al, 1986c). Analysis of a Mn tetrameric structure, two antiferromagnetic coupled Mn dimers with ferromagnetic exchange between the two dimers, was proposed to be capable of generating either the $S=3/2$ or $S=1/2$ states depending on the spin state of one of the dimers. This model also provided an explanation of the complexity of the $S=1/2$ multiline signal, with tuning of the magnetic exchange between the $S=1/2$ dimer and the other ESR silent Mn dimer capable of increasing the hyperfine complexity of the simulated spectra (de Paula and Brudvig, 1985b, de Paula, et al, 1986c). For such a structure to be able to give rise to an $S=3/2$ ground state, the exchange between each Mn ion in the $S=1$ dimer and those of the $S=1/2$ Mn dimer was required to be equivalent, with the $S=1/2$ Mn dimer reducible to an $S=1/2$ centre in the Heisenberg exchange coupling scheme (ie strongly coupled) (de Paula, et al, 1986b). This structure, proposed by Brudvig and coworkers, led to a cubane type model for the Mn tetramer (Brudvig and Crabtree, 1986). However, this structure was inconsistent with the X-ray absorbance data. These indicated the Mn to be structured as μ -oxo bridged dimers with separations of 2.7\AA , with only one other possible Mn-Mn distance at 3.3\AA . The number of nearest Mn neighbours for Mn was consistent only with dimer structures (Yachandra, et al,

1987, Yachandra, et al, 1993, George, et al, 1989, MacLachlan, et al, 1992, Kusunoki, et al, 1989, Penner-Hahn, et al., 1990, see below).

The ferromagnetically exchange coupled dimer of antiferromagnetic exchange coupled Mn dimers was, however, maintained as the major accepted model for the Mn site. On the basis of the ratio of the exchange couplings between the Mn ions in the $S=1/2$ centre and each of the other Mn ions, forming either an $S=1$ or $S=2$ dimer, an $S=3/2$ or $S=5/2$ total spin state could be generated by a single electron withdrawal from the Mn tetrameric state (de Paula, et al, 1986c, Haddy, et al, 1992, Yachandra, et al, 1993).

Line shape studies of the $g=4.1$ signals generated at 200K or in inhibited samples treated with either F^- or NH_3 to suppress the multiline state formation and multifrequency simulations of model Hamiltonians led to the proposal that the $g=4.1$ signal arose from the quasi-isotropic middle Kramers doublet of a rhombic $S=5/2$ state (Haddy, et al, 1992). The addition of F^- or NH_3 to PSII led to an increase of the rhombicity of the signal (Haddy, et al, 1992). However, the analysis of such an $S=5/2$ state indicated additional ESR signals should be observable at lower g value (de Paula, et al, 1986c) although arguments based on transition probabilities and the quasi-isotropic nature of the signal argued against this (Haddy, et al, 1992, Kim, et al, 1992).

Examination of the magnetic moment for each of the $g=4.1$ and multiline signals indicated the total magnetic susceptibility change from a proposed $S=5/2$ $g=4.1$ state to the $S=1/2$ multiline state at 200K was inconsistent with the observation (Baumgarten, et al, 1990, de Paula, et al, 1986c, Hansson, et al, 1987, Sivaraja, et al, 1989). A further conclusion was that the ligand rearrangement required for the interconversion from an $S=5/2$ state to an $S=1/2$ state at 200K was too great (de Paula, et al, 1986c). It was claimed that only an $S=3/2$ state could be generated at 140K, giving rise to the $g=4.1$ signal (de Paula, et al, 1986c).

Based on the model structure for the multiline signal, the minimum being an $S=1/2$ antiferromagnetically coupled mixed valence Mn III-IV dimer, an additional model for the $g=4.1$ signal was proposed by Pace et al, based on comparison to model Mn compounds (Pace, et al., 1991). For an isolated mixed valence Mn III ($S=2$) Mn IV ($S=3/2$) pair antiferromagnetic exchange coupling leads to a ground state $S=1/2$ species. The populatable states of the total $S=7/2$ system are then $S=1/2, 3/2, 5/2, 7/2$. The multiline is observed as the ground state $S=1/2$ species with the free electron interacting with both Mn ($I=5/2$) nuclei resulting in a complicated hyperfine pattern. The first excited state, the $S=3/2$, for a quasi axial system, suggested by the line shape at X and Q bands (Pace, et al., 1991, Smith, et al, 1993), leads to an ESR resonance near $g=4$. Slight rhombic distortion in the fine structure, zero field terms, and spin state mixing from higher spin states leads to the apparent g value being slightly above 4 (Pace, et al., 1991), similar to that observed for model Mn dimer compounds (Chang, et al., 1988a, Chang, et al., 1988b, Diril, et al., 1987).

The modelling of the multiline and cogenerated $g=4.1$ signals as arising from an isolated Mn dimer was discounted on the H_1 field dependence of the pulsed ENDOR signal intensity of the $g=4.1$ signal (Astashkin, et al., 1994b, Kawamori, et al., 1993). A pulsed Mn ENDOR study on the multiline signal gave results consistent with the presence of significant Mn nuclear quadrupole components (Britt, et al., 1995). However, based on low level simulations of this signal, a tetramer Mn complex was proposed as more closely matching the signal line shape arising from the multiline S_2 state (Britt, et al., 1995). The electron spin echo (ESE) study on the $g\sim 4$ region of S_2 state PSII indicated that the H_1 field dependence of the signal line shape was consistent with the signals in the $g\sim 4$ region arising from a rhombically distorted $S=5/2$ state (Astashkin, et al., 1994b, Kawamori, et al., 1993). However, the H_1 field dependence of signal intensity of the background Fe signal at $g=4.3$, this signal being an ideal rhombic distorted $S = 5/2$ signal, should be close to the simulation model proposed. This was not obvious for the data presented (Astashkin, et al., 1994b, Kawamori, et al., 1993), with the assignment of any signal to a rhombic $S=5/2$ state being as yet inconclusive.

At present modelling studies based on Hamiltonian simulations related to ESR and ENDOR experiments have not provided a clear model for the number of Mn associated with each of the multiline and $g=4.1$ signals, and the absolute spin state for the $g=4.1$ signal.

1.8. X Ray Studies

ESR has advanced the knowledge of the structure of the OEC through studies on the chemical nature of the Mn complexes which generate the ESR signals in the S_2 state. To relate these Mn complexes to the protein environment, studies using X ray spectroscopic techniques have examined the oxidation state changes and ligand coordination environment of Mn within the OEC and the protein.

The ability to observe the environment of the Mn cluster using ESR on functional and inhibited PSII is limited to the few ESR/ENDOR signals available. The use of X-ray techniques has examined the oxidation state, ligand environment and ligand symmetry for the Mn ions within PSII and observed changes in the local structure and redox environment upon advancement through the S states and in reduced states upon treatment with NH_2OH and NH_2NH_2 .

The X-ray absorption K edge for the S_1 state of PSII samples was similar in energy to Mn containing compounds with an average oxidation state of either Mn III (McDermott, et al, 1988, George, et al, 1989, Kusunoki, et al, 1989), or a mixture of Mn III and Mn IV (Guiles, et al, 1990a, Yachandra, et al, 1986a, Yachandra, et al, 1987, MacLachlan, et al, 1992, Sauer, et al, 1988, Penner-Hahn, et al., 1990). This result was echoed across the comparison of various PSII containing materials; whole chloroplasts (Kirby, et al, 1981a, Kirby, et al, 1981b, George,

et al, 1989), detergent solubilised thylakoid PSII samples from spinach (Cole, et al, 1987, Goodin, et al, 1984, Kusunoki, et al, 1989, Yachandra, et al, 1986a, Yachandra, et al, 1987), cyanobacteria *Synechocystis* (DeRose, et al, 1994, McDermott, et al, 1988) and oriented chloroplast samples (George, et al, 1989, Mukerji, et al, 1994). Examination of the absorption edge fine structure, with a k^n weighted Fourier transform analysis of the edge modulations, leading to information of the numbers of ligands, the radial distances of the ligands from the Mn ions and the overall symmetry of the Mn environments, led to the generally accepted model of the Mn organised as μ -oxo bridged dimers, with two oxygen (O) or nitrogen (N) ligands at $\sim 1.8\text{\AA}$, 3 or 4 O or N ligands per Mn ion at $\sim 2.0\text{\AA}$, each Mn ion observing between 0.5 and 1.0 Mn at 2.7\AA and less than one metal ion, either Mn or Ca, at 3.3\AA (George, et al, 1989, Kusunoki, et al, 1989, MacLachlan, et al, 1992, Penner-Hahn, et al., 1990, Yachandra, et al, 1993). The natures of the Mn- metal distances have resulted in the greatest discussion over the structure of the Mn OEC.

Studies on the near edge features of the X-ray absorption spectrum proposed details of the symmetry and homogeneity of the Mn ions ligand environment. The near edge feature in PSII samples is said to be relatively intense in comparison to model Mn containing compounds, indicating that the Mn ions were not homogeneously ligated to the protein (Kirby, et al, 1981b, Kusunoki, et al, 1989, Penner-Hahn, et al., 1990). The intensity of the peak and its line shape and peak position were compared to model compounds, concluding that some of the Mn may be ligand deficient, being 5 coordinate in the protein (Kusunoki, et al, 1989). This was also implied from ENDOR studies (Dismukes, et al, 1994), allowing the high oxidative potential for the enzyme. The non centrosymmetric nature of the Mn ions, drawn from the near edge feature, indicated a range of different ligand types to the Mn (Kusunoki, et al, 1989).

The environment was proposed to consist of oxygen ligands, as μ -oxo bridges, either as μ -oxo-oxygens or derived from water as μ -hydroxo-protein salt bridged structures; carboxylato bridges, either as bridging μ -carboxylato or as terminal carboxyl ligands, arising from acidic amino acid groups, and nitrogen ligands from histidine amino acid residues as terminal ligands (Kusunoki, et al, 1989, George, et al, 1989, MacLachlan, et al, 1992, Penner-Hahn, et al., 1990, Sauer, et al, 1988, McDermott, et al, 1988, DeRose, et al, 1994).

Cl^- as a ligand was neither confirmed nor discounted due to the insensitivity of the data being modelled to the presence of a single Cl^- (Yachandra, et al, 1993, Klein, et al, 1993). With Electron spin echo envelop modulation (ESEEM) spectroscopic data indicating the binding of the NH_3 to Mn in inhibited PSII systems (Britt, et al, 1989), leading to the generation of a $g=4.1$ signal upon illumination at 200K and an altered multiline signal in short term annealed samples illuminated at 273K (Beck and Brudvig, 1986, Beck, et al, 1986), Cl^- has been proposed to be bound to the Mn (Yachandra, et al, 1993). However, the inability to observe any alterations in S_2 state multiline superhyperfine features with the exchange of Br^- for Cl^- in

functional PSII (Yachandra, et al, 1986b) and the inability to observe major changes of the X-ray absorbance data for the exchange of Br⁻ (a better X-ray scatterer due to its larger atomic mass and electron cloud) (Yachandra, et al, 1986b, Klein, et al, 1993), the Cl⁻ (and hence Br⁻) binding, as indicated by Cl NMR (Preston and Pace, 1985), may be located away from the direct Mn ligand shells.

The EXAFS peak at 3.3Å has been the object of major discussion throughout the literature. This peak, observed as a Mn-metal distance, has been conjectured to arise from either a longer Mn-Mn distance, with the μ -oxo bridged Mn dimers bridged by flexible μ -carboxylate bridges (Yachandra, et al, 1993), or from a Mn-Ca scattering distance (George, et al, 1989, MacLachlan, et al, 1992, Nugent, et al, 1993, Liang, et al, 1994, DeRose, et al, 1994). The number of Mn or metal ions as nearest neighbours for Mn is proposed to be 0.5 to 1.0, based on the peak at 3.3Å (Yachandra, et al, 1993, Klein, et al, 1993, Penner-Hahn, et al., 1990, DeRose, et al, 1994). The proposal for the 3.3Å distance being a Mn-Mn distance was based on comparison to μ -carboxylato bridged Mn compounds (George, et al, 1989, Penner-Hahn, et al., 1990, Yachandra, et al, 1993) and the proposed model structure for the centre giving rise to the multiline and $g=4.1$ signals (Haddy, et al, 1989, Haddy, et al, 1992, Kim, et al, 1992, Kusunoki, 1992). The X-ray absorbance data discounted the possibility of a cubane like Mn tetramer, proposed by Brudvig (Brudvig and Crabtree, 1986), and for a symmetric butterfly tetramer proposed by George et al (George, et al, 1989). The data remained consistent with an asymmetric butterfly type structure (Kusunoki, et al, 1989, Yachandra, et al, 1993) with the two Mn dimers linked by a di- μ -carboxylato- μ -oxo bridged structure.

The alternative proposal for the 3.3Å Mn-metal peak is for Mn-Ca separation (George, et al, 1989, MacLachlan, et al, 1992, Nugent, et al, 1993). In PSII depleted of Ca, the EXAFS peak at 3.3Å is decreased in intensity, indicating a correlation to the Ca content (Nugent, et al, 1993, Yachandra, et al, 1993) With the exchange of Sr for Ca, the peak at 3.3Å is enhanced, expected if the Mn-metal distance is now Mn-Sr with Sr being a better X-ray scatterer (Yachandra, et al, 1993). This data suggests strongly the interaction between Mn and Ca in the X-ray absorbance data. The detection of a carboxyl bridge between Mn and Ca in PSII, using IR spectroscopy (Noguchi, et al., 1995) indicated that such a Mn-Ca distance could be mediated by at least one μ -carboxylato type bridge. The data for Ca depletion and Sr exchange has led to two proposals, that the 3.3Å separation arises from both a Mn-Mn and Mn-Ca distance (Klein, et al, 1993, Yachandra, et al, 1993, DeRose, et al, 1994) or as a direct Mn-Ca separation (Nugent, et al, 1993, Evans, et al, 1994), with the uncertainty at high separation distances in the EXAFS Fourier transform too great to give further detail of the separation of the Mn - Mn dimers (MacLachlan pers comm).

Comparison of the X-ray absorbance data for the S₁ state to that for the other S states gives detail on the changes occurring during the oxidation process of the complex in both

functional and inhibited PSII. Illumination generating the S₂ state dominated by the multiline signal resulted in little change in the ligand environment of the Mn ions, although the K edge spectrum was observed to shift toward lower λ (or higher energy) by about 1eV, indicating an oxidation of a Mn (III) to Mn (IV) (Goodin, et al, 1984, Liang, et al, 1994, George, et al, 1989, MacLachlan, et al, 1992, Kusunoki, et al, 1989, Yachandra, et al, 1987, McDermott, et al, 1988) or a change in the Mn environment (MacLachlan pers comm). Initial studies on the S₂ to S₃ transition indicated little change in terms of the XAS inflection point and the EXAFS peaks with the turnover by illumination / short anneal / illumination technique (Guiles, et al, 1990b). This illumination protocol transformed the S states through the multiline visible state to another ESR silent state, presumably the S₃ state (Guiles, et al, 1990b). A possible change in the X-ray absorption near edge structure (XANES) region indicated a rearrangement of ligand charge for this S state turnover event, as well as possible changes in the Mn-Mn distances, with a more heterogeneous distribution of the Mn-Mn within the dimer structures (Guiles, et al, 1990b). More recent studies have indicated that the XAS inflection point is shifted by almost equivalent energies for both the S₁ to multiline S₂ state and the multiline S₂ to ESR silent S₃ state, indicating oxidation events within the Mn environment for both S state steps (Evans, et al, 1994, MacLachlan, et al, 1994b, Ono and Inoue, 1992, Ono, et al, 1993, Ono, et al, 1994).

Illumination of NH₂OH treated PSII results in reduction of the OEC forming an S₀^{*} state (Guiles, et al, 1990a, Messinger, et al, 1991a). The dark-adapted, essentially S₁ state, in the presence of the NH₂OH was observed to be identical to the normal S₁ state, indicating that the illumination is prerequisite to the reduction to the S₀^{*} state with NH₂OH (Guiles, et al, 1990a). This S₀^{*} state was observed to be significantly different to that of the dark adapted S₁ state. The EXAFS and XANES spectra for the S₀^{*} state indicated changes in the ligand environment of one of the Mn ions, with significant ligand rearrangement (Guiles, et al, 1990a). The XAS inflection point shifted to lower energy indicating that one Mn ion was reduced, Mn III to Mn II, upon the illumination of the NH₂OH treated PSII (Guiles, et al, 1990a).

The illumination of functional PSII at or below 140K generates the S₂ state dominated by the g=4.1 signal (Casey and Sauer, 1984, Zimmermann and Rutherford, 1984, de Paula, et al, 1985a). X-ray spectroscopic studies indicated significant changes between the dark stable S₁ state and the g=4.1 S₂ state. The XAS inflection point shifted to higher energy, consistent with an oxidation event within a Mn environment (Cole, et al, 1987, Liang, et al, 1994, Yachandra, et al, 1987), although the correlation of the XAS inflection point for the multiline S₂ state formed by either 200K illumination or 273K illumination in the presence of DCMU, showed a strong dependence of the inflection point shift on the amount of multiline signal formed (Cole, et al, 1987, Liang, et al, 1994, Yachandra, et al, 1987). This type of correlation was not observed to be as strong for the formation of the g=4.1 S₂ state, with a different linear

dependence. Thus, although indicating an oxidation within a Mn environment, this oxidation may have occurred within a Mn environment (generating the $g=4.1$ S_2 state) different to that generating the multiline S_2 state (Cole, et al, 1987, Yachandra, et al, 1987). More recent EXAFS spectroscopic studies have reported a shift to greater Mn environment heterogeneity especially in the Mn-Mn distances, in samples illuminated to form the $g=4.1$ S_2 state. The EXAFS data indicate an increase in the separation of one of the Mn dimers, such that two distinct Mn-Mn dimer separations are evident, one at $\sim 2.7\text{\AA}$, the other at $\sim 2.86\text{\AA}$ (Liang, et al, 1994).

The substitution of F^- for Cl^- in PSII samples is observed to inhibit O_2 evolution and lead to the generation of a $g=4.1$ signal with illumination of F^- treated PSII at 200K (Casey and Sauer, 1984, Baumgarten, et al, 1990, Damoder, et al, 1986, Ono, et al, 1987). X-ray spectroscopy on the F^- PSII samples poised in the S_1 state show an apparent increase in disorder of the Mn environment in comparison to the control S_1 PSII (DeRose, et al., 1995). The Mn-Mn $\sim 2.7\text{\AA}$ separation was observed to split with two Mn-Mn separations differing by $\sim 0.08\text{\AA}$ (deRose, et al., 1995, Yachandra, et al, 1993). No overall large structural rearrangements in the ligand environment were evident (deRose, et al., 1995). For F^- PSII suspended in the S_2 state, the Mn-Mn separations were observed to become more heterogenous in comparison to control samples, with one Mn-Mn separation being extended from $\sim 2.7\text{\AA}$ to 2.8\AA , with the other Mn-Mn separation apparently unchanged from the F^- PSII S_1 state (deRose, et al., 1995, Yachandra, et al, 1993). The disorder was also observed to be consistent in the Mn-metal $\sim 3.3\text{\AA}$ separation being less intense in the F^- PSII S_1 and S_2 states (deRose, et al., 1995). The changes in observable properties of the Mn OEC have been discussed earlier for the functional PSII, where the turnover from the S_2 state results in a loss of the multiline ESR signal leading to an ESR silent state, and the changes in X-ray absorbance data consistent with the oxidation of Mn, K edge energy increase upon S_2 - S_3 , without major structural changes in the Mn environment.

In PSII treated with agents which slow S state turnover and inhibit O_2 evolution, the generation of the S_3 state by either flashing illumination or by continuous illumination (Boussac, et al, 1989, Boussac, et al, 1990a) leads to the observation of an ESR signal centred near $g=2$, with a peak to peak separation dependant on the inhibitory condition applied. This altered S_3 state signal is thought to arise from the interaction of the Mn OEC, in similar oxidation state to the S_2 state, and an organic radical from an oxidised amino acid residue, either tyrosine (Hallahan, et al., 1992) or histidine (Boussac, et al, 1989, Boussac, et al, 1990a, Boussac, et al, 1990b, Tso, et al, 1991a). X-ray absorbance studies on PSII samples treated to inhibit O_2 evolution and S state turnover beyond the S_3 state show effects which also are dependent on the inhibitory treatment.

X-ray studies on PSII samples treated with NH_3 indicated either little difference to the control sample (Dau, et al., 1995) or slight shift of the K edge energy shift to lower energy by $\sim 1\text{eV}$ (MacLachlan, et al, 1994b). Upon illumination to generate the S_2 state, significant changes were observed, with the ligand environment proposed to be different to that of the native S_2 state (Dau, et al., 1995, MacLachlan, et al, 1994b). With illumination at 200K, observed to generate mostly $g=4.1$ signal (Beck and Brudvig, 1988a, Andreasson and Vangaard, 1988), the EXAFS indicates similar results to those with other samples treatments which fix the OEC into the $g=4.1$ S_2 state, such as 140K illumination of EG cryoprotected control samples (Liang, et al, 1994) and 200K illumination of F^- treated PSII (deRose, et al., 1995). The second EXAFS peak, indicative of Mn-Mn separations was observed to be more heterogenous. The generation of the $g=4.1$ S_2 state in NH_3 treated PSII leads to an increased separation in one Mn dimer, to $\sim 2.85\text{\AA}$, with the other dimer unchanged from the S_1 state, $\sim 2.7\text{\AA}$ (Dau, et al., 1995). Illumination to generate the altered S_3 state in the NH_3 treated PSII indicated the K edge inflection point shifted by approximately equivalent amounts for the S_1 to S_2 and for the S_2 to S_3 transitions, indicating an oxidation event within the Mn environment for each transition (MacLachlan, et al, 1994b).

The EXAFS data for the S_1 state in PSII samples depleted of Ca^{2+} by low pH citrate treatment (Ono and Inoue, 1988) displayed a striking difference to the control PSII samples. The Mn-Mn separations were heterogenous in the S_1 state, with one Mn-Mn dimer similar to the control samples, $\sim 2.7\text{\AA}$, while the Mn-Mn separation for the second dimer was extended to $\sim 3.0\text{\AA}$ (Nugent, et al, 1993, Nugent, et al, 1994, Evans, et al, 1994) The third EXAFS peak indicative of a second Mn-metal separation at ~ 3.3 to 3.7\AA (George, et al, 1989, Yachandra, et al, 1993, MacLachlan, et al, 1992, Kusunoki, et al, 1989, Penner-Hahn, et al., 1990) was observed to be significantly reduced, indicating the involvement of Ca^{2+} close to the Mn cluster (Yachandra, et al, 1993, Nugent, et al, 1993). The changes in the Mn-Mn separations were observed to be reversible upon readdition of Ca^{++} to the sample (Ono and Inoue, 1991, Ono, et al, 1993, Ono, et al, 1994). It was concluded that Ca was located close to the Mn cluster and that it was involved in maintaining a structural integrity of the protein environment around the Mn OEC site (Nugent, et al, 1993, MacLachlan, et al, 1994b, MacLachlan, et al, 1994a, Ono and Inoue, 1991, Ono, et al, 1993, Ono, et al, 1994). The K edge inflection energies for the S_1 to S_2 and S_2 to altered S_3 states transitions in the Ca depleted PSII samples were observed to shift to higher energies across these transitions, indicative of oxidation within the Mn environment for each transition (Nugent, et al, 1993, MacLachlan, et al, 1994b, Ono and Inoue, 1991, Ono, et al, 1993).

1.9. Summary: Aim of Project.

The current model of the Mn centre in PSII is based upon X ray absorbance data indicating Mn is structured within PSII as magnetically coupled μ -oxo bridged dimers. The conclusion that these dimers interact to form a tetrameric structure has been influenced by simulations of the line shapes of the multiline and $g=4.1$ signals and by pulsed ESR and ENDOR experiments on these signals. The results presented so far are not conclusive in terms of the spin states and nuclearities of the Mn centres giving rise to the S_2 state signals. In an endeavour to shed light on these Mn structures, this project was aimed at determining the spin states of the multiline and $g=4.1$ signals observed under various illumination and cryoprotectant regimes through careful measurement of their temperature dependences. The studies were aimed at clarifying the relationship between the $g=4.1$ signal and the multiline signal using PSII in control samples and PSII inhibited by various protocols. Based on the data gathered for the S_2 state, some experimentation on the altered S_3 state signals in the inhibited PSII was undertaken to gain further information on how the OEC is structured and on its functioning.

Chapter 2

Electron Spin Resonance Overview

2.1 Introduction

This chapter introduces some simple theory and background behind the electron spin resonance spectroscopic technique with particular reference to its application in this project. Electron spin resonance (ESR) or electron paramagnetic resonance is based on a microwave radiation spectroscopy of materials possessing sites which are paramagnetic in nature. That is, the atomic or molecular components of the system contain centres which possess unpaired electrons, giving rise to a net magnetic moment within the sample.

The fundamental physical properties of an electron are its mass, charge, spin and its magnetic moment. The electron spins around its own axis and gives it an intrinsic angular momentum. This angular momentum is a vector and is denoted by S . The angular momentum has the value $\pm 1/2\hbar$, \pm as the spin may be in either a clockwise direction, so as its spin moment is 'down', or in an anticlockwise direction, and is referred to as having spin 'up'.

The magnetic moment of the electron is related to its angular momentum by

$$\mu_e = -g_e \mu_B S$$

where g_e = Landé g factor, a proportionality constant between the angular momentum and the magnetic moment, μ_B = Bohr magneton which is equivalent to $e\hbar / 2 m_e c$. As an isolated electron has a magnetic moment of one Bohr magneton, and its (dimensionless) angular momentum is $1/2$, g_e has a value of 2 in this case. Its actual value is 2.0023, the slight shift from 2.00 being due to relativistic effects.

For electrons with $\mu_e = -g_e \mu_B S$ the maximum measurable value of S along the direction of a magnetic field is $\pm 1/2$. The absolute magnitude of the vector S is $\sqrt{1/2(3/2)} = \sqrt{3}/2$. That is, the magnetic moment of the electron along the field direction may align either parallel or antiparallel to the field, but the angular momentum and magnetic moment vectors are not coincident with the field, and maintain set orientations with the field based on the ratio of the measurable and absolute values of the moment vector. The reference frame typically used for defining the system places the applied magnetic field along the Z direction. The component of S measurable along the field is termed the Z component, ie $S_z = 1/2$.

The two orientations will have different energies, according to the value of S . For the components of S aligned with H_z , $S_z = \pm 1/2$, the energies will be

$$E = -g_e \mu_B \mathbf{S} \cdot \mathbf{H} = -g_e \mu_B S_z H_z$$

for $S_z = +1/2$ or $-1/2$ then

$$E = -g_e \mu_B H / 2 \text{ or } +g_e \mu_B H / 2$$

The energy of the electrons within the magnetic field will differ in proportion to the field. The energy difference between the two orientations will be

$$\Delta E = (g_e \mu_B H / 2) - (-g_e \mu_B H / 2) = g_e \mu_B H.$$

The ESR experiment applies an electromagnetic radiation which, at the appropriate energy, is absorbed by the electrons allowing transitions between the two energy orientations. The relationship between the energy of the electron in the field and the applied radiation of frequency ν , produces resonance at $h\nu = \Delta E = g_e \mu_B H$. For a field of $\sim 3000\text{G}$, the energy of the electromagnetic radiation is within the microwave region with frequency of the order of 9GHz and wavelength of $\sim 3\text{cm}$. This gives the resonance condition for the ESR experiment for “free” electrons. Within a compound the electrons are subject to set energy levels and orbitals and may produce resonance at g values different from 2 (ie at fields different from the free electron value).

2.2. Quantum Mechanical Analysis

Quantum mechanics applies an energy operator to the wave functions of the atomic or molecular system to determine the energy eigenfunctions and eigenvectors. The energy operator is more commonly named the Hamiltonian. The Hamiltonian contains a number of distinct components describing the full energy levels of the atomic/molecular system under consideration. For this study, only those terms whose components are applicable to the magnetic moments or spin functions of the atomic or molecular system are required. This restricted Hamiltonian is referred to as the “Spin” Hamiltonian and consists of components due to the Zeeman interaction between the magnetic moments and the field, Hyperfine interaction between the individual electrons and magnetic nuclei within the molecular system, nuclear Zeeman terms, electronuclear quadrupole interactions and a removal of spin degeneracy by the ligand or crystal field, termed zero field interactions. Each of these interaction terms are important to understand, especially for systems containing transition metals, and give an indication of the environment in which the atomic or molecular systems possessing the net spin is located.

The overall Hamiltonian has the form (Abragam and Bleaney 1970)

$$\mathbf{H} = \mu_B \mathbf{S} \cdot \mathbf{g} \cdot \mathbf{H} + \mathbf{S} \cdot \mathbf{A} \cdot \mathbf{I} + \mathbf{S} \cdot \mathbf{D} \cdot \mathbf{S} + \mathbf{I} \cdot \mathbf{Q} \cdot \mathbf{I}$$

The nuclear Zeeman interaction is also included in the Spin Hamiltonian, but the interaction energy and the resultant effect is extremely small due to the nuclear mass being nearly 2000 times heavier than the electron, and so this term will not be included here.

2.2.1. Zeeman Term $\mu_B \mathbf{S} \cdot \mathbf{g} \cdot \mathbf{H}$

The Zeeman term appears analogous to the classical splitting of the energy levels as discussed before, where, for a spin only system

$$E = \mu_B g_e H_z S_z$$

or, if the system has non zero orbital momentum, \mathbf{L} ,

$$E = \mu_B g_L \mathbf{H} \cdot \mathbf{J}$$

where $\mathbf{J} = \mathbf{S} + \mathbf{L}$ and g_L is the Lande g factor (Abragam and Bleaney 1970, Pake and Estle 73), which is the combination of electronic spin, g_e , and orbital, g_L , g factors, such that

$$g_L = 1 + (J(J+1) + S(S+1) - L(L+1)) / 2J(J+1)$$

$g_L = 2$ for a spin only contribution and $g_L = 1$ for orbital only contributions. For systems where $\mathbf{L} = 0$, ie. where the orbital angular momentum is zero and hence no spin orbit coupling is present, the g factor is equivalent in form to the electronic g factor. In the presence of orbital angular momentum, the g factor is no longer necessarily a scalar single value entity, and is represented as a tensor (MacMillan 68, Poole 67), such that

$$H_z = \mu_B \mathbf{S} \cdot \mathbf{g} \cdot \mathbf{H}$$

$$\text{ie, } \mathbf{g} = \begin{bmatrix} g_{xx} & g_{xy} & g_{xz} \\ g_{yx} & g_{yy} & g_{yz} \\ g_{zx} & g_{zy} & g_{zz} \end{bmatrix}$$

and with \mathbf{S} and \mathbf{H} both vector quantities, $\mathbf{S} = \{S_x, S_y, S_z\}$ and $\mathbf{H} = \{H_x, H_y, H_z\}$. This tensor may be diagonalised by using a suitable frame of reference (Pake and Estle 1973, Pilbrow 90, Poole 67, Schlichter 90), so that

$$H = \mu_B [S_x \ S_y \ S_z] \begin{bmatrix} g_{xx} & 0 & 0 \\ 0 & g_{yy} & 0 \\ 0 & 0 & g_{zz} \end{bmatrix} \begin{bmatrix} H_x \\ H_y \\ H_z \end{bmatrix}$$

$$= \mu_B [S_x g_{xx} H_x + S_y g_{yy} H_y + S_z g_{zz} H_z]$$

The case of an axially anisotropic environment represents a situation in which the molecular x and y axes are equivalent, ie. $g_{xx} = g_{yy} = g_{\perp}$ and $g_{zz} = g_{\parallel}$ ($\neq g_{\perp}$) (MacMillan 68, Pake and Estle 73). We represent the g components for “x” (g_{xx}) and “y” (g_{yy}) projections as the perpendicular components, the “z” (g_{zz}) component as a parallel component. The effective g factor can be written as $g_{\text{eff}} = \sqrt{g_{\parallel}^2 \cos^2 \theta + g_{\perp}^2 \sin^2 \theta}$, where θ is the angle between H and the molecular Z axis (Poole 67).

For a cubic or spherical symmetric environment, the g tensor collapses to a scalar value (MacMillan 68), not necessarily equivalent to g_e . A tensor g value implies a splitting in the ESR signal such that transitions are observed to cluster around the principle g values in solid samples. This splitting is not, however, equivalent to hyperfine splitting, and becomes of greater importance at higher microwave frequencies where the field differences between the different $g_{(\perp)}$ components are magnified, with increased resolution of these signal components.

2.2.2. Hyperfine Interactions S.A.I

If the nucleus of the atom containing the unpaired electron, or a nearby closely interacting nucleus possesses a non zero nuclear magnetic moment, $I > 0$, the nuclear magnetic moment will interact with the electronic magnetic moment, causing a splitting of the Zeeman energy levels in an external magnetic field (Bernsohn and Baird 1966, MacMillan 68). The nuclear magnetic moment, like the electronic, is subject to a quantisation of the spin and orientation of the magnetic moment about the nucleus. The energy differences of the nuclear magnetic moments are very small compared to that of the electron, and consequently the populations of spins in each state is essentially equivalent.

For a nuclear spin of I, there are $2I+1$ energy levels, corresponding to quantised values of the magnetic moment

$$\mu_N = g_N \mu_N I \quad \text{where } \mu_N = e \hbar / 2 m_N c \text{ is the nuclear Bohr magneton.}$$

The electron experiences the effect of the external field, a field due to these nuclear magnetic moments and a variable direct coupling to the nuclear magnetic dipole when the electron density at the nucleus is non zero. The interaction is represented by

$$H_{HF} = \mathbf{S} \cdot \mathbf{A} \cdot \mathbf{I}$$

The hyperfine tensor \mathbf{A} is made up of two contributions; an isotropic component, occurring when the electron density at the nucleus is non zero, termed the Fermi contact interaction; and an anisotropic component, due to magnetic interaction between the electronic and nuclear spins.

2.2.2.1. Isotropic Term

The isotropic hyperfine term, or Fermi contact interaction requires there to exist electron density at the nucleus (Assenheim, 1965, Bernsohn and Baird, 1966, MacMillan, 1986). The coupling term for the interaction reduces to

$$\mathbf{S} \cdot \mathbf{A} \cdot \mathbf{I} = a (S_x I_x + S_y I_y + S_z I_z)$$

where

$$a = 8\pi/3 \cdot g_e g_N \mu_B \mu_N |\Psi(0)|^2$$

and $|\Psi(0)|$ is the wave function of the electron at the nucleus, $|\Psi(0)|^2$ is non zero when the electron is located in either an s atomic orbital or a molecular orbital containing atomic s character (Assenheim, 1965, Ayscough, 1967, MacMillan, 1968). Electrons in p, d, f atomic orbitals, or π molecular orbitals generally have $|\Psi(0)|^2 = 0$, as the electron wave function at the nucleus has a node, with lobes projecting away from the nucleus (Assenheim, 1968, Bernsohn and Baird, 1966). However, electrons in the p, d etc orbitals of multi-electron atoms generally exhibit an isotropic hyperfine coupling due to differential induced 'polarisation' of up and down spins in filled, lower lying s orbitals (Ayscough, 1967, Pake and Estle, 1973, Symons, 1978).

2.2.2.2. Anisotropic Term

The isotropic term, hence, appears in connection with the s character of unpaired electrons in ions and atoms and is often accompanied by an anisotropic term, arising from dipolar interaction. If the orbital of an unpaired electron embraces an atom with a nuclear magnetic moment μ_N and spin \mathbf{I}_N , the electron energy will be split due to electron / nuclear dipole dipole interaction. The Hamiltonian for the interaction is of the form (Assenheim, 1965, Bernsohn and Baird, 1966)

$$H_{DIP} = -(1/r^3) \cdot g_e g_N \mu_B \mu_N (\mathbf{I} \cdot \mathbf{S} - \frac{3}{r^3} (\mathbf{L} \cdot \mathbf{r})(\mathbf{S} \cdot \mathbf{r}))$$

\mathbf{r} is the radius vector from the nucleus to the electron (\mathbf{r} the unit vector along \mathbf{r}), and this interaction is qualitatively an interaction between the electron moment $\boldsymbol{\mu}_e = g \mu_B \mathbf{S}$ with the magnetic field of the nucleus $H_{\text{HFS}} \approx g_I \mu_N \mathbf{I} / r^3$ (Pilbrow, 1990). To first order, this interaction Hamiltonian may be rewritten as

$$H_{\text{DIP}} = g_e g_N \mu_B \mu_N ((3\cos^2\theta - 1) / r^3) I_Z S_Z$$

where r is the distance between the nucleus and the electron, and θ being the angle between the applied field and the radius vector between the nucleus and the electron (Assenheim, 1965, Pilbrow, 1990). The first order dipole dipole Hamiltonian defines the interaction energy for non spherical electron density, when the electron and nuclear spins are approximately collinear, ie either parallel or antiparallel. If the electron charge distribution is spherical, the dipole dipole term vanishes.

This summarises the physical significance of the Hyperfine interaction term \mathbf{A} for isotropic and anisotropic systems. The quantum mechanical significance of the term $\mathbf{S.A.I}$ still remains to be answered, and involves the calculation of energy interactions for \mathbf{I} , m_I , \mathbf{S} and m_S with the overall Hamiltonian

$$\mathbf{H} = \mu_B g \mathbf{H.S} + \mathbf{S.A.I.}$$

To first order

$$\mathbf{H} = g \mu_B H_Z S_Z + S_Z A_{ZZ} I_Z \quad (\text{ie } A_{ZZ} = a + H'_{\text{DIP}})$$

for an energy state $|m_S\rangle |m_I\rangle (= |m_S m_I\rangle)$

$$E(m_S, m_I) = g \mu_B H_Z m_S + A_{ZZ} m_S m_I$$

where m_S and m_I are respectively the Z component quantum numbers for the electron and nucleus (eg $m_S = \pm 1/2$ etc). Each of m_S and m_I act independently of each other. The energy levels for such a system then depend on the individual spin alignments and the magnitude and sign of \mathbf{A} . As the absorption of a photon may only affect the electron magnetic levels and not the nuclear magnetic moments in first order, the transition selection rules for the Hyperfine interaction requires $\Delta E = h\nu$ arises from $\Delta m_S = 1$ transitions, with $\Delta m_I = 0$ (Assenheim, 1968). The transitions for $\Delta m_I = 1$ are forbidden, as changes in both the electronic and nuclear angular

momentum ($\Delta m_S = 1$ $\Delta m_I = 1$) are not probable for a single photon absorption (Bernsohn and Baird, 1966, Schlicter, 1990). The differences in energy between electron status for each transition are then,

$$\Delta E = g \mu_B H_Z + m_I A_{ZZ} (\Delta m_S=1)$$

The Zeeman transition is thus split into $2I + 1$ levels corresponding to the m_I values ($-I, -I+1, \dots, I$). The splittings are equally spaced to first order, with separation of the order $A_{ZZ} / g\mu_B$ (Pake and Estle, 1973, Schlicter, 1990) At this level, multiple local nuclei each with $I > 0$, produce an 'additive' effect with each nucleus generating a splitting of the levels of the electron energy states, such that the electron levels are split by the first nuclei, the split levels of which are subsequently split, and so on to produce a multiple effect (Pake and Estle, 1973, Poole, 1967)

$$H = g \mu_B H_Z m_S + \sum_j A_{jzz} m_{Ij} m_S \quad (\text{for each } j\text{th nucleus})$$

This usually results in an overlap of individual splittings within the total hyperfine interaction, dependent on the environment of the unpaired electron.

When the hyperfine interaction is large, and in particular when quadrupole effects are significant, generation of a hyperfine pattern requires solving the Hamiltonian matrix exactly for the basis vectors $|m_I m_S\rangle$.

$ m_S m_I\rangle$	$ -m_S - m_I\rangle$	$ -m_S - m_I + 1\rangle$	$ -m_S + 1 - m_I\rangle$	$ m_S m_I - 1\rangle$	$ m_S m_I\rangle$
$ -m_S - m_I\rangle$							
$ -m_S - m_I + 1\rangle$							
.							
.							
$ -m_S + 1 - m_I\rangle$							
$ m_S m_I - 1\rangle$							
$ m_S m_I\rangle$							

The matrix typically has a block diagonal (Åhring and Pace, 1995) form indicated schematically above. If the Zeeman term, $g \mu_B H_Z$, is dominant, off diagonal terms may be neglected and solution collapses to the first order form. For a less dominant Zeeman term, the solution requires the diagonalisation of the secular matrix for completeness.

The major physical consequence of the lower symmetry environment and higher off diagonality of the matrix is that the splittings observed for the different m_I levels will be no longer

symmetrical and the $2I+1$ separations of the Zeeman levels generated by the hyperfine will no longer be equally spaced (MacMillan, 1968, Pake and Estle, 1973). Such calculations are beyond the scope of this project. However, the general appearance of the Hyperfine splitting pattern will allow us to draw qualitative conclusions about the environment of the spin centres with which we deal.

2.2.3. Fine Structure - Zero Field Terms $S.D.S$

For an $S=1/2$ ($m_S = 1/2, -1/2$) ion, the spin associated with the unpaired electron may take only set quantised orientations with respect to the applied field. These quantised orientations are not necessarily set with respect to any atomic self axis, ie. with respect to some internal axis compared to other (paired) electrons. In the triplet (or higher) state, where for the triplet $S=1$ ($m_S = -1, 0, 1$), there is commonly a strong tendency for the spins of the unpaired electrons to be in fixed orientations with respect to the line joining the spins, ie. an atomic axis. This dipolar interaction typically has an energy of the same order as the Zeeman interaction, ie. between the unpaired electron magnetic moment and the applied field H_Z (Bernsohn and Baird, 1966). If the two spins are interdependent in orientation and interaction, the usual flipping of the states which gives rise to $\Delta m_S = 1$ involves the transitions: $|0\rangle \rightarrow | +1\rangle$ and $| -1\rangle \rightarrow |0\rangle$. The transition between $| -1\rangle \rightarrow | +1\rangle$, giving $\Delta m_S = 2$ is usually forbidden (as this requires the flipping of two independent spins with one quantum of energy) (Abragam and Bleaney, 1970, Al'tschuler and Kozyrev, 1964, Bernsohn and Baird, 1966). In triplet (or higher) states, this no longer necessarily holds true. The interdependent system may be flipped as a whole, with a join of the $| -1\rangle \rightarrow |0\rangle$ to the $|0\rangle \rightarrow | +1\rangle$ realising the net spin flipping $| -1\rangle \rightarrow | +1\rangle$ (Abragam and Bleaney, 1970, Al'tschuler and Kozyrev, 1964).

This type of spin spin interaction changes the energy levels associated with the transitions $| -1\rangle \rightarrow |0\rangle$ and $|0\rangle \rightarrow | +1\rangle$, in an orientation dependent way.

The difference in energy between the different spin transitions means two separate ESR resonances are observed when an external field is applied for any given orientation of the system. This so called fine structure effect is represented by the Hamiltonian

$$H = S.D.S$$

where D is a second rank symmetric tensor (Orton, 1968), defined by subtracting any necessary scalar component to have zero trace.

$$\mathbf{S.D.S} = [S_x \ S_y \ S_z] \begin{bmatrix} \uparrow \uparrow S_x \uparrow \\ | \mathbf{D}_{xyz} | | S_y | \\ \downarrow \downarrow S_x \downarrow \end{bmatrix}$$

The form of the tensor depends upon the symmetry of the environment (Abragam and Bleaney, 1970). An axis system (the 'molecular axis' system) may always be suitably defined such that the tensor is diagonal.

$$\mathbf{D}_{xyz} = \begin{bmatrix} D_{xx} & 0 & 0 \\ 0 & D_{yy} & 0 \\ 0 & 0 & D_{zz} \end{bmatrix}$$

and $D_{xx} + D_{yy} + D_{zz} = 0$ for a traceless tensor (Pake and Estle, 1973). In symmetry terms

Orthorhombic	$D_{xx} \neq D_{yy} \neq D_{zz}$
Axial	$D_{xx} = D_{yy} = D_{\perp} \quad D_{zz} = D_{\parallel}$
Cubic	$D_{xx} = D_{yy} = D_{zz} = D$

For Cubic symmetry,

$$\begin{aligned} \mathbf{S.D.S} &= D (S_x^2 + S_y^2 + S_z^2) \\ &= D [S(S+1)] \end{aligned}$$

so that an environment of cubic symmetry will not remove spin degeneracy to the second order in S (MacMillan, 1968). For a system with non cubic symmetry, we may define parameters

$$\begin{aligned} E_{zf} &= 1/2 (D_{xx} - D_{yy}) \\ D_{zf} &= D_{zz} - 1/2 (D_{xx} + D_{yy}) = 3/2 D_{zz} \end{aligned}$$

where E_{zf} and D_{zf} are referred to as zero field splitting parameters (Bernsohn and Baird, 1966, MacMillan, 1968). E_{zf} and D_{zf} have units of energy. At zero applied field (ie. $H_z = 0$), the presence of $S \geq 1$ and D_{zf} and E_{zf} means that different magnetic energy levels exist, and the energy differences between these zero field energy levels depend on D_{zf} and E_{zf} (Assenheim, 1968).

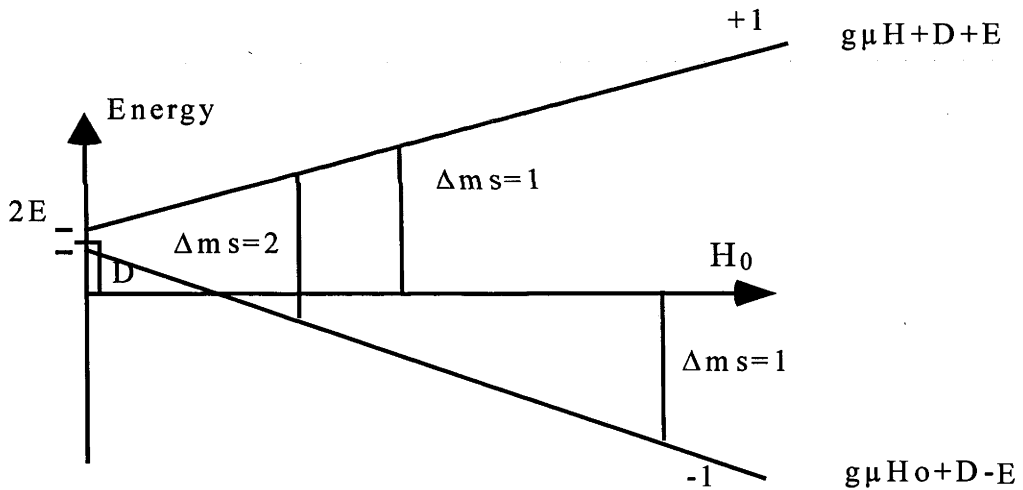
For such a system, the applied field H_0 is no longer referred to as the z direction. The magnetic moments may then lie on any coordinate plane of the ion or molecule. D represents then

the interaction energy of the two spins when the magnetic field is in the z direction. It is the axial parameter, and $|D|$ depends on the separation of the two spins of the ion or molecule. E measures the distinction between the x and y coordinate directions and so is a measure of deviation from axial symmetry (Al'tschuler and Kozyrev, 1964, Poole, 1967). If the x and y components are equivalent, ie. the environment has axial symmetry, $E = 0$.

The zero field term may be re expressed as

$$H_{zfs} = D [S_z^2 - 1/3 S(S+1)] + E (S_x^2 - S_y^2)$$

The values of the energy levels depend on the direction of H_0 with respect to the molecular axis (Abragam and Bleaney, 1970). For $S=1$, $H_0 \parallel z$ direction and $E_{zf} = 0$, adjacent transitions (ie $|-1\rangle \rightarrow |0\rangle$ and $|0\rangle \rightarrow |+1\rangle$) differ in energy (δE) by D_{zf} (Bernsohn and Baird, 1966). For $H_0 \parallel x$ direction, $\delta E = D_{zf} - E_{zf}$, for $H_0 \parallel y$ direction, $\delta E = D_{zf} + E_{zf}$. At zero field, ie. $H_0 = 0$ mT, the two energy levels are separated by $2E_{zf}$ and the average of these energy levels separated from the third by D_{zf} (Bernsohn and Baird, 1966). Diagrammatically,



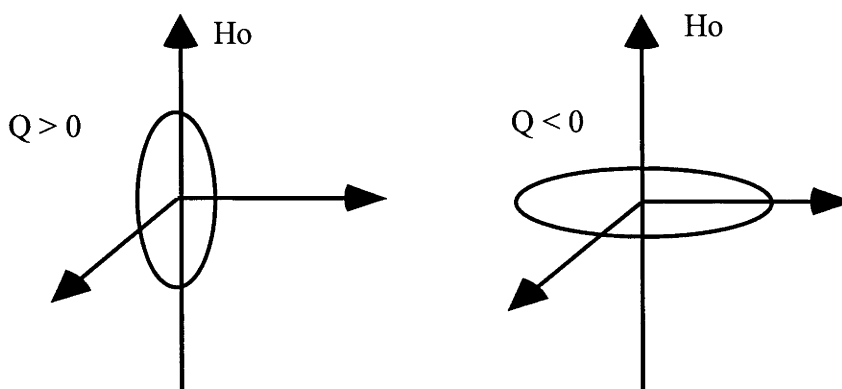
Usually, higher order orientational effects are applicable to ions, the energy levels then being dependent also on $(g_{\perp}, g_{\parallel})$.

2.2.4. Quadrupole Interaction I.Q.I

The interactions described above involve the interaction of the electron spin with environmental components; the applied field H_0 , nuclear spins I , etc. The Quadrupole interaction is a wholly nuclear spin term.

If a nucleus has spin $>1/2$, the nucleus may possess an electric quadrupole moment, Q . The quadrupole moment is a measure of departure of the nuclear charge distribution from spherical symmetry (Schlicter, 1990). The quadrupole moment may have either +ve or -ve sign, depending

on the form of departure from spherical symmetry. The nucleus usually retains symmetry about its axis of spin, with an elongated (oblate or rugby ball) shape with $Q > 0$, and a flattened (prolate or disc) shape with $Q < 0$ (Assenheim, 1965, Schlichter, 1990).



The quadrupole interaction is an electrostatic effect that varies with nuclear orientation. This interaction is measured by the Quadrupolar coupling tensor, Q . The interaction is the product of the nuclear quadrupole moment with the electrostatic field gradient due the surrounding electrons (Orton, 1968, Wertz and Bolton, 1972). The greatest contribution to electric field gradients in paramagnetic ions are usually due to electrons in d orbitals (paired and unpaired) (Orton, 1968, Wertz and Bolton, 1972). The quadrupolar interaction is dependent on the nuclear magnetic quantum number, I , which describes the nuclear orientation.

If the electron distribution has cubic symmetry (or regular octahedral or tetrahedral) the electric field gradient is zero (Schlichter, 1990). In a chemical bond, the nature of the bond has a strong influence on the electric field gradient. Strong covalent bonds tend to have high axial field gradients (Al'tschuler and Kozyrev, 1964, Schlichter, 1990). Ionic bonds usually have small gradients due to high charge symmetry near the nucleus (Schlichter, 1990).

The quadrupolar interaction leads to an additional term in the Spin Hamiltonian;

$$H_Q = \mathbf{I} \cdot \mathbf{Q} \cdot \mathbf{I}$$

which may be expanded in a similar manner to the fine structure term (Abragam and Bleaney, 1970) as

$$Q' [I_z^2 - 1/3 I(I+1)] + Q'' [I_x^2 - I_y^2]$$

The first term describes the interaction for axial symmetry. Q' is related to the nuclear electric quadrupole moment, Q , by

$$Q' = 3e / [4I(2I-1)] (d^2V/dz^2) Q$$

Here d^2V/dz^2 is the electric field gradient at the nucleus along the symmetry axis (Abragam and Bleaney, 1970). The second term, Q' , accounts for orthorhombic symmetry. For axial symmetry and H_0 parallel to the symmetry axis, $\mathbf{I} \cdot \mathbf{Q} \cdot \mathbf{I}$ reduces to $Q_{||} [I^2_z - 1/3I(I+1)]$. If the charge distribution is spherically symmetric, Q is zero.

In summary, the energy of the quadrupole interaction is based on the product of the nuclear electric quadrupole moment, Q , and the electric field gradient, d^2V/dz^2 . The interaction is observed to lead to two main effects, a broadening of resonance lines and an uneven separation of spectrum components (Abragam and Bleaney, 1970).

2.3. Electron Spin-Spin Interactions

When paramagnetic centres within a system are in close approach, ie the system is no longer magnetically dilute, interactions between the different paramagnetic centres can occur. One of these is a dipolar interaction and leads to a line broadening, the other is a coulombic interaction known as the exchange interaction. When unpaired spins become close in space, it is possible for them to affect each other in such a way that it is possible to exchange their spin orientation between different atomic or molecular orbitals (Bencini and Gatteschi, 1990, MacMillan, 1968, Pilbrow, 1990). This arises as a consequence of the Heisenberg uncertainty principle and occurs even when negligible binding exists between the molecules having unpaired spins (MacMillan, 1968).

2.3.1. Dipolar Interaction

The Hamiltonian of the dipole dipole interaction is of the form

$$H = \mu_i \cdot \mu_j / r^3 - 3(\mu_i \cdot \mathbf{r}_{ij})(\mu_j \cdot \mathbf{r}_{ij}) / r^5$$

where $\mu_i(\mathbf{j}) = \mu_B g_i(\mathbf{j}) \cdot \mathbf{S}_i(\mathbf{j})$ and \mathbf{r}_{ij} is the distance between the paramagnetic dipoles (Pake and Estle, 1973, Pilbrow, 1990). This interaction is important in ESR as it leads to a broadening of ESR signals from the individual spin centres which are within dipole interaction range (as discussed above).

2.3.2. Heisenberg Exchange Interaction

The exchange interaction is typically a stronger effect that arises from a coulombic interaction between the electrons of two or more neighbouring paramagnets which leads, via the Pauli Exclusion principle, to an effective interaction between the spins of the electrons (Bencini

and Gatteschi, 1990, Pake, 1962, Pake and Estle, 1973). The Hamiltonian of the interaction is of the form

$$H_{ijEx} = -2 J_{ij} \mathbf{S}_i \cdot \mathbf{S}_j$$

where J_{ij} is the exchange integral

$$J_{ij} = \iint \Psi_A^*(\mathbf{r}_i) \Psi_B^*(\mathbf{r}_j) (q_e^2 / r_{ij}) \Psi_A(\mathbf{r}_j) \Psi_B(\mathbf{r}_i) \partial\tau_i \partial\tau_j$$

where r_{ij} is the distance between the two electrons i and j and the integral is carried out over all space $\partial\tau_i \partial\tau_j$ with reference to the electrons i and j (Bencini and Gatteschi, 1990, Pake, 1962, Pake and Estle, 1973). J_{ij} is dependent on some overlap of the orbital wave functions Ψ_A and Ψ_B (Pake and Estle, 1973). J_{ij} falls off sharply with distance between the ions and $\Psi_A(\mathbf{r}_i)\Psi_B(\mathbf{r}_j)$ vanishes with J_{ij} (Pake, 1962). This interaction is heavily spin concentration and distance dependent, leading to two effects on the spin system.

2.3.2.1. Dilute - Exchange Narrowing

If the concentration of paramagnets becomes sufficiently high in a sample such that they become physically close, energy can be transferred from one paramagnet to another (Bencini and Gatteschi, 1990). This interaction modulates the spin orientations of the unpaired electrons of the paramagnets. The electrons exchange between the orbitals of the different molecules and so affect the linewidth of the ESR transition by decreasing the lifetime of the spin in its m_S state (Pake and Estle, 1973). This interaction shortens the lifetime of the resonance to times shorter than the Spin Lattice time, T_1 . This exchange is the basis for the Spin Spin Relaxation time T_2 .

Exchange narrowing may be viewed as the higher order portion of the Hamiltonian - $2J\mathbf{S}_i \cdot \mathbf{S}_j$, ie. $J(S_{kx}S_{jx} + S_{ky}S_{jy})$ (Pake and Estle, 1973). It may be thought of as flipping the neighbouring oppositely oriented spins at a rate J/h , leading to an effective migration of spin orientation through the lattice (Pake, 1962, Pake and Estle, 1973). This exchange interaction does not contribute to the mean square field position of the resonance (Pake, 1962, Schlichter, 1990). The exchange does affect the mean square width (linewidth) of the main resonance line centred at some $g\mu_B H_0$ (Pake, 1962, Pake and Estle, 1973) The spin flipping at the rate J/h leads to a change in the T_2 relaxation rate (Pake, 1962, Pilbrow, 1990);

$$1 / T_2 \propto E_d^2 / J$$

where E_d is the dipolar interaction energy. A change in J will affect T_2 , the spin spin relaxation rate, and hence will affect the linewidth (Pake and Estle, 1973) as

$$\Delta H_{1/2} \propto 1 / T_2$$

where $\Delta H_{1/2}$ is the half width of the resonance line absorption spectrum. In this study, the exchange narrowing is mentioned only in passing so as to acknowledge existence. The second exchange interaction is of higher importance here and deals with spin-spin interaction between molecules containing more than one paramagnet.

2.3.2.2. Strong Exchange

Strong exchange occurs when overlaps of the orbitals associated with the individual paramagnetics is significant. The form of this interaction Hamiltonian is, as noted above for spins S_i, S_j

$$H = -2 J_{ij} S_i \cdot S_j$$

where J_{ij} is the exchange integral. The exchange integral is a strictly quantum mechanical entity, and is dependent on the existence of wave function overlap of the electronic orbitals. The spectrum for these interacting paramagnets results from the solution of the Hamiltonian consisting of the two separate spin Hamiltonians for each paramagnet plus the interaction Hamiltonian.

The exchange integral leads to many physically fundamental interactions. It is the influence that aligns the elementary magnets in ferromagnetic and antiferromagnetic domains (Pake, 1962). This interaction is present in all paramagnetic substances, but cooperative alignment occurs only when the temperature is low enough that kT is comparable to the exchange energy between the spin pairs (Bencini and Gatteschi, 1990).

Two different types of exchange interaction resulting in orbital overlap between interacting paramagnets are definable by the directness of the orbital approach. Direct exchange is where there is direct overlap of atomic orbitals of two interacting paramagnets, ie. the paramagnetic centres are directly "bonded" (Bencini and Gatteschi, 1990), eg. H_2 exchange couples to form a singlet state molecule, O_2 exchange couples to a triplet. Indirect exchange, or superexchange, occurs when two paramagnetic ions have negligible direct wave function overlap (Bencini and Gatteschi, 1990). Exchange occurs via one or more intermediate diamagnetic ions which foster atomic orbital overlap with each of the two interacting paramagnets (Bencini and Gatteschi, 1990).

The exchange interaction leads to a molecular spin value, where the spins from the individual paramagnets S_1 , S_2 couple to give total spin, S , values in the range (Bencini and Gatteschi, 1990, Pake and Estle, 1973)

$$|S_1 - S_2| \leq S \leq |S_1 + S_2|$$

If spin dependent terms in the overall Hamiltonian can be neglected in determining the exchange, the overall spin S is a good quantum number (Pake and Estle, 1973). The exchange interaction splits the lower orbital level of the molecule into spin singlets, doublets, triplets,.... The Heisenberg Exchange Hamiltonian becomes

$$H = -2 J_{ij} \mathbf{S}_i \cdot \mathbf{S}_j = -J (S^2 - S_i^2 - S_j^2)$$

The energy levels become dependent on the total spin, S (Bencini and Gatteschi, 1990, Sinn et al, 1970), as

$$E(S) = -J [S(S+1) - S_i(S_i+1) - S_j(S_j+1)]$$

and the difference in energy between adjacent levels (Bencini and Gatteschi, 1990) is

$$E(S) - E(S-1) = 2JS$$

We may then write the spin Hamiltonian in terms of the total spin, S , derived from the parameters describing the Spin Hamiltonian in terms of the individual centres S_i and S_j

$$H = \mu_B g_S \mathbf{H} \cdot \mathbf{S} + \sum \mathbf{S} \cdot \mathbf{A}_{Sk} \cdot \mathbf{I}_k - J [S(S+1) - S_i(S_i+1) - S_j(S_j+1)]$$

Here g_S and A_{Sk} are the 'effective' values of the g tensor and hyperfine tensors for the combined spin system, in total spin state S . These effective values depend on the extents to which the individual paramagnets quantum mechanically couple in the total spin system (eg see Bencini and Gatteschi, 1990).

2.4. Transition Probability

From time dependent perturbation theory (Al'tschuler and Kozyrev, 1964, Merzbacher, 1961, Schlichter, 1990), it is known that the rate, W_{nm} , at which some interaction (represented by Hamiltonian H') induces transitions between two quantum states, $|n\rangle$, $|m\rangle$, obeys

$$W_{nm} = W_{mn} \propto |\langle m | H' | n \rangle|^2$$

In magnetic resonance, H' , represents the interaction between μ_e and the oscillating magnetic field component of the applied radiation, $H_1(t)$, so

$$H'(t) = \mu_e \cdot H_1(t) = g_e \mu_B H_1(t) \cdot S$$

Now, only S_x or S_y have non zero matrix elements between states such as $|1/2\rangle$, $|-1/2\rangle$, so $H_1(t)$ must be in the x, y plane to induce magnetic resonance transitions. Because $W_{nm} = W_{mn}$, the radiation field induces transitions equally in both directions. This rate, W_h , depends on the magnitude of H_1^2 , ie. is proportional to the microwave power, P , applied to the sample.

2.5. Magnetic Resonance and the Rapid Passage Condition

The phenomenon of magnetic resonance is readily observable only when the resonance condition $h\nu = g\beta H_0$ is fulfilled. In ESR experiments, it is usually the approach to work under the continuous wave (CW) condition; that is, to work at a fixed frequency (and applied power of microwave radiation) and vary the steady field H_0 . There is a restriction on the rate at which H_0 may be varied (Pake, 1962). A rapidly changing field will have oscillatory components capable of inducing transitions between the atomic energy levels (Pake and Estle, 1973). When the steady field is varied slowly, such transitions do not occur, and the change is said to be 'adiabatic' (Pake and Estle, 1973, Pilbrow, 1990). If the magnetic field is swept through the resonance condition slowly enough, ie. at a rate much less than the precession frequency, μ closely follows H (Pake, 1962, Pake and Estle, 1973, Pilbrow, 1990). This is important when signal intensity is to be reliably measured under conditions of slow spin relaxation rates, such as are obtained at low temperatures (see below).

2.6. Spin State Populations, Transitions and Saturation

With a large assembly of paramagnets, with spin either $+1/2$ or $-1/2$, there will exist two spin state populations dependent on their energies in an applied magnetic field H_0 . The ratio of these populations at thermal equilibrium is, from the Boltzmann relation

$$n_\beta / n_\alpha = \exp(E(-1/2) - E(+1/2)) / kT = \exp (g\mu_B H_0 / kT)$$

where n_α , n_β are the spin up (+1/2) and spin down (-1/2) populations. The total spin population, $N = n_\alpha + n_\beta$. Writing $x = \mu_B H_0 / kT$ (as $g_e m_s = 1$), the resultant magnetisation (Kittel, 1976) is;

$$\begin{aligned} \mathbf{M} &= (n_\alpha - n_\beta) \mu = N \mu \{ \exp(+x) - \exp(-x) \} / [\exp(+x) + \exp(-x)] \\ &= N \mu \tanh(x) \end{aligned}$$

In nearly all cases, $\mu_B H \ll kT$ ($x \ll 1$), $\tanh(x) \propto x$, and

$$\mathbf{M} \propto N \mu (\mu_B H / kT).$$

If the magnetic species has total angular momentum \mathbf{J} , having $2J+1$ equally spaced m_j levels, the magnetisation is given by

$$\mathbf{M} = N g_e \mathbf{J} \mu_B B_j(X) \quad \text{where } X = g_e m_j \mu_B H / kT$$

and $B_j(x)$ is the Brillouin Function (Kittel, 1976, MacMillan, 1968)

$$B_j(X) = \frac{2J+1}{2J} \coth\left(\frac{(2J+1)X}{2J}\right) - \frac{1}{2J} \coth\left(\frac{X}{2J}\right)$$

For $\mu_B H \ll kT$ (ie $x \ll 1$),

$$\coth(X) = 1/X + X/3 + X^3/45 + \dots$$

Working through the simplification gives the magnetisation. The susceptibility is the more commonly measured property, and is given by

$$\chi = \mathbf{M} / \mathbf{H} = N J(J+1) g_e^2 \mu_B^2 / 3kT = C / T$$

where C is called the Curie constant (Kittel, 1976, Pake and Estle, 1973). This is the Curie Law for the magnetic susceptibility, ie. the total magnetisation of all states within the sample (MacMillan, 1968), placed in an external field H .

The resonance condition $h\nu = g\mu_B H$ implies an input of energy to the electron spins, causing transitions, with the spins in the lower energy state shifted to the higher state. Without coupling between the paramagnetic centres and to the environmental lattice, the application of the resonant microwave energy to the spin system would lead to rapid saturation of these transitions.

2.7. Relaxation Times

Spin relaxation processes arise from two interactions, one between the spins of the system and one between the spins and the lattice or environment within the sample. During the resonance condition or after a shift in the system to change the ratio of the higher and lower energy state populations, the relaxation processes determine the time course by which the system shifts toward equilibrium in the new state.

The two relaxation processes are termed the Spin-Spin relaxation and Spin-Lattice relaxation.

2.7.1. Spin Lattice Relaxation

The spin-lattice relaxation relates to the lifetime of an electronic state and is determined by exchange of spin energy via thermal vibrations to the lattice (Pilbrow, 1990), bringing the spin system into thermal equilibrium with the lattice (Bernsohn and Baird, 1966, Pake, 1962, Symons, 1978). The spin lattice interaction controls the time for recovery of the magnetisation of the paramagnetic system along the applied magnetic field direction after a disturbance of the system from equilibrium (Pilbrow, 1990, Schlichter, 1990). This time is called the Spin Lattice relaxation time, T_1 , or alternatively, the longitudinal relaxation time (ie. along the field direction) (Bernsohn and Baird, 1966). T_1 is usually temperature dependent, which is expected as the lattice has higher numbers of vibrational energy states with increasing temperature (Pake and Estle, 1973), allowing higher rates of energy absorption from the spin system (Pake, 1962, Pilbrow, 1990).

2.7.2. Transverse Relaxation

The transverse relaxation process is mainly concentration dependent and measures the characteristic time taken, T_2 , for the oscillating components of the magnetisation in the plane normal to the applied field H_0 , ie in the plane of H_1 , to become out of phase with each other (Bernsohn and Baird, 1966, Pilbrow, 1990). At equilibrium, the transverse components of the spin, S_x and S_y , are randomly oriented. Following application of the microwave field, H_1 , the spin system becomes more coherent. With time the spin coherence decays as different local environmental static and dynamic effects (spin spin dipolar interactions) induce a separation of phase for each spin traversing the x-y plane, with the H_1 field (Mims, 1976, Pilbrow, 1990). This process leads to a finite width for the transition (line width) which is proportional to the transverse relaxation rate. The relaxation time T_2 , is related to the signal linewidth $\Delta H_{1/2}$ by

$$1/T_2 = \pi g \mu_B \Delta H_{1/2} / h$$

where $\Delta H_{1/2}$ represents the half height width of the absorbance signal (Bernsohn and Baird, 1966).

2.8. Spin Transitions and Saturation

The application of a steady field, H_0 , to a system of unpaired electrons leads to two energy states, with relative populations of unpaired electrons in each state based on Boltzmann statistics of the energies of each orientation of the magnetic dipoles in the field. The spin system, although linked to the lattice via relaxation processes, may be described by a spin temperature, T_S , which at thermal equilibrium, must be equal to the temperature of the lattice (Pake, 1962, Pilbrow, 1990). At thermal equilibrium,

$$n_\alpha / n_\beta = \exp(-g \mu_B H_0 / k T_S) \text{ as from before.}$$

By definition, the total population of unpaired spins, $N = n_\alpha + n_\beta$ and the population difference, $n = n_\alpha - n_\beta$ ($= n_0$ at thermal equilibrium). The populations of each state may be redefined in terms of N and n , $n_\alpha = 1/2 (N - n)$ and $n_\beta = 1/2 (N + n)$. With a disturbance of the system away from equilibrium, by changing the applied field H_0 (in the absence of a microwave field) or the lattice temperature T for example, the system undergoes transitions to reach an equilibrium state (Pilbrow, 1990). The transitions between each state are governed by the rate parameters, P_\pm , induced by the coupling of the spin system to the lattice, where P_+ is determined by the transition probability for $n_\beta \rightarrow n_\alpha$ and P_- for the transition $n_\alpha \rightarrow n_\beta$. The rate of change of n is

$$\begin{aligned} dn / dt &= 2n_\beta P_+ + 2n_\alpha P_- \\ &= N (P_- - P_+) - n (P_- + P_+) \end{aligned}$$

as at equilibrium,

$$n_0 = N(P_- - P_+) / (P_- + P_+)$$

the rate of change of n is

$$dn/dt = (n_0 - n)(P_- + P_+)$$

This is a simple first order kinetic equation with an exponential time dependent solution.

$$n = n_0 [1 - \exp(-t/T_1)]$$

where $T_1 = 1/(P_- + P_+)$.

The spin lattice relaxation time, T_1 , is the time constant for re-establishment of equilibrium spin population after a disturbance.

With the application of a microwave field, additional transitions arise due to the absorption of the radiation close to or at resonance, the transitions having probability W_h , which is the same for $\alpha \rightarrow \beta$ or $\beta \rightarrow \alpha$ processes (see above). Resonant absorption of the microwave power at frequency $\nu = \Delta E / h$, increases the spin temperature T_S above the lattice temperature T_L , the spin system is effectively heated. To limit saturation, where n_α approaches n_β , the relaxation processes must be greater in effect than the radiatively induced transitions, ie. $W_h \ll P_-$. Combining the thermal and radiative processes;

$$dn/dt = -1/T_1 (n - n_0) - 2n W_h$$

If n_s is the steady state population of n in the presence of the H_1 field, at steady state,

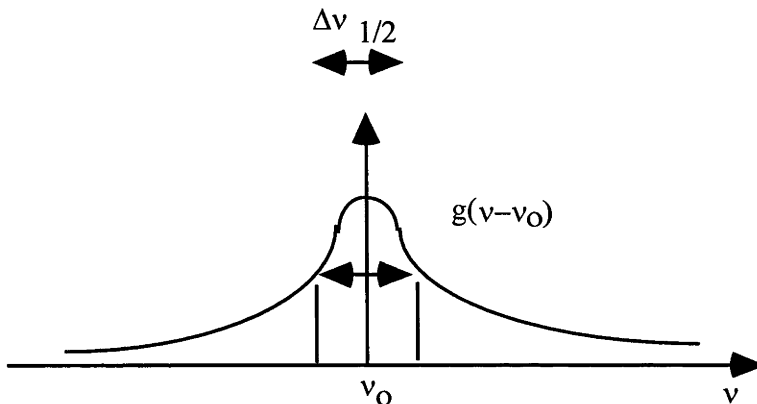
$$dn_s/dt = 0 = (n_0 - n_s)/T_1 - 2n_s W_h$$

$$\text{and } n_s/n_0 = 1/(1+2W_h T_1)$$

W_h is a function of the microwave power and of the line shape of the signal

$$W_h \propto H_1^2 g(\nu - \nu_0), \text{ since } H_1^2 \text{ is proportional to microwave power (Pilbrow, 1990).}$$

Here $g(\nu - \nu_0)$ is the line shape function, which typically has a gaussian or lorentzian form centred on the central transition frequency, ν_0 .



The width at half height is related to T_2 , for a lorentzian line shape (Pilbrow, 1990),

$$\Delta\nu_{1/2} = 1 / \pi T_2 \quad (\text{as noted above in field units})$$

Integrating the transition rate for the total signal (ie over the whole line), one may show that;

$$\begin{aligned} \text{Signal Transition Intensity} &\propto \text{Power absorbed} \\ &\propto n_s * \text{Power applied} \\ &= C H_1^2 / (1 + 1/4 \gamma^2 H_1^2 T_1 T_2) \end{aligned}$$

where γ is the gyromagnetic ratio for the electron and C is a constant containing n_0 (Yim et al, 1982). Defining $P_{1/2}$ to be the microwave power at which the signal attains half its maximal value, then $P_{1/2} \propto 1 / T_1 T_2$ and as H_1^2 is a proportional to the microwave power applied (P) (Yim, 1982), we may write

$$1/4 \gamma^2 H_1^2 T_1 T_2 = P / P_{1/2}$$

the signal intensity is then related to the applied microwave power (Pilbrow, 1990, Sahlin et al, 1986) as

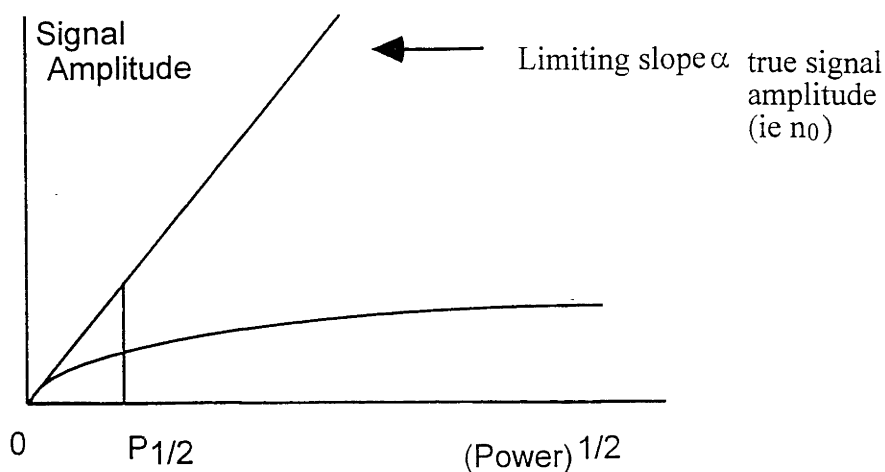
$$\text{Intensity} = C P / (1 + P / P_{1/2})$$

The measured signal amplitude is proportional to the square root of the power dependent component of the above expression and so

$$\text{Signal Amplitude} = C' P^{1/2} / (1 + P / P_{1/2})^{1/2}$$

which is the relationship between the measured signal amplitude, the power incident on the microwave cavity and the saturation condition $P / P_{1/2}$ for an inhomogenously broadened ESR line, consisting of a large number of overlapping individual resonance transition envelopes. At low power, where $P \ll P_{1/2}$, the signal amplitude increases linearly with the square root of the applied power. With increasing power applied, with $P \rightarrow P_{1/2}$, the signal diverges from this linearity, with signal saturation occurring as the rate of stimulated transitions due to the microwave radiation becomes of the order of the relaxation process decay times (T_1 and T_2). This

relationship of the signal amplitude to the saturation factor and the applied microwave power enables determination of the true signal amplitude and the $P_{1/2}$, diagrammatically,



It is important to measure the saturation behaviour over a range of temperatures as $P_{1/2}$ ($\propto 1/T_1 T_2$) is a complex function of the temperature of measurement and dependent on the mechanism of the Spin lattice relaxation, (see Abragam, 1970, Orton, 1968, Pake, 1973, Pilbrow, 1990).

Chapter 3

Materials and Methods

3.1. Spinach

The spinach used throughout this project was obtained from two sources, one a greenhouse under the supervision of Dr Jan Anderson, located at CSIRO Division of Plant Industry, Black Mountain, Canberra, the second a controlled environment chamber under the supervision of Dr Tom Wydrzynski, located at the Plant Culture Facility, Research School of Biological Sciences, Australian National University, Canberra. Both sources used the same cultivar of English Spinach, Yates variety 102, and cultivated the spinach hydroponically using a Hoaglands style liquid media. The isolation of PSII containing membranes using spinach from these two sources gave almost identical results. The growth patterns of the spinach from the two sources resulted in two distinct leaf forms, the greenhouse producing large relatively thin leaves, while the controlled environment chamber producing smaller leaves of much greater thickness. Many research groups working on Photosystem II (PSII) use market spinach as the source of plant material. Market spinach was not used throughout this project as an isolation procedure trialed with market spinach before the commencement of this work showed the presence of very high levels of copper ions, probably as a copper containing systemic fungicide sprayed onto the spinach during growth. Some copper signals are present in the ESR spectra from PSII samples due to the presence of copper in light harvesting complex II (Sibbald and Green, 1987) and bound loosely to other PSII polypeptides (Baron, et al, 1993) and the ubiquitous copper in watered plants, which adheres very tightly to protein surfaces. The level of copper signal in the market spinach was two or more orders of magnitude greater than the stray copper signals observed in the PSII ESR spectra normally observed.

3.1.1. Spinach Harvesting

For each PSII containing membrane isolation procedure, sets of > 50 gram of spinach leaves were harvested early in the morning to allow only minimal sunlight incidence and photosynthetic activity (realising large starch loads in the leaves). Leaves were harvested from plants which had not begun flowering by “pinching off” the leaf along the petiole approximately 1.5 centimetres from the leaf. Flowering plants usually showed a significant reduction of PSII containing membranes and a reduced quality of PSII S₂ state signal. Usually > 100 grams were harvested. The leaves were wrapped in wet absorbent paper (paper towel) to maintain leaf turgor. The leaves were placed in the dark at 4°C for about one hour to halt photosynthetic processes within the chloroplasts.

Preparation of the leaves for the isolation procedures involved removing the major vein along the abaxial surface by tearing the vein away from the leaf and washing the leaves in double distilled water to remove any pesticides sprayed on the leaves and salt crusts which form on the leaves due to evaporation of the nutrient solution splashed on the leaves, and due to guttative processes. The major vein was removed to maximise the mesophyll weight in the sets of “50 grams” of leaves used during the blending processes (see later). Pesticides were only encountered on the CSIRO greenhouse spinach, these not being systemic and not containing paramagnetic compounds (such as metal ions) as no ESR signals were evident in the samples undertaken from spinach material sprayed prior to harvesting (which did however perturb the author). The washed, deveined leaves were wrapped in fresh paper towel wetted with distilled water and placed back in the dark at 4°C while glassware was cooled to 4°C.

3.2. PSII Preparation

Two protocols for isolating PSII containing chloroplast membrane fragments were utilised. Both protocols used a Triton X-100 detergent solubilisation technique to remove the stromal (single lamellar membrane) regions of thylakoid membranes. This leaves the granal (multi-lammellar membrane) regions intact. The protocols were based on the methods of Bricker, Pakrasi and Sherman (Bricker prep) (Bricker, et al, 1985) and of Berthold, Babcock and Yocum (BBY prep) (Berthold, et al, 1981). All homogenisation, centrifugation and incubation steps were undertaken at 4°C in either a darkened refrigerator or cold room under dim room light or dim green light. Solutions containing the chloroplast and/or thylakoid suspensions were carried to the centrifuge in a covered ice filled container.

3.2.1. PSII Preparation Protocol of Bricker et al. (Bricker, et al, 1985) as Modified for this Work

The preparation method described is based on a 100g sample of leaves as this amount was sufficient to isolate sub-chloroplast fragment end product to concentrate to ~ 14 - 18 gl^{-1} [Chl]. The leaves were obtained as per section 3.1 fresh for each preparation.

a/. The sets of deveined, washed leaves were shredded by hand and loaded into a Waring blender. Approximately 100 mls Buffer 1 was added per 50 gram set and the leaves blended for 15 seconds at high speed. The homogenate was loaded onto filtration material, consisting of either one layer of Miracloth[®] and four layers of gauze or 4 layers of muslin. After the blending of the second set of leaves the blender bowl was washed with 50ml Buffer 1 to rinse excess homogenate, and this was poured into the filtering solution.

b/. The filter material was parcelled around the homogenate and squeezed by hand to accelerate the drainage of the homogenate juice. The homogenate was then centrifuged at 6500 rpm (5000xg) in an SS34 rotor (using eight 40ml centrifuge tubes) for 10 minutes.

c/. The supernatant was decanted and discarded, the pellet homogenised in Buffer 2 and the homogenate centrifuged at 6500 rpm in an SS34 centrifuge (using two 40 ml tubes) for 10 minutes.

d/. The supernatant was decanted and discarded, the pellet homogenised in sufficient Buffer 2 to obtain a chlorophyll concentration ([Chl]) of approximately 4 g l^{-1} . The chlorophyll content was determined by the method of Arnon (Arnon, 1949) and the homogenate left on ice in the dark for approximately one hour to allow the thylakoid membranes to undergo stacking and lateral segregation into granal (PSII containing) and stromal regions. No agitation nor stirring was applied to the broken chloroplast containing suspension.

NB. The steps from blending the leaves to the dark incubation of the broken chloroplast suspension were undertaken rapidly, endeavouring to place the broken chloroplast solution in dark incubation within 75 minutes of blending the leaves. This protocol of pre solubilisation steps significantly enhanced the quality of the final PSII material.

e/. After the period of dark incubation, Buffer 3 was added to obtain a Triton X-100 detergent : chlorophyll ratio of 20:1 w:w. The solubilising thylakoid suspension was rapidly agitated to enhance mixing and centrifuged at 18300 r.p.m. (35000 x g) for 30 minutes. The contact time of the Triton X-100 in the thylakoid suspension, before centrifugation, was typically less than two minutes. Longer contact times resulted in a greater membrane solubilisation, and hence, lower final return of granal membranes.

The detergent was added as a 20% w:v solution in buffer (2) to avoid pH changes, buffer solute dilution and to allow mixing of the Triton X-100 without detergent micellisation, as is observed when placing Triton X-100 from undiluted form into an aqueous solution. The detergent solubilises the single membrane layer (stromal) regions. The granal membranes reseal forming thylakoidal micelles.

f/. The supernatant was decanted and discarded, leaving a pellet containing the granal membrane regions and starch from within the thylakoid. The pellet was suspended and homogenised in Buffer 4 and centrifuged at 9000 r.p.m. (9700 x g) for 1 minute. The supernatant was transferred to a clean centrifuge tube and centrifuged at 18300 r.p.m. for 30 minutes. The remaining pellet after supernatant transfer, containing $\geq 90\%$ of the starch content was discarded.

g/. The supernatant was decanted and discarded and the pellet suspended and partially homogenised in the centrifuge tube using ~ 0.5 ml Storage Buffer with an homogenising pestle (Thomas size AA). The homogenate was stirred vigorously by shaking in a Vortex shaker / stirrer. The chlorophyll content was redetermined. Typically, the chlorophyll content was $\sim 18 \text{ g l}^{-1}$ for a 100 gram leaf preparation. The volume of the final PSII containing suspension was

adjusted to $\sim 15 \text{ g l}^{-1}$ chlorophyll content. Aliquots of 0.3 to 0.6 ml were placed into cryotubes (Nunc[®]), the tubes sealed and the samples placed into liquid nitrogen (77K) for storage until use.

3.2.1.1. Buffers used for the Bricker Type protocol

For all buffers, the chemical components were AR grade and measured as dry chemical into the flask and made to volume using deionised water passed through a Milli-Q[®] water purification system. The original protocol menu called for the buffering species to be pre-pHed, allowing the final buffer pH to be determined by the mixing of the components. The modification of adding all ingredients in their “pure” AR state, diluting to the set volume with the purified water and then setting the pH ensured that the final pH of each buffer was as required. No protease inhibitor was added to these buffers. A sacrificial protein, Bovine Serum Albumin (BSA) (Aldrich Sigma fraction V), was added to the pre-incubation buffers. The pH of the buffers was adjusted using 2 M NaOH and 2 M HCl.

Buffer 1: Blending Buffer

Sucrose	0.1 M		
KH ₂ PO ₄	0.05 M	}	constitute Phosphate Buffer
Na ₂ HPO ₄	0.05 M		
NaCl	0.2 M		

The pH of the final solution was set to 7.5. BSA was added to the buffer on the day of each isolation procedure to a content of 2 g l^{-1} . 0.25 l was required for each 100 gram of leaves in the preparation.

Buffer 2: Wash / Incubation Buffer.

Sucrose	0.4 M
NaCl	0.015 M
MgCl ₂	0.005 M
2-[N-Morpholino] ethane sulfonic acid (MES)	0.05 M
Ethylene diamine tetra acetic acid (as disodium salt) (EDTA.Na ₂)	0.005 M

The pH of the final solution was set to 6.0. BSA was added to the solution on the morning of the preparation to 2.5 g l^{-1} . 0.07 l of buffer was required for each 100 gram of leaves in the preparation.

Buffer 3: Solubilisation Buffer.

It was found that the easiest method of preparing this buffer, which consisted of Buffer 2 with 0.2 kg l^{-1} Triton[®] X-100 detergent, was to prepare the components of Buffer 2 into

approximately 1/3 of the required volume. This was added to the required mass of the detergent, liquid at room temperature. This high ionic strength solution of buffer components enabled the dissolution of the aqueous solution into the detergent with minimal micellisation, a major problem with trying to dissolve the detergent into low ionic strength solution. This buffer was made as a high volume stock solution due to the difficulty of preparing this buffer. The pH was checked and set to pH 6.0 for each isolation procedure.

Buffer 4: Post Detergent Wash Buffer.

NaCl	0.05 M
MgSO ₄	0.005 M
MES	0.05 M

This solution was made as a stock and the pH checked and adjusted to 6.0 for each isolation procedure.

Storage Buffer.

Sucrose	0.4 M
NaCl	0.015 M
MgCl ₂	0.01 M
MES	0.02 M

This buffer was prepared as a stock and the pH checked and adjusted to 6.0 for each isolation procedure. For the Bricker preparations requiring ethylene glycol as the cryoprotectant, ethylene glycol was added to the Post Detergent and Storage buffers to a level of 30% v:v and the sucrose omitted from the Storage Buffer.

3.2.2. Protocol for BBY preparation (Berthold, et al, 1981) with Modifications as per Beck et al (Beck, et al, 1985) and further modifications by the author

Spinach was sourced and prepared as per the Bricker protocol, see above. Typically 100 grams of leaves were used per preparation procedure.

1/. Leaves were shredded in 50 gram bundles by hand into a Waring type blender and blended in ~100 mls buffer A at high speed for 15 seconds. The homogenate was poured into filtering material. The blender bowl was rinsed with ~50 mls buffer A to wash excess homogenate into the filter material.

2/. The homogenate was filtered through either one layer of Miracloth[®] and four layers of gauze or four layers of cheesecloth. The filter material was parcelled around the homogenate and squeezed to accelerate the drainage of homogenate “juice”. The homogenate was then centrifuged at 6500 rpm (5000 x g) in an SS34 rotor for 10 minutes. For 100 grams of leaves blended, 8 x 40 ml SS34 tubes were used.

3/. The supernatant was decanted and discarded. The pellet was suspended and homogenised in Buffer B and the homogenate centrifuged at 6500 rpm for 10 minutes. Two x 40 ml SS34 tubes were required for 100 grams of leaves.

4/. The supernatant was decanted and discarded. The pellet was suspended and homogenised in Buffer C to a [chlorophyll] of $\sim 4 \text{ g l}^{-1}$. The chlorophyll concentration was determined, by the method of Arnon (Arnon, 1949) and the homogenate covered and incubated at 4°C for about 45 minutes to allow thylakoid stacking and photosystem partitioning. A magnetic stirrer bar was placed into the thylakoid suspension at this stage, but no stirring was applied during the stacking incubation.

These pre-incubation steps were undertaken quickly, usually less than 75 minutes between the start of blending and the incubation, enhancing the final PSII quality.

5/. After the ~ 45 minutes incubation, Buffer D was added to obtain a Triton[®] X-100 detergent : Chlorophyll ratio of $\sim 25:1$ w:w. The thylakoid / detergent solubilisation was stirred at 4°C in darkness for ~ 15 minutes to allow extensive solubilisation. The solution was centrifuged at 18300 rpm (40000 x g) for 30 minutes.

Buffer D consisted of Buffer C with 20% w:v X-100 detergent so as to avoid pH changes, solute dilution and detergent micellisation in the thylakoid / detergent solubilisation step.

6/. The supernatant was decanted and discarded. The pellet, consisting of granal membranes and starch, was suspended and homogenised in Buffer E and centrifuged at 9000 rpm (12000 x g) for one minute. The supernatant was decanted and transferred to another centrifuge tube and centrifuged at 18300 rpm for 30 minutes. The pellet, mainly starch, was discarded.

7/. The supernatant was decanted and discarded. The pellet was resuspended in the centrifuge tube using 0.5 to 0.75 ml Buffer E and an homogenising pestle (Thomas size AA). The resulting suspension was vigorously shaken using a Vortex[®] to aid homogenisation. The chlorophyll content was redetermined. Typical chlorophyll concentration was ~ 12 to 14 g l^{-1} for a 100 gram leaf preparation. Aliquots of 0.3 to 0.6 ml were placed into Nunc[®] cryotubes, sealed and stored in liquid nitrogen (77K) until required for experimentation.

3.2.2.1. Buffers for the BBY Type Isolation Procedure

For all buffers, the chemical components were AR grade and measured as dry chemical into the flask and made to volume using deionised water passed through a Milli-Q water purification system as per the Bricker isolation protocol. No protease inhibitor was added to these buffers. A sacrificial protein, BSA was added to the pre-incubation buffers. The pH of the buffers was adjusted using 2 M NaOH and 2 M HCl.

Buffer A: Blending Buffer.

NaCl	0.4 M
MgCl ₂	0.01 M
Tricine	0.02 M
EDTA.Na ₂	0.005 M

The solution pH was adjusted to 8.0 before the isolation procedure. BSA was added to the solution to a concentration of 2 g l⁻¹ on the morning of the isolation procedure.

Buffer B: Wash Buffer.

NaCl	0.15 M
MgCl ₂	0.01 M
Tricine	0.02 M
EDTA.Na ₂	0.005 M

The pH of the solution was set to 8.0 before the isolation procedure. BSA was added to the buffer to a level of 2.5 g l⁻¹ on the morning of the isolation procedure.

Buffer C: Incubation Buffer.

NaCl	0.015 M
MgCl ₂	0.01 M
MES	0.05 M
EDTA.Na ₂	0.005 M

The pH of the solution was set to 6.0 before the isolation procedure and BSA was added on the morning of the isolation procedure to a level of 2.5 g l⁻¹.

Buffer D: Solubilisation Buffer.

The normal components of Incubation Buffer were dissolved into 1/3 of the normal volume. To this was added Triton[®] X-100 and ultra-pure water to achieve a normal strength Incubation buffer containing 200 g l⁻¹ X-100 detergent. This buffer was prepared in the same fashion as the equivalent Bricker protocol buffer to enable efficient solubilisation of the detergent with minimal micellisation. This buffer was prepared as a stock and the pH checked and adjusted to 6.0 before each isolation procedure.

Buffer E: Resuspension / Storage Buffer.

NaCl	0.015 M
MgCl ₂	0.005 M
MES	0.02 M
EDTA.Na ₂	0.005 M
1,2-Ethandiol	30 % v:v

The buffer solution was made as a stock and the pH checked and adjusted to 6.0 before each isolation procedure. For the BBY preparations utilising sucrose as cryoprotectant, 0.4 M sucrose was included in this buffer and the ethandiol omitted.

3.3. Inhibited Sample Preparation

Previously prepared PSII samples were used as the starting material for all inhibition protocols. The main form of inhibition used was to chloride deplete the PSII material and to exchange tightly bound chloride with fluoride. The fluoride exchange inhibition followed the protocol of Ono (Ono, et al, 1987). The procedure for chloride depletion and fluoride exchange was undertaken on both BBY type and Bricker type PSII samples, with equivalent results observed for each starting material.

PSII samples containing about 30 mg (total) chlorophyll were used for each chloride depletion / fluoride inhibition procedure. Very low light levels were required for these procedures, to maintain OEC intactness. Very dim green light or a far red safety light were used in an otherwise darkened room.

1/. PSII samples of about 30 mg total chlorophyll content were thawed from liquid nitrogen storage. The sample was suspended into ~ 30 mls Buffer (i) in an SS34 centrifuge tube. The suspension was shaken by hand to enhance mixing of the PSII containing membranes and centrifuged at 17200 rpm (35000 x g) for 15 minutes.

2/. The supernatant was decanted and discarded. The pellet was suspended and homogenised in ~ 15 ml Buffer (ii) and transferred to a 15 ml Corex centrifuge tube. The solution was centrifuged at 17200 rpm for 15 minutes.

3/. The supernatant was decanted and discarded. The pellet was resuspended into 15 mls Buffer (ii). The pellet remained in the same centrifuge tube during this suspension. The suspension was centrifuged at 17200 rpm for 15 minutes. This step was repeated to give a second wash in Buffer (ii), keeping the PSII sample in the same centrifuge tube.

4/. After the second wash, the supernatant was decanted and discarded. The pellet was resuspended, in the same centrifuge tube, to a volume of 5 ml. The chlorophyll content was determined by the method of Arnon (Arnon, 1949). A [chlorophyll] of $\geq 5 \text{ g l}^{-1}$ was desired. This suspension, with $[\text{Cl}^-]$ of ~ 1mM, was left to incubate in darkness at 4°C for 60 to 90 minutes.

After the incubation time, the suspension was transferred to a larger vessel, whereby the PSII was diluted to ~ 120 ml, [chlorophyll] of ~ 0.25 g l^{-1} , using Buffer (iii). This diluted the $[\text{Cl}^-]$ to ~ 0.03 mM. 1 M NaF was added to the diluted solution to yield a final $[\text{F}^-]$ of 50 mM. The sample was incubated in darkness at 4°C for 10 minutes to allow F^-/Cl^- exchange within the protein.

The resultant solution was transferred to SS34 centrifuge tubes and centrifuged at 17200 rpm for 10 minutes.

5/. The supernatant was decanted and discarded. The pellet was suspended and homogenised to a volume of 15 ml in Buffer (iv) and transferred to a clean Corex centrifuge tube. The solution was centrifuged at 17200 rpm for 10 minutes.

6/. The supernatant was decanted and discarded. The pellet was suspended in Buffer (iv) to a final volume of 3 ml. The suspension of the F⁻ exchanged PSII particles was in the same centrifuge tube. The chlorophyll content was redetermined.

Typically, the final [Chl] was between 8 and 11 g l⁻¹, The concentration being dependent on the ability to suspend the very 'gluggy' PSII sample without extensive smearing on the walls of the centrifuge tube. This material became viscous and adherent upon addition of the F⁻. This may have been due to the lack of divalent cations in the buffers, as these tend to form a counter ion layer on the surface of the protein, neutralising the negative charge density on the protein surface, reducing the adherent properties of the proteinaceous samples.

The PSII suspension was transferred directly into quartz ESR tubes without any further modifications, such as quinone acceptors, etc. The samples were frozen into liquid nitrogen (77 K) and stored in the ESR tubes until required. This material was used within three days of the anion exchange procedure, the shelf life of these samples being severely reduced by the absence of Cl⁻ and counter divalent cations.

3.3.1.1. Buffers for the Cl⁻ Depletion / F⁻ Inhibition protocol

All buffers were prepared with AR grade reagents to minimise Cl⁻ contamination and were pH adjusted using 2 M NaOH and 1 M H₂SO₄. The dissolution of the dry reagents resulted in an initial pH well below that required for the exchange procedure, ie the un-pHed buffers were more acidic than the required pH, so most pH adjustment required only NaOH, the H₂SO₄ content being minimised as it has been observed to be a PSII oxygen evolution inhibitor (Ono, et al, 1987).

Buffer (i):

NaCl	0.02 M
MES	0.04 M
EDTA.Na ₂	0.002 M
Sucrose	0.4 M

This buffer was prepared as a stock solution and the pH checked and adjusted to 6.5 for each anion exchange procedure.

Buffer (ii):

NaCl	0.001 M
MES	0.04 M
Sucrose	0.4 M

This buffer was prepared as a stock buffer and the pH checked and adjusted to 6.5 before each anion exchange procedure.

Buffer (iii):

HEPES	0.04 M
Sucrose	0.4 M

This buffer was made fresh for each anion exchange procedure and the pH checked and adjusted to 7.5.

Buffer (iv):

HEPES	0.04 M
NaF	0.05 M
NaCl	0.00003 M *
Sucrose	0.4 M

The solution was prepared as a stock buffer and the pH checked and adjusted to 7.5 before each anion exchange procedure. * NaCl was included in this buffer at a concentration of 30 μ M as this was suggested to be sufficient to maintain protein integrity while not allowing physiological electron transfer capability out of the donor side of the PSII (Ono, et al, 1987).

3.4. Experimental Apparatus

The majority of experiments in this project involved the use of CW EPR on PSII containing samples trapped in the S₂ state. The paramagnetic signals arising from the S₂ state were examined in detail in attempts to define the magnetic species and spin state giving rise to each signal. Mainly, this involved examining the power saturation properties of each signal at varying temperatures in order to define the non saturated temperature dependence behaviour of the signals. This work sought to determine the number of manganese ions involved in each of the S₂ state signals and to decipher the location of these ions within the protein structure.

3.4.1. Sample Illumination

Under steady illumination at physiological temperatures, the OEC cycles continuously through the S states, with a population ratio of 25% in each S state under steady state conditions. To obtain the S₂ state in high yield, a number of techniques have been used. Using saturating light flashes, PSII may be made to step through each S state of the Kok cycle (Kok, et al., 1970) with high yields of the S₂ state obtained by rapid freezing after the first and fifth flashes (Dismukes and Siderer, 1980, Dismukes and Siderer, 1981), although some population of S₁ and S₃ states are observed due to double hits and misses. Freezing of samples while under continuous illumination yields a significant S₂ state population, which is enhanced when DCMU in ethanol is added to the sample (Hansson and Andreasson, 1982, Andreasson, et al,

1983). The addition of DCMU inhibits electron transfer from Q_A to Q_B. This prevents double advancement beyond the S₂ state and allows a more complete turnover of OEC centres into the S₂ state, but also allows possible side path electron transfer. These may create additional paramagnetic sites which could interact with the Mn sites, causing changes in signal structure and power saturation behaviours. Illuminating PSII containing samples at temperatures below 220K (Brudvig, et al, 1983, Casey and Sauer, 1984) blocks functional electron transfer from Q_A to Q_B without the addition of inhibitors and solvents. This technique was generally used here and generates different regimes of the multiline and g~4.1 signals, dependent on the temperature of illumination and cryoprotectant used in the PSII isolation storage buffer.

3.4.1.1. Illumination System

To cool PSII samples to temperatures between 125K and 240K for illumination, a nitrogen gas flow system was used. This system consisted of a Varian transparent quartz, NMR flow cryostat and heater controller. Calibration of temperature at the sample position was possible between 100K and 300K. Temperature calibration was performed using a gold-chromel thermocouple located at the sample position with an ice water bath reference.

Illumination of the samples was achieved by either a Leits Wetzlar Epidiascope fitted with a 1000W tungsten filament lamp or by use of a Kodak SAV2000 Carousel slide projector fitted with a 250W Halogen lamp. For both light sources, the light was passed through 15cm of water and filtered using Corning type filters; one yellow realising a sample illuminance of ~ 600 Wm⁻², or a combination of yellow and blue filters realising a sample illuminance of ~ 150 Wm⁻².

3.4.2. Electron Spin Resonance Experiments

The Electron Spin Resonance experiments undertaken throughout this project utilised two different spectrometers; 1). A Varian V-4502 X Band Spectrometer and 2). a Bruker ESP300E spectrometer.

3.4.2.1. Varian Spectrometer

The Varian V-4502 spectrometer was used to record spectra at X Band (9GHz), at both 100kHz and 400Hz Modulation Frequency, and Q Band (35 GHz). The instrument consisted of the base spectrometer supported by a Varian V-4560 100Kc Field Modulation and Control Unit, a Varian Fieldial Mark II Field Regulated Magnetic Power Supply, and a Varian X Band Microwave Bridge, using a rectangular microwave cavity operating in the TE₁₀₂ mode. For X Band experiments, the microwave radiation frequency was measured using a Hewlett Packard HP 5245L Electronic Counter recording via an HP 5257A Transfer Oscillator.

For Q Band experiments, the X Band Microwave bridge and associated waveguide and cavity was replaced by a Varian V-4561 35Gc Microwave bridge, using a home built cylindrical cavity operating in the TE₁₀₂ mode (Bramley Unpublished).

For each frequency band, the field was required to be manually calibrated. For this purpose, either a Resonance Technology Ltd model CX 86 Teslameter, or a Home built Teslameter (Bramley Unpublished) recording via an alternative mode of the HP 5245L Electronic Counter were used.

For power saturation and temperature dependence experiments on Signal II, it was necessary to work at low modulation frequency. This was required to ensure the intensity of Signal II recorded at low powers and low temperatures was not subject to Rapid Passage effects. The possibility that this was occurring was raised by Dr R Bramley after some discussion of the signal temperature dependence recorded at 100KHz, see later. Any rapid passage artefacts were overcome by working at a modulation frequency of 400Hz. This was possible due to the Varian being equipped with a low frequency sweep unit, allowing experimentation at modulation frequencies at between 20 Hz and 400 Hz.

Microwave power was recorded using an HP 8481 Power Sensor and an HP 435A Power meter. In some experiments on the power saturation behaviour of Signal II, power levels below the standard capability of the Varian X Band Microwave Bridge were required. The power levels below the standard maximum attenuation of the bridge were achieved by in line HP 8735A Pin Modulator with a set 20dB pre-calibrated bias voltage.

The spectra were recorded to computer for manipulation and presentation. This was achieved through the use of two computer systems consisting of an IBM clone PC fitted with A / D interface boards. These systems were (1) a DAS 16 A / D interface controller board within an AT 286 clone PC, with programs home written by the author, (P. Smith unpublished), and (2) an A/D interface board within a 386 clone PC, with software home written by Luca and Wang (V. Luca and D. Wang unpublished). Further data presentation was undertaken using the Jandal Scientific SigmaPlot program using a 486 DX2 66 clone PC.

3.4.2.2. Bruker Spectrometer

The Varian Instrument was the only ESR Spectrometer available for this work at the start of this project. Acknowledgment is due to Dr R. Bramley for allowing access to this spectrometer at the start and during the course of this project. During the course of this project, availability of the Varian instrument declined severely limiting progress. In late '93 a new Bruker ESP300E spectrometer was obtained for biological work. This instrument is almost fully automated, with inbuilt 486 equivalent PC, automated Field and microwave power level adjustment and microwave frequency calibration. The computer controlled data acquisition system improved the capability of data recording, with auto tuning, amplification, digital acquisition on the field and signal recording. The Modulation frequency was software

selectable between 1.56kHz and 100kHz. The spectrometer was used only at X Band, using a standard rectangular cavity and waveguide operating in the TE 102 mode.

The spectra were recorded directly to the spectrometer's inbuilt PC hard drive, and transferred via WIN EPR Kermit function to a Clone 486 DX2 66MHz PC for analysis and manipulation using Bruker WIN EPR. Data presentation was done using the Jandal Scientific Sigma Plot software package.

3.4.2.3. Cryogenic Temperatures

Measurements on each spectrometer were carried out at cryogenic temperatures. For this purpose, experiments carried out at X Band (9GHz) frequencies utilised an Oxford Instruments ESR9 Helium flow cryostat fitted to each spectrometer, with temperature control between ~4.5K and ~70K using an Oxford Instruments ITC4 Intelligent Temperature Controller, with helium flow controlled by an Oxford Instruments VC40 Gas flow controller. For Q Band (35GHz) frequency experiments, the cylindrical cavity and waveguide was wholly contained within an Oxford Instruments Helium flow cryostat, utilising also an ITC 4 and VC40 controllers. Sample temperature calibration was by either using a pre calibrated Carbon resistor or a gold chromel thermocouple each located at the sample position.

Chapter 4

Results and Discussion

This study was aimed at examining the signal line shapes, temperature dependencies and spin states for the S_2 and S_3^* states in the catalytic cycle of functional and inhibited photosystem (PS) II. Two protocols of PSII isolation were utilised for generating functional S_2 state signals, and a comparison of the line shapes of each signal type studied, under the sample conditions generated during the different isolation protocols, was undertaken.

4.1. Comparison of the Two Preparations:

BBY- and Bricker- type PSII

The preparation of PSII by two different protocols was undertaken to examine the similarity of the S_2 state signals observed when generated in samples of the two different preparations. For simplicity, only the multiline signal formed by illumination of samples at 200K with the different cryoprotectants and the $g=4.1$ signals generated by illuminating the ethylene glycol cryoprotected PSII at 130K are compared. These signals, the multiline and $g=4.1$ signals generated by these regimes, have been the most studied signals and, hence, will best allow observation of any differences in the PSII samples.

The Bricker preparation (Bricker, et al, 1985) maintains a high osmolarity buffer through the preparation to the solubilisation step. The only low osmolar buffer, providing an hypo-osmolar swelling of the membranes, is applied to wash the excess Triton X-100 (TX-100) detergent from the membranes. For sucrose cryoprotected PSII, this protocol has been the preferred method of PSII preparation due to the osmotic insulation of the PSII complexes and the relatively rapid solubilisation step.

The BBY protocol (Berthold, et al, 1981) places the broken chloroplasts into low osmolar buffer from the post blending wash stage. This procedure works to maintain the thylakoids in a swollen state throughout the preparation. The solubilisation procedure of stirring the thylakoids in the presence of the detergent for 15 to 20 minutes leads to a much lower final yield of active PSII, as a fraction of the pre solubilisation chlorophyll content, when compared to the Bricker method. The buffers for the post solubilisation steps for the BBY procedure have higher osmolarity as they contain the final concentration of the cryoprotectant species.

The following spectra are presented only for the comparison. More detailed analyses of these signal types will be presented later.

4.1.1. Multiline Signal for Sucrose and Ethylene Glycol as Cryoprotectants

Figure 4.01 shows the multiline signals generated in sucrose cryoprotected PSII illuminated at 200K for (a) the Bricker type samples and (b) the BBY type samples. These two spectra indicate the multiline signals generated under these conditions are almost equivalent in overall width, number of hyperfine peaks and superhyperfine structure. Figure 4.02 shows the multiline signals generated in ethylene glycol (EG) cryoprotected PSII illuminated at 200K for (a) the Bricker type samples and (b) the BBY type samples. The comparison of these two signals show them to be very similar to the sucrose cryoprotected sample spectra.

4.1.2. $g=4.1$ Signal for Ethylene Glycol as Cryoprotectant

Figure 4.03 shows the $g=4.1$ signals for the (a) Bricker and (b) BBY type PSII samples cryoprotected with ethylene glycol and illuminated at 130K. The signals are almost equivalent in terms of the g value and peak to trough width of the signal.

These comparisons were intended to confirm that the PSII samples from the different preparations give rise to the same overall forms of the multiline and $g=4.1$ signals in terms of the spectral features. The following results are presented as a combination of the results for the two types of PSII preparations undertaken.

4.2. Multiline Signal. PSII Illuminated at 200K

This study was aimed at examining PSII samples suspended in the S_2 state with minimal additions to the sample buffer, such as electron acceptors and DCMU. The addition of small monoalcohols to the sample buffer prior to illumination was avoided, allowing the development of both multiline and $g=4.1$ signals.

4.2.1. PSII Cryoprotected with 0.4M Sucrose

The multiline signal generated in sucrose cryoprotected PSII illuminated at 200K is shown in figure 4.04. The spectrum is the addition of many recordings over many samples to improve signal to noise. The number of hyperfine peaks observable is subject to some uncertainty. The main hyperfine features are observable to lines -9 and +9 from the central region. The insets on fig.4.04 show the edge regions of the multiline spectrum expanded to determine additional features. The downfield edge shows a -10th peak and possibly a -11th feature, although the signal to noise in this region makes the identification of the -11th peak rather uncertain. The upfield edge of the spectrum indicates the possibility of +10th, +11th and possibly +12th peaks. These

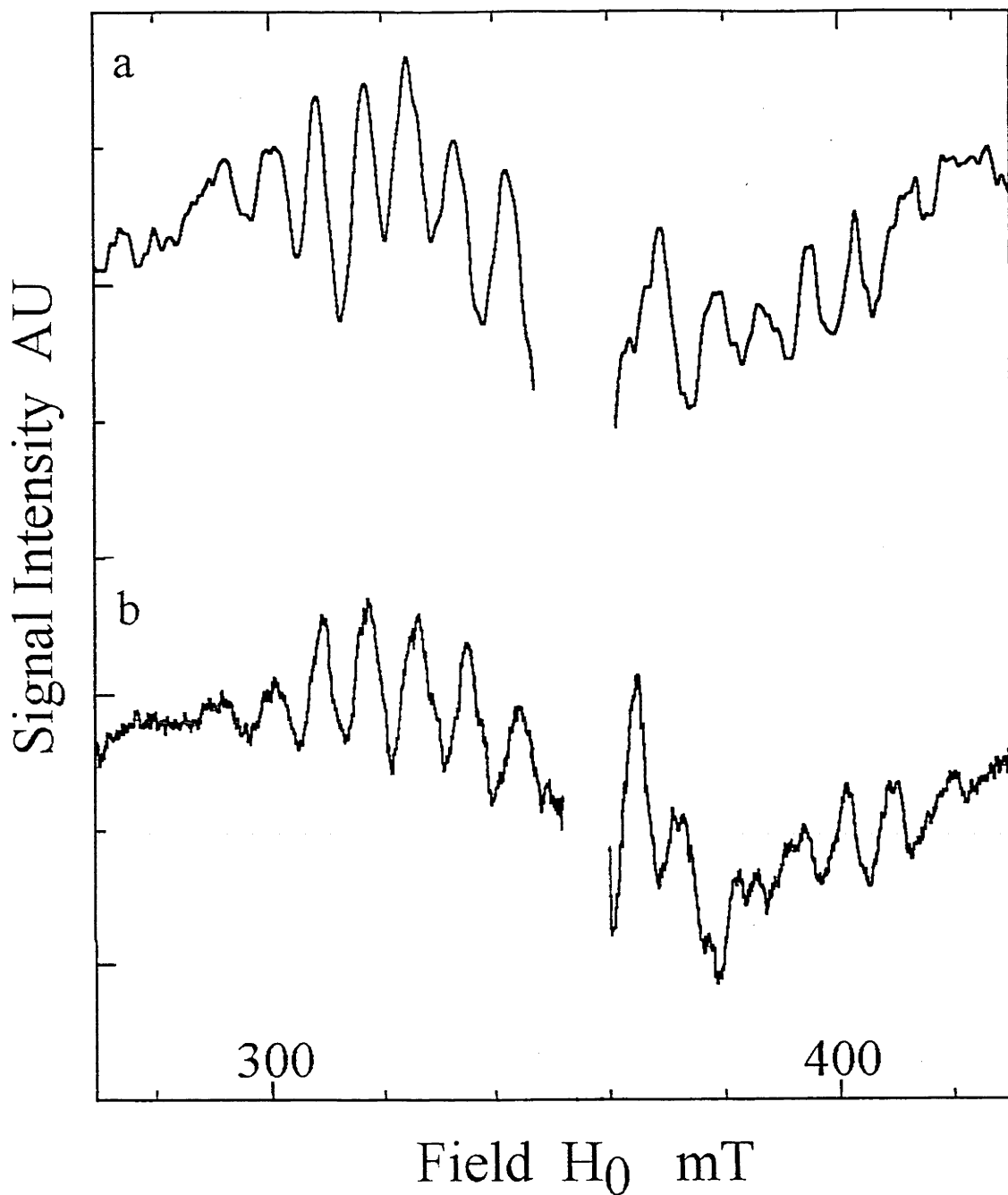


Figure 4.01. Comparison of the S_2 state multiline signals generated in PSII cryoprotected with 0.4M sucrose, illuminated at 200K. a). Bricker type PSII particles (as per Bricker, et al, 1985), b). BBY type PSII particles (as per Berthold, et al, 1981). Spectrometer conditions: temperature 9K, microwave frequency 8.97 GHz, microwave power 100 μ W, modulation frequency 100 KHz, modulation amplitude 1.3mT.

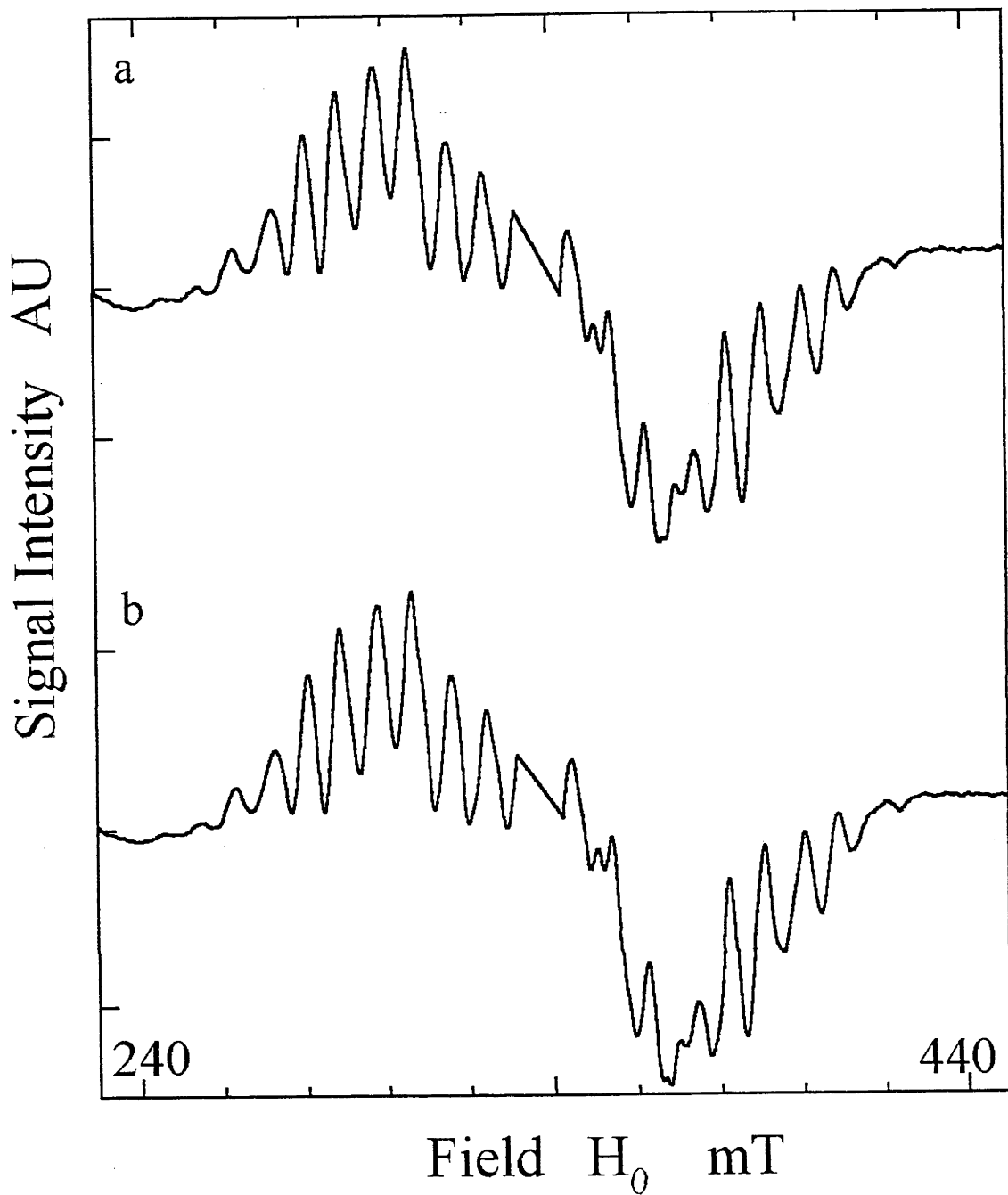


Figure 4.02. Comparison of S_2 state multiline signals generated in PSII cryoprotected with 30% v:v ethylene glycol, illuminated at 200K. a). Bricker type PSII particles, b). BBY type PSII particles. Spectrometer conditions as per fig. 4.01.

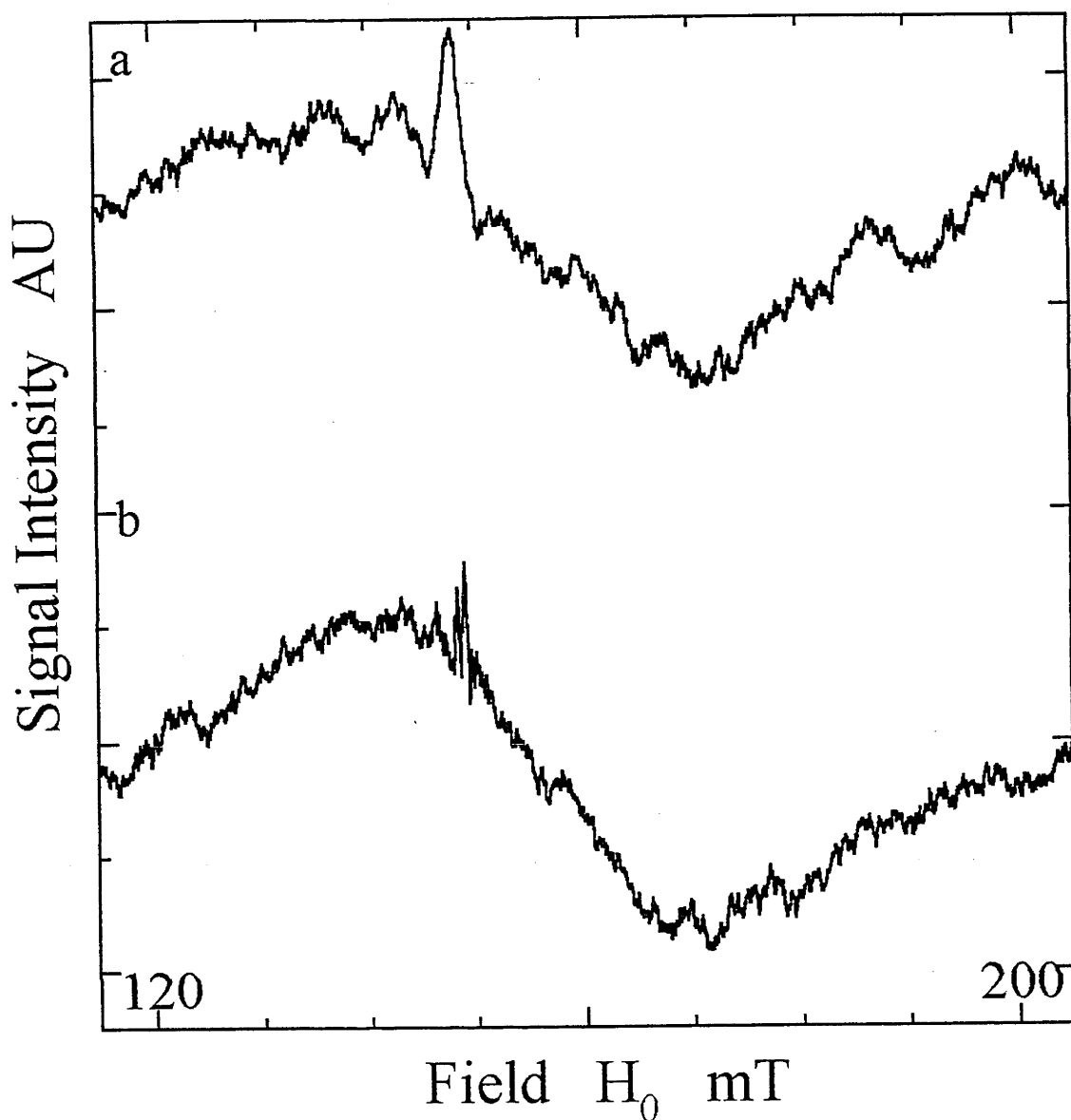


Figure 4.03. Comparison of the S_2 state $g=4.1$ signals generated in PSII cryoprotected with 30% v:v ethylene glycol, illuminated at 130K. a). Bricker type PSII particles, b). BBY type PSII particles. Spectrometer conditions as per fig. 4.01.

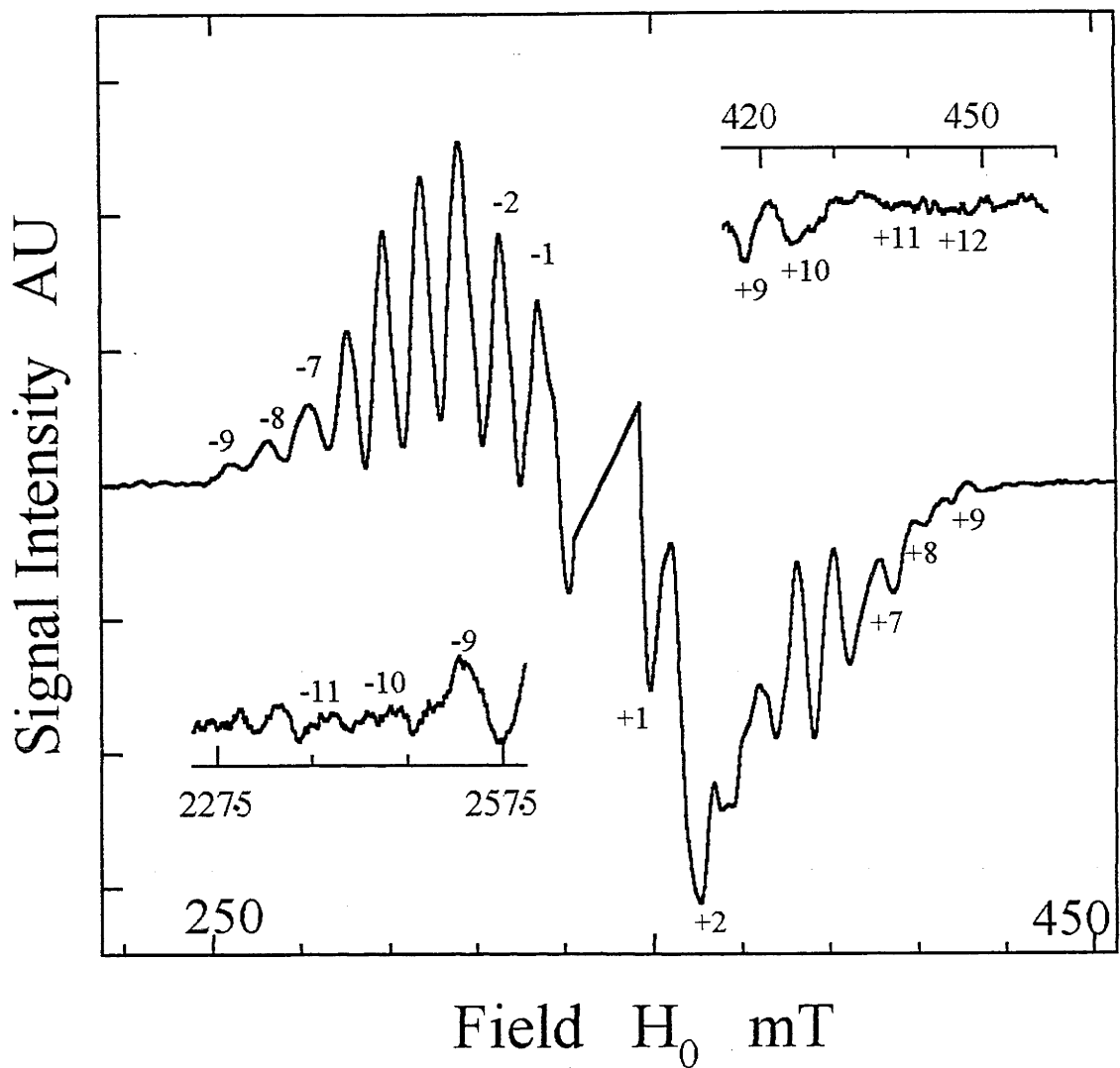


Figure 4.04. S_2 state multiline generated in PSII cryoprotected with 0.4M sucrose, illuminated at 200K. Inserts indicate the fine features on the edges of the hyperfine pattern. Spectrometer conditions: temperature 9K, microwave frequency 9.42 GHz, microwave power 6.3mW, modulation frequency 100 KHz, modulation amplitude 2mT. Numbering of the peaks is as per Pace and coworkers (Pace, et al, 1991), and differs from that of the Kusunoki numbering (Kusunoki, 1992) by the numbering of the peak overlain by signal II, which would raise the indicated peak numbers by one.

additional peaks on the spectrum edges are predicted in the multiline signal simulation spectrum (Åhrling and Pace, 1995) although the intensity of these features is frequency dependent (Åhrling pers. comm.).

4.2.2. PSII Cryoprotected with 30% v:v Ethylene Glycol

The illumination of polyalcohol cryoprotected (eg glycerol or EG) PSII at 200K in the absence of additional alcohol has been shown previously to develop both multiline and $g=4.1$ signals (Zimmermann and Rutherford, 1984, Zimmermann and Rutherford, 1986). Figure 4.05a shows the multiline generated in EG PSII illuminated at 200K. This signal is very similar in overall features to that of the sucrose PSII multiline, see fig.4.04. The hyperfine features on the upfield edge of the $g\sim 2$ region, at about $g\sim 1.9$, show significant superhyperfine differences to those of the equivalent region of the sucrose PSII multiline spectrum. The differences in superhyperfine structure between the sucrose cryoprotected and the EG cryoprotected PSII multilines are almost equivalent to the superhyperfine structure differences in the multiline signals generated in sucrose cryoprotected PSII illuminated at 200K in the absence and presence of added alcohols (Smith, et al, 1993), although alcohols cause the disappearance of the $g=4.1$ signal..

The number of observed hyperfine peaks is similar to that of the sucrose PSII multiline. The insets show the downfield and upfield edges expanded to determine hyperfine features beyond the readily observable -9th and +9th peaks. The expanded regions indicate that the spectrum extends out to the -10th and possibly -11th peaks downfield and the +10th and possibly +11th features upfield.

Figure 4.05b shows the multiline signal generated by annealing the EG PSII sample, in darkness at 200K for 100s, following initial illumination at 130K to generate $g=4.1$ signal, (see below). The multiline signal generated by this protocol is essentially identical to the multiline generated by simple 200K illumination. The equivalence of the multiline signals implies that the environment of the Mn centre giving rise to this signal reaches the same ligand status. This comparison suggests that the reorganisation of the oxidative equivalent during the annealing process may be a transfer between separate sites rather than a ligand rearrangement of a Mn tetramer, which may be subject to cofactor access limitation in the frozen state. The process could have conceivably led to different end results in the superhyperfine features, since the time between 130K illumination and the annealing process was only 100 seconds, while the illumination at 200K was ~ 200 seconds.

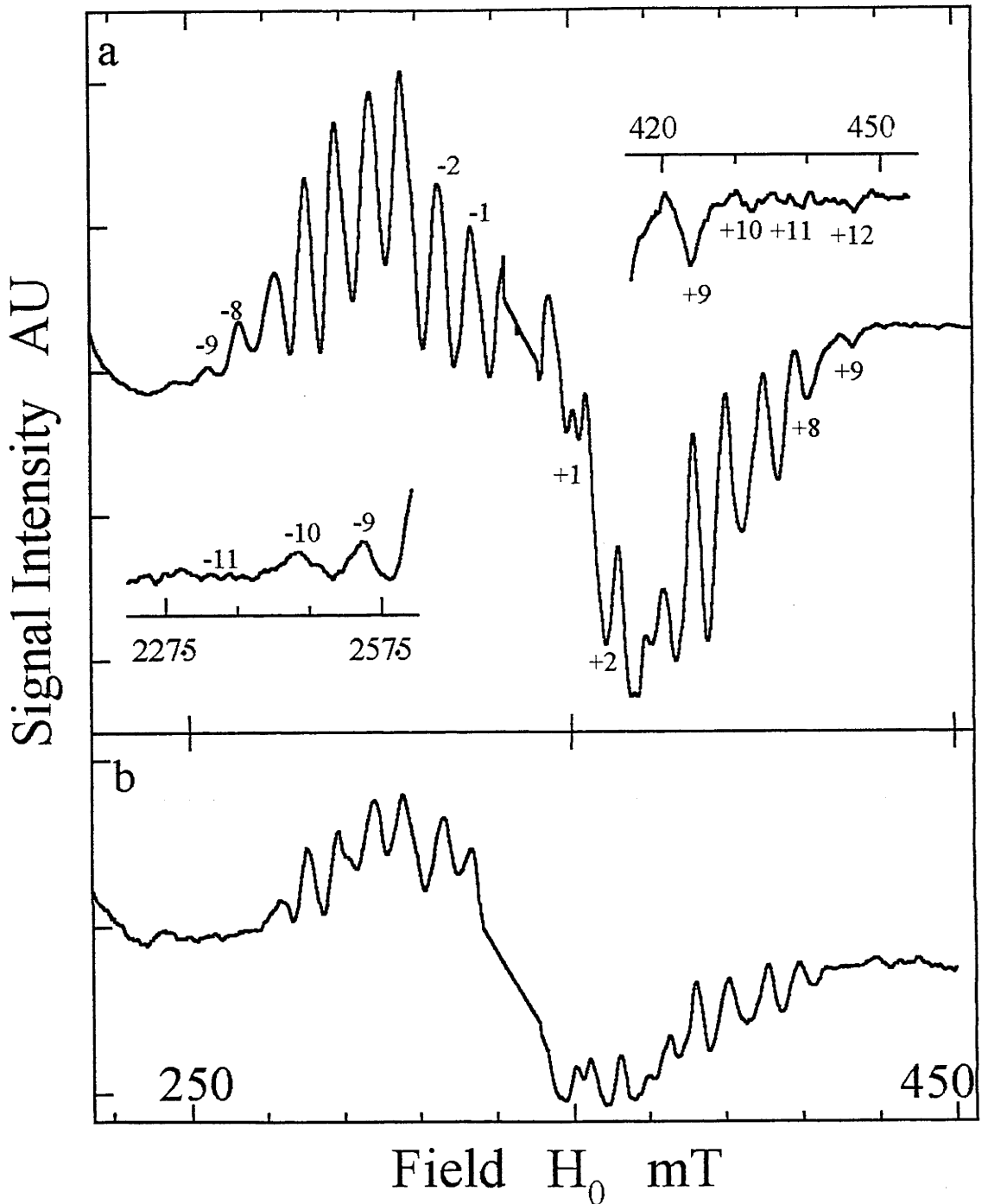


Figure 4.05. S_2 state multiline signals in PSII cryoprotected with 30% v:v ethylene glycol, a). illuminated at 200K, b). generated via annealing at 200K of samples previously illuminated at 130K to generate the $g=4.1$ signal. Spectrum (a) is illuminated minus dark 295K annealed spectrum, (b) is 200K annealed minus 130K illuminated spectrum. Multiline hyperfine peak numbering and spectrometer conditions are as per fig. 4.04.

4.3. g=4.1 Signals. PSII Illuminated at either 200K or 130K

The development of g=4.1 signal intensity has been deliberately promoted by the omission of monoalcohols from the sample buffer. The g=4.1 signals in the sucrose PSII illuminated at 200K and the EG PSII illuminated at both 200K and 130K have been examined and compared in terms of the g value, peak to trough width and overall spectral features.

4.3.1. Sucrose PSII Illuminated at 200K

The g=4.1 signal cogenerated in the presence of the multiline signal in sucrose cryoprotected PSII illuminated at 200K is shown in figure 4.06a. The signal displays a strong axial nature, with a g value of 4.10 ± 0.02 and peak to trough width of 33mT. No evidence of splitting of the signal due to anisotropy of the g tensor is evident, nor are there any resolvable hyperfine features which arise on oriented g=4.1 from both uninhibited material (Smith, et al, 1993) and that inhibited by NH₄Cl addition (Kim, et al, 1990, Kim, et al, 1992).

4.3.2. EG PSII Illuminated at 130K

The g=4.1 signal generated by illumination at 130K of EG cryoprotected PSII is shown in figure 4.06b. This g=4.1 signal shows a strong axial line shape with g value 4.11 ± 0.02 and peak to trough width of 31mT. The g=4.1 signal generated by 130K illumination of EG PSII is very similar in line shape to that of the g=4.1 signal generated in sucrose PSII illuminated at 200K. However, some differences are observed, with the EG PSII 130K illuminated g=4.1 signal being ~10% narrower than the sucrose g=4.1. No development of hyperfine features is apparent, similar to the sucrose g=4.1 spectrum.

The EG PSII 130K illumination g=4.1 signal shows a slight splitting at the crossing point of the signal, indicative of a significant difference in the g_⊥ components. This splitting of the g=4.1 signal is only tentatively assigned, however, and is insufficiently developed to make judgement of the g_⊥ components, so only the g_{av} value is reported.

4.3.3. EG PSII Illuminated at 200K

Figure 4.07a shows the g=4.1 signal generated in EG PSII illuminated at 200K. The line shape shows strong axial nature, and is quite similar to both the g=4.1 signals presented in fig.4.06. The g value of this g=4.1 signal was observed to be 4.14 ± 0.02 , with a peak to trough width of 30mT. The g value and linewidth of this EG PSII 200K illumination g=4.1 signal appears most similar to that of the EG PSII 130K illumination g=4.1 signal.

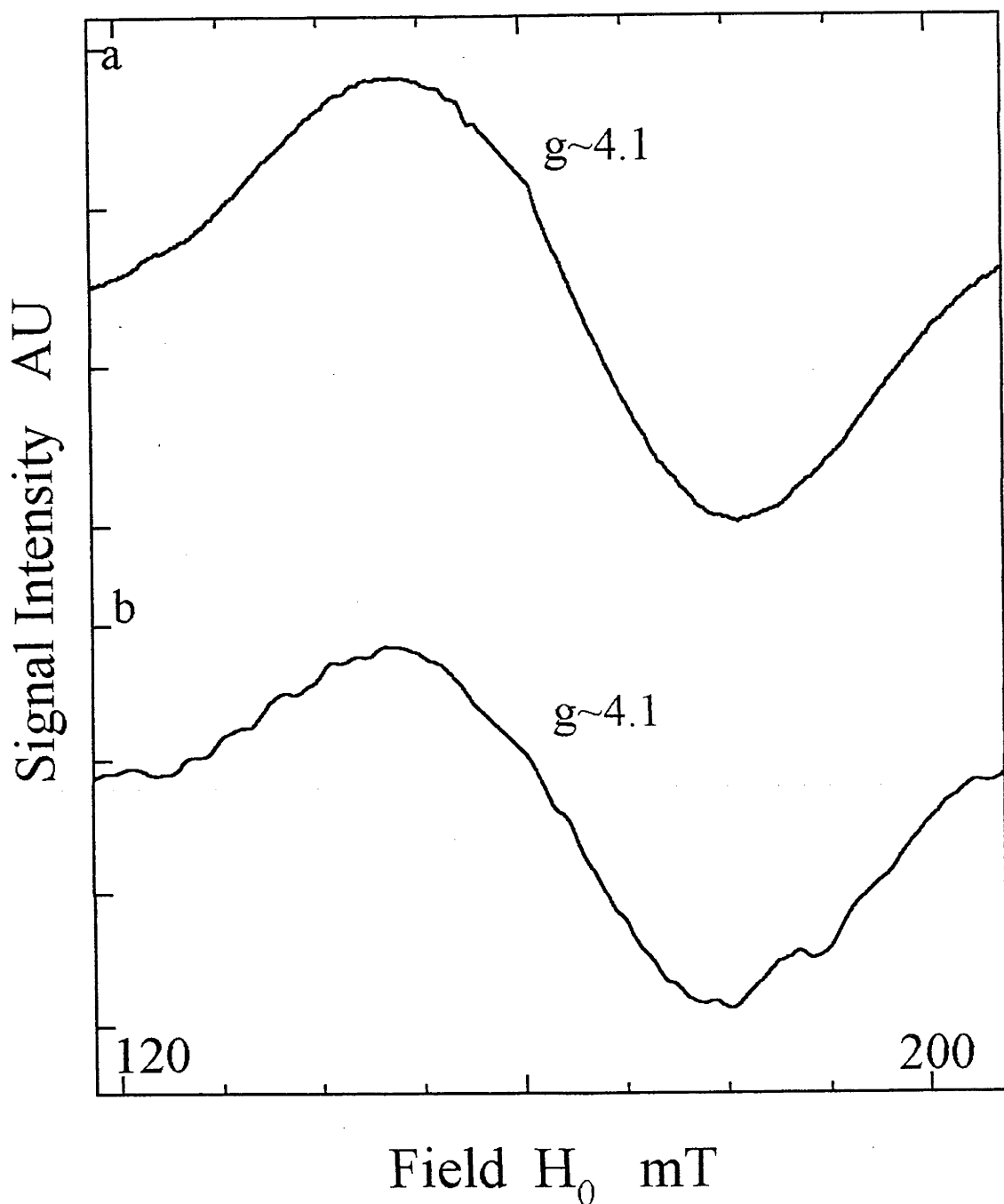


Figure 4.06. S_2 state $g=4.1$ signals generated under the two main protocols of illumination and cryoprotectant preparation. a). PSII cryoprotected with 0.4M sucrose, illuminated at 200K, b). PSII cryoprotected with 30% v:v ethylene glycol, illuminated at 130K. Spectrometer conditions as per fig. 4.04 with modulation amplitude 1.4mT.

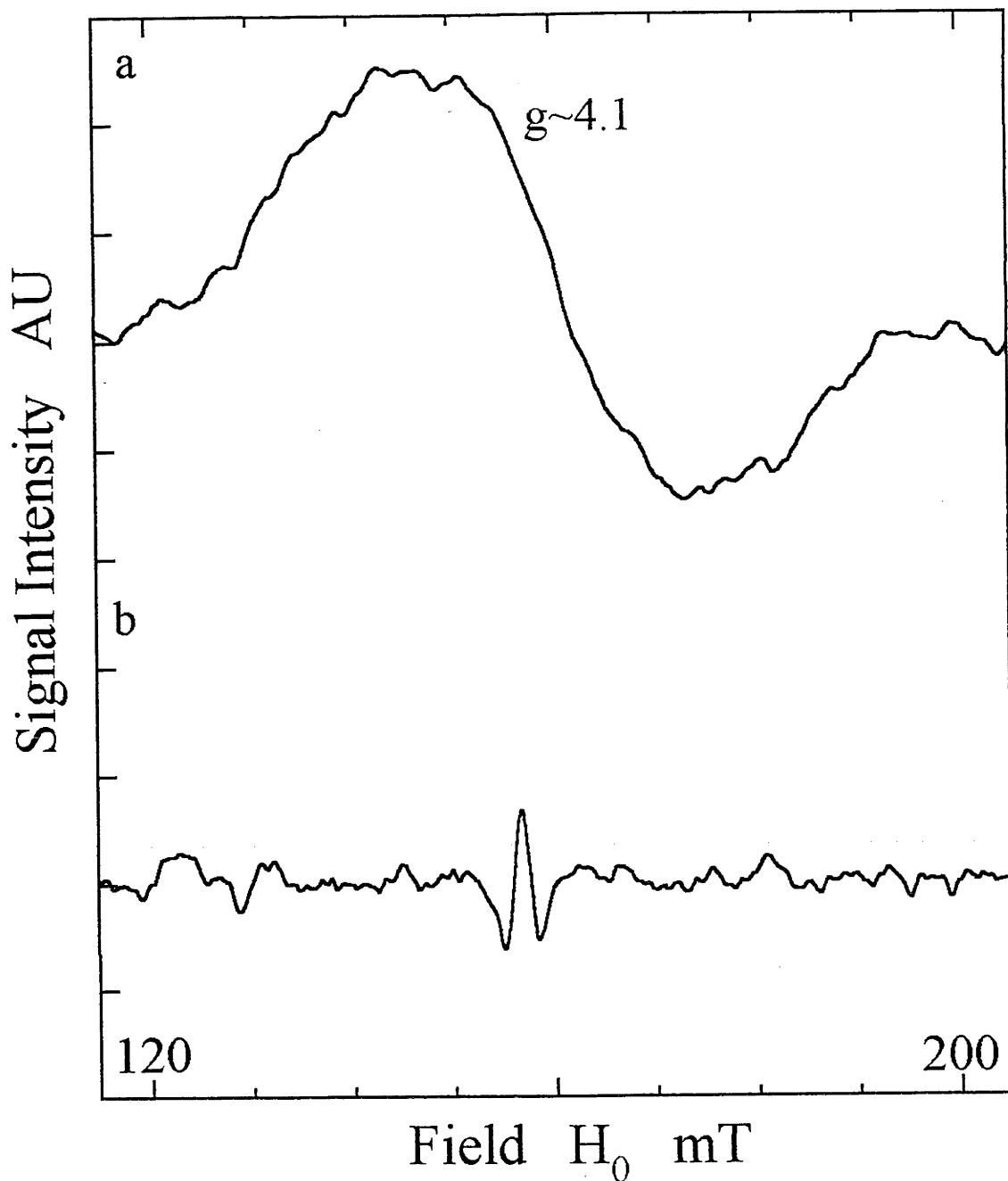


Figure 4.07. PSII cryoprotected with 30% v:v ethylene glycol, S_2 state $g=4.1$ regions a). illuminated at 200K forming $g=4.1$, b). recorded in sample annealed at 200K previously illuminated at 130K to generate the $g=4.1$ signal. Spectrometer conditions as per fig. 4.04 with modulation amplitude 1.4mT.

Figure 4.07b shows the $g=4.1$ region for EG PSII which has been dark annealed at 200K, previously having been illuminated at 130K to generate the $g=4.1$ signal observed in figure 4.06b. No $g=4.1$ signal is observed for this post 200K annealed EG PSII sample. The multiline developed in the post 200K annealed EG PSII is most likely of the added alcohol form, as observed earlier (fig.4.05b) (Pace, et al., 1991, Smith, et al, 1993). The presence of $g=4.1$ signal in the 200K illuminated sample may represent generation of the low temperature illumination form in this sample.

4.4 Relationship of $g=4.1$ signals to the Multiline Signal

4.4.1. EG PSII Illuminated at 130K, Annealed 200K

The intensity of the $g=4.1$ signal developed in the S_2 state of EG cryoprotected PSII samples illuminated at temperatures between 125K and 145K showed no correlation to the development of multiline signals in the same samples (data not shown). Typically, only small intensities of multiline signal were observed under these illumination conditions (between effectively zero (multiline undiscernible) and ~20% of maximal multiline intensity as developed with 200K illumination). The line shape of the $g=4.1$ signal remained consistent across the illumination temperature range 125K to 145K.

Upon annealing at 200K for 100 seconds, the $g=4.1$ generated by 130K illumination is lost, and multiline signal intensity increases, indicative of an interconversion of redox states between the sites responsible for the low temperature $g=4.1$ and the multiline signals, fig.4.08. The apparent interconversion between the low temperature generated $g=4.1$ and the multiline signal has been suggested to arise from the $g=4.1$ acting as an intermediate state between the S_1 and the S_2 states (Casey and Sauer, 1984) or the S_2 and S_3 states (Zimmermann and Rutherford, 1984) of the OEC cycle. The Zimmermann interpretation is made questionable by the generation of the low temperature $g=4.1$ form with 200K illumination, which is the case for inefficiently mixed PSII in EG or glycerol storage buffer (data not shown).

The development of $g=4.1$ signal by 130K illumination and interconversion to multiline signal upon 200K annealing may be carried out in a cyclic manner, with 130K illumination generating $g=4.1$ signal intensity, with subsequent annealing at 200K interconverting the $g=4.1$ signal into multiline signal intensity, figure 4.09. The signal intensity of the $g=4.1$ signal formed by the second illumination is less than that for the initial illumination, and implies that the interconversion of the first generation of $g=4.1$ signal blocks out the PSII centres from subsequent turnover, suggesting that the $g=4.1$ signal is an intermediate electron transfer event between the S_1 and S_2 states, as was proposed by Casey and Sauer (Casey and Sauer, 1984). That only one type of Mn based ESR signal may arise from each PSII centre implies that either the signals arise

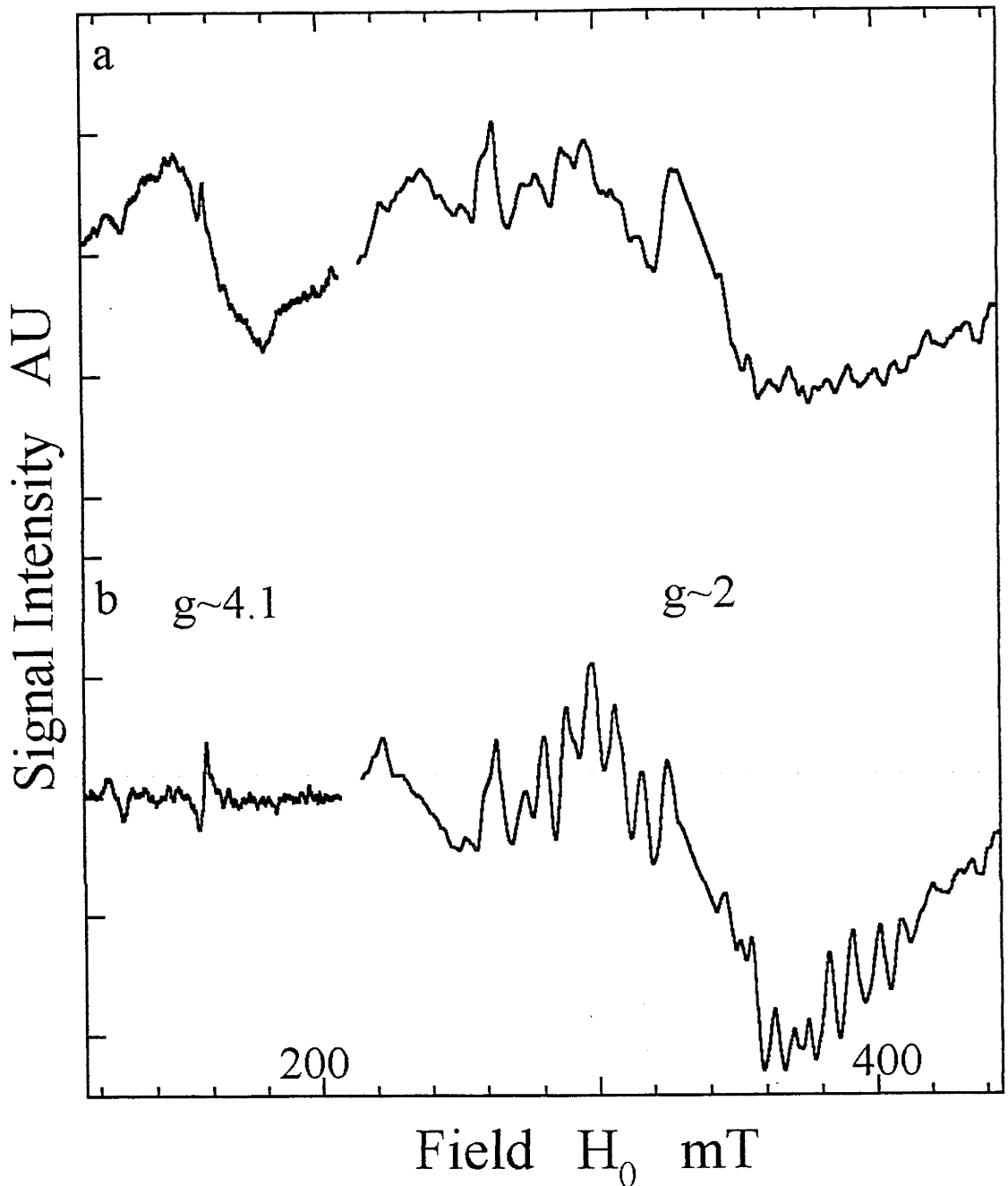


Figure 4.08. S_2 state signals generated in PSII cryoprotected with 30% v:v ethylene glycol a). illuminated at 130K indicating $g=4.1$ signal formation independent of multiline signal formation, b). sample from (a) annealed in darkness at 200K for 100s, showing the loss of $g=4.1$ signal leading to formation of multiline signal. Spectrometer conditions as per fig. 4.04.

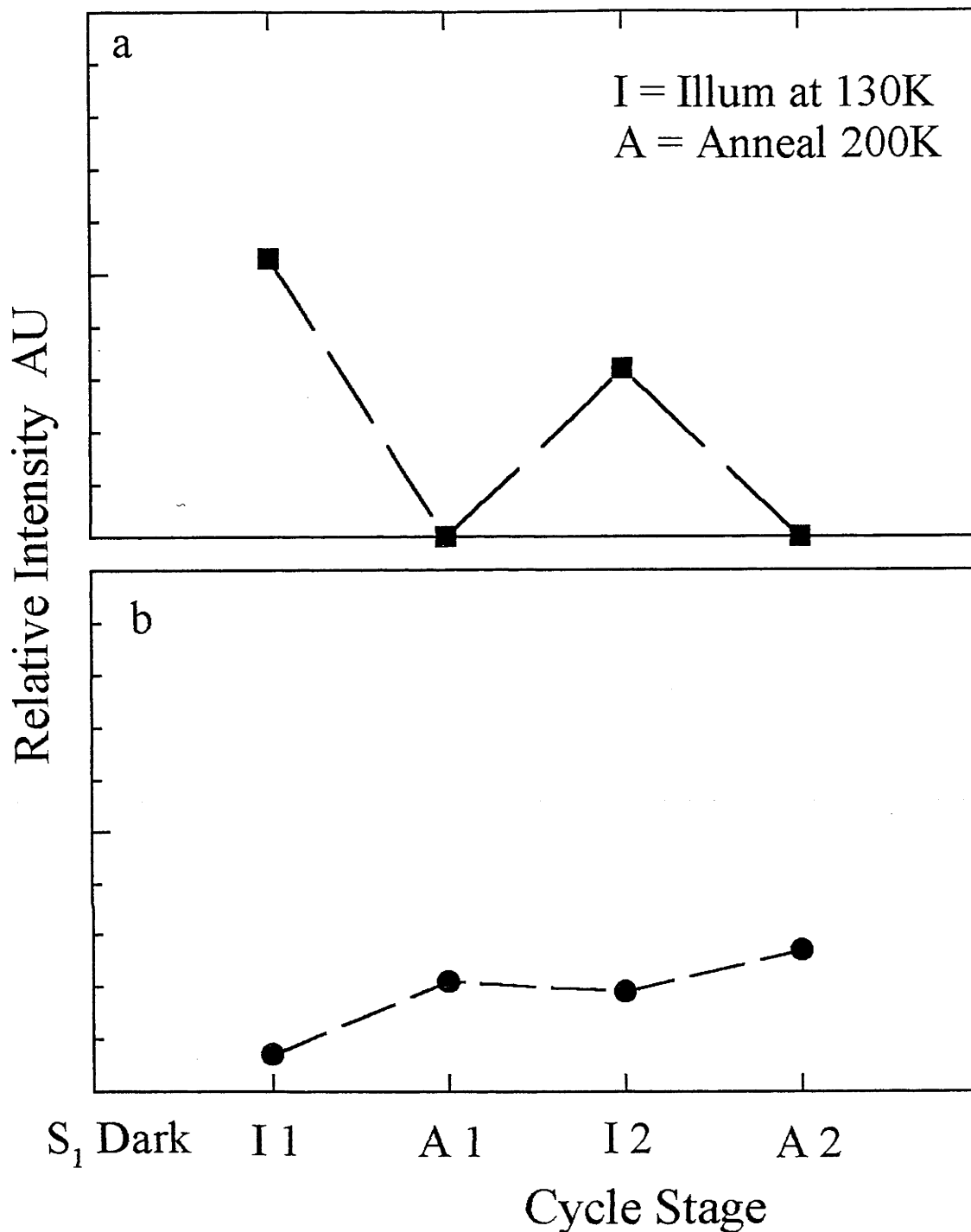


Figure 4.09. Effects of cyclic illumination at 130K and subsequent annealing at 200K on PSII cryoprotected with 30% v:v ethylene glycol. a). the $g=4.1$ signal intensity measured during two illumination at 130K / dark anneal at 200K cycles, b). the multiline signal developed during two illumination at 130K / dark anneal at 200K cycles. Relative intensities are based on the (a) combined $g=4.1$ signal intensity developed during the two illumination cycles and (b) the multiline signal intensity developed by illumination of equivalent samples at 200K.

from different states of a single Mn complex, with interconversion due to an electron reshuffle (deRose, et al., 1995) and possible ligand rearrangement upon warming the sample to 200K (de Paula, et al, 1985) or that the intermediate centre generating the $g=4.1$ signal is prevented from undergoing a second electron transfer due to electrostatic effects at the illumination temperature (Styring and Rutherford, 1988), implying a change in protein environment being required with each electron transfer event (compensating H^+ transfer or release perhaps).

The generation of $g=4.1$ signal by illumination at 130K and interconversion to the multiline signal occurs both with and without additional alcohol in the sample buffer, figure 4.10. However, some differences between the two sets of samples were found, with a signal developed in the samples without additional alcohol when compared to the additional alcohol present samples. Upon annealing, the non alcohol treated samples displayed interconversion of the $g=4.1$ to multiline signal states and also the generation of a broad signal, centred at $g\approx 2.04$ width $\sim 40mT$, underlying the multiline signal.

4.5 ESR Line shape Measurements Q Band (35GHz)

4.5.1 Multiline Signal

Measurements of ESR spectra at higher microwave frequencies allows one to alter the balance between the separate magnetic interactions which contribute to the spin Hamiltonian. The ESR line shapes vary with frequency reflecting the various field dependences of each Hamiltonian component. Measurements of the multiline signal generated in sucrose cryoprotected PSII illuminated at 200K and for the EG cryoprotected PSII illuminated at 130K are shown in figure 4.11.

It should be noted that the significant multiline signal intensity observed in the 130K illuminated EG PSII arises as a consequence of the relative sizes of the samples for the X and Q band experiments. The Q band sample is only one fourth the volume of the X band sample, and so has a much lower thermal mass. The Q band samples are subjected to greater temperature changes due to effects such as; (i) non fluorescent energy quenching during illumination, decay of the Chl^* excited state back to the ground state with release of the photon energy as heat, and (ii) sample temperature increases during loading of the sample through the waveguide aperture into the cavity and cryostat. As shown in section 4.4, raising the temperature of the PSII samples leads to electron redistribution which seriously affect the observability of the ground state $g=4.1$ signal. Serendipitously, this allows the measurement of the multiline signal in the EG PSII 130K illuminated samples. Procedures were refined to enable observation of the ground state form of the $g=4.1$ signal; illumination at lower temperatures (120K - 125K) and improving the loading

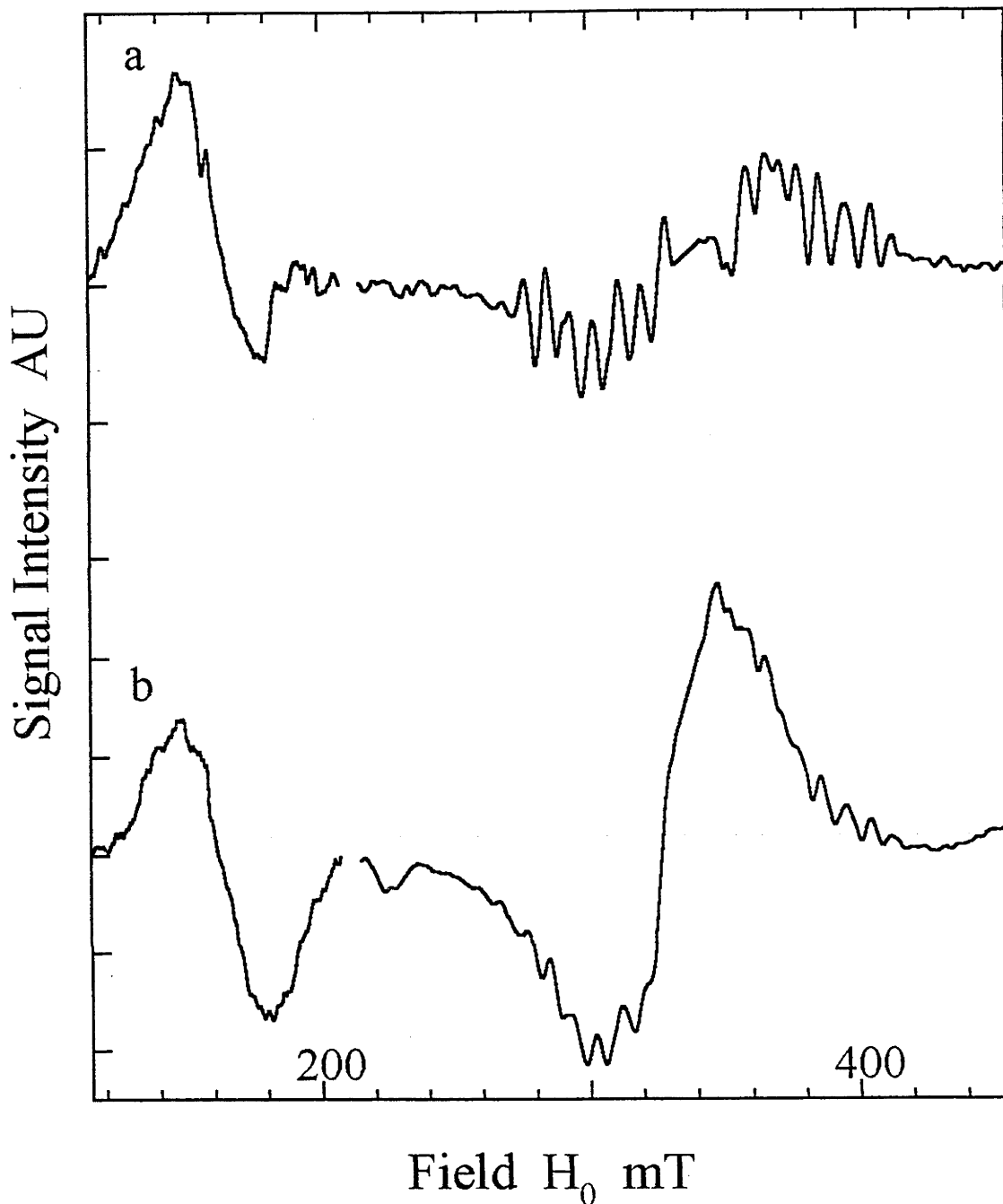


Figure 4.10. S_2 state signals developed in PSII cryoprotected by 30% v:v ethylene glycol. Spectra are the subtraction difference for samples illuminated at 130K minus post dark annealed at 200K spectra. a). PSII sample with 4% v:v ethanol added to the sample buffer prior to the illumination step, b). PSII sample in which no additional alcohol was added, ie illuminated without additional ethanol in the sample buffer. Spectrometer conditions as per fig. 4.04.

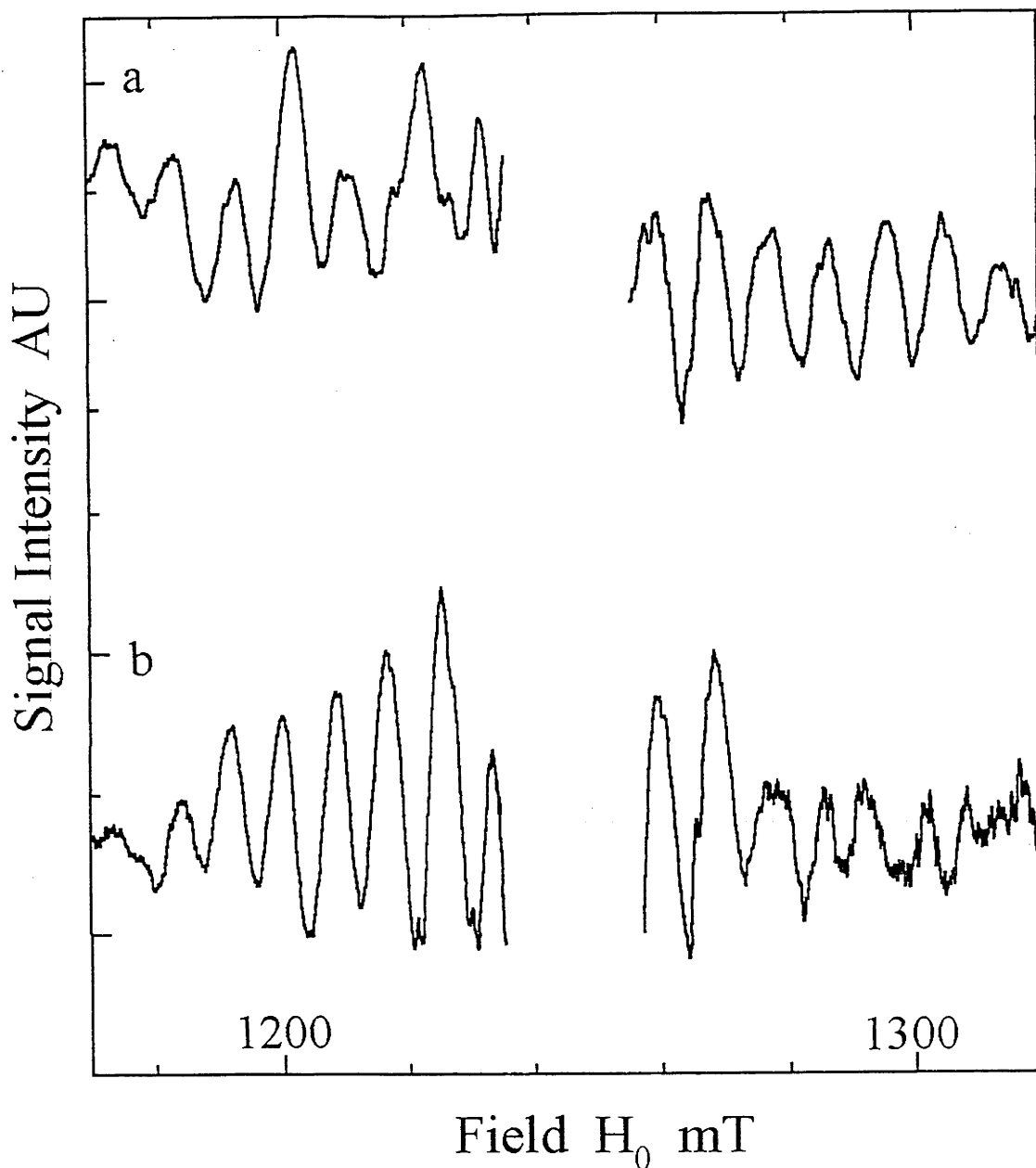


Figure 4.11. Q Band S_2 state multiline signals a). PSII cryoprotected with 0.4M sucrose illuminated at 200K, b). PSII cryoprotected with 30% v:v ethylene glycol illuminated at 130K. The presence of significant multiline intensity in (b) arises due to the small volume of sample used in the Q band experiment, $\sim 12\%$ of the volume of the X band sample. This Q band sample is subject to greater temperature changes during the processes of insertion into the ESR cavity, see text. Spectrometer conditions: temperature 9K, microwave frequency 34.7 GHz, microwave power $100\mu\text{W}$, modulation frequency 100KHz, modulation amplitude 1.1mT.

procedure to quickly seal the loading aperture, reapply the liquid helium flow to reduce the temperature, and adjusting the sample position with the helium flow on.

4.5.2. The $g=4.1$ signal

As the signals generated in PSII samples observed near $g=4$ arise from centres of spin $3/2$, contributions from Hamiltonian terms which affect the apparent g value (such as the zero field splitting (ZFS) terms) will be exaggerated. The contribution of the ZFS terms to the g tensor components will be highlighted due to the frequency dependence of the Zeeman term at the higher field of Q band ($g=2$ being at $\sim 1.2\text{T}$ at 35GHz cf $\sim 0.34\text{T}$ at 9.4GHz). The $g=4.1$ signals generated in the Sucrose PSII illuminated at 200K and the EG PSII illuminated at 125K are shown in fig.4.12. In comparison to the line shapes of these signals at X band (9GHz), where the g value and line shape were almost identical, at Q band, the two $g=4.1$ signals are significantly different. Both signals show strong axial nature.

The sucrose PSII spectrum shows a splitting due to slight deviation from axial symmetry of the g tensor. The g_{\perp} components are $g_{\perp 1} = 4.34 \pm 0.02$ and $g_{\perp 2} = 4.08 \pm 0.02$, with a $g_{\perp av} = 4.25 \pm 0.02$ and a peak to trough width of 48mT .

The EG PSII spectrum displays a much broadened line shape with a peak to trough width of $\sim 67\text{mT}$. The $g_{\perp av}$ for this signal has shifted upfield (to lower g value) to 3.98 ± 0.02 . The crossing region of this signal is very narrow, with broad upfield and downfield wings. This may be due to the presence of slight orthorhombic distortion (as above) from axial symmetry within the environment of the centre giving rise to this signal.

Previous modelling studies on the $g=4.1$ signal on unoriented and oriented PSII samples measured at different frequencies have assumed that all observations of the $g=4.1$ were of one type of signal (Haddy, et al, 1992, Kim, et al, 1992, Brudvig and Crabtree, 1986, Zimmermann and Rutherford, 1984, Zimmermann and Rutherford, 1986, Astashkin, et al., 1994a). All the differences between the $g=4.1$ signals generated by different illumination protocols and sample buffer regimes have been assumed to arise from changes in the magnetic interactions of a single Mn tetramer (de Paula, et al, 1986c, Beck and Brudvig, 1988a, Kim, et al, 1992, Haddy, et al, 1992, Astashkin, et al., 1994a). The spectra shown in figures 4.06 and 4.12 clearly show the ability to generate two distinct forms of the $g=4.1$ signal and outline the conditions under which each is generated. Although the X band line shapes of the $g=4.1$ signals generated by the different cryoprotectant and illumination regimes are quite similar, the Q band line shapes indicate that these signals are quite distinct, arising from separate Mn structures, possibly within different environments within the protein.

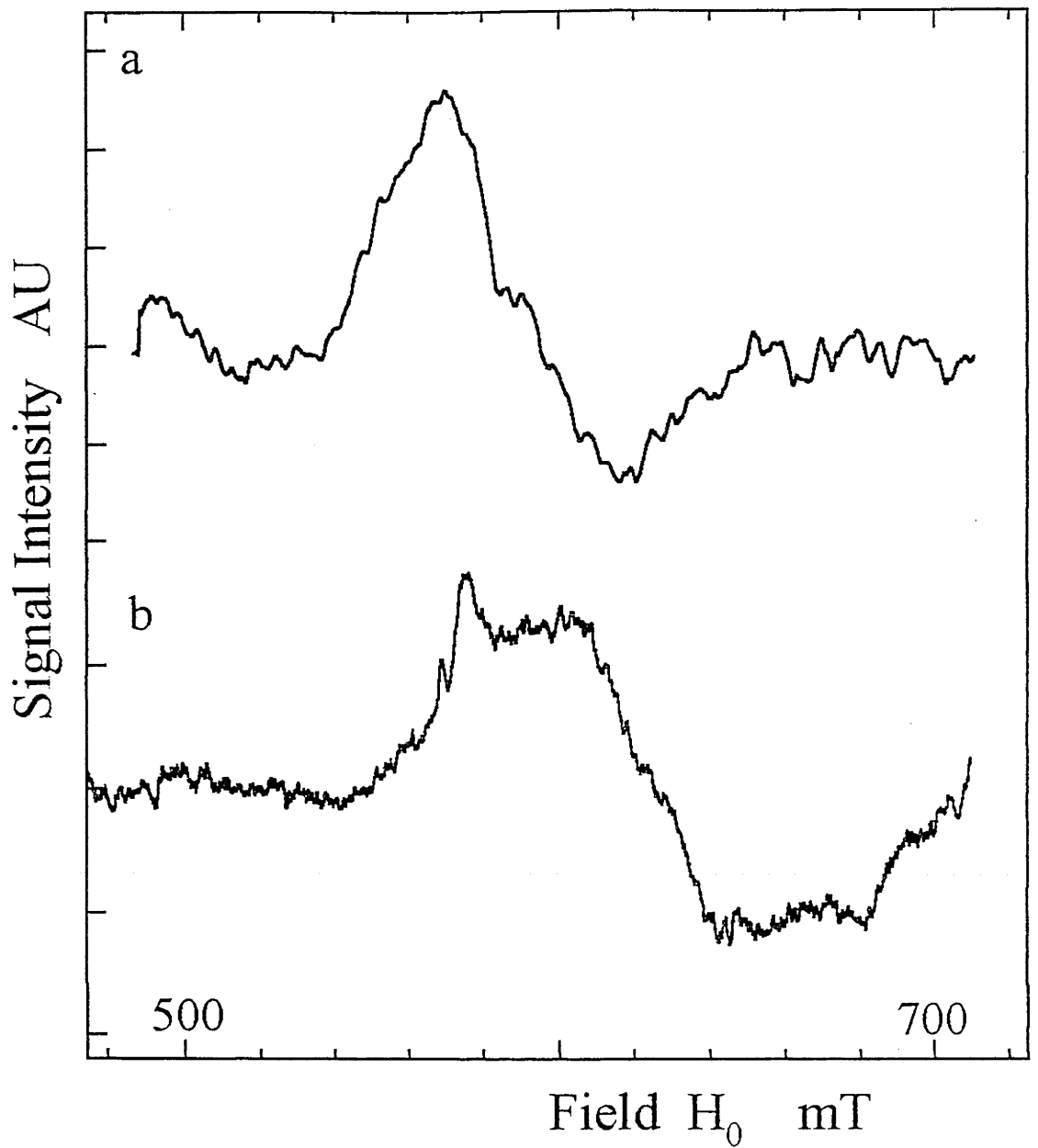


Figure 4.12. Q Band S_2 state $g=4.1$ signals. a). PSII cryoprotected with 0.4M sucrose, illuminated at 200K, b). PSII cryoprotected with 30% v:v ethylene glycol, illuminated at 130K. Spectrometer conditions as per fig. 4.11.

4.6. Temperature Dependence Studies

Most studies to date have used the line shapes of the multiline and $g=4.1$ signals at different microwave frequencies as the basis for modelling analyses, using Hamiltonian simulations to probe the spin state and paramagnetic centre environment giving rise to each of these signals. Along with temperature dependence data for the multiline in the presence of monoalcohols and the $g=4.1$ signal from EG PSII illuminated at 130K or from inhibited PSII, it has been hypothesised that all four Mn interact as a tetrameric site to generate these signals, with slight changes to terminal and bridging ligand structures giving rise to the changes in magnetic interactions required to develop each of the multiline and $g=4.1$ signals (Kim, et al, 1992, Zimmermann and Rutherford, 1986). Pace and coworkers (Pace, et al., 1991) have observed that, under conditions where alcohol is omitted from the PSII sample buffer, the multiline and a $g=4.1$ signal are cogenerated, displaying complimentary deviations from Curie temperature dependence behaviour. This is in apparent conflict with earlier conclusions that the $g=4.1$ signal arose from an isolated ground state (de Paula and Brudvig, 1985b, de Paula, et al, 1986c, Hansson, et al, 1987).

We now consider this ambiguity in the nature of the $g=4.1$ signals observed. The overall aim of this section is to re-examine the temperature dependences of each of the multiline and $g=4.1$ signals generated in the S_2 state of PSII with either sucrose or EG as cryoprotectant. This will give insight into the spin state of each signal as, if higher excited states are detected, the nature of the exchange interactions leading to the development of each signal may be clarified.

From the spectra of the multiline and $g=4.1$ signals presented earlier, the different protocols for isolating PSII containing samples, ie the Bricker and BBY procedures, resulted in essentially equivalent ESR signal line shapes for the multiline and / or the $g=4.1$ signals generated under equivalent illumination and cryoprotectant conditions. That the two procedures generate equivalent S_2 state behaviours leads to the conclusion that the properties of the PSII giving rise to the individual multiline and $g=4.1$ signal types must be due to cryoprotectant, illumination and sample buffer modification effects only. The temperature dependences presented are from a combination of the results for each illumination and cryoprotectant regime for the two procedures used for PSII preparation.

To avoid effects of power saturation of signal amplitude, the procedure outlined in Chapter 3 whereby the signal intensities were measured from the initial slopes of the power saturation plots, extrapolated to zero power, were utilised for all signal temperature dependences.

4.6.1 Sucrose PSII Illumination at 200K

The combined results for the multiline and $g=4.1$ signals generated in sucrose PSII illuminated at 200K are shown in fig.4.13. These results are consistent with those of Pace et al

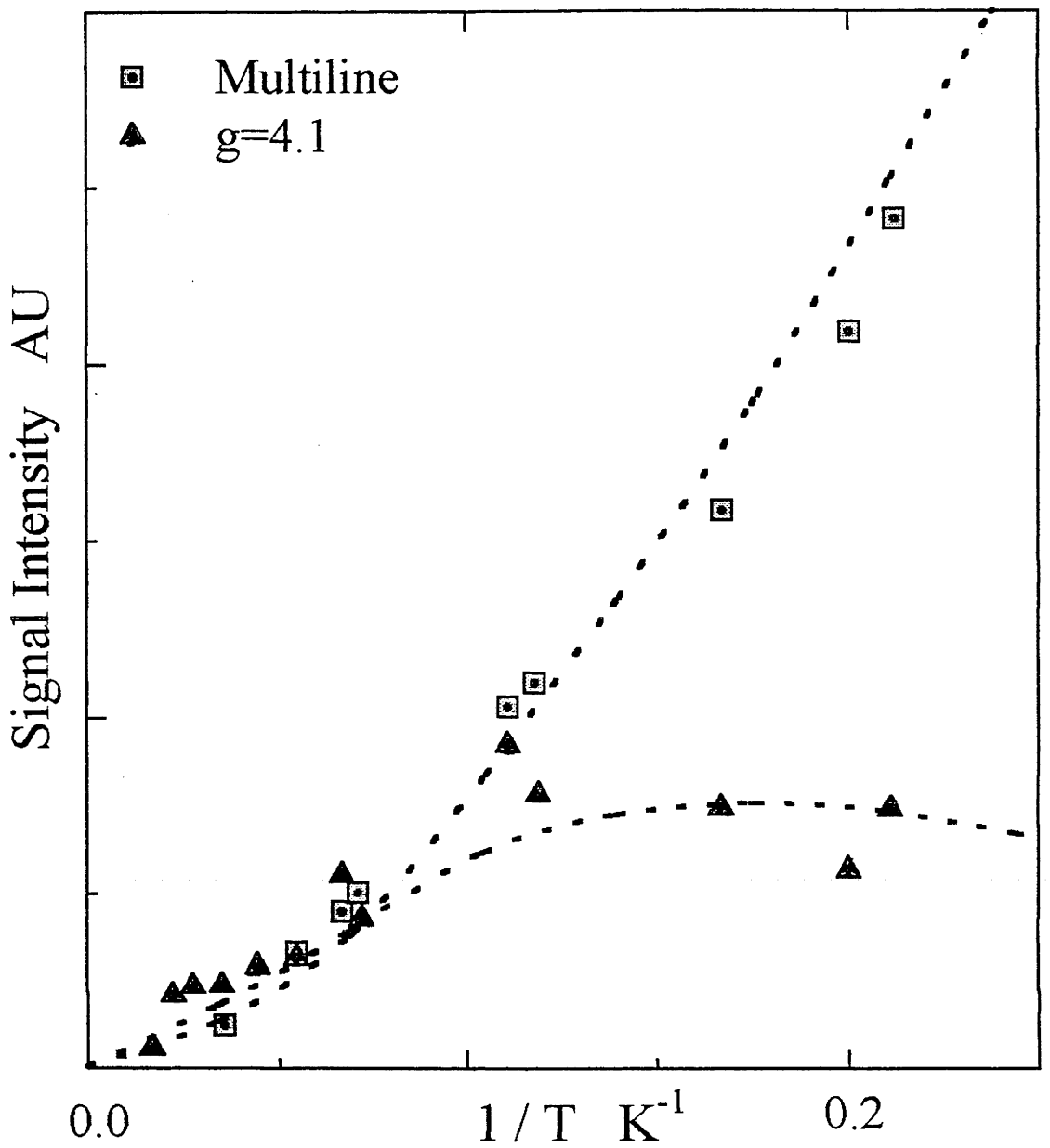


Figure 4.13. Temperature dependence of the S_2 state multiline (\square) and $g=4.1$ (\blacktriangle) signals cogenerated in PSII cryoprotected with 0.4M sucrose illuminated at 200K. Signal intensities are determined from extrapolating the power saturation curve to zero microwave power at each temperature for each signal. Dotted lines represent the estimation of the signal intensities for the $S=1/2$ (multiline) and $S=3/2$ ($g=4.1$) spin states based on the Boltzmann energy statistics according to equation 4.1, see text, with an exchange constant $|J/k| = 3K$, as per Pace, et al, 91.

(Pace, et al., 1991), whereby the multiline and $g=4.1$ signals show complimentary deviations from Curie behaviour. The most simple magnetic exchange system containing Mn which may give rise to such signals and their respective temperature dependence behaviours is an antiferromagnetically exchange coupled Mn III - IV dimer, with $S=1/2$ ground state of a total spin $7/2$ (Pace, et al., 1991). The ground state gives rise to the multiline signal ($S=1/2$) and the first excited state gives rise to the $g=4.1$ signal ($S=3/2$). From figures 4.06 and 4.12, in which the X band and Q band line shapes could be considered consistent with a quasi axial system, the temperature dependence behaviour supports the spin state assignment, $S=3/2$ for the $g=4.1$ signal. The signal intensity of the first excited state, ie this $g=4.1$ signal, is observed to be significant at low temperatures. An antiferromagnetically exchange coupled Mn III - IV dimer with a low lying first excited state is consistent with the model of Pace and coworkers, where the exchange constant J was suggested to be of the order of $J/k \approx -3K$ (Pace, et al., 1991). Figure 4.13 shows the spin populations $I(T)$ calculated for such a Mn III - IV exchange coupled dimer, whereby;

$$I(T) = I_0 \frac{S(S+1) \exp(-E_S / kT)}{T \sum_S (S(S+1) \exp(-E_S / kT))} \quad (4.1)$$

where $E_S = J(S_1(S_1+1) + S_2(S_2+1) - S(S+1))$

$S = 1/2, 3/2, 5/2, 7/2$ (Total spin)

$S_1 = 2, S_2 = 3/2$ (Mn III, Mn IV)

$k =$ Boltzmann constant

$T =$ temperature in Kelvin

$J =$ Exchange coupling constant (J/k set to -3K as per Pace et al 91)

$I_0 =$ total spin centre population

Previous multifrequency studies and spectral simulations based on model spin Hamiltonians have asserted that four Mn ions must be magnetically exchange coupled to explain the complexity of the multiline signal, especially at S band (Dismukes and Siderer, 1981, Dismukes, et al, 1982, Haddy, et al, 1989, Kim, et al, 1992, Kusonoki, 1992). More recently, a spectral simulation of the multiline signal at each of S, X and Q bands has shown that an isolated Mn dimer in a suitably anisotropic ligand environment may generate a spectrum very similar to that observed for the S_2 state multiline signal (Åhrling and Pace, 1995). This infers that such a dimer generating the multiline signal in the ground state should also generate a $g=4$ signal. Depending on the magnitude of the exchange coupling, this signal may also be visible at low temperature. In part, the question of whether a Mn tetramer or a Mn dimer is required to explain the ground state multiline signal, may be clarified by close examination of the low field region (high g value), examining for possible higher spin states. If, for the moment, we assume a dimer

model for the system giving rise to the multiline signal, such as in fig 4.14a, then the next thermally accessible higher energy spin state should be an $S=5/2$ state. As the first excited state ($S=3/2$) gave rise to a signal which displayed a line shape consistent with quasi axial symmetry, the signal line shape for a quasi axial $S=5/2$ state should generate intensity mainly in the $g=6$ region.

To explore the possibility of thermally accessible higher spin states, close examination of the line shape of the $g=4.1$ signal generated in the sucrose PSII illuminated at 200K was undertaken. Figure 4.15 shows the $g=4.1$ signal line shape over the temperature range 5K to 60K. All spectra were recorded with the same microwave power, 6.32 mW. The signal line shapes and intensities for the lowest temperature will be subject to minor saturation effects. This is the widest temperature range for observation of a $g=4.1$ line shape reported. The most significant change in the line shape of the $g=4.1$ signal over the temperature range 5K to ~ 35 K appears as an intensity development below the low field edge. This is not accompanied by comparable changes on the higher field edge of the $g=4.1$ signal, as would be the case for a simple temperature broadening effect. This extra intensity at the low field edge builds in magnitude so that, at ~ 28 K, it rises above that of the diminishing $g=4.1$ signal intensity. At higher temperatures, it is apparent that this intensity builds as an independent signal at a field position overlapping with the low field edge of the $g=4.1$ signal. To deconvolute this 'new' signal from that of the overlying $g=4.1$ signal, it was assumed that the symmetrical line shape of the 5K spectrum of the $g=4.1$ signal corresponded to the 'pure' signal shape for this species. By scaling the $g=4.1$ signal recorded at 5K to its signal intensity at each of the other temperatures, subtraction should leave only the line shape of the new $g\sim 6$ signal, fig. 4.16. This process was undertaken for the temperature range 9K to 36K, fig.4.17, allowing examination of the "new" signal arising at higher temperatures. This signal, centred at $g\approx 6.11\pm 0.05$ (named here as the $g\sim 6$ signal) has field position consistent with that expected for a quasi axial spin $5/2$ centre, and is assigned to the second excited state of the sucrose PSII multiline centre. The main feature of this signal is the absorbance resonance centred at $g\sim 6.1$. The line shape of the $g\sim 6$ signal appears to evolve as intensity is developed below ~ 25 K, and decays, above ~ 37 K, where hyperfine features on or underlying the $g\sim 6$ signal appear ($T = 45$ K to 60K). In the $g\sim 6$ region, both signal line shape and intensity are observed to develop as could be expected for the populating of the proposed second excited $S=5/2$ state.

The temperature dependence of this $g\sim 6$ signal gives an insight into the overall magnetic exchange interplay between the four Mn ions within the OEC. The temperature dependence of the $g\sim 6$ signal is measured using the double integral intensity of the signal between the field range 70mT and 110 mT. Figure 4.18 shows the temperature dependence plots for the multiline (a), the $g=4.1$ (b) and the $g\sim 6$ (c) signals. The dashed lines are theoretical curves for the spin state populations for the exchange coupled isolated Mn dimer model from fig. 4.14 with $J/k = -3.5$ K. Each of the experimental temperature dependences are observed to be similar to the Boltzmann

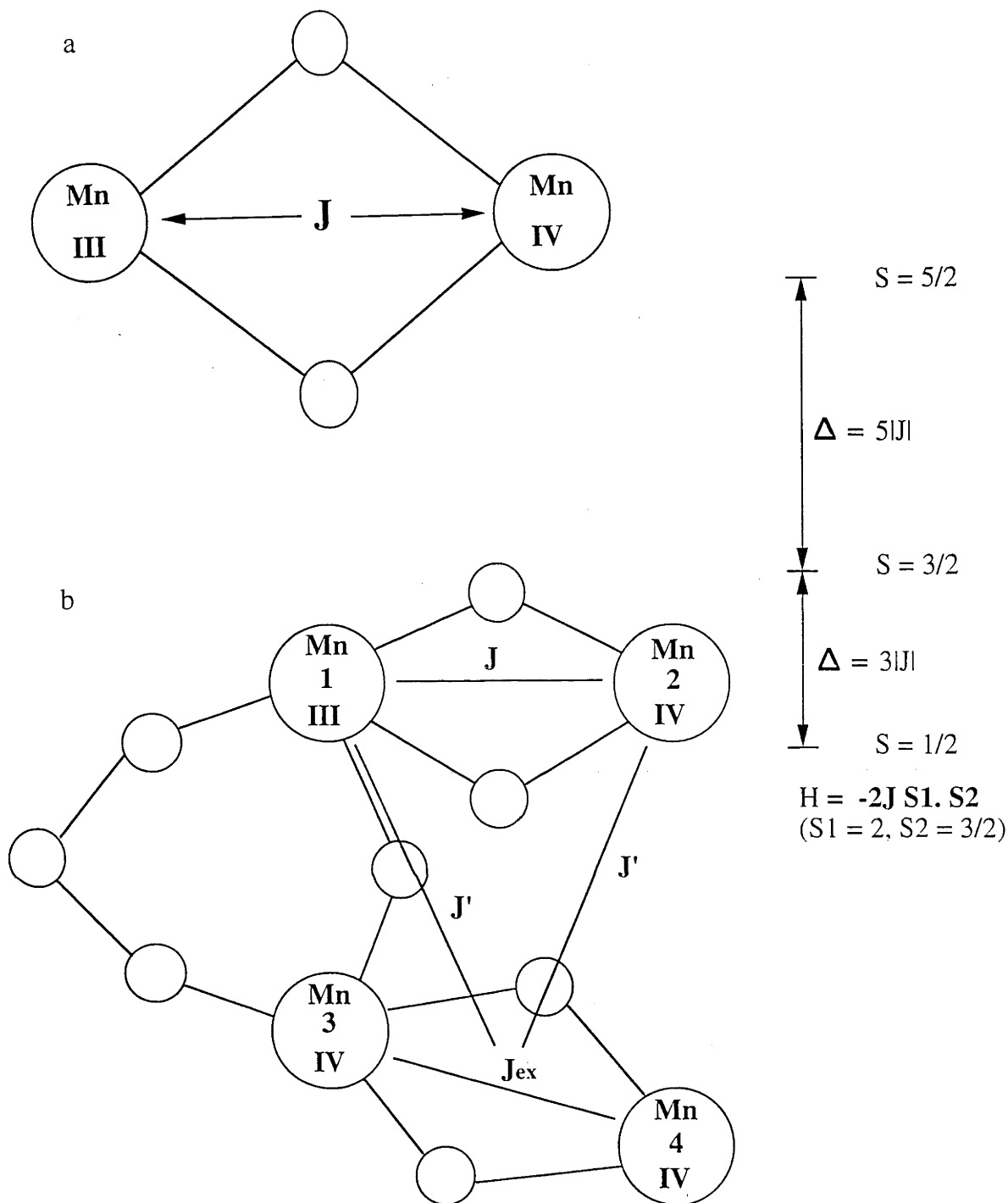


Figure 4.14. Model structures for the centre giving rise to the S_2 state multiline and $g=4.1$ signals generated in PSII cryoprotected with 0.4M sucrose illuminated at 200K. a). Representation of an antiferromagnetically exchange coupled Mn heterodimer, nominally Mn III-IV. Energy levels are as indicated for exchange interaction $H = -2J S_1 \cdot S_2$ b). Coupled dimer of dimers tetramer model based on the models of Yachandra, et al, 93 and Kusunoki, 92. Spin states initially determined by exchange at one of the Mn dimers (similar in nature to the dimer in (a)), the second dimer (nominally Mn III-III or Mn IV-IV) influencing the Hyperfine and Zero Field interactions. Higher spin states of the heterodimer component may be affected by population of “excited” higher spin states of the second dimer.

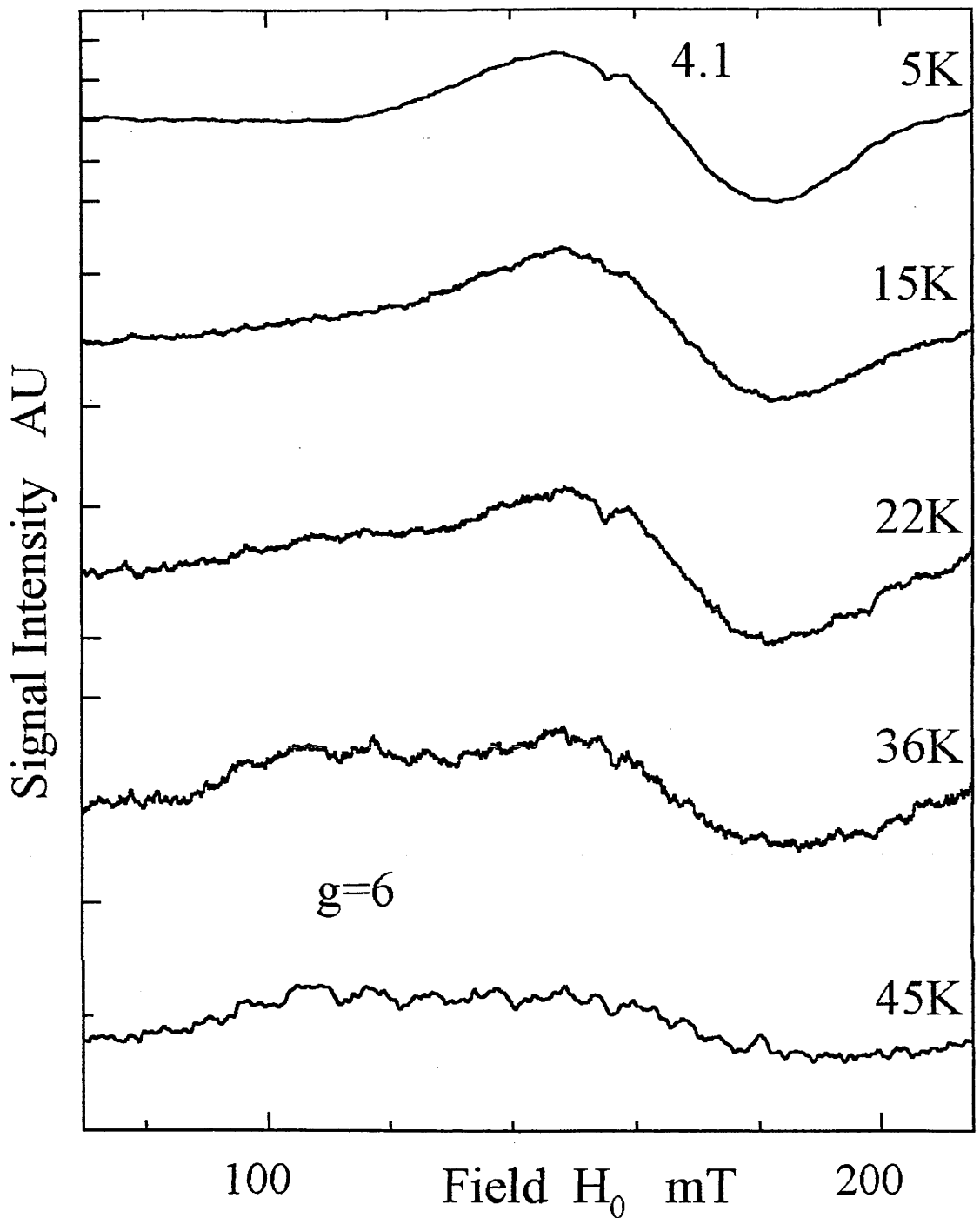


Figure 4.15. Temperature dependence of the line shape of the S_2 state $g=4.1$ signal generated in PSII cryoprotected with 0.4M sucrose illuminated at 200K. Spectra are resultant of illuminated minus dark 295K annealed spectra. Spectrometer conditions: temperatures as indicated, microwave frequency 9.42 GHz, microwave power 6.32mW, modulation frequency 100 KHz, modulation amplitude 1.4mT.

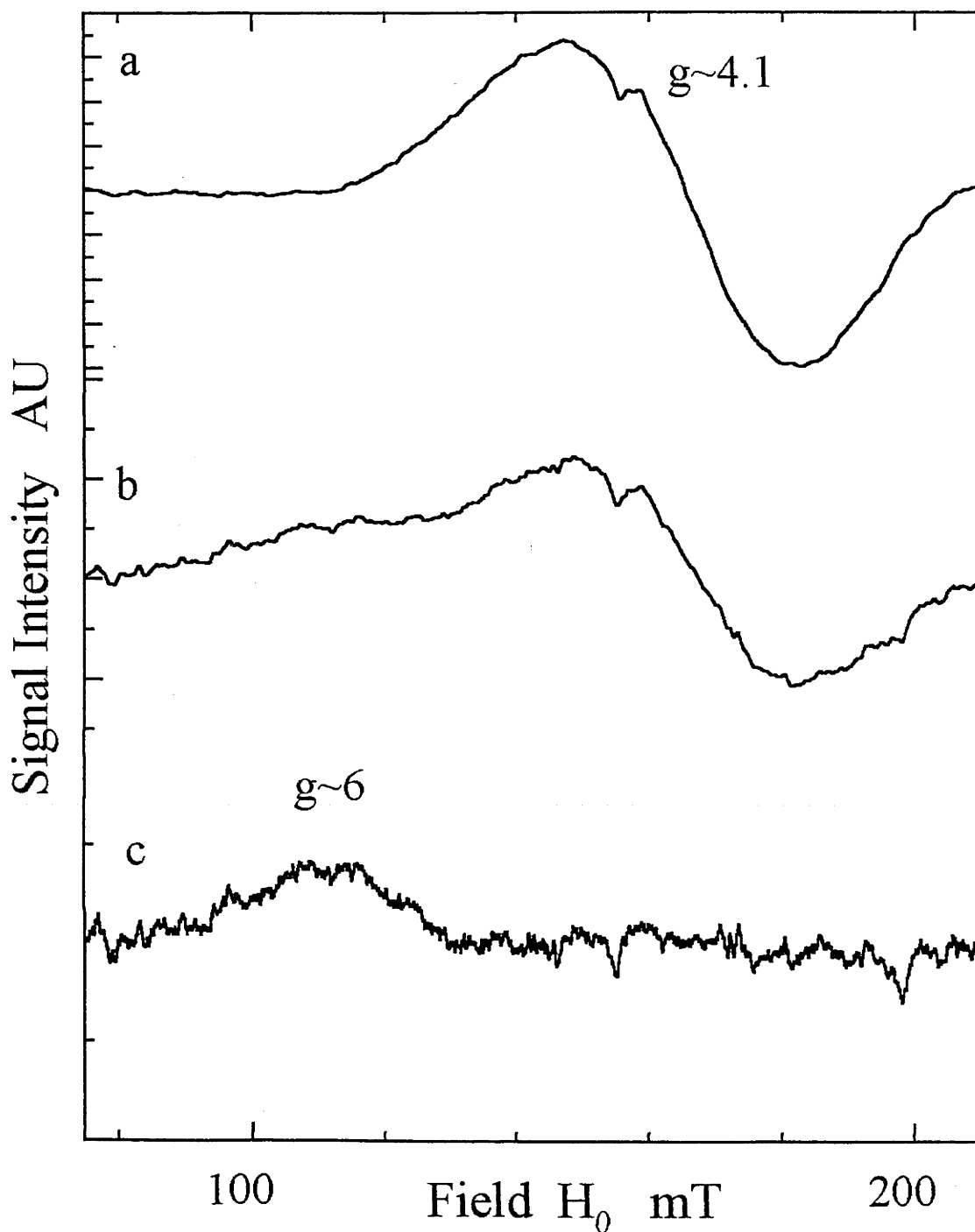


Figure 4.16. Deconvolution of the signal intensity developed on the low field shoulder of the S_2 state $g=4.1$ signal generated in PSII cryoprotected with 0.4M sucrose, illuminated at 200K. a). $g=4.1$ signal recorded at 5K, b). $g=4.1$ signal recorded at 22K, c). spectrum of the subtraction resultant for the $g=4.1$ signal intensity measured at 5K scaled to the intensity measured at 22K. Spectrometer conditions as per fig. 4.15.

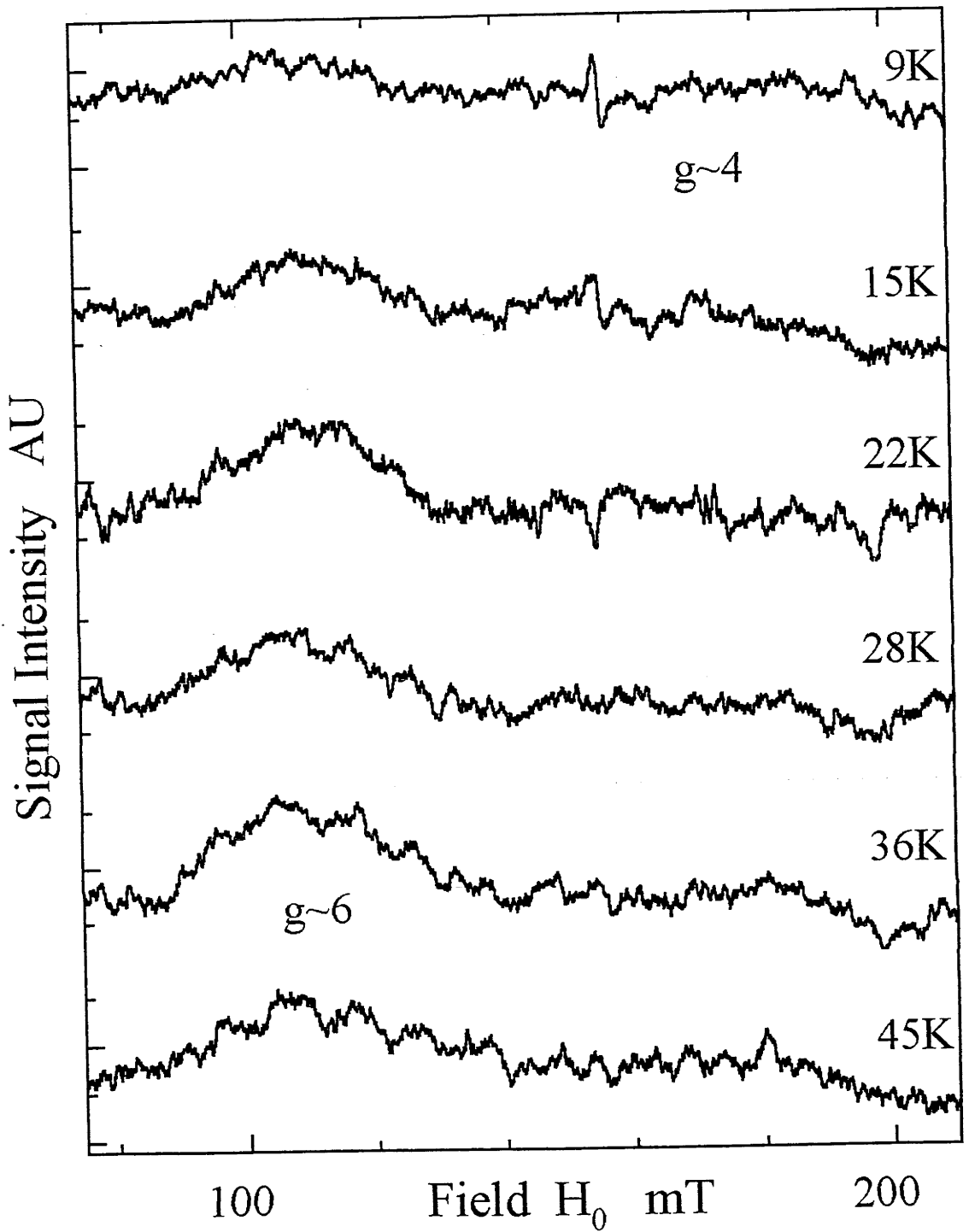


Figure 4.17. Temperature dependence of the line shape of the resultant spectra as per fig. 4.16, undertaken for the temperature range 9K to 45K. All spectra are shown for an equivalent intensity scale. Spectrometer conditions as per fig. 4.15.

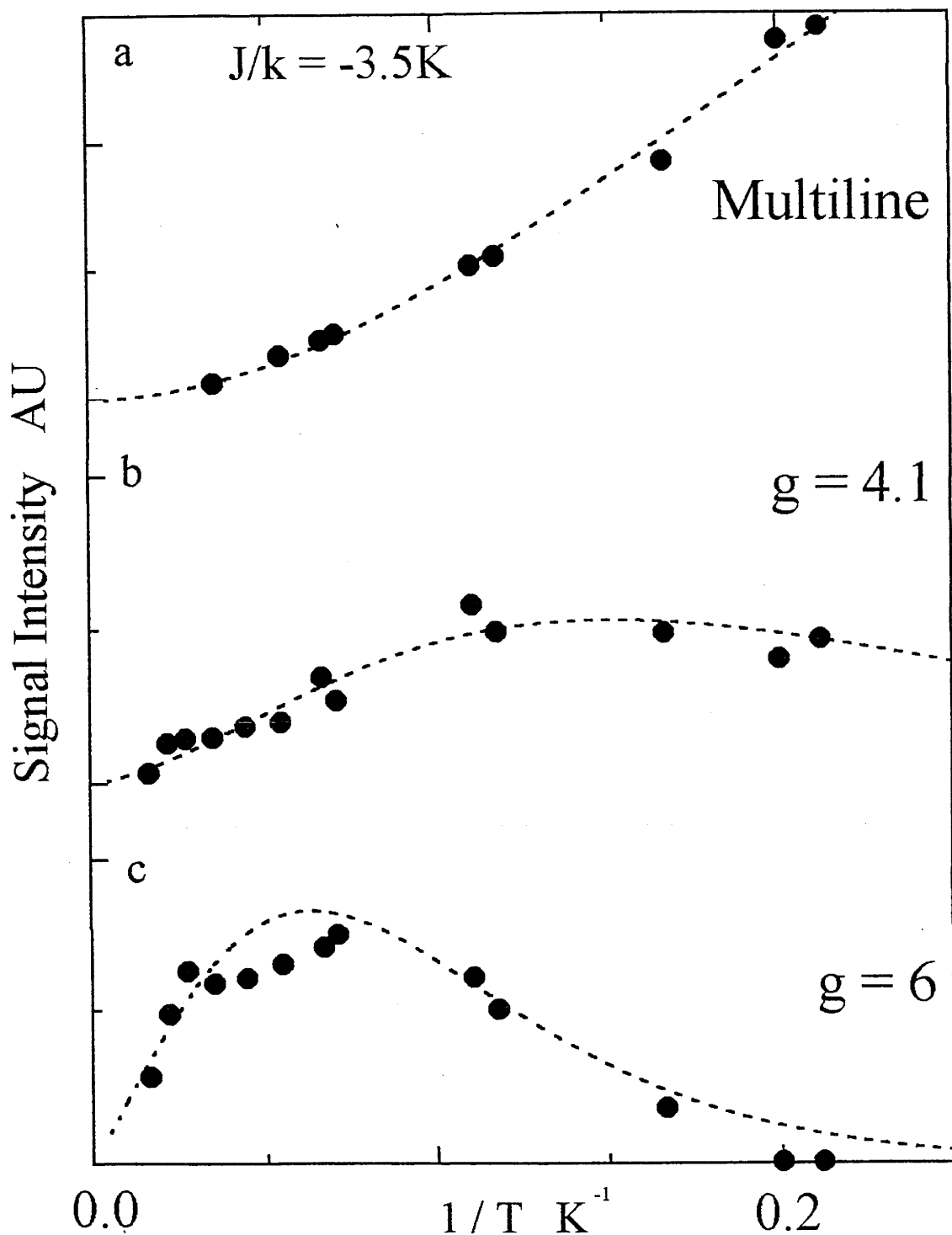


Figure 4.18. Temperature dependences of the signal intensities of the S_2 state multiline, $g=4.1$ and $g\sim 6$ signal deconvoluted from the difference spectra displayed in fig. 4.17. Signal intensities of the multiline and $g=4.1$ signals measured from the extrapolation of the power saturation to zero microwave power, the signal intensity of the $g\sim 6$ signal determined by double integration of the signal resolved between 85mT and 145mT. Dotted lines are the spin populations based on Boltzmann statistics as per fig. 4.13 with exchange constant $|J/k| = 3.5K$. The intensity scales are arbitrary due to the different methods of signal quantisation.

statistical spin state population for the $S=1/2$ ground (multiline), $S=3/2$ first excited ($g=4.1$) and $S=5/2$ second excited ($g\sim 6$) states of the isolated dimer model, with single population number and single exchange coupling constant.

At this point, several preliminary conclusions may be drawn. (1). Only two Mn ions are required to form a magnetically exchange coupled complex that explains the spin states and signal intensities for the multiline, $g=4.1$ and $g\sim 6$ signals arising in the S_2 state of sucrose PSII illuminated at 200K. (2). The multiline signal, observed in various forms depending on the presence of alcohols and type of cryoprotectant, arises from a centre most probably consisting of a single magnetically isolated, antiferromagnetically exchange coupled Mn III - IV dimer. (3). As the multiline signal arises within one of the functional steps of the oxygen evolving cycle, as observed from the generation of the S_2 state by flashing through the S states and its period four periodicity (Dismukes and Siderer, 1981, Dismukes, et al, 1982, Hansson and Andreasson, 1982, Zimmermann and Rutherford, 1984), it is possible that the catalytic centre undertaking the water oxidation process requires only two functional Mn for oxygen evolution.

4.6.2. Ethylene Glycol Cryoprotected PSII

4.6.2.1. EG PSII Illuminated at 200K

With the illumination of EG PSII at 200K generating both multiline and $g=4.1$ signal intensity, (see figs 4.05 and 4.06, the comparison of these signals to those of the sucrose PSII illuminated at 200K is of interest. Rutherford and coworkers observed the cogeneration of both $g=4.1$ and multiline signal intensity in sucrose cryoprotected PSII in which additional polyalcohol (glycerol) was added to the sample buffer (Zimmermann and Rutherford, 1984, Zimmermann and Rutherford, 1986). The decay kinetics of the $g=4.1$ signal was observed to be biphasic, indicating the presence of two forms of the $g=4.1$ signal. The more rapid phase of the $g=4.1$ signal decay was observed to lead to an increase in multiline signal intensity (Zimmermann and Rutherford, 1984, Zimmermann and Rutherford, 1986). This was most probably due to the low temperature form of the $g=4.1$ signal interconverting to the multiline signal during the decay process. The second, slower phase component displayed parallel decay kinetics to the multiline signal. This slower decay component most likely represents the contribution of the excited state $g=4.1$ form, as per the sucrose PSII.

4.6.2.1.1. Multiline Signal

Figure 4.19 shows the temperature dependence of the multiline signal generated by 200K illumination of EG PSII. The temperature dependence indicates that the multiline signal generated under this condition arises from a ground state centre. The curve is almost Curie in nature, which is quite different to the temperature dependence of the sucrose PSII multiline

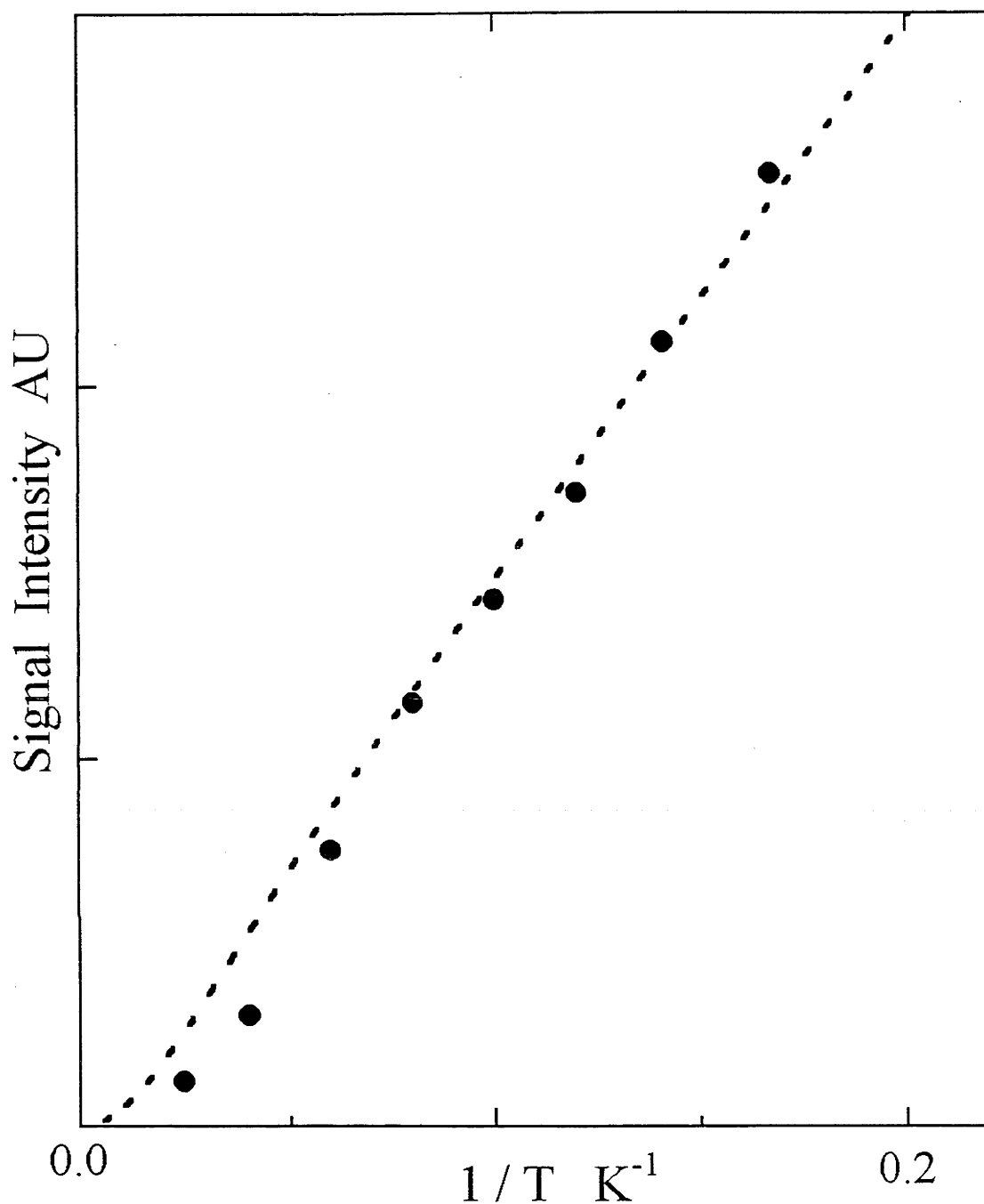


Figure 4.19. Temperature dependence of the S_2 state multiline signal generated in PSII cryoprotected with 30% v:v ethylene glycol, illuminated at 200K. Signal intensity recorded from the extrapolation of the power saturation to zero microwave power. Dotted line is the calculated intensity for the ground state ($S=1/2$) multiline signal based on the Boltzmann spin state model using equation 4.1, with exchange constant $|J/k| = 25\text{K}$.

signal, (see fig.4.13). The temperature dependence resembles that of the +alc multiline (Pace, et al., 1991) which is consistent with the presence of polyalcohol (EG) in the buffer.

Using the same model scheme as for the sucrose PSII multiline signal, the temperature dependence of the multiline arising in the EG PSII could be modelled by the same Boltzmann statistical approach for an exchange coupling constant of $J/k \sim 25K$.

4.6.2.1.2. $g=4.1$ Signal. Illumination at 200K

The temperature dependence of the cogenerated $g=4.1$ signal observed in the 200K illuminated EG PSII sample, figure 4.20, demonstrates that this $g=4.1$ signal arises from a ground state centre. In this study, illumination of EG PSII at 200K cogenerates ground state multiline and $g=4.1$ signals only. Further discussion on the nature of this ground state $g=4.1$ signal is presented in the next section.

The data presented here indicates that there exists two forms of the $g=4.1$ signal. From previous observations by other groups, these ground state and excited state $g=4.1$ signals may be cogenerated under some circumstances (Zimmermann and Rutherford, 1984). In the author's hands, the duality of the $g=4.1$ signal behaviour in the presence of EG has been observed to arise from inhomogenous mixing of the EG PSII storage buffer. In the preparation of BBY or Bricker PSII, the cryoprotectant is only introduced in the post solubilisation steps, and the mixing of polyalcohols (EG or glycerol) into sucrose cryoprotected PSII (Zimmermann and Rutherford, 1986), may generate the ground state $g=4.1$ in centres mixed well into the polyalcohol buffer, with the excited state $g=4.1$ form developed in centres not so well mixed (Zimmermann and Rutherford, 1986 and data not presented).

Comparing the temperature dependences of the multiline signals generated in EG PSII and sucrose PSII each illuminated at 200K and taking into account the data for the respective cogenerated $g=4.1$ signals, the EG PSII multiline signal must be of similar origin to that of the sucrose PSII illuminated in the presence of alcohols (Pace, et al., 1991). Previous studies on coupled metal complexes made to examine exchange interactions, have indicated that the coupling constant J is dependent on the nature of the ligand groups bridging the metal ions. For metal complexes with either μ -oxo or μ -hydroxo bridging ligands, the exchange constant was dependent on the protonation state of the bridging ligands (Knopp and Wieghardt, 1991, Baldwin, et al., 1993, Larson, et al., 1992b, Larson, et al., 1992a, Baldwin, et al., 1994). In essentially equivalent metal complexes, J for the μ -oxo ligands was observed to be large antiferromagnetic, (Cooper, et al., 1978, Inoue, 1978, Plaksin, et al., 1972, Goodson, et al., 1990, Baldwin, et al., 1993, Baldwin, et al., 1994) while the corresponding μ -hydroxo bridged complexes showed a J value that was much less antiferromagnetic, and in some complexes was observed to be slightly ferromagnetic, (Knopp and Wieghardt, 1991, Larson, et al., 1992b,

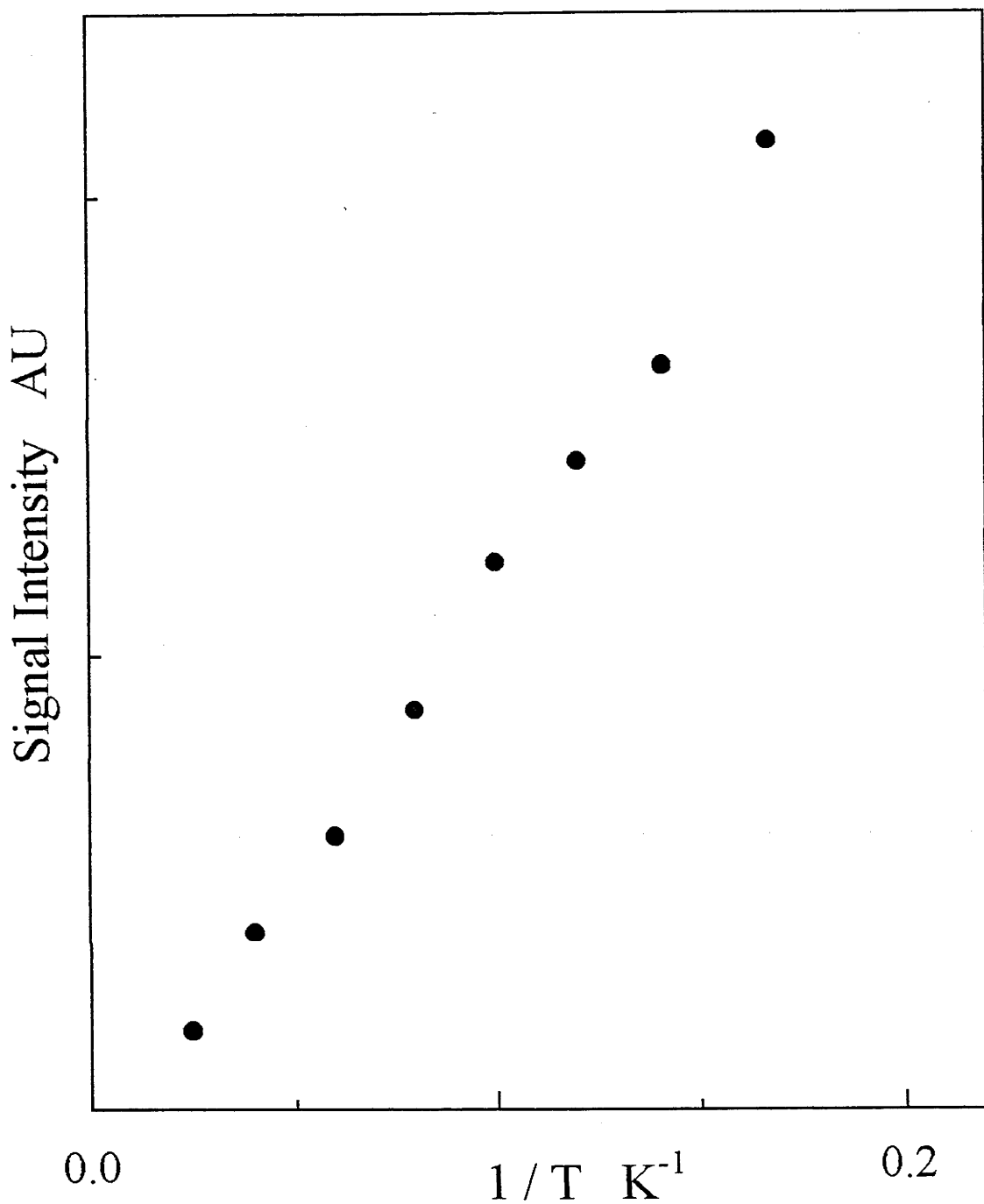


Figure 4.20. Temperature dependence of the S_2 state $g=4.1$ signal generated in PSII cryoprotected with 30% v/v ethylene glycol, illuminated at 200K, ie cogenerated with S_2 state multiline signal in these samples. Signal intensity determined by extrapolation of the power saturation curve to zero microwave power.

Larson, et al., 1992a, Baldwin, et al., 1993, Baldwin, et al., 1994). The temperature dependence behaviours of the multiline signals generated in sucrose PSII and EG PSII appears to show that the presence of the alcohol leads to an increase in J for what must be essentially an equivalent Mn containing complex. The inference from this is that the presence of the alcohol, as a monoalcohol (Pace, et al., 1991), or as polyalcohol (EG) here, leads to a change in the bridging ligand environment of the OEC complex, with the alcohol leading to an effective deprotonation of possible μ -hydroxo type ligands. This may arise from a 'loosening' of the protein environment, leading to movement of proton acceptor amino acid residues away from the bridging ligands and to an increase in the distance of the protons from the resultant μ -oxo ligands. In addition, the spin state population model predicts the presence of an excited state $g=4.1$ signal in the EG PSII multiline sample, and it is left for future work to examine for each of these possibilities.

4.6.2.2. $g=4.1$ signal. Illumination at 130K

The $g=4.1$ signal generated by illuminating ethylene glycol or glycerol cryoprotected PSII at 130K has been the main form of the $g=4.1$ signal studied. Previous reports have shown that this signal arises from a ground state centre (Hansson, et al, 1987, Vanngård, et al, 1992, de Paula, et al, 1986c). Line shape and Hamiltonian simulation studies of this $g=4.1$ signal ESR spectrum at different microwave frequencies, S band (4GHz), X band (9GHz) and P band (16GHz), have led to the suggestion that the signal arises from the middle Kramer's transition of a rhombic $S=5/2$ ground state centre (Haddy, et al, 1992). This assignment was recently supported by spin echo studies of the $g=4$ region signals (Kawamori, et al., 1993, Astashkin, et al., 1994b). However, Brudvig and coworkers have argued that, on the basis of the interconversion of this signal to the $S=1/2$ multiline signal upon warming of the sample to 200K, such a spin state change, from $S=5/2$ to $S=1/2$, would appear to require a too large exchange coupling interconversion for a Mn tetramer, requiring significant ligand shifting within an effectively frozen state (at 200K or -70°C) (de Paula, et al, 1986c). The model proposed by Brudvig and coworkers was for an $S=3/2$ ground state.

To generate a spin $3/2$ or $5/2$ ground state from a single electron turnover, the interaction of at least three spin centres is required. To date, no direct measurement of physical spin states has been undertaken, with the assignment of spin state being made as a result of the modelling of the ESR line shapes (at S, X and P band) (Vänngård, et al, 1992, Haddy, et al, 1992) and the fact that this $g=4.1$ signal arises from a ground state (de Paula, et al, 1986c, Hansson, et al, 1987). The spin state assignment was examined by measurement of the microwave field (H_1) dependence of the $g=4.1$ signal intensity in a two pulse ESEEM experiment (Kawamori, et al., 1993, Astashkin, et al., 1994b). Based on the Hamiltonians used for simulating the $g=4.1$ signal, the H_1 field

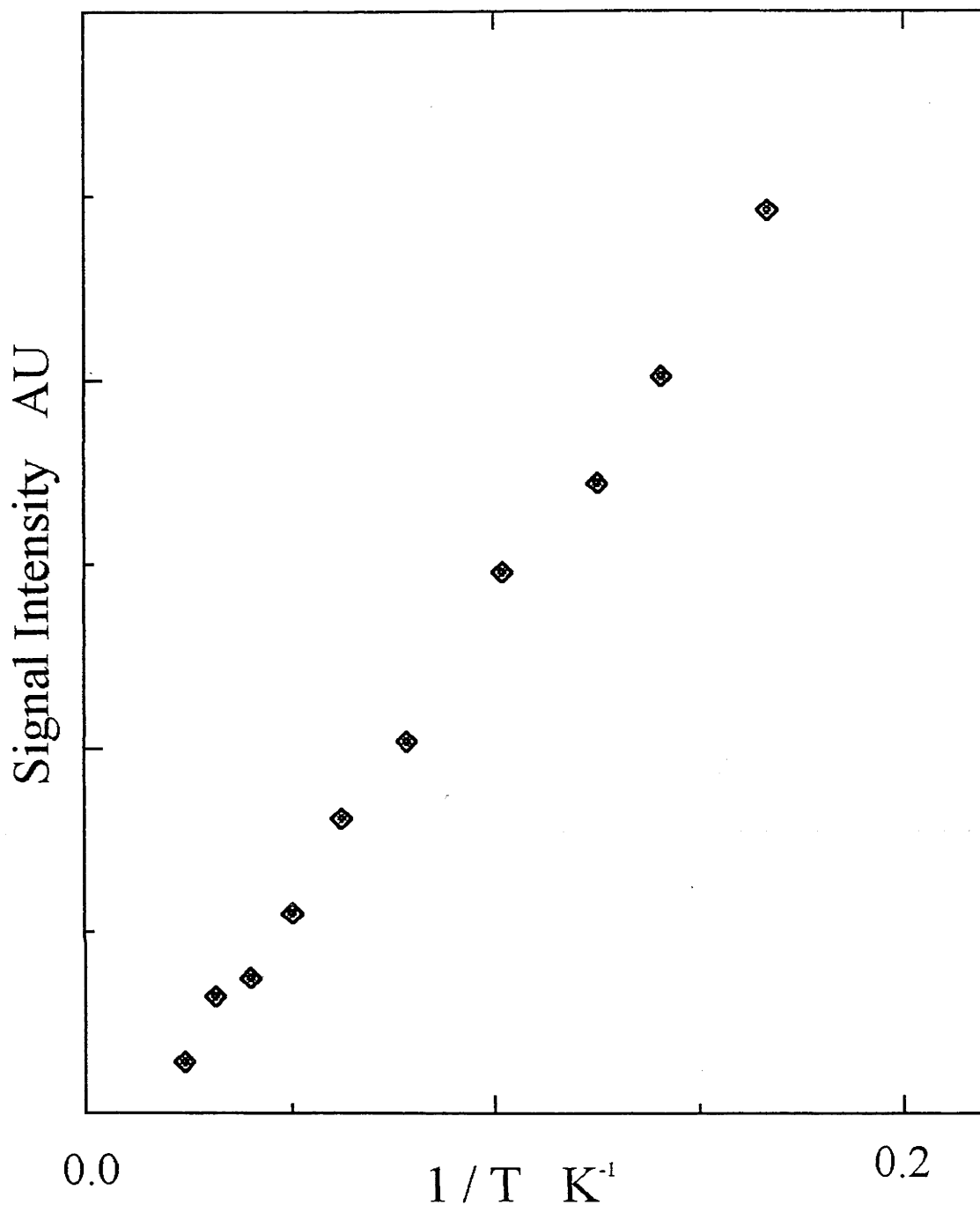


Figure 4.21. Temperature dependence of the S_2 state $g=4.1$ signal generated in PSII cryoprotected with 30% v:v ethylene glycol, illuminated at 130K, ie independent of the S_2 state multiline signal. Signal intensities are determined by extrapolation of the power saturation plot to zero microwave power. Signal temperature dependence appears very similar to that of the S_2 state $g=4.1$ signal generated by 200K illumination of these PSII samples.

dependence was proposed to be best fit by the middle Kramer's transition of a rhombic $S=5/2$ centre (Astashkin, et al., 1994b). The difficulty with the assignment of the spin state by this method is further discussed in the next chapter.

To examine the above question, measurements were made of the temperature dependence of the signals generated within EG cryoprotected PSII illuminated at either 130K or at 200K. Without the presence of monoalcohols prior to illumination, both illumination regimes generate $g=4.1$ signal intensity, although the signal intensity showed a poor correlation to the multiline signal generated under each illumination regime.

Figure 4.06 shows that the $g=4.1$ signal generated by illuminating EG PSII at 130K is very similar in overall line shape (at X band) to the $g=4.1$ generated as an excited state signal in the S_2 state produced by illuminating sucrose PSII at 200K. The temperature dependence of the $g=4.1$ signal intensity in EG PSII illuminated at 130K was measured over a wide temperature range (5K to ~ 40 K), (fig.4.21). The signal intensities are derived from the extrapolation to zero microwave power as performed in the previous temperature dependence studies. The temperature dependence of the $g=4.1$ signal generated in 130K illuminated EG PSII, as shown in fig.4.21, supports the earlier conclusion that this signal arises from a ground state centre. Close examination of the temperature dependence indicates one interesting feature; the curve of the temperature dependence is non linear (concave up) near the origin of the graph. This suggests that a thermally accessible excited spin state lies less than $\sim 10 - 15 \text{ cm}^{-1}$ above the ground state. Such behaviour has been previously reported by Hansson and coworkers (Vänngård, et al, 1992) but not commented upon. Likewise, the data of Brudvig and coworkers (de Paula and Brudvig, 1985b, de Paula, et al, 1986c) suggests similar behaviour, although no origin point is presented on their choice of axes. If a thermally accessible excited spin state lies close to the $g=4.1$ signal ground state, then this should give insight into the nature of the coupled system from which the signal arises. An exchange coupled Mn tetramer model was proposed by Brudvig and coworkers, (de Paula, et al, 1986c), to explain the behaviour of the multiline and ground state $g=4.1$ signals. This model consisted of two antiferromagnetically exchange coupled Mn dimers, one with net spin $1/2$, the other net spin 1 (for the $g=4.1$ signal S_2 state) ferromagnetically coupled to give rise to a spin $3/2$ ground state. The model required that the spin $1/2$ Mn dimer was strongly coupled such that it remained always a net spin $1/2$ centre. Figure 4.22a depicts this model. It should be noted that this model requires strong equivalent coupling between each of the $S=1$ dimer metal centres and the $S=1/2$ dimer unit. The model of the Mn arrangement proposed by both Kusunoki and Klein and coworkers (Kusunoki, et al, 1989, Yachandra, et al, 1993) generally does not support this exchange coupling requirement. However, representing the $S=1/2$ dimer as a single spin centre, then for $J = J_{12}$, $J' = J_{1D} = J_{2D}$ (note equivalent coupling requirement), $S_{12} = S_1 + S_2$ and $S_T = S_{12} + S_D$, then the energy state $E(S_T, S_{12})$ for the spin state S_{12} and S_T is

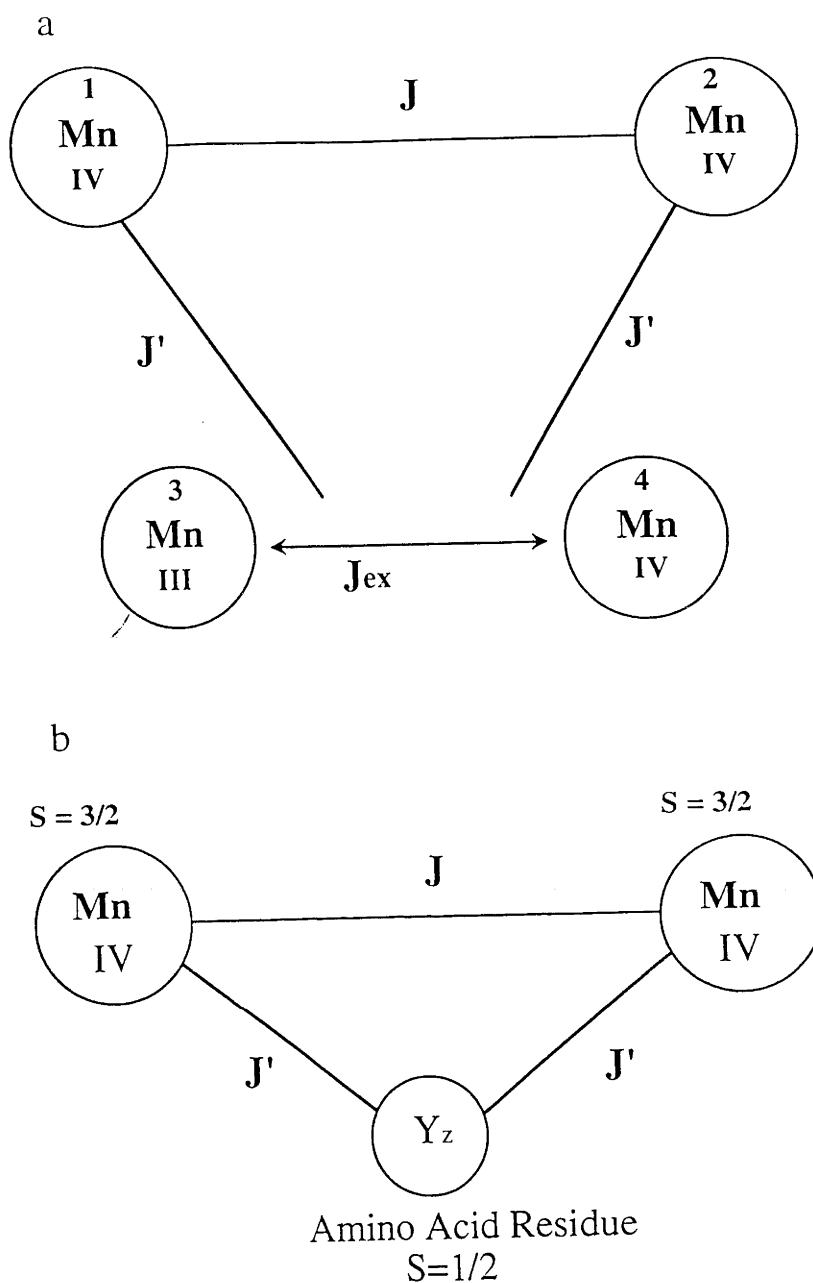


Figure 4.22. Model structures for the structure giving rise to the S_2 state $g=4.1$ signal generated in PSII cryoprotected with 30% v:v ethylene glycol, illuminated at either 200K or 130K, see figs 4.20 and 4.21. a). Model based on a tetramer construct of the Brudvig group (Brudvig and Crabtree, 1987), modified by Kusunoki (Kusunoki, 1992) and the Klein group (Yachandra, et al, 1993). Model requires the exchange coupling between each of the Mn in the effective homodimer and the spin $S=1/2$ heterodimer unit to be equivalent. This is satisfied by the cubane model of the Brudvig group (Brudvig and Crabtree, 1987), but not supported by the Xray diffraction data, and not by the modified tetramer of the Klein group (Yachandra, et al, 1993) and Kusunoki (Kusunoki, 1992). b). Alternate proposal for such a minimum three spin centre model for generating the spin $S=3/2$ or $S=5/2$ ground state centre leading to the formation of the S_2 state $g=4.1$ signal. The $S=1/2$ centre need NOT be a Mn heterodimer but may be represented by a spin $S=1/2$ centre, an organic radical. This satisfies the exchange coupling requirement between the Mn ions in the homodimer to this spin $S=1/2$ centre with less constraint on the overall geometry of the bridging structure.

$$E(S_T, S_{12}) = 1/2 (J - J') [S_{12}(S_{12}+1) - 12] + 1/2 J' [S_T(S_T+1) - 5/4] \quad (4.2)$$

where $S_1 = 3/2$, $S_2 = 3/2$ and $S_{12} = 1/2$ (a tightly exchange coupled Mn III - IV dimer). Figure 4.23 presents the energy level diagram for the different spin states of S_T and S_{12} , various ratios of J and J' , with J corresponding to antiferromagnetic and J' ferromagnetic coupling. From these exchange interactions, such a spin coupled system will give rise to an $S = 3/2$ ground state for $2|J| < |J'| < 4|J|$. The system will give rise to an $S = 5/2$ ground state for $4|J| < |J'|$. The same effective spin state pattern arises regardless of the Mn homodimer being III-III ($S_1 = S_2 = 2$) or IV-IV ($S_1 = S_2 = 3/2$) (de Paula, et al, 1986c).

An important feature of this model is that it is independent of the detailed nature of the $S_D = 1/2$ species. The scheme is equivalent for S_D being either an $S = 1/2$ exchange coupled Mn III - IV dimer or for any other spin $1/2$ centre, eg a radical. The major requirement is simply that it has net spin $1/2$ and couples ferromagnetically to each of the other Mn ions equivalently. From the spin level diagram, figure 4.23, the first excited state for such a system depends on the ratio $|J'|/|J|$ and has the possibilities; either $S = 5/2$ or $S = 1/2$ first excited state for an $S = 3/2$ ground state, or $S = 3/2$ excited state for an $S = 5/2$ ground state.

4.6.2.2.1. Case 1: $S = 3/2$ Ground State

The case for the spin $3/2$ ground state for the model implies minimal changes in ligand and exchange coupling interactions from interconverting from the $S=3/2$ state generated by the 130K illumination to the $S=1/2$ state during annealing at 200K. The $S=3/2$ ground state requires that the $g=4.1$ signal arise from a quasi axial centre, whereby one allowed transition generates ESR signal intensity in the $g\sim 4$ region, with shift from $g=4.00$ due to slight mixing of higher excited states in the manifold (D significant compared to J) (Diril, et al., 1987, Chang, et al., 1988a, Chang, et al., 1988b, Pace, et al., 1991).

The first excited state of such a system, assuming an $S=3/2$ ground state, would have either $S=1/2$, which would presumably give an ESR signal in the $g\sim 2$ region, or $S = 5/2$, which with quasi axial symmetry, would lead to an ESR signal in the $g\sim 6$ region.

4.6.2.2.2. Case 2: $S = 5/2$ Ground State

For an $S=5/2$ ground state, the interaction between the two exchange coupled Mn dimers must be of the form of the $S = 2$ dimer ferromagnetically coupled to an $S = 1/2$ centre. This will require the ratio of the exchange coupling constants to be of the range $4|J| < |J'|$, with high exchange interaction equivalence between the two Mn ions of the $S = 2$ dimer and the $S = 1/2$

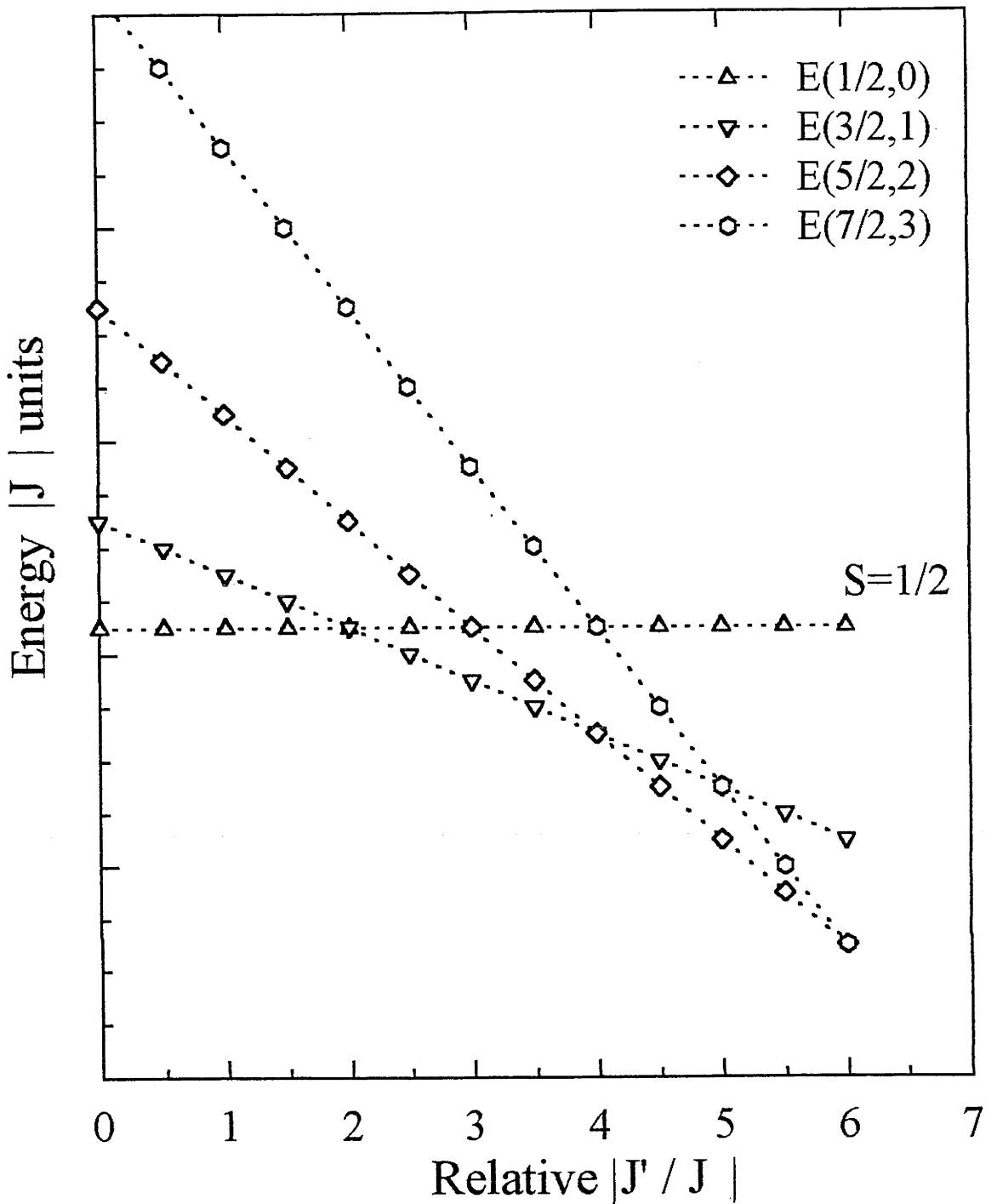


Figure 4.23. Energy level diagram for the spin states populatable for either structure of fig. 4.22, (spin states are identical). The energy plots are based on the exchange energies from $E(S_T, S_{12}) = \frac{1}{2}(J-J')[S_{12}(S_{12}+1)-15/2]+1/2J'[S'(S'+1)-33/4]$ (Beck, et al, 1986). For an $S=3/2$ ground state, $2|J| < J' < 4|J|$. For an $S=5/2$ ground state, $4|J| < J' < 6|J|$.

centre. The exchange equivalence requirement would not be consistent with the “open butterfly” model (Kusonoki, et al, 1989, Yachandra, et al, 1993). For an $S=5/2$ state, the $g=4.1$ signal is modelled to arise from the centre Kramer's transition in a near rhombic centre. If this were the case then other ESR signals should probably be measurable from the centre, with signal intensity possible from $g\sim 8$ through to $g<2$ (Schlichter, 1990, Castner, et al., 1960). The first excited state for the $S=5/2$ ground state, based on the $S=2$ dimer arising from a Mn IV-IV pair, would be an $S=3/2$ state. Such a rhombic $S=3/2$ centre should give rise to a highly anisotropic ESR signal across the $g\sim 5$ to $g\sim 2$ region. This would give rise to an alteration in the rhombic $S=5/2$ state “ $g=4.1$ ” signal line shape due to additional signals in this region arising with thermal population of the first excited, $S=3/2$ state.

4.6.2.2.3. Analysis of Ground and Excited States

The spectral line shape for the S_2 state of EG cryoprotected PSII illuminated at 130K over the field range 50mT to 450mT for temperatures 8K, 16K and 30K are presented in figure 4.24. This field range allows the line shape to be observed over the “ g range” ~ 11 to ~ 1.5 . Figure 4.25 shows the line shape of the $g=4.1$ signal generated under the same conditions for the equivalent temperature range as per fig.4.24. From these spectra, both $g=4.1$ and multiline signal intensity is generated. The $g=2.97$ turning point of the oxidised cyt b559 heme complex is observable, offering a clean g marker for these samples. However, no other signals are apparent in the 8K spectrum which may be due to other transitions of a rhombic $S=5/2$ centre. As the temperature is raised, no additional signals arise either in low field (high g) regions nor in the centre field ($g\sim 2$) region which should arise for the spin state interconversion from an $S=3/2$ ground to either an $S=5/2$ or $S=1/2$ excited state, and little change of the line shape of the $g=4.1$ signal occurs, apart from line broadening in the 30K spectrum. There is no evidence of additional signals arising in this region, underlying the $g=4.1$ signal, due to spin state interconversion from a rhombic $S=5/2$ ground to an $S=3/2$ excited state. The spectra do not support the model of the Mn tetramer consisting of either an $S=5/2$ or $S=3/2$ ground state as no other Mn signals arise over the field ranges expected and the temperature range shown to provide a thermal depopulation of the ground state to some as yet unidentified excited state. It should be noted that both Brudvig and coworkers (de Paula, et al, 1986c) and Haddy and coworkers (Haddy, et al, 1992) reported that they could not observe any additional ESR signals arising from the thermal population of any putative excited spin states which may be assigned to an exchange coupled Mn tetramer.

If we examine the Brudvig model for the Mn organisation within the OEC giving rise to the multiline and specifically the ground state $g=4.1$ signal (whether it arises from the $S=5/2$ or $S=3/2$ state is of no consequence), the same exchange coupling system may give rise to an $S=5/2$ or $S=3/2$ ground state *independent* of the physical nature of the $S=1/2$ centre, ie. an $S=1/2$ organic

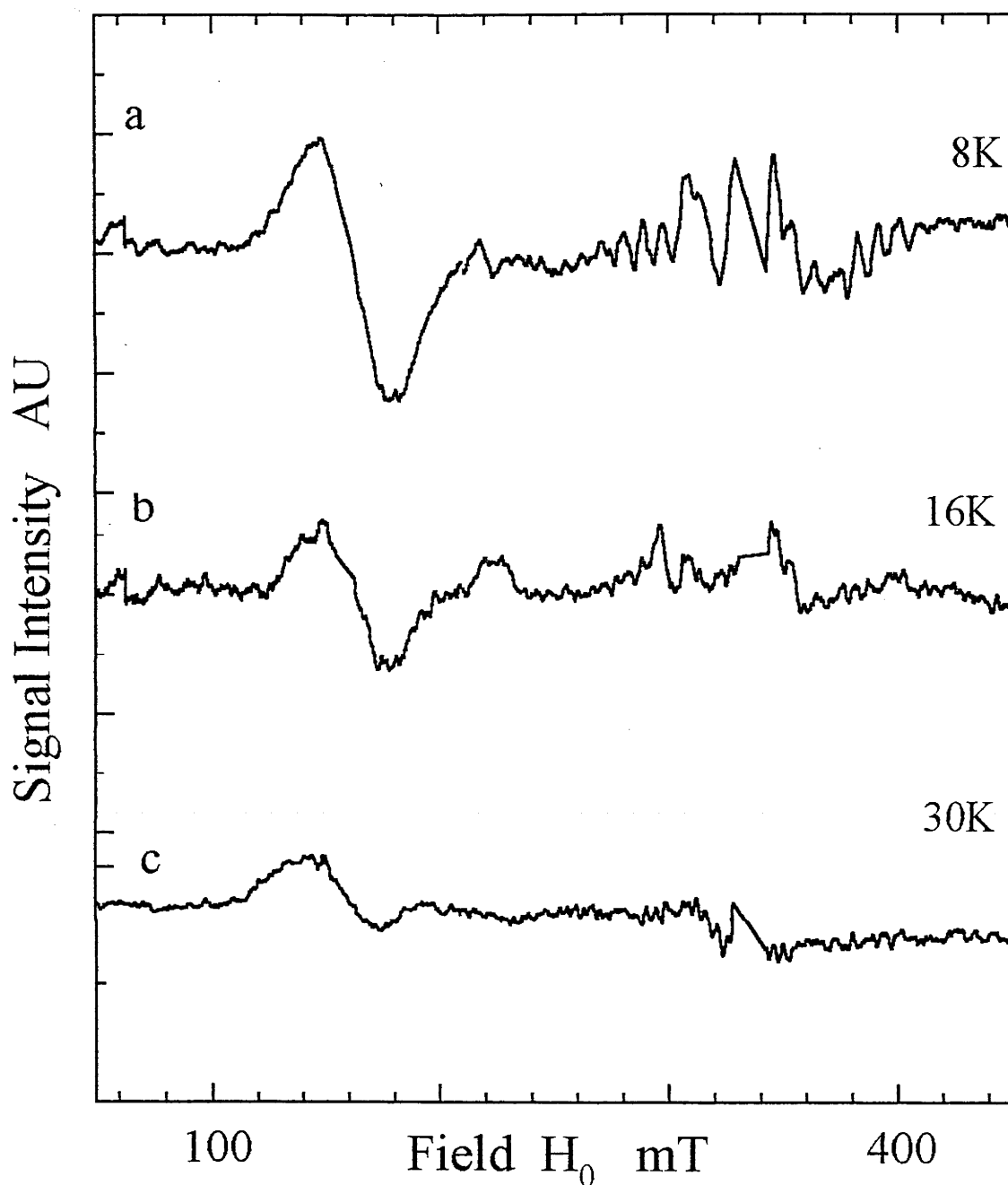


Figure 4.24. Temperature dependence of the line shape of the $g \sim 2$ and $g \sim 4$ regions of the S_2 state generated in PSII cryoprotected with 30% v:v ethylene glycol, illuminated at 130K, recorded for a). 8K, b). 16K, c). 30K. Multiline signal observed in the spectrum recorded at 8K (a) is observed to decline at higher temperatures indicating it is the ground state species and not developed as an excited state expected for depopulation of the ground state $g=4.1$ signal system. Spectrometer conditions as per fig. 4.15.

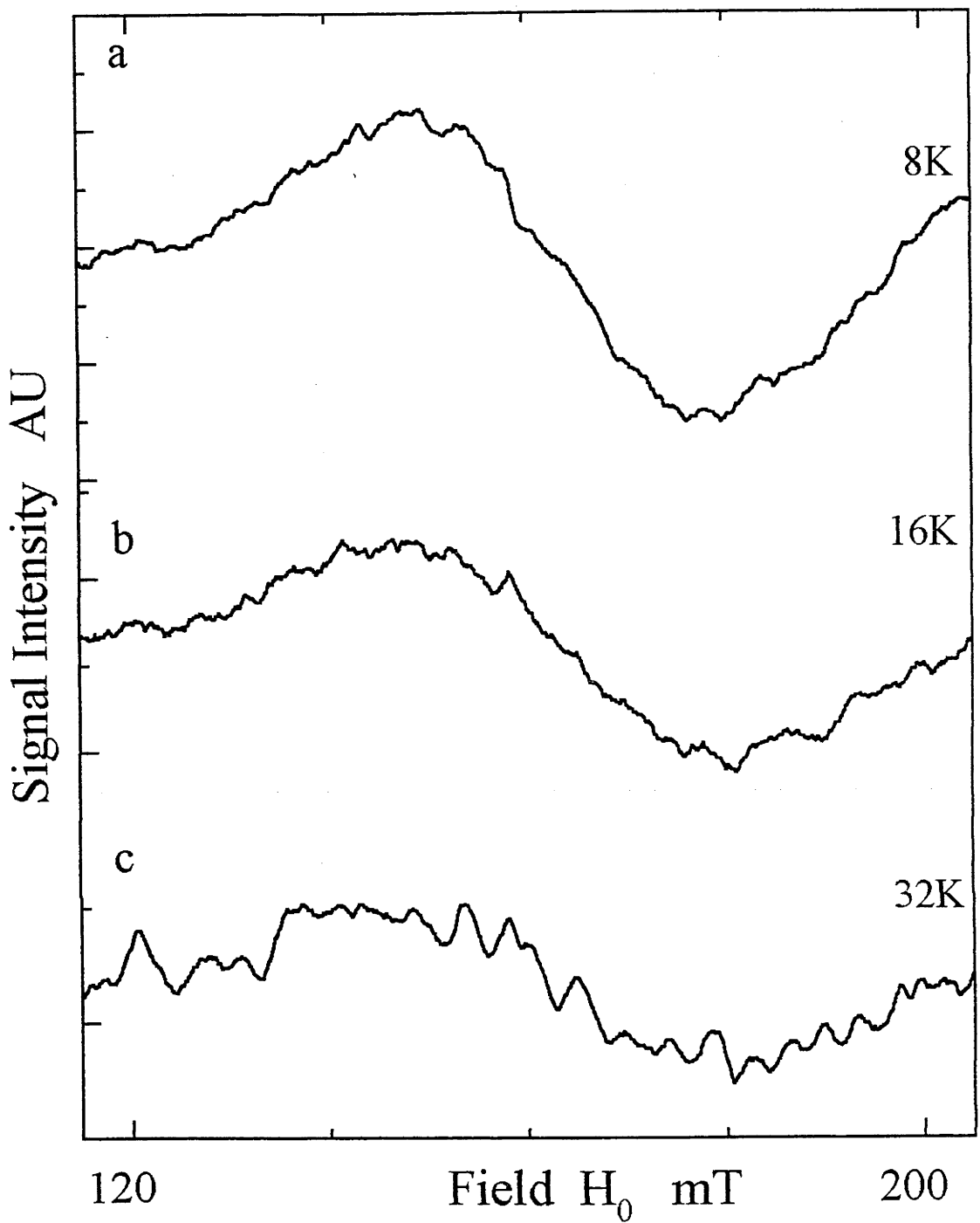


Figure 4.25. Temperature dependence of the line shape of the S_2 state $g=4.1$ signal generated in PSII cryoprotected with 30% v:v ethylene glycol, illuminated at 130K, recorded at a). 8K, b). 16K and c). 30K. Spectrometer conditions as per fig. 4.15.

radical bridging an $S=2$ or $S=1$ antiferromagnetically coupled Mn homodimer may give rise to the same exchange coupling interaction, figure 4.22b. That is, the requirement for an $S=3/2$ ground state requires only that the $J'=J_{1R}=J_{2R}$, $2|J| < |J'| < 3|J|$ and that J' be ferromagnetic and $J (=J_{12})$ be antiferromagnetic, with similar requirements for an $S=5/2$ ground state except that $4|J| < |J'|$.

4.6.3. An Excited State Signal

As no broad Mn derived nor altered signals were observed to arise due to the thermal population of an excited spin state of a Mn tetramer, close examination of the $g=2$ region was undertaken. If some effect occurs in the $g=2.00$ region, the source of the excited state may be an organic radical $S=1/2$ centre bridging the Mn homodimer. The centre field region of the ESR spectrum is dominated by a dark stable radical, which arises from the oxidation of a specific amino acid residue, tyrosine 160 on the D2 polypeptide (known as Y_D) (Barry and Babcock, 1987, Debus, et al, 1988a, Barry and Babcock, 1988, Vermaas, et al, 1988). This signal has been studied for many years, and is known as Signal II_S (Babcock and Sauer, 1973a). Other $g=2.00$ region signals known include; Signal II_f and Signal II_{vf}, arising from the transient oxidation of the electron transfer intermediate tyrosine 161 on the D1 polypeptide (known as Y_Z) (Barry and Babcock, 1987, Debus, et al., 1988b, Noren and Barry, 1992, Barry and Babcock, 1988, Metz, et al., 1989), which, as discussed in Chapter 1, is the transfer redox component between the Mn containing OEC and P680⁺ (Boska, et al., 1983, Babcock, et al, 1983, Hoganson and Babcock, 1988). These signals are similar in shape to Signal II_S and are normally observed as a very fast transient during turnover (Babcock and Sauer, 1975b, Blankenship, et al., 1977, Warden, et al., 1976, Hoganson and Babcock, 1989, Babcock, et al, 1983, Hoganson and Babcock, 1988) or in samples in which the Mn cluster has been removed by inhibitory washes such as 0.8M Tris (Astashkin, et al., 1994a, Hoganson and Babcock, 1988, Mino and Kawamori, 1994, Babcock and Sauer, 1975b, Babcock and Sauer, 1975a, Boska, et al., 1983, Gilchrist, et al., 1995, Diner, et al., 1995). In addition, a chlorophyll radical which is proposed to interact with cyt b559 in a cyclic manner, may be photo accumulated at low temperature. This species is believed to protect P680 from double turnover under conditions which slow electron flow out of the OEC and from Y_Z (Thompson, et al, 1988, Thompson and Brudvig, 1988).

Figure 4.26 shows the temperature dependence of the total signal intensity (extrapolated to zero microwave power) in the Signal II region measured either under illumination at 130K, in the presence of the ground state $g=4.1$ signal, and for the sample annealed for 100s at 200K, whence the $g=4.1$ signal interconverts to the multiline signal. The data for the illuminated sample shows a non Curie deviation, at low temperatures, from the temperature dependence behaviour of the annealed sample data, where the only signal expected is that of Signal II_S, which exhibits

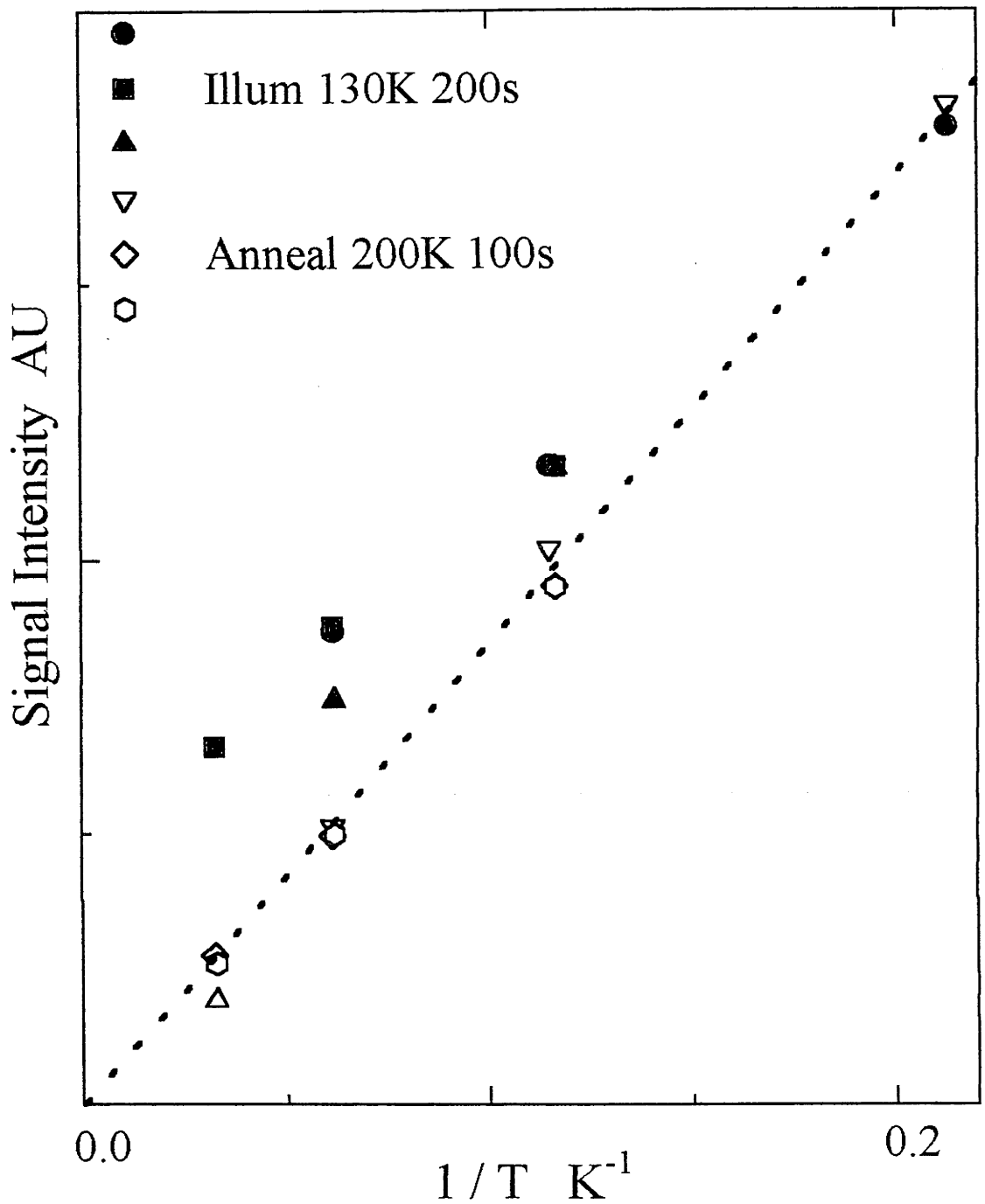


Figure 4.26. Temperature dependence of the total signal intensity measured in the Signal II ($g=2.00$) region in the S_2 state generated in PSII cryoprotected with 30% v:v ethylene glycol illuminated at 130K. Signal intensities determined by extrapolation of the power saturation to zero microwave power. Spectrometer conditions for spectral recording: microwave frequency 8.98 GHz, modulation frequency 100 KHz, modulation amplitude 0.4mT.

expected Curie behaviour. The deviation observed is not of great magnitude and may imply a rapid passage effect was involved (R. Bramley pers comm). The data for fig.4.26 was recorded with a modulation frequency (MF) of 100KHz, which is the standard MF used in ESR experiments.

To limit the influence of any possible rapid passage artefact, the experiments on the Signal II region were repeated at a MF of 400Hz using the Varian spectrometer and a MF of 1.56KHz using the Bruker spectrometer. Figure 4.27 shows the temperature dependence curves for the total signal intensity (again extrapolated to zero microwave power) in the Signal II region for the sample illuminated at 130K and for the sample annealed at 200K, the equivalent conditions as for figure 4.26 but with the lower MF. The data for the illuminated sample shows a definite non Curie curvature in comparison to the annealed data, where the only signal expected is that of Signal II_S, which again exhibits the expected Curie behaviour. This suggests that signal intensity is present in the illuminated sample in addition to and independent of Signal II_S, and that this additional signal has excited state behaviour. Figure 4.28 replots this data in a spin population format, where the signal intensity multiplied by the temperature is plotted against inverse temperature. The signal amplitudes are scaled to that of the 5K spectrum of the annealed sample to indicate relative intensity. The data is the average of three experiments and clearly shows the development of additional 'excess' spin population within the illuminated signal data. For strict Curie behaviour, the graph would follow a constant level. This behaviour is observed for the annealed sample data. The data curve for the illuminated sample does not follow this Curie behaviour. The spin population graph clearly indicates the development of additional signal intensity above the background level of Signal II_S. At low temperatures, below ~7K, the curves merge, indicating that the additional intensity is due to the populating of an excited state, observable at temperatures above ~10K. Figure 4.29 indicates the line shapes of the Signal II region for the illuminated, $g=4.1$ present, and 200K annealed, $g=4.1$ interconverted to multiline, conditions as well as the difference spectrum of the non Curie component. It was important that the measurement of the annealed spectrum was undertaken without time delay between the annealing and the spectral recording. Upon annealing the 130K illuminated sample at 200K, subsequent storage at 77K (in liquid nitrogen) prior to measurement of the annealed spectra led to an increase in Signal II region intensity, fig. 4.30. This change in Signal II intensity is a result of electron redistribution within PSII with transfer from oxidised Mn in the multiline state of the OEC to Y_D^+ . With minimal delay between the annealing process and measurement, a decrease in intensity of the Signal II region of 45% at 16K was observed. No intensity difference was observed at the lowest temperature (6K), consistent with there being no change in the background Signal II_S intensity on short annealing, and the virtual disappearance of the non Curie component at this temperature.

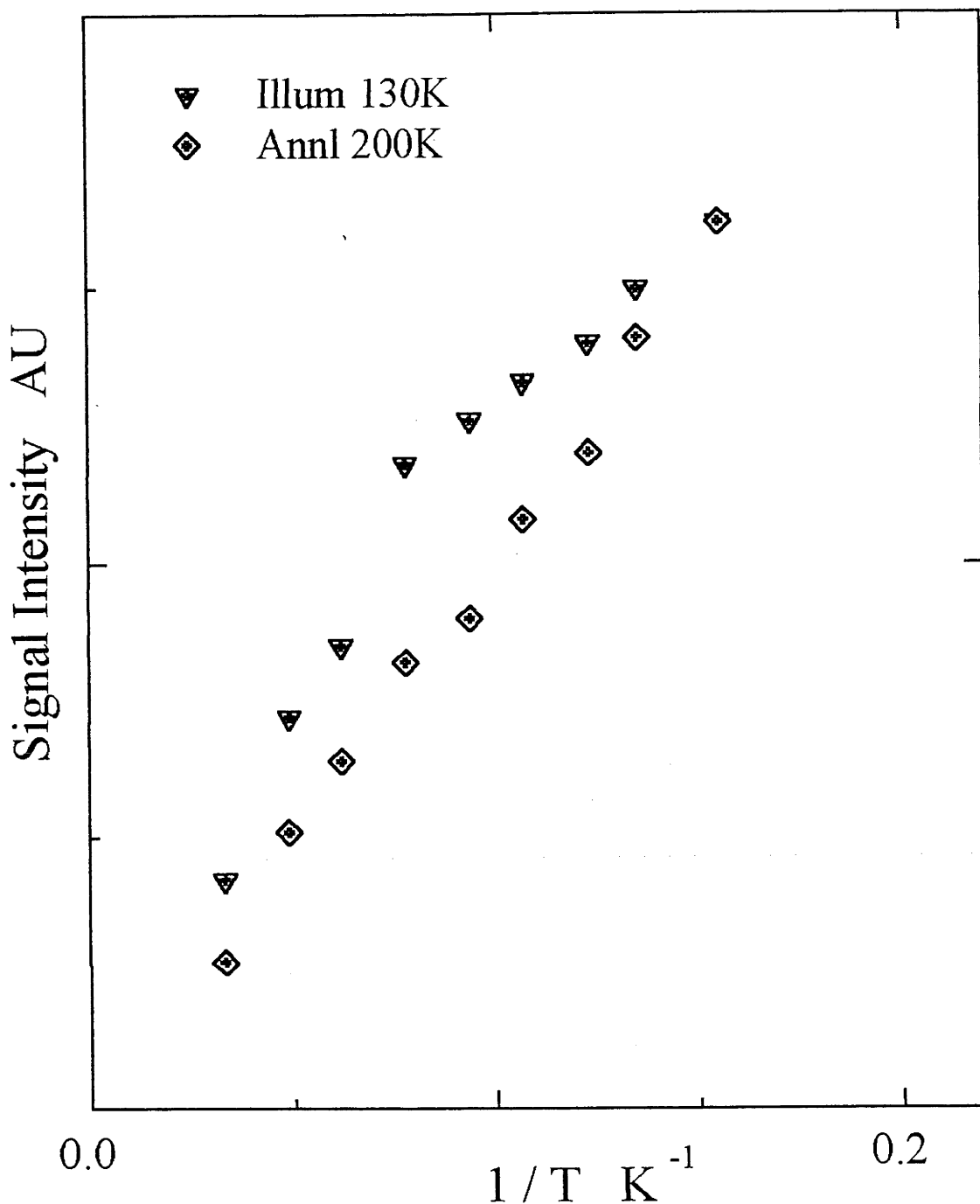


Figure 4.27. Temperature dependence of the total signal intensity measured in the Signal II ($g=2.00$) region as per fig. 4.26 remeasured for a modulation frequency of 400Hz (with the Varian spectrometer) and 1.56KHz (with the Bruker spectrometer). Use of the lower modulation frequency reduces the possible influence of rapid passage artifacts. Signal intensities determined by extrapolation of the power saturation to zero microwave power. Spectrometer conditions: modulation amplitude 0.2mT, microwave frequency (Bruker) 9.42GHz; (Varian) 8.98GHz, modulation frequency (Bruker) 1.56KHz; (Varian) 400Hz.

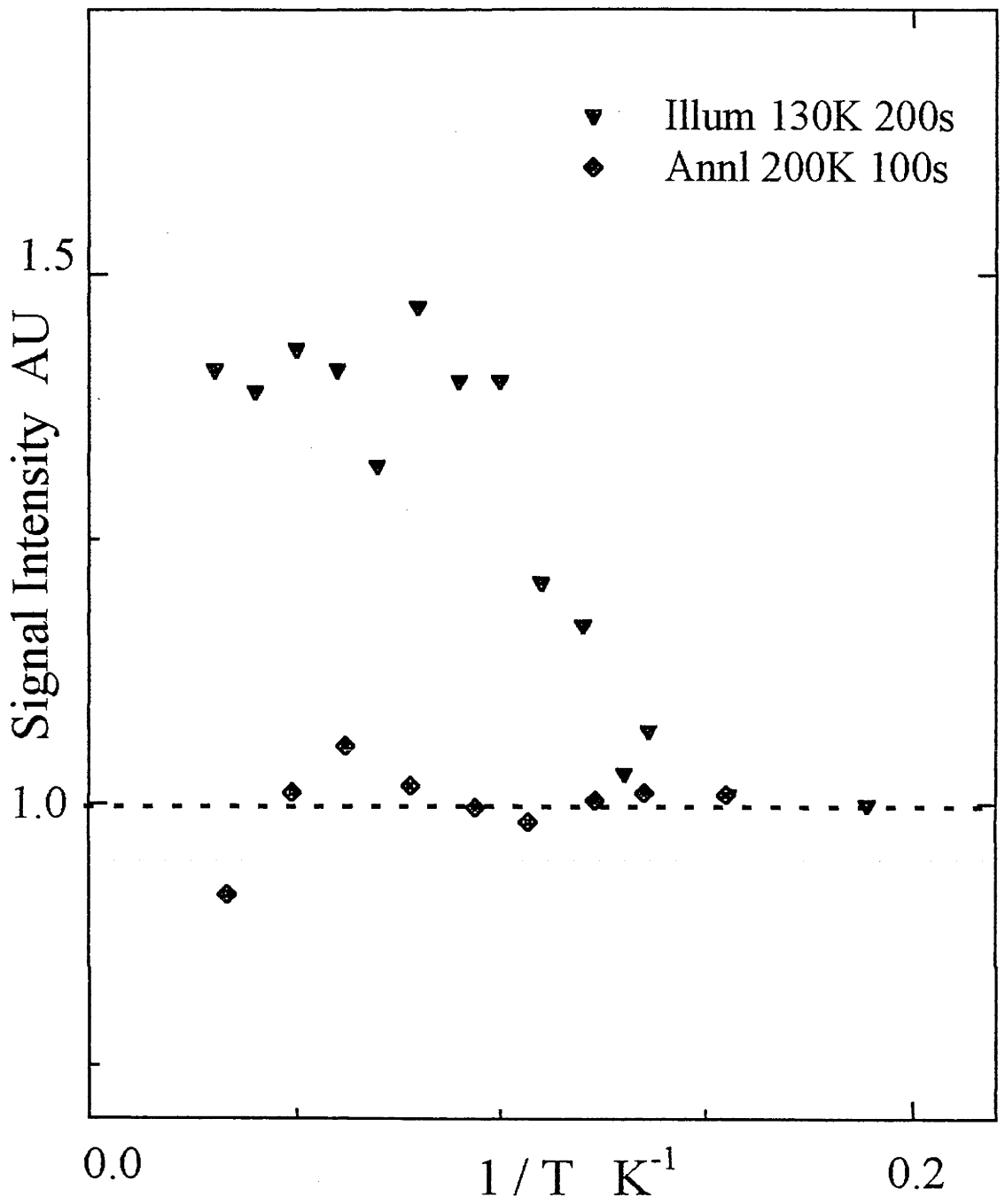


Figure 4.28. Re examination of the Signal II temperature dependence data from fig. 4.27 presented in a spin population format, ie $SI * T$ versus T , see text. Intensity axis is rescaled to a relative intensity. Dotted line at $SI * T = 1$ defines Curie behaviour.

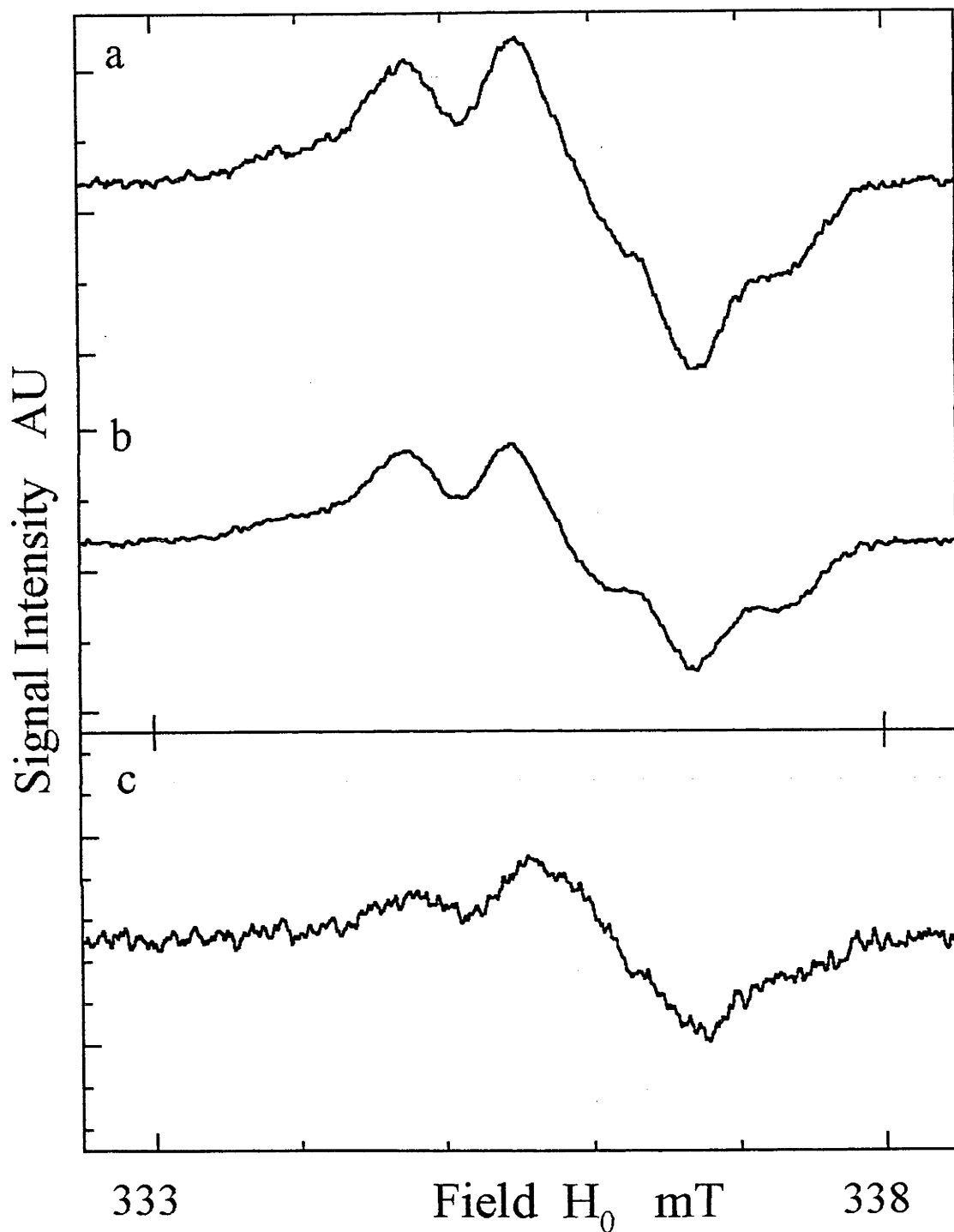


Figure 4.29. S_2 state Signal II spectra recorded from PSII cryoprotected with 30% v:v ethylene glycol, a). illuminated at 130K (in the presence of the ground state $g=4.1$ signal) and b). dark annealed at 200K for 100 seconds (where the ground state $g=4.1$ signal is no longer present). Spectrum c). is the resultant spectrum for the illuminated minus annealed subtraction. Spectrometer conditions: temperature 16K, microwave frequency 9.42 GHz, microwave power $20\mu\text{W}$, modulation frequency 1.56 KHz, modulation amplitude 0.2mT.

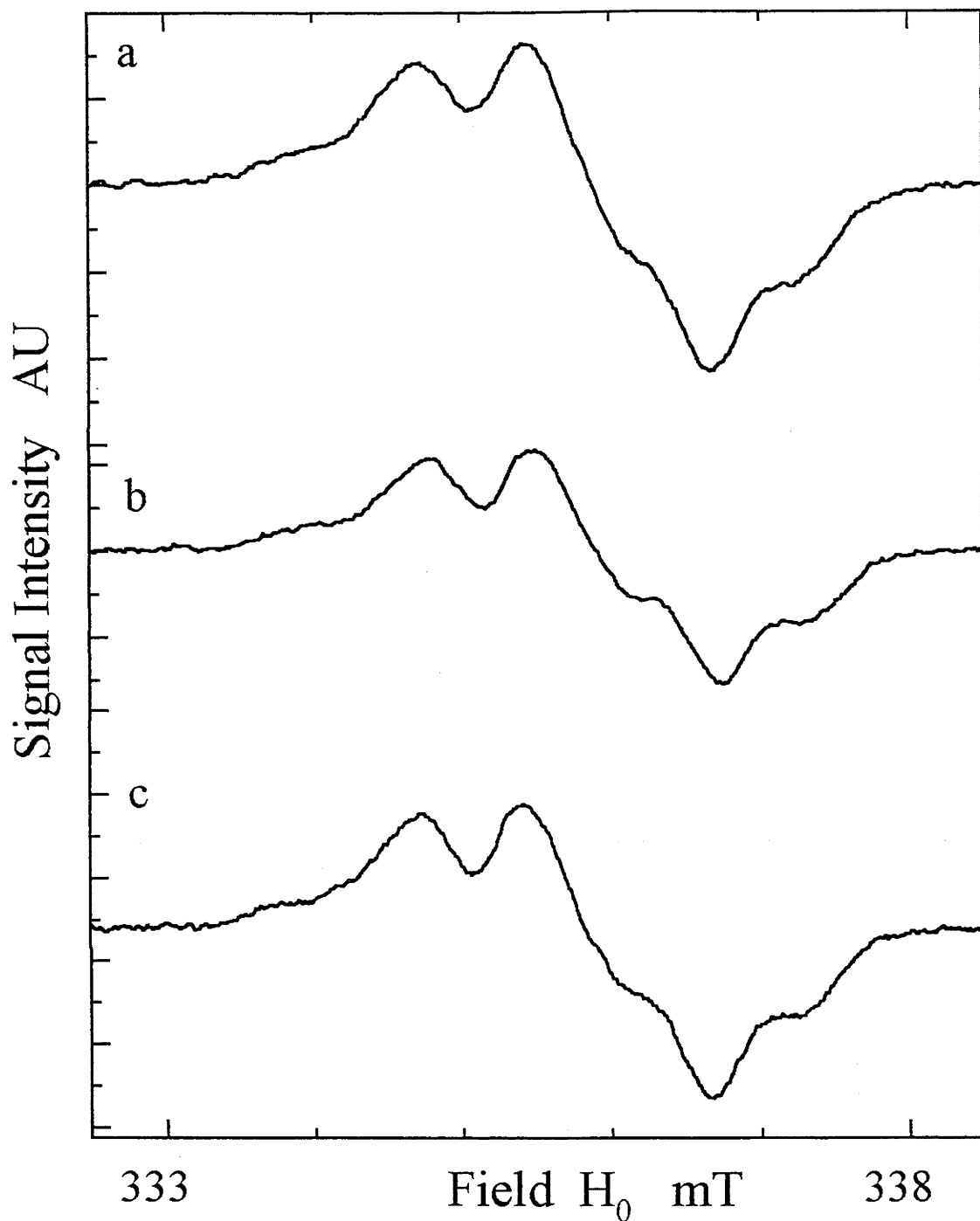


Figure 4.30. S_2 state Signal II spectra recorded from PSII cryoprotected with 30% v:v ethylene glycol, a). illuminated at 130K (recorded in the presence of the ground state $g=4.1$ signal), b). subsequently dark annealed at 200K for 100 seconds (where the ground state $g=4.1$ signal is no longer present), with recording of the spectrum subsequent to the annealing process, and c). the sample from (b) stored overnight at 77K (liquid nitrogen) in darkness and remeasured to determine changes in intensity of Signal II slow (Y_D^-). Spectrometer conditions: temperature 13K, microwave frequency 9.42 GHz, microwave power $20\mu\text{W}$, modulation frequency 1.56 KHz, modulation amplitude 0.2mT.

The spectrum of the non Curie component in fig.4.29c clearly resembles that of an organic radical, similar in overall form to an oxidised tyrosine, but with less resolution of the proton hyperfine. Its shape, temperature dependence, absence of significant Mn hyperfine broadening and its close association with the ground state $g=4.1$ signal, are all consistent with it arising as the first excited $S_T=1/2$, state of a Mn homodimer bridged by an oxidisable protein side chain. The electron transfer event which accompanies the loss of the $g=4.1$ signal and formation of the multiline signal on annealing (fig.4.08) at 200K, presumably results in reduction of the oxidised bridging ligand, leading to a diamagnetic centre.

This implies also that an organic type radical signal arises as an excited state signal, displaying ESR intensity overlying the dark stable Y_D^+ . This in itself is of significant physical interest. From before, the interaction of a spin $1/2$ radical centre with a spin 1 Mn homodimer may be theoretically shown to have a spin $3/2$ ground state, dependent on the magnetic exchange couplings between the dimer and the radical centre. The temperature dependence behaviours of ESR signals arising in ethylene glycol cryoprotected PSII illuminated at 130K are consistent with the theoretical model for the ground and proposed first excited states. This is possibly the first observation of the interaction between an organic radical and a metal dimer centre whereby the interaction of the exchange couplings generates a mixed state, probably $S=3/2$, as the ground state, the first excited state arising with the metal dimer changing to $S=0$ diamagnetic, with the isolated radical observed the first excited state signal.

The spin changes which must occur for such an organic radical - Mn dimer interaction are such that the transition from the ground $S=3/2$ to first excited $S=1/2$ state occurs via one spin transition in the Mn dimer exchange levels. From the exchange coupling interactions, the ground state being $S=3/2$ with an $S=1/2$ first excited state, (see fig. 4.23), the ratio of the exchange couplings must be in a narrow range, to accommodate both the energy gap to the $S=1/2$ state and the fact that no evidence of the next excited, spin $5/2$ state is seen in the temperature range used. Figure 4.31 re-plots the temperature dependences of the $g=4.1$ and $S=1/2$ state signals and models these curves based on the population statistics for the postulated exchange interaction system. The dotted curve shows the best fit curve for the model to be with $J/k \approx 65K$, with a $|J' / J|$ ratio of ~ 2.6 . As a comparison to the exchange coupling within the other proposed (multiline) dimer, where the J_{ex} / k was only $\sim 3.5K$ to $\sim 25K$, depending on the presence of alcohol (see above), the J_{ex} for this dimer is large and more typical of oxo bridged high valence systems (Cooper, et al., 1978). This may well represent the differences in environments of the two dimers, where the multiline dimer is more easily accessed by the lumen while the "ground $g=4.1$ " dimer is buried more deeply within the membrane bound protein region. It suggests that the multiline dimer maintains some significant proton binding to the μ -oxo bridging ligands of the dimer, weakening the antiferromagnetic coupling, while the bridging in the other dimer is

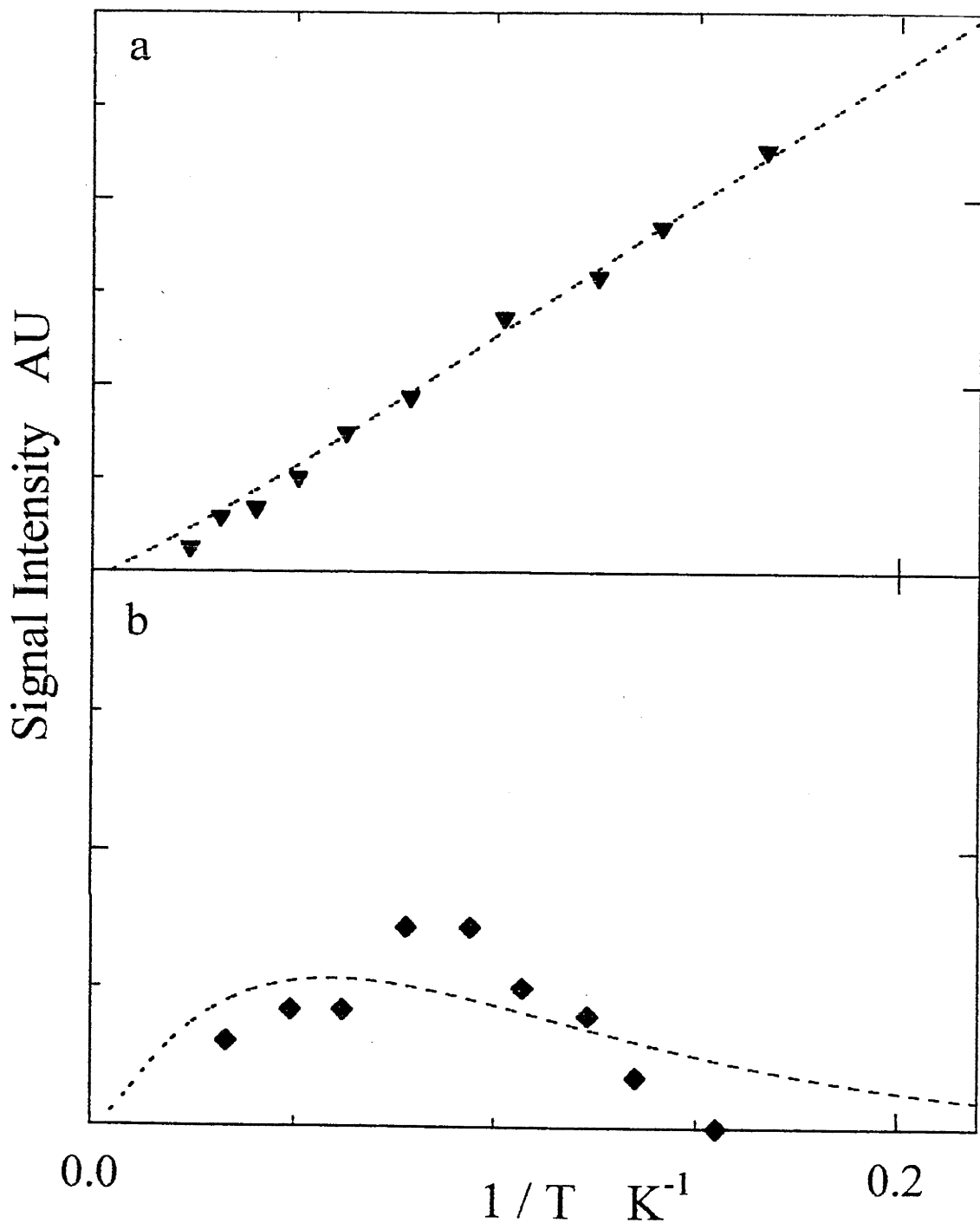


Figure 4.31. Temperature dependences of the a). ground state $g=4.1$ signal and b). light induced component of Signal II generated in ethylene glycol cryoprotected PSII, illuminated at 130K. Dotted lines are the signal intensities calculated for a Boltzmann energy model according to equation 4.2, see text. The exchange couplings for the calculation are $|J'/k| = 65\text{K}$, $J'/J = -2.6$. The intensity scale is arbitrary due to the different methods of signal quantitation for the $g=4.1$ and Signal II.

strongly antiferromagnetic indicating a bridging ligand that is non protonated, “pure” μ -oxo in nature, if not some other ligand.

The nature of the organic radical signal is of major significance as it bears upon the postulated ligand environment of the Mn associated with the ground state $g=4.1$ signal. Using a MF of 400Hz and a MA of 0.025mT (0.25G) and microwave power of 1μ W, with the Varian spectrometer, careful line shape observations of the Signal II region in 130K illuminated and post 200K annealed samples of EG cryoprotected PSII were recorded. Figure 4.32 shows the 130K illuminated (a) and post 200K annealed (b) spectra recorded under these rapid passage artefact, modulation broadening and microwave power saturation limited conditions. Figure 4.32c shows the difference spectrum from the summation of 25 recording scans for each of the illuminated and annealed spectra (from 5 different sample illuminations) under the above conditions. This spectrum shows strong similarity to the dark stable Signal II_S. The g value for this signal is 2.0045, with a peak to trough width of 4.0mT. The g value is typical of a neutral tyrosine radical (Evelo, et al., 1989, Barry and Babcock, 1988), This suggests the involvement of a redox active tyrosine moiety with the ground state $g=4.1$ signal.

Close examination of this signal shows little of the line broadening that would be expected for the interaction of the organic radical with two highly paramagnetic Mn ions (Gilchrist, et al., 1995). However, the presumed state giving rise to the signal is one in which the strong antiferromagnetic exchange between the Mn ions yields an $S_{12}=0$ first excited spin interaction, for the Mn dimer, resulting in an effective diamagnetic state interacting with the radical. Further, the radical signal shows slight differences to that for Y_D^+ such that one of the proton hyperfine peaks is absent and a low amplitude hyperfine pattern of ~ 0.2 mT spacing appears to overly the signal. The g value for the signal is slightly shifted from that of Y_D^+ , but remains well within the range of g values observed for oxidisable tyrosines observed in other protein systems (Barry and Babcock, 1988, Bender, et al, 1992).

The interconversion of the ground state $g=4.1$ to the multiline signal during 200K annealing raises questions concerning the electron transfer through PSII. The kinetics of P680 charge separation and rereduction through the donor side of PSII have been shown to contain evidence of only one electron transfer intermediate between $P680^+$ and the Mn OEC site. Kinetic analysis has shown that the rereduction kinetics of $P680^+$ match that of the oxidation kinetics of YZ closely (Babcock and Sauer, 1975a, Warden, et al., 1976, Boska, et al., 1983). If the electron transfer through PSII were to be slowed due to illumination at very low temperature, then YZ is the likely site for the steady state intermediate. Indeed, in preparations in which the Mn has been removed, eg by Tris washing, the electron transfer through the donor side of PSII can be trapped on YZ^+ , which has been the main approach to the study of this signal by ESR, ENDOR and ESSEM

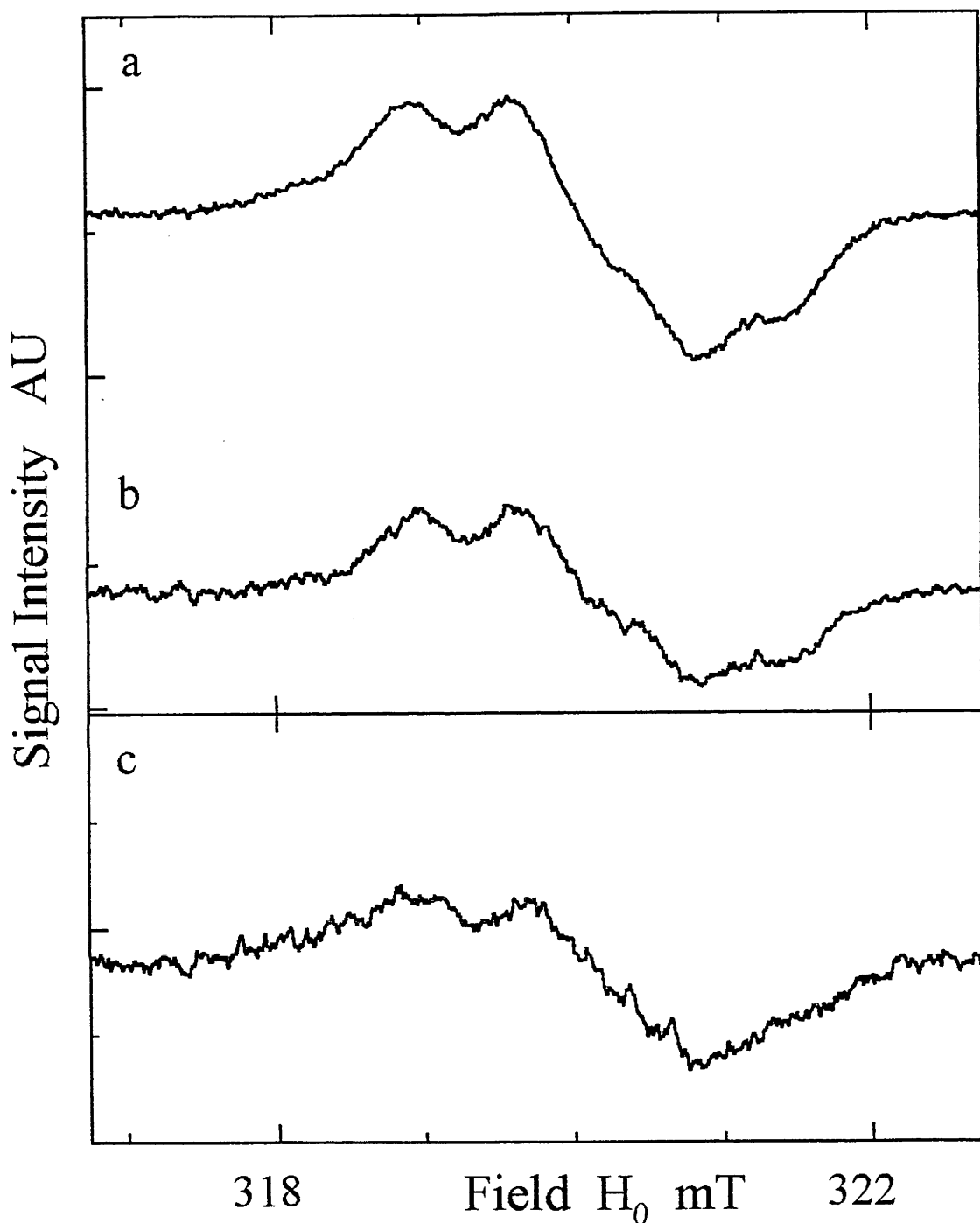


Figure 4.32. Examination of the S_2 state Signal II spectra from PSII cryoprotected with 30% v:v ethylene glycol, a). illuminated at 130K, and b). subsequently dark annealed at 200K for 100 seconds. c). The resultant difference spectrum for the illuminated minus dark annealed subtraction. Spectrometer conditions have been chosen to avoid (i) rapid passage artifacts, (ii) microwave power saturation, and (iii) modulation broadening effects. Spectrometer conditions: temperature 16.5K, microwave frequency 8.98 GHz, microwave power $9.2\mu\text{W}$, modulation frequency 400 Hz, modulation amplitude 0.05mT. Spectrum (c) is the resultant of ~ 25 sets of illuminated and annealed scans over five separate experiments.

techniques (Evelo, et al., 1989, Babcock and Sauer, 1975b, Babcock and Sauer, 1975a, Boska, et al., 1983, Astashkin, et al., 1994a, Britt, et al., 1995, Gilchrist, et al., 1995, Diner, et al., 1995, Astashkin, et al., 1994a, Barry and Babcock, 1988, Hoganson and Babcock, 1988, Mino and Kawamori, 1994). The initial conclusion of Casey and Sauer was that, with the development of the $g=4.1$ with 140K illumination and its interconversion to the multiline signal with 200K annealing, the $g=4.1$ must be an intermediate state between the S_1 and multiline S_2 states (Casey and Sauer, 1984). The development of ESR signals in PSII due to variable temperature illuminations has shed light on the interactions of the ground state $g=4.1$ and the multiline S_2 states. Brudvig and coworkers studied the temperature dependence of the development of ESR signals arising from electron donors to $P680^+$ and / or YZ^+ , showing that at low temperatures, cyt b559 competed with YZ for electron transfer to $P680^+$ (de Paula, et al, 1985a, Thompson, et al, 1988). The ESR signals arising from the Mn site were observed to be dependent on temperature also. At very low temperature, the $g=4.1$ state competed with electron donation by cyt b559. At higher temperatures, the multiline signal began to be developed. A thermal study of both the development and annealing kinetics, by ESR (de Paula, et al, 1985a) and FTIR (Koike and Inoue, 1987, Noguchi, et al, 1993), indicated electron donation from the Mn OEC was temperature dependent as well as S state dependent. For the S_2 state, electron transfer from the Mn OEC site had an activation temperature of 160K, with the terminal site generating the multiline signal (de Paula, et al, 1985a, Styring and Rutherford, 1988, Koike and Inoue, 1987, Noguchi, et al, 1993). This temperature is in excess of that required to develop the ground state $g=4.1$ signal, indicating that the $g=4.1$ centre is an intermediate state of the electron transfer through the donor side of PSII. Rutherford and coworkers were able to cogenerate $g=4.1$ and multiline signal intensity in sucrose PSII with added glycerol illuminated at 200K, in the absence of added alcohols (Zimmermann and Rutherford, 1984, Zimmermann and Rutherford, 1986). The study included a kinetic examination of the recombination back to the S_1 state from the multiline and $g=4.1$ S_2 state manifold. The decay of the $g=4.1$ signal was shown to be biphasic. It was found that a fast decay component of the $g=4.1$ signal coincided with an initial increase in multiline signal intensity, while a slower component of $g=4.1$ signal decay paralleled the decay of the multiline signal (Zimmermann and Rutherford, 1984, Zimmermann and Rutherford, 1986). Although the conclusion from this data, that the $g=4.1$ was an intermediate between the S_2 and the S_3 states, was shown to be in error, the result of the kinetic analysis that the interconversion from the $g=4.1$ state to the multiline state was more rapid than the decay of the multiline signal (Zimmermann and Rutherford, 1984, Zimmermann and Rutherford, 1986), suggests that at least some component of the total observed $g=4.1$ signal intensity is derived from an intermediate state of electron transfer. From figures 4.05 and 4.08, the generation of the multiline state either by direct

with inclusion of probable ligand and magnetic interactions with the amino acids proposed as metal binding sites.

4.8. Studies on Inhibitory Treatments on PSII

The magnetic and spin population behaviours of the “physiological” PSII have led to a model for the organisation of the Mn ions within the OEC. There have been many reports concerning the effects of inhibitory treatments on the ESR signals arising in different S states in PSII. These studies on inhibited PSII have mainly involved an examination of the effects on the S₂ and ‘S₃’ states of Cl⁻ depletion, with or without low molecular weight inhibitory anion addition, and Ca²⁺ depletion. In this study, the effects of Cl⁻ / F⁻ exchange and addition of inhibitory levels of Acetate and NaCl on the S₂ and ‘S₃’ states have been examined, and interpretations presented in terms of the Mn model proposed.

4.8.1. Cl⁻ / F⁻ exchange

The depletion of Cl⁻ from PSII has been shown to inhibit O₂ evolution (Damoder, et al, 1986, deRose, et al., 1995, Itoh and Uwano, 1986, Theg, et al, 1984, Homann, 1988a, Homann, 1988b, Sinclair, 1984, Coleman and Govindjee., 1987), restrict the formation of the multiline under single turnover conditions generating the S₂ state (Baumgarten, et al, 1990, Casey and Sauer, 1984, Damoder, et al, 1986, deRose, et al., 1995, Ono, et al, 1986, Ono, et al, 1987, Mavankal, et al, 1986, Boussac and Rutherford, 1994a) and electron transfer through the donor side of PSII under continuous turnover conditions (Baumgarten, et al, 1990, Damoder, et al, 1986, Jursinic and Stemler, 1988, Ono, et al, 1986, Sinclair, 1984, Theg, et al, 1984, Coleman, et al, 1987b). A split ESR signal proposed to arise from an altered S₃ state is observed after the second turnover (Baumgarten, et al, 1990, Boussac and Rutherford, 1994a). The physical nature of this inhibition is not well understood, with Cl⁻ reported to play numerous physiological roles in the PSII complex, from enhancement of electron transfer (Damoder, et al, 1986, Jursinic and Stemler, 1988, Coleman, et al, 1987b, Coleman and Govindjee., 1987), modulation of the redox potentials of various oxidative equivalent storage groups (Damoder, et al, 1986, Homann, 1988b, Itoh and Uwano, 1986, Ono, et al, 1986, Ono, et al, 1987, Sinclair, 1984, Theg, et al, 1984, Coleman and Govindjee, 1987, Boussac and Rutherford, 1994a), to a structural role for organising the polypeptide complex (Homann, 1988a, Homann, 1988b, Mavankal, et al, 1986, Coleman, et al, 1987b).

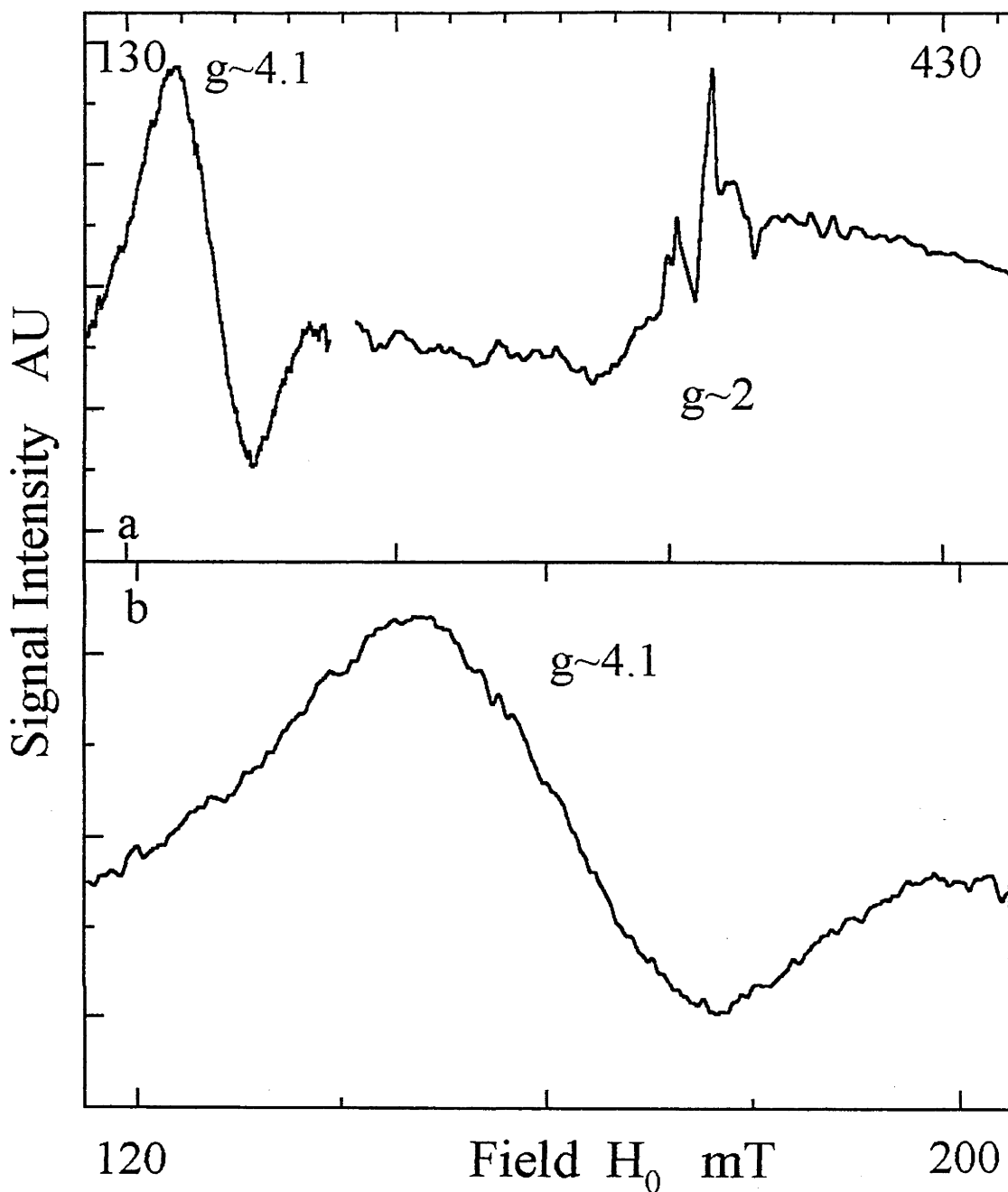


Figure 4.34. S_2 state signals from PSII samples inhibited by the Cl^- depletion / F^- exchange protocol as per Ono, et al 1987. Samples were illuminated at 200K. a). $g \sim 4$ and $g \sim 2$ regions, b). expansion of the $g \sim 4$ region. No multiline signals are generated in these samples. Illumination at temperatures up to 275K (in the presence of $100 \mu M$ DCMU) generate only the $g = 4.1$, data not shown. Spectrometer conditions: temperature 9K, microwave frequency 9.42 GHz, microwave power 2mW, modulation frequency 100 KHz, modulation amplitude 1.4mT.

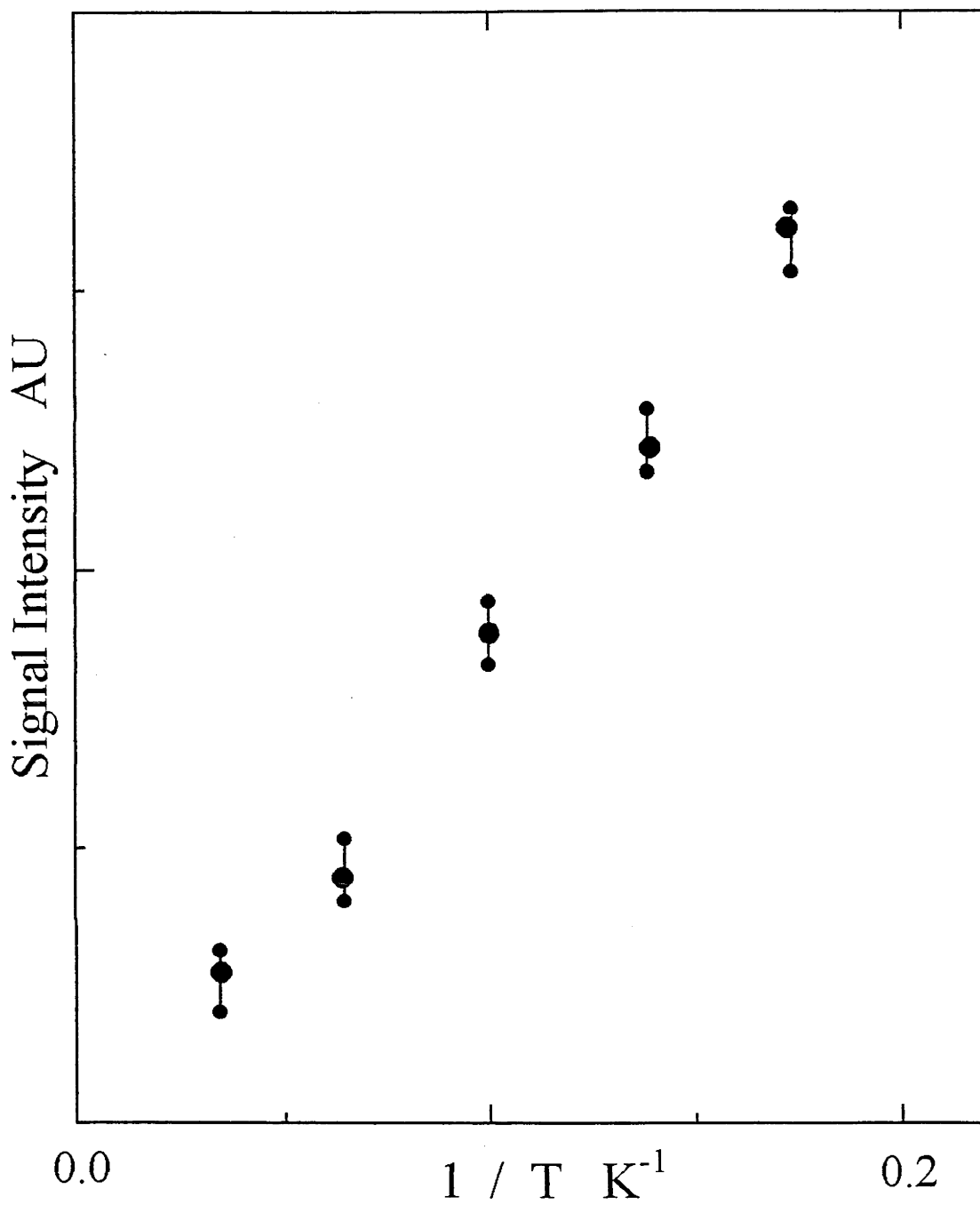


Figure 4.35. Temperature dependence of the S_2 state $g=4.1$ signal generated in PSII inhibited by Cl^- depletion / F^- exchange, illuminated at 200K. Signal intensities determined from the extrapolation of the power saturation to zero microwave power.

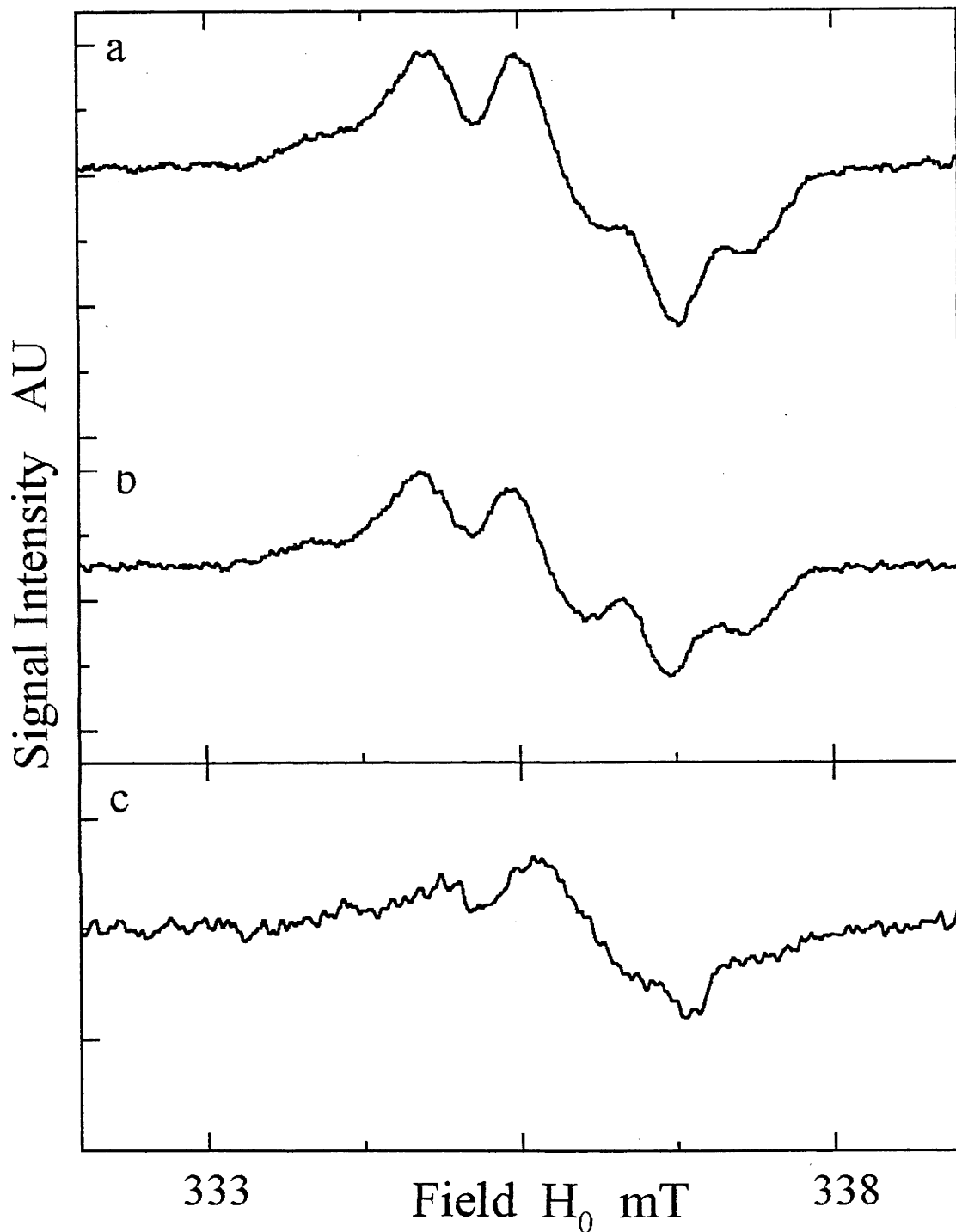


Figure 4.36. S_2 state Signal II line shapes for PSII inhibited by Cl^- depletion / F^- exchange, a). illuminated at 200K (in the presence of the $g=4.1$ signal), b). dark annealed at 295K for 10 minutes, where the samples relax back to the dark stable S_1 state. c). Subtraction difference spectrum for the illuminated spectrum minus the annealed spectrum manipulation. Line shape is similar to that of fig. 4.29. Spectrometer conditions as per fig. 4.29.

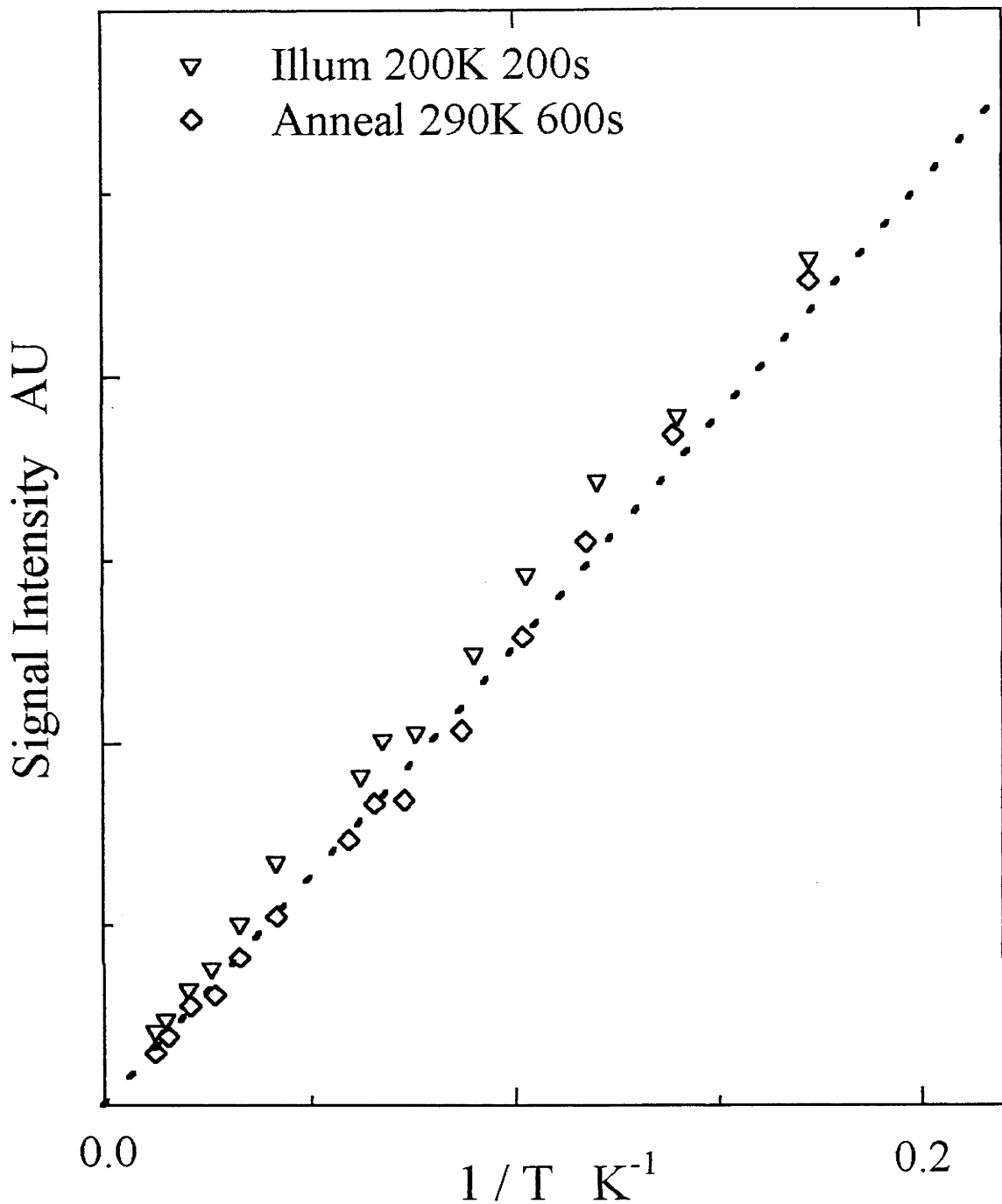


Figure 4.37. Temperature dependence of the total Signal II intensity recorded from PSII inhibited by Cl^- depletion / F^- exchange, (∇) illuminated at 200K (in the presence of the $g=4.1$ signal), (\diamond) subsequently dark annealed at 295K for 10 minutes (with the PSII relaxed to the S_1 state). Signal intensities determined from the extrapolation of the power saturation to zero microwave power.

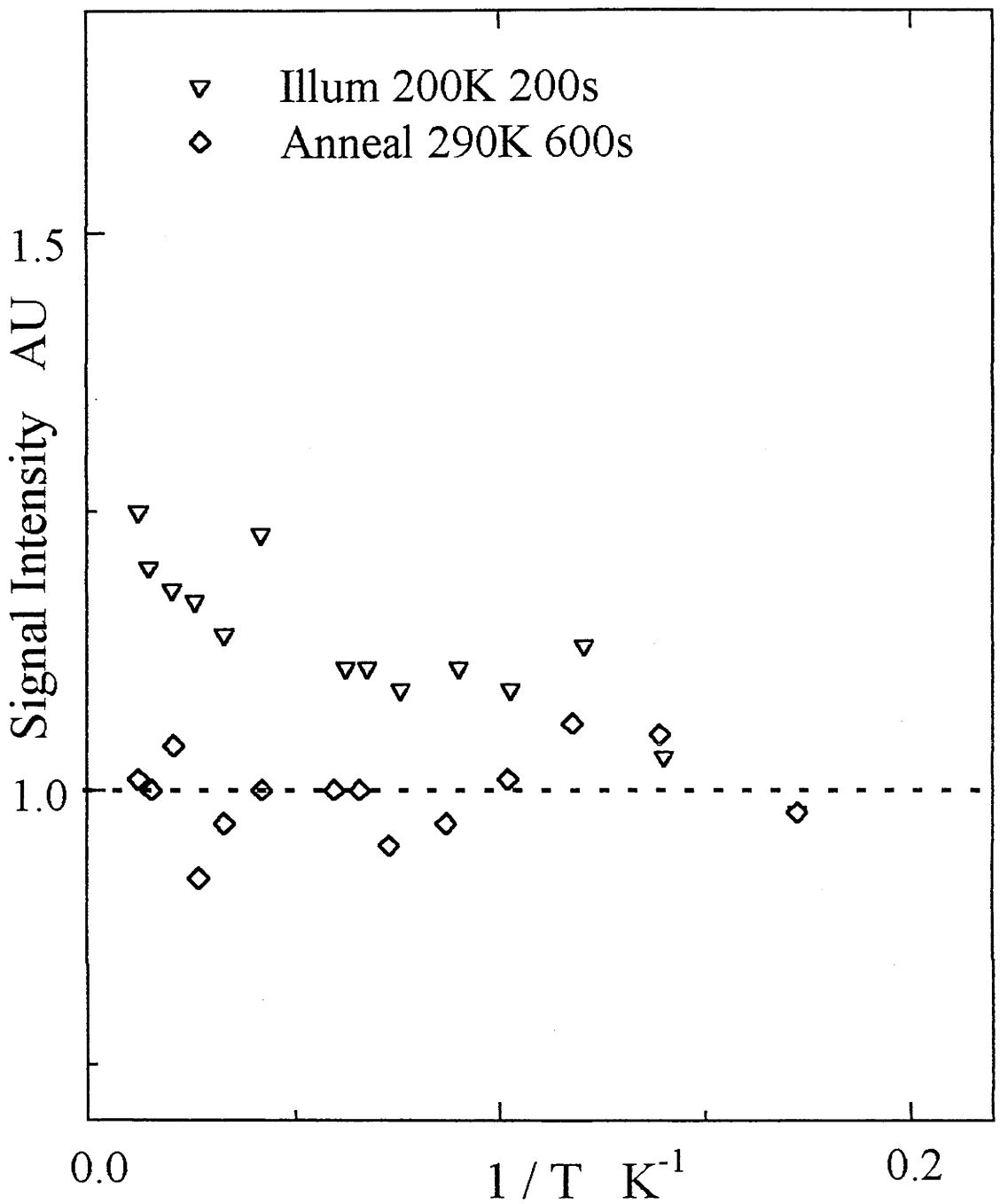


Figure 4.38. Presentation of the data from fig. 4.37 in a spin population format (signal intensity * T), as per fig. 4.28. Signal population scale is shown as a relative format scale based on the signal intensity of the signal recorded from the illuminated sample relative to the intensity of the signal recorded from the annealed sample. Dotted line indicates relative intensities expected for Curie behaviour.

between the S₁ state and the 'functional' S₂ state, displaying the multiline signal, as originally postulated by Casey and Sauer (Casey and Sauer, 1984). Both treatments developing the ground state g=4.1 signal, Cl⁻ depletion / F⁻ exchange and the extreme low temperature illumination (in the presence of the polyalcohol as cryoprotectant) appear to trap the oxidative equivalent transfer from P680⁺ at the secondary donor site, YZ. This adds evidence for the model presented in fig.4.33, in which YZ, the redox active electron transfer intermediate, acting as a bridging ligand across a strongly antiferromagnetically coupled Mn dimer, gives rise to the ground state g=4.1 signal upon YZ oxidation. The oxidation of YZ leads to the development of a spin 3/2 or 5/2 ground state, with the first excited state of the system arising from the conversion of the spin 1 or spin 2 dimer component to the next lowest spin state. The fact that the first excited state of the total system appears to be an isolated, YZ like species, suggests that the ground state g=4.1 signal system must be as a spin 3/2 state converting to a spin 1/2 first excited state, ie with the dimer component diamagnetic as discussed above. Previous reports have concluded that this F⁻ PSII g=4.1 arises from a spin 5/2 ground state species (Casey and Sauer, 1984, deRose, et al., 1995, Haddy, et al, 1992, Kawamori, et al., 1993, Vanngård, et al, 1992, Astashkin, et al., 1994b). However, it seems unlikely from the exchange coupling scheme spin state energy levels (fig. 4.23) that the first excited state from an S=5/2 ground state would result in a spin 1/2 state.

4.8.1.2. Illumination at 275K

Illumination of Cl⁻ depleted / F⁻ exchanged PSII at 275K, with subsequent rapid freezing under illumination, traps the OEC cycle into an electron transfer suspended state (Baumgarten, et al, 1990, Boussac and Rutherford, 1994a, Boussac and Rutherford, 1994b, Boussac, et al, 1992a). This suspended state has been inferred to consist of an altered S₃ state (S₃^{*}), with electron donation from the water oxidation site at the S₄ state blocked due to inhibition of turnover of YZ either after or during the development of the S₃ state (Nugent, et al, 1994, Sinclair, 1984, Theg, et al, 1984, Van Vliet and Rutherford, 1996, Boussac and Rutherford, 1994b, Boussac and Rutherford, 1992b, Boussac, et al, 1992a). Fig 4.39 shows the g~2 region of the spectrum formed by illumination of F⁻ PSII at 275K, cooling rapidly under illumination to ~100K and rapidly transferring the illuminated sample to liquid nitrogen (77K). This illumination regime generates an ESR signal centred at g~2.0 with an apparent peak to trough width of 9.5mT. This signal is similar to that observed previously for Cl⁻ depleted and Cl⁻ depleted / F⁻ exchanged PSII (Boussac and Rutherford, 1994a, Baumgarten, et al, 1990, van Vliet, et al., 1994, Van Vliet and Rutherford, 1996, Boussac and

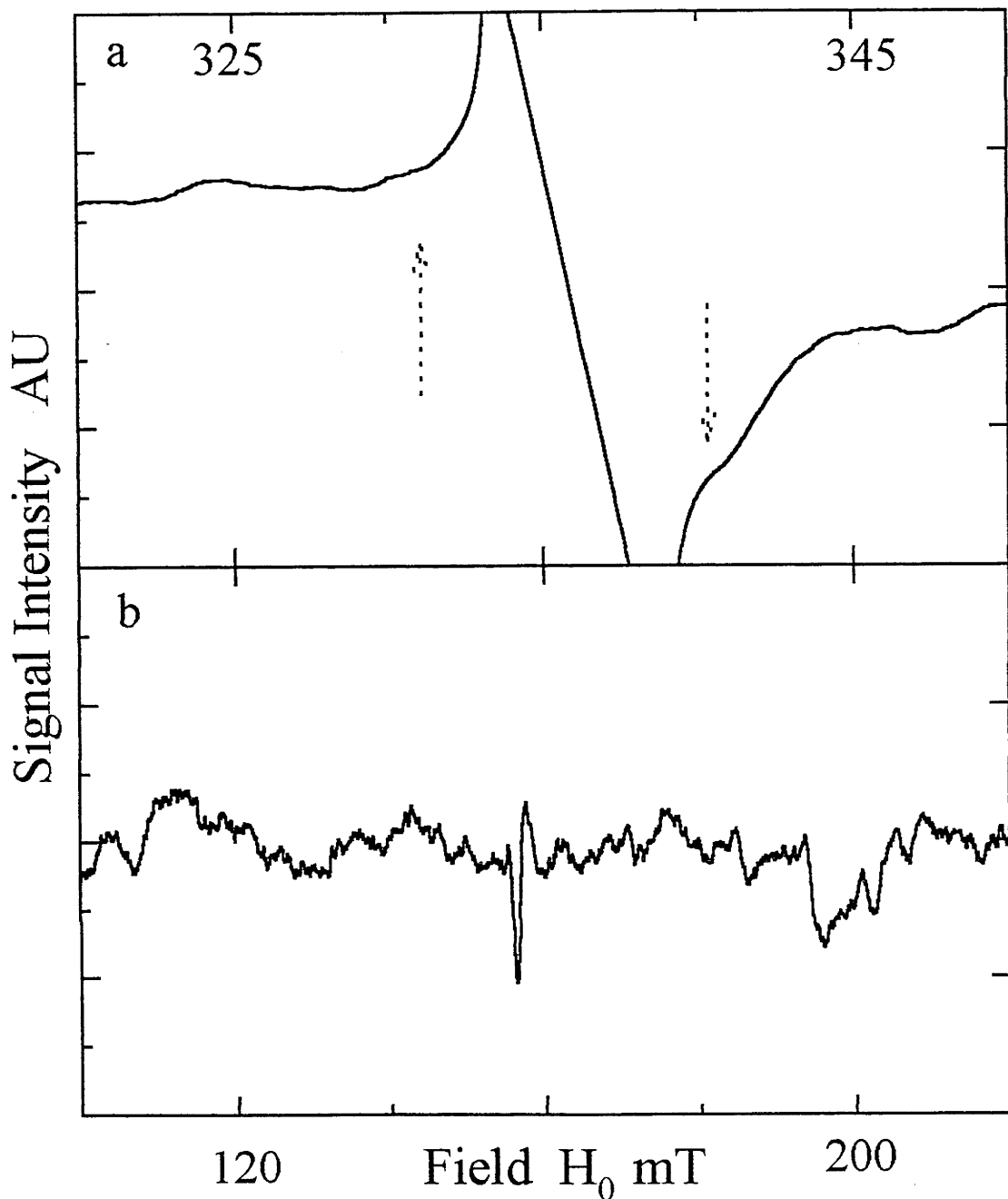


Figure 4.39. ‘Altered S_3 state’ signals recorded from PSII inhibited by Cl^- depletion / F exchange, illuminated at 275K for 90 seconds and cooled under illumination to ~ 120 K, see text. a). $g\sim 2$ region, arrows indicate the peak and trough positions of the S_3^* split signal. Signal is overlain by Signal II slow (Y_D^+), which hinders elucidation of the true line shape of this signal. b). $g\sim 4$ region indicating absence of any signal intensity in this region cogenerated with the $g\sim 2$ ‘split signal’. Spectrometer conditions: temperature 10K, microwave frequency 9.42 GHz, microwave power (a) 0.632mW, (b) 6.32mW, modulation frequency 100 KHz, modulation amplitude (a) 1mT, (b) 1.4mT.

Rutherford, 1994b, Boussac and Rutherford, 1994a, Boussac, et al, 1992a, Boussac and Rutherford, 1992b). This S_3 state signal has been postulated to arise from a spin-spin interaction between a Mn containing centre and an organic radical centre (Baumgarten, et al, 1990, Boussac, et al, 1990a), possibly an oxidisable amino acid residue such as an Histidine (Boussac and Rutherford, 1994b, Boussac and Rutherford, 1992b) or YZ (Boussac and Rutherford, 1994a, Baumgarten, et al, 1990, Hallahan, et al., 1992). This interaction is proposed to arise between two spin $1/2$ centres, generating a net spin 1 split signal. No other signals have been reported to be associated with this signal, eg signals in the $g=4$ region due to $\Delta m_S=2$ transitions from the spin 1 state. Figure 4.40 shows the temperature dependence of this altered S_3 state signal. This temperature dependence indicates that the altered S_3 state $g=2$ signal arises from an apparent ground state centre, displaying Curie behaviour between $\sim 6K$ and $\sim 50K$.

The model proposed for the S_2 state signals arising in the F PSII sample suggest that the $g=4.1$ signal arises from an $S=3/2$ centre. It is expected that this centre is a transitional state in the formation of the altered S_3 state, so that the altered S_3 state signal is a spin-spin exchange interaction between this $S=3/2$ centre with another centre, possibly another oxidisable amino acid residue. Such an interaction may lead to signal intensity in the $g=4$ region due to $\Delta m_S=2$ transitions for a centre with even spin $S=1$. Figure 4.39b shows the ESR spectrum for F⁻ PSII illuminated at 275K over the g range $g\sim 8$ to $g\sim 3$. This spectrum suggests no signal intensity is observed in the $g\sim 4$ to $g\sim 6$ region.

The $g\sim 2.0$ split signal has been postulated to arise from an $S=1$ centre (Boussac and Rutherford, 1988b, Boussac, et al, 1989, Hallahan, et al., 1992) generated by the spin-spin interaction of an organic radical with a Mn containing centre (Boussac and Rutherford, 1994a, Baumgarten, et al, 1990, Hallahan, et al., 1992, Nugent, et al, 1994, Boussac and Rutherford, 1994a, Boussac and Rutherford, 1994b, Boussac and Rutherford, 1992b). If the Mn centre is the same as that responsible for the ground state $g=4.1$ signal, generated in the S_2 state, the interaction must be antiferromagnetic between the organic radical and the (probable) $S=3/2$ $g=4.1$ centre. An alternative explanation may be that the Mn dimer involved in this centre may reside in the $S=0$ state, with the split S_3 state signal arising due to ferromagnetic spin-spin exchange between the oxidised YZ^+ and the organic radical, (discussed in chapter 5).

4.8.2. Treatment with 1M NaCl

The incubation of PSII in the presence of 1M NaCl has been shown to lead to the displacement of the 17 and 23 KDa extrinsic polypeptides (Blough and Sauer, 1984,

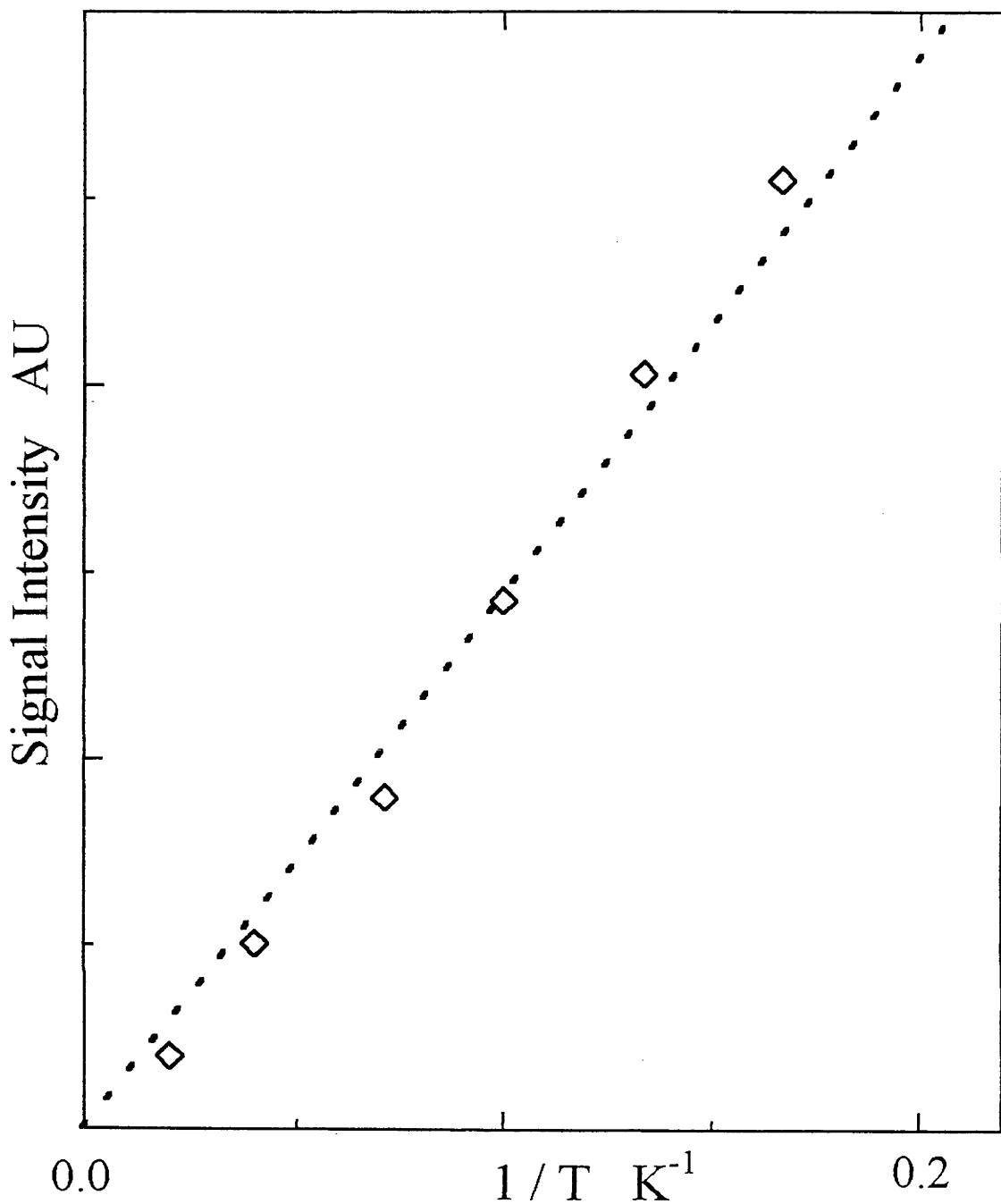


Figure 4.40. Temperature dependence of the S_3^* state $g \sim 2$ split signal generated in Cl^- depleted / F^- inhibited PSII, illuminated at 275K. Signal intensities are determined from the extrapolation of the power saturation to zero microwave power. The Curie type behaviour for this signal, apparent for temperatures between $\sim 5\text{K}$ and 50K , infers strong exchange between two $S=1/2$ centers coupled to form the spin $S=1$ state.

Cammarata and Cheniae, 1987, Shen, et al, 1988, Åkerlund, et al., 1982, Kuwabara and Murata, 1982) located on the luminal surface of the PSII complex, which is postulated to perturb Ca^{2+} binding near the OEC functional site (Boussac, et al, 1985b, Boussac, et al, 1985a, Cammarata and Cheniae, 1987, de Paula, et al, 1986a, Ghanotakis, et al, 1984, Boussac and Rutherford, 1988b, Boussac, et al, 1990a). The effect of these influences on the oxygen evolving site has been examined in the S_2 state, illuminating the sample at 200K and at higher temperatures in the presence of DCMU, and in the S_3 state, illuminating the sample at 275K.

4.8.2.1. Illumination at 200K

Incubation of functional PSII in the presence of 1M NaCl for 20 minutes, in the dark at room temperature, appears to have minimal affect on the generation of S_2 state signals upon illumination, as evidenced by the lineshapes and intensities of the multiline and $g=4.1$ signals. The multiline signals presented were generated by three illumination regimes; (i) illumination at 200K, (ii) illumination at 200K in the presence of 250 μM DCMU, and (iii) illumination at 275K in the presence of 250 μM DCMU, figure 4.41. The overall width and hyperfine / superhyperfine features are essentially identical for the three illumination regimes. The spectra for the $g\sim 4$ region are shown for the equivalent treatments in figure 4.42. The comparison of the multiline and $g=4.1$ signals averaged for the three illumination regimes generating this S_2 state are compared with the spectra for the multiline and $g=4.1$ signal generated in the S_2 state of uninhibited PSII, illuminated at 200K, figure 4.43. The spectra for the 1M NaCl incubated samples are observed to be almost equivalent to those for the uninhibited sample.

The spectra for the NaCl incubated PSII also evidence the presence of oxidised cyt b559, as seen from the features at $g\sim 3$ and $g\sim 2.2$ in figs. 4.41 and 4.43. This suggests a change in the electron transfer capabilities of the donor side of PSII. This 'competition' between cyt b559 and the Mn OEC for electron donation to P680^+ (de Paula, et al, 1985a, de Paula, et al, 1986a, Noguchi, et al, 1993) may be due to a partial breakdown of the OEC, possibly due to a slow loss of Ca^{2+} from binding sites close to the Mn structure within the OEC site. This was examined by allowing a sample to incubate in the presence of 1M NaCl for a period of 20 hours before illumination. If the 1M NaCl was to loosen the binding of and/or remove the 17 and 23 KDa extrinsic polypeptides, which are proposed to protect Ca^{2+} binding site(s) near the OEC, a slow leaching of Ca^{2+} will occur. Upon illumination of the PSII at 275K in the presence of 100 μM DCMU sample incubated in the presence of 1M NaCl

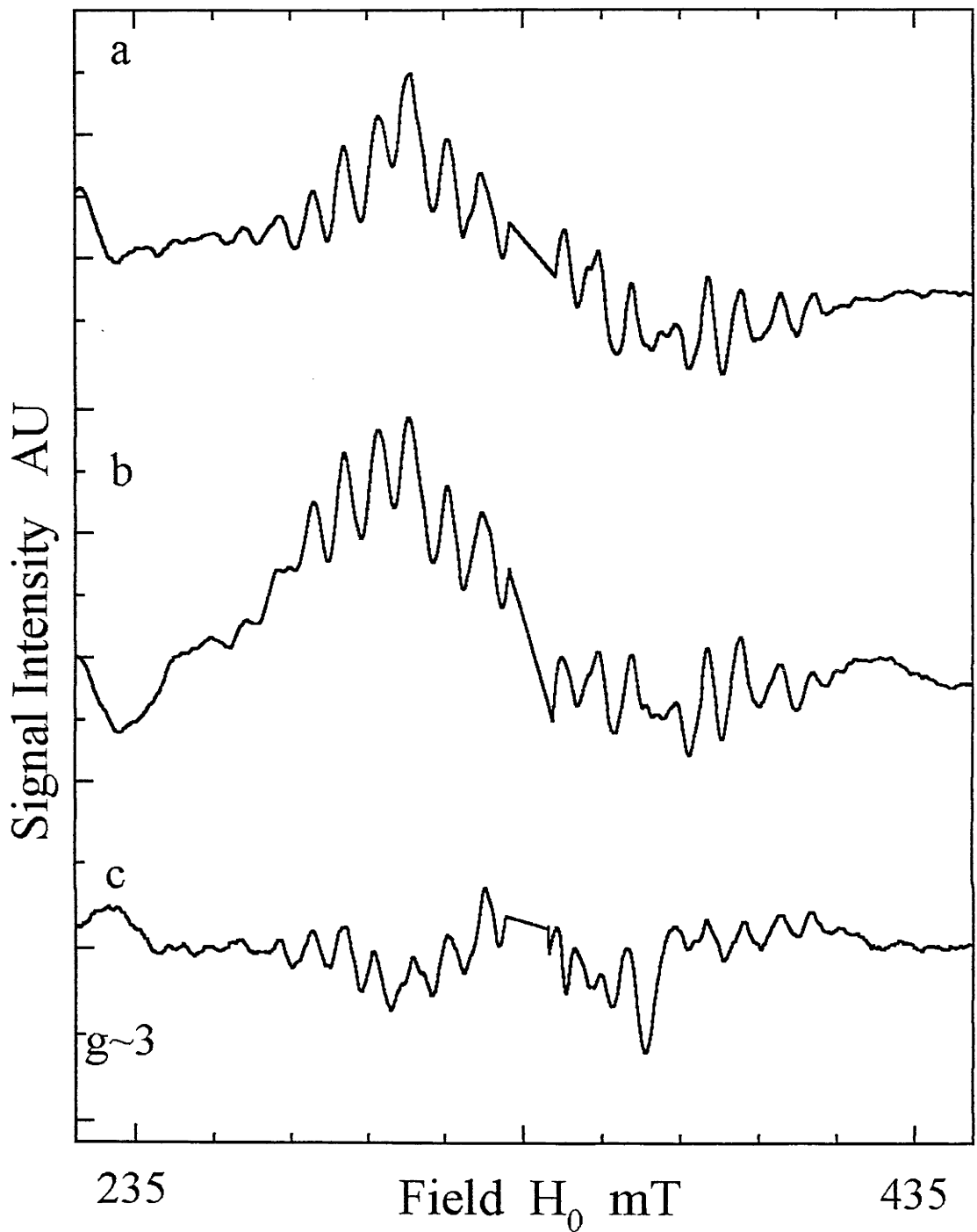


Figure 4.41. Comparison of S_2 state multiline signals generated in PSII incubated in the presence of 1M NaCl, a). illuminated at 200K, b). illuminated at 200K in the presence of 100 μ M DCMU (in DMSO), and c). illuminated at 275K in the presence of 100 μ M DCMU (in DMSO). Spectrometer conditions: temperature 9K, microwave frequency 9.42 GHz, microwave power 2mW, modulation frequency 100 KHz, modulation amplitude 2mT.

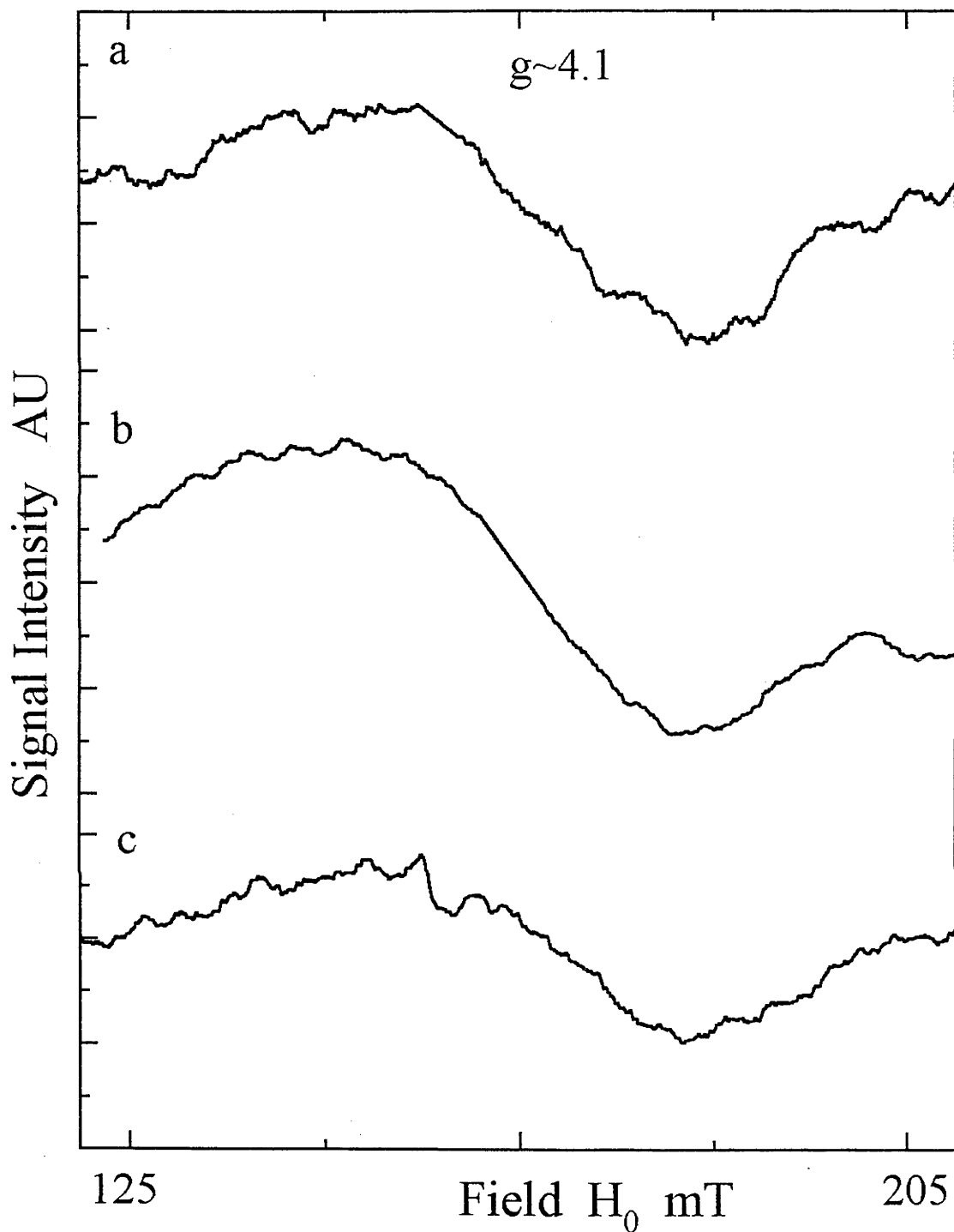


Figure 4.42. Comparison of S_2 state $g=4.1$ signals generated in PSII incubated in the presence of 1M NaCl, a). illuminated at 200K, b). illuminated at 200K in the presence of 100 μ M DCMU (in DMSO), and c). illuminated at 275K in the presence of 100 μ M DCMU (in DMSO). Spectrometer conditions as per fig. 4.41 with modulation amplitude 1.4mT.

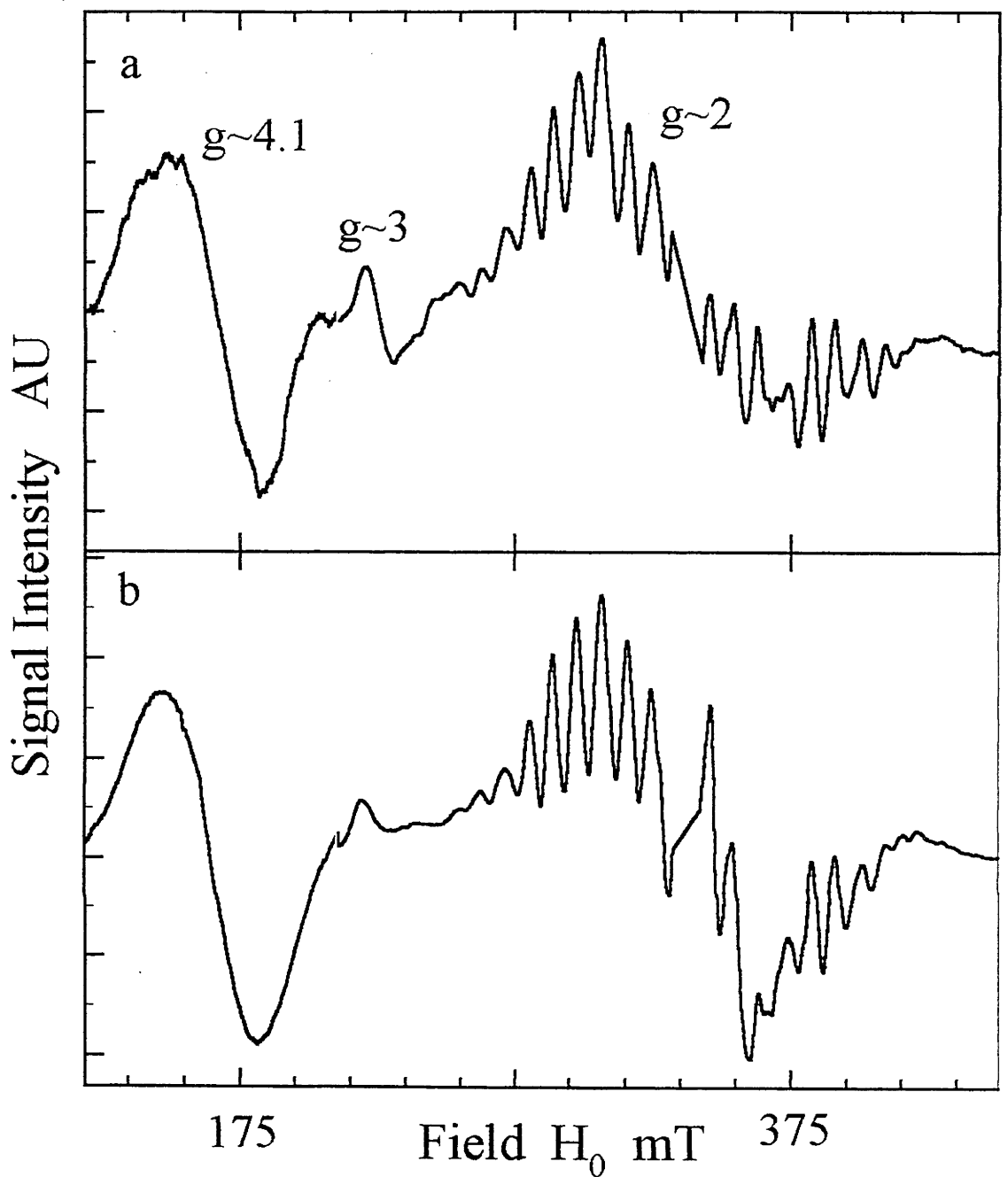


Figure 4.43. Comparison of S_2 state $g=4.1$ and multiline signals generated in PSII illuminated at 200K. a). PSII cryoprotected with 0.4M sucrose incubated in the presence of 1M NaCl, b). PSII cryoprotected with 0.4M sucrose. Spectrometer conditions as per fig. 4.41.

for 20 hours, no signals are generated in the $g \sim 2$ nor $g \sim 4$ regions which may be assigned to the OEC, fig 4.44. These spectra show some cyt b559 is still capable of rereducing $P680^+$ with intensity developed on the 2.97 and 2.20 resonance positions. The inability to develop either multiline or $g=4.1$ signal intensity indicates a serious disruption in functioning of the Mn cluster of the OEC. This may well be due to the slow loss of Ca^{2+} from the Mn OEC site leading to a degradation of the protein environment, effectively breaking apart the Mn OEC binding site, over a slow period.

The short term incubated PSII was still able to develop significant multiline intensity with illumination at 200K. The overall similarity of the 1M NaCl incubated multiline and the uninhibited PSII multiline suggests that the initial weakening of the binding of the 17 and 23 KDa extrinsic polypeptides does not necessarily affect the immediate functioning of the Mn OEC site (de Paula, et al, 1986a, Ono and Inoue, 1988, Boussac, et al, 1990a). Longer incubation in the presence of 1M NaCl, which appears to lead to a full breakdown of the Mn OEC site, suggests slow leaching of Ca^{2+} and the requirement of Ca^{2+} for the stability not only of the oxygen evolving Mn site, but the Mn site responsible for the ground state $g=4.1$ also. This is consistent with the accepted view for the role for Ca^{2+} and the 17 and 23 Kda extrinsic polypeptides in maintaining the stability of the luminal region of the D1D2 complex influencing the efficiency of water oxidation (Andreasson, et al, 1994, Blough and Sauer, 1984, Boussac, et al, 1985b, Boussac, et al, 1989, Cammarata and Cheniae, 1987, Ghanotakis, et al, 1984).

4.8.2.2. Illumination at 275K

The slow development of S_2 state dysfunction over many hours indicates a loss of Mn from the OEC. This Mn depletion must involve an initial loss of Ca^{2+} , which is well known to be severely inhibitory (Boussac, et al, 1985b, Boussac, et al, 1989, Boussac, et al, 1992a, de Paula, et al, 1986a, Boussac, et al, 1990a). Illumination of PSII at 275K allows multiple turnovers of the OEC through the S states. The presence of an inhibitory condition leading to a blockage of S state turnover has been shown to allow generation of a signal centred near $g \sim 2$. These signals are considered to consist of 'spilt' resonances arising in a perturbed S_3 states (Boussac, et al, 1989, Boussac, et al, 1992a). They have been proposed, as noted above, to arise from $S=1$ centres consisting of the exchange interaction between a Mn containing centre and an organic radical (Boussac, et al, 1989, Hallahan, et al., 1992, de Paula, et al, 1986a, Boussac, et al, 1990a). The effect of illuminating PSII, inhibited by Cl^- depletion / F^- exchange at 275K, to generate such an S_3 state resonance has been demonstrated earlier. The effect of illuminating PSII incubated in the presence of 1M NaCl at 275K, followed by

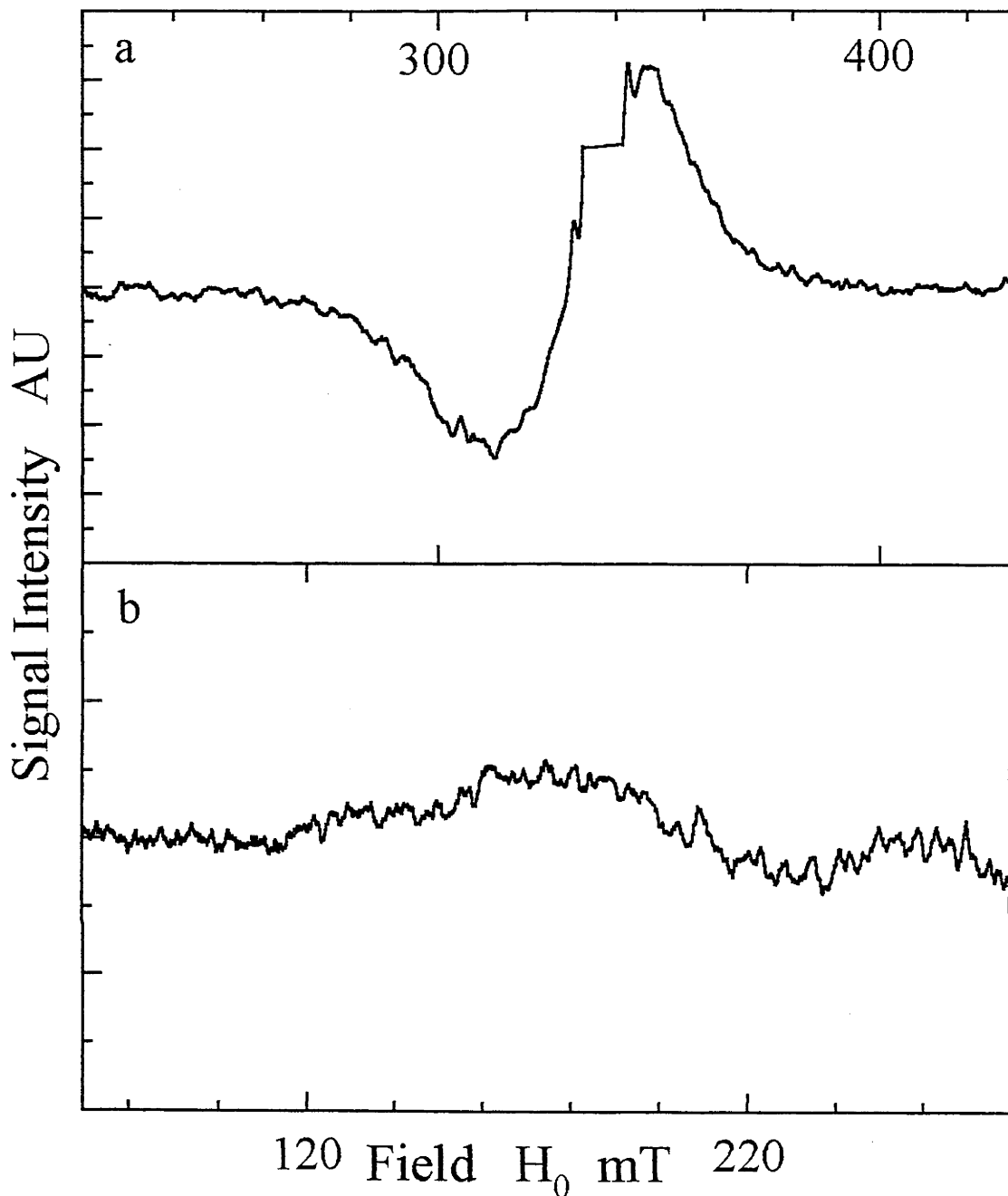


Figure 4.44. Examination of the $g \sim 2$ and $g \sim 4$ regions in the “ S_2 state” of PSII incubated in the presence of 1M NaCl and $100 \mu\text{M}$ DCMU for 24 hours on ice, followed by illumination at 275K. a). $g \sim 2$ region indicating the absence of multiline signal formation, b). $g \sim 4$ region indicating possible formation of an altered $g=4.1$ signal, the signal shifted to higher field compared to the functional state $g=4.1$ signal, likely due to an altered Mn environment. Spectrometer conditions as per fig. 4.41.

illumination under cooling to $\sim 100\text{K}$, was to generate an S_3 state 'split' signal centred at $g \approx 2.003$ with a peak to trough width of $\sim 15\text{mT}$, figure 4.45. The effects of various treatments of NaCl samples prior to 275K illumination are shown in 4.46. During illumination, and in the transfer process to liquid nitrogen (for post illumination storage), some multiline signal is generated. Comparison of the multiline signal formed in the presence of the S_3^* signal with that of the uninhibited multiline S_2 state, figure 4.47, indicates that the single recombination step, from the ' S_3 ' state back to the ' S_2 ' state, in the presence of 1M NaCl does not lead to a modification of the multiline signal, as has been observed for the equivalent treatment of NH_3 incubated PSII (Beck and Brudvig, 1986, Beck and Brudvig, 1986, Beck and Brudvig, 1988a, Boussac, et al, 1990c). This is in contrast to the report of Rutherford and coworkers, where the treatment with 1.2M NaCl and EGTA generated an altered multiline signal with reduced hyperfine spacing $\sim 5.5\text{ mT}$ (Boussac, et al, 1989). The differences observed here may well be a consequence of the non-addition of EGTA, which 'aggressively chelates Ca^{2+} aiding in its withdrawal from the protein (Boussac, et al, 1985b, Boussac, et al, 1985a, Boussac and Rutherford, 1988a, Boussac, et al, 1989, Boussac, et al, 1990a). This indicates that while the high concentration NaCl treatment may alter the S state turnover properties of the OEC, in the absence of Ca^{2+} chelators, it does not alter the hyperfine and superhyperfine features of the multiline signal generated in the S_2 state, either by direct single electron withdrawal turnover, or upon single electron recombination from the altered S_3 state.

The nature of the spin centre forming this altered S_3 state, characterised by the 15mT p-p 'split' signal, is examined with regard to its temperature dependence in figure 4.48. The temperature dependence indicates behaviour consistent with the signal arising from a ground state centre. The temperature dependence also suggests that the centre may interconvert to an excited state upon increase in temperature, with the ground state split signal intensity collapsing toward zero at $1/T \sim 0.05\text{K}^{-1}$ or $T \approx 20\text{K}$. This apparent depopulation of the ground spin state, which might still be only a relaxation effect, follows a roughly similar temperature regime to that for the uninhibited PSII S_2 state multiline generated by illumination at 200K in the absence of alcohols (see fig 4.12 and Pace, et al., 1991). The proposed origin of the split S_3 state signal is a spin-spin interaction between an $S=1/2$ organic radical and the centre giving rise to the S_2 state multiline signal. The S_3 state signal arising from this illumination and 'inhibition' regime would therefore arise from an $S=1$ state, which is the resultant of the spin-spin interaction of the multiline $S=1/2$ centre with a second donor site, an oxidisable organic radical with spin $S=1/2$. The first excited state of the functional PSII multiline S_2 state is observed to be an $S=3/2$ state, giving rise to the

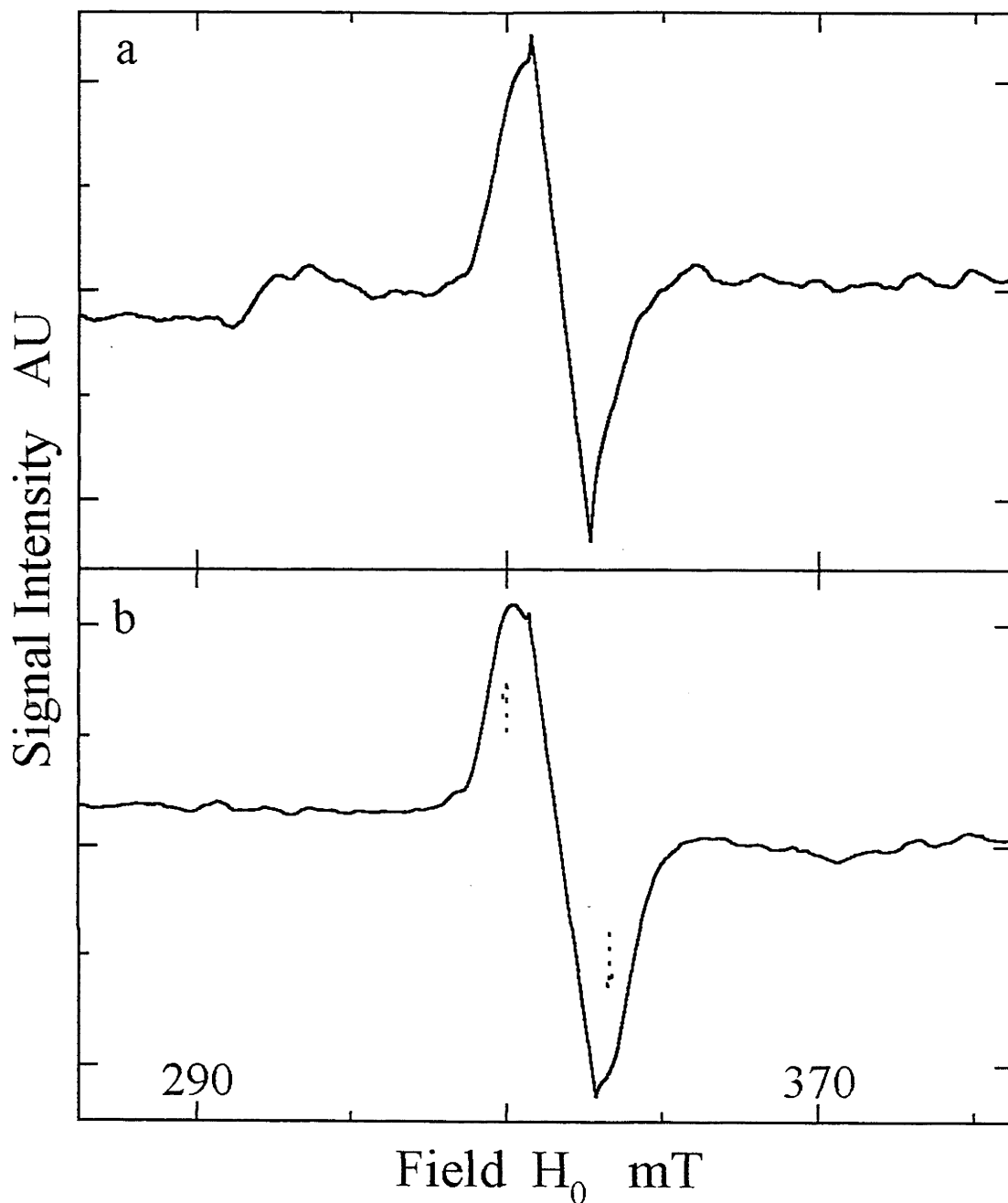


Figure 4.45. Comparison of S_3^+ state signals generated in PSII incubated in the presence of 1M NaCl, illuminated at 275K for 90 seconds. a). PSII with 100 μ M PpBQ, b). PSII with 5mM EDTA. Spectrometer conditions: temperature 9K, microwave frequency 9.42 GHz, microwave power 0.63mW, modulation frequency 100 KHz, modulation amplitude 1mT.

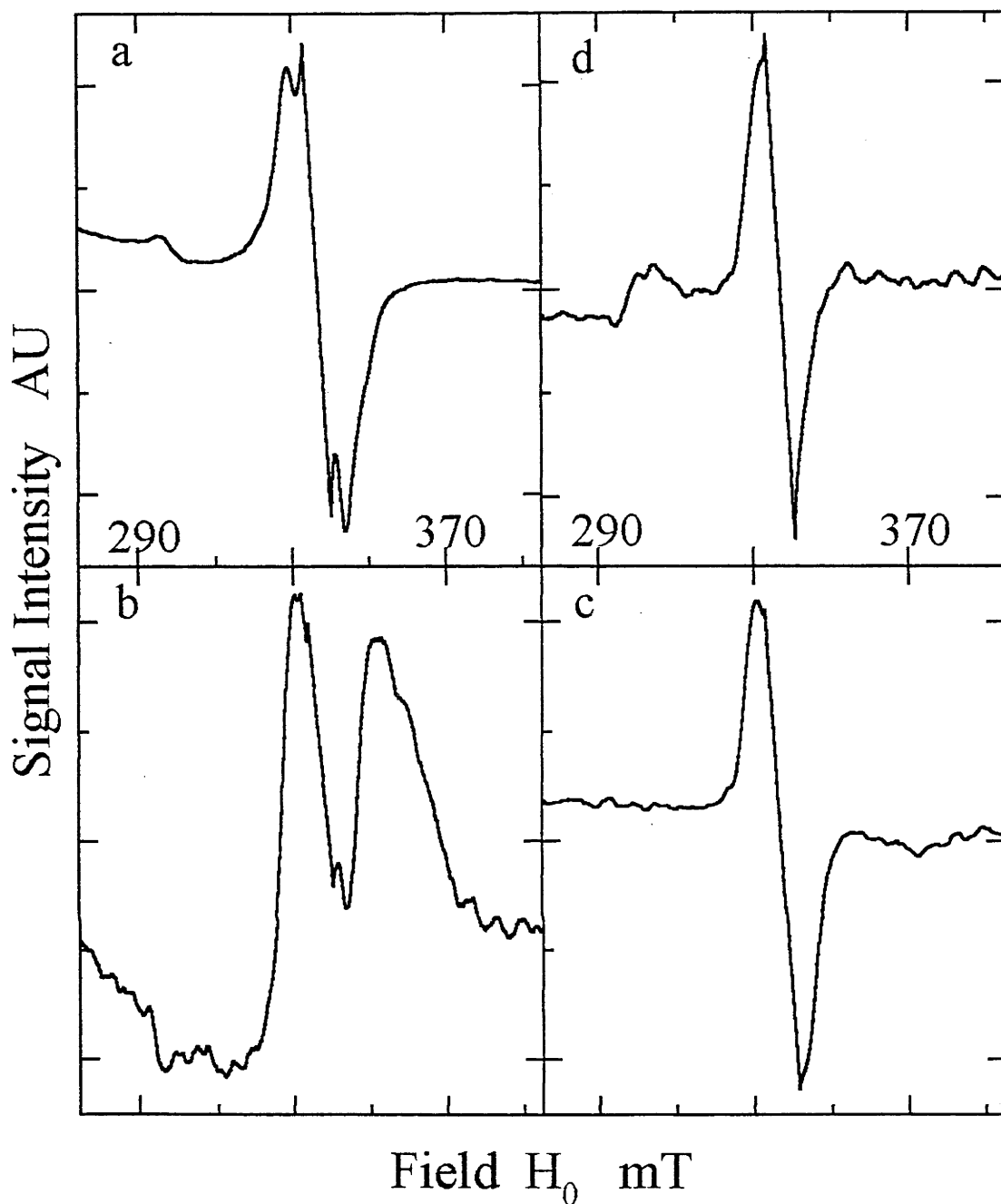


Figure 4.46. Comparison of signals arising from different methods of generating the S_3^* state signals in PSII incubated in the presence of 1M NaCl, illuminated at 275K. a). PSII with 10mM $K_2Fe(CN)_6$, b). PSII left overnight on ice, the S_3^* state $g \sim 2$ signal is cogenerated with a broad signal similar in nature to that observed in fig. 4.44(a), c). PSII with 5mM EDTA, illuminated at 275K, annealed at 290K for 20 minutes and reilluminated at 275K, indicating the capability of the donor side electron transfer, and the blockage of the OEC cycling before the S_4 state, d). PSII with 100 μ M PpBQ, as per fig. 4.45(a). Spectrometer conditions: temperature 9K, microwave frequency 9.42 GHz, microwave power 0.63mW, modulation frequency 100 KHz, modulation amplitude 1mT.

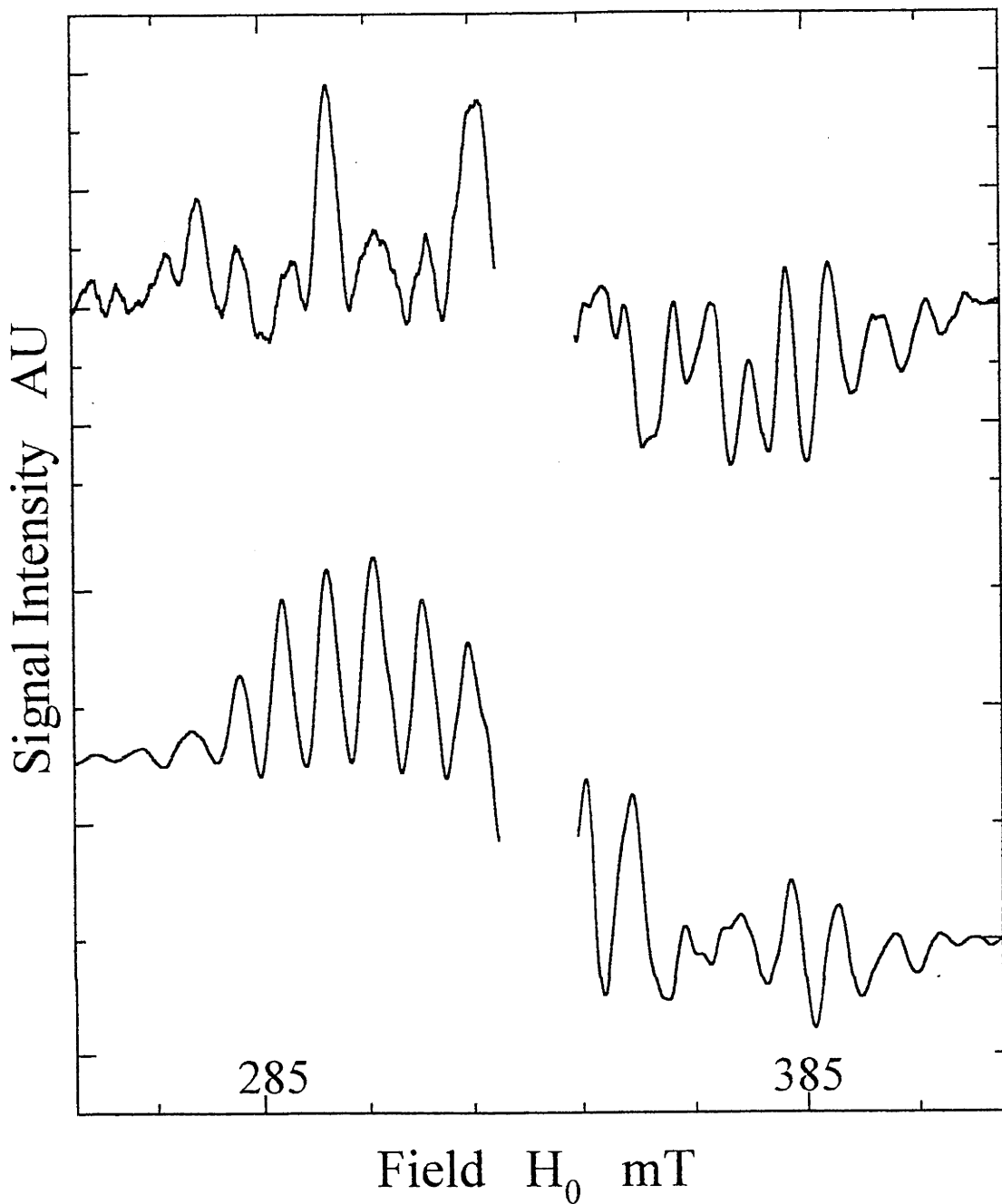


Figure 4.47. Comparison of multiline signals generated in PSII cryoprotected with 0.4M sucrose, a). samples incubated with 1M NaCl, illuminated at 275K, the multiline signal underlies the S_3^* state $g\sim 2$ split signal, b). functional PSII illuminated at 200K, forming the S_2 state. Spectrometer conditions, (a) as per fig. 4.46, (b) as per fig. 4.01.

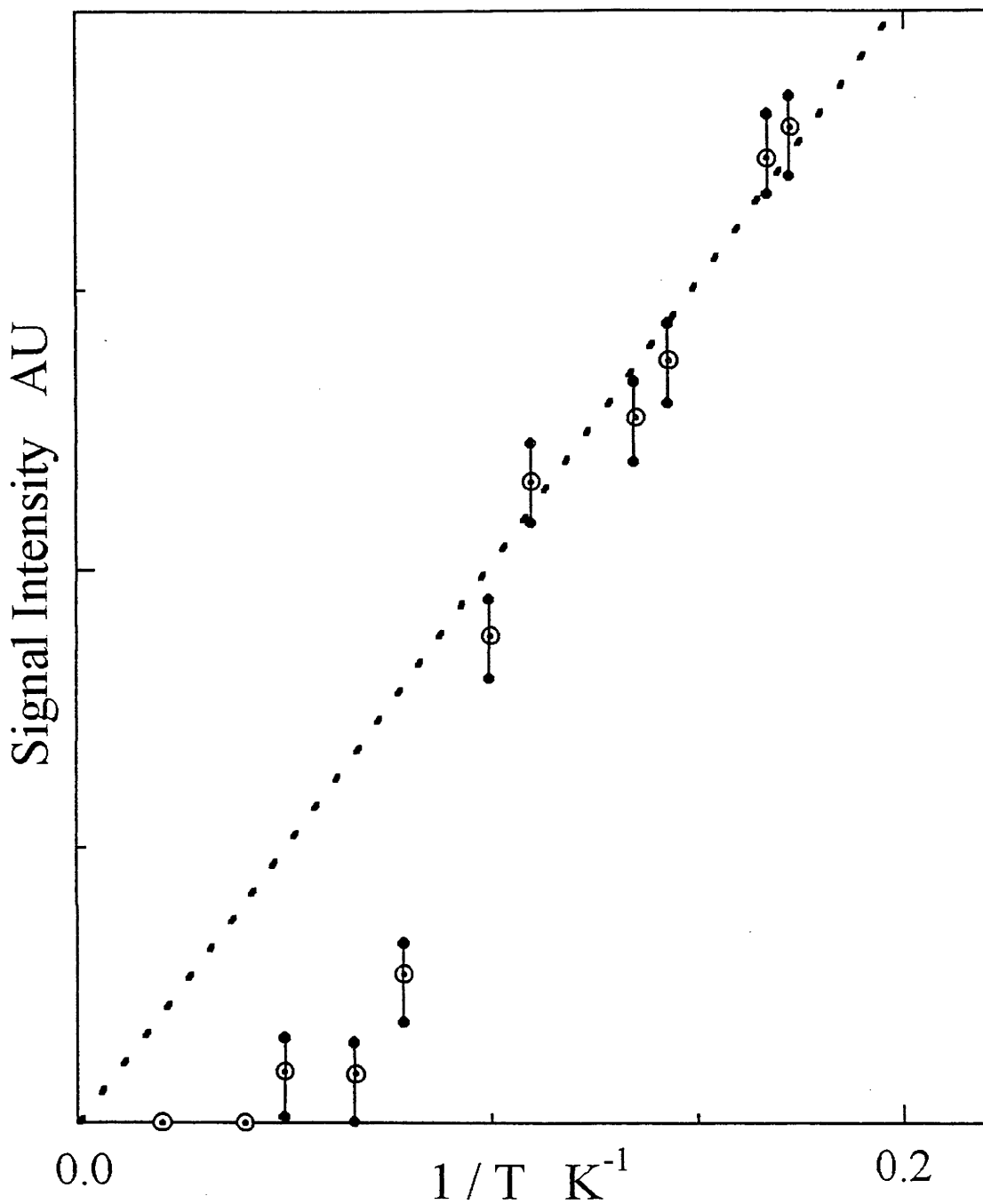


Figure 4.48. Temperature dependence of the S_3^* state $g \sim 2$ split signal generated in PSII incubated in the presence of 1M NaCl, illuminated at 275K. Data taken from all variations of 1M NaCl treated PSII S_3^* state forms, see fig. 4.45. Signal intensities are derived from extrapolation of the power saturation to zero microwave power. Dotted line indicated intensities expected for Curie behaviour. Exchange constant is estimated from the temperature at which the signal intensity is estimated to fall to $1/e$ (0.368) of the Curie behaviour approximation, see chapter 5.

excited state form of the $g=4.1$ signal (see earlier). Examination of the $g\sim 4$ region, actual range $g\sim 8$ to $g\sim 3$, figure 4.49, indicates that the $g=4.1$ associated with the multiline is not generated. The spectrum does indicate the presence of a resonance at low field, in the $g\sim 5$ to 6 region, however. The temperature dependence behaviour of this $g\sim 5.5$ signal, figure 4.50, indicates that it follows the same temperature dependence as the $g\sim 2$ 'split' signal. This suggests that this low field signal ($g\sim 5$) could be the $\Delta m_s = 2$ transition of the $S=1$ ground state. It also appears that no excited state signals arise due to the transition of the multiline centre from the $S=1/2$ ground to the $S=3/2$ first excited state.

The nature of the signal examined here is somewhat different to that of the Cl^- depletion / F^- exchange treated sample. The F^- PSII sample appeared not to be able to remove electrons from the OEC site, the multiline signal site, evidenced by the inability to develop a multiline signal with illumination at 275K in the presence of DCMU, with the S_2 and S_3 state signals arising from the oxidation of the Mn centre responsible for the ground state $g=4.1$ signal. Here, with the inhibition due to 1M NaCl incubation loosening the binding of the 17 and 23 Kda polypeptides and possibly loosening Ca^{2+} binding close to the OEC site, at least partial oxidation of the oxygen evolving Mn is possible to the multiline S_2 state, and the second electron withdrawal, leading to the S_3 state, giving rise to a broader 'split' signal. It is interesting to ponder the turnover capability of this high concentration NaCl treated PSII, as although the S_3 state signal appears consistent with previous reports (Boussac, et al, 1989, Hallahan, et al., 1992, Boussac, et al, 1990a), the 1M NaCl treated PSII withdraws electrons from a Mn containing site different to that for the F^- PSII, from the pattern of signals generated. From our data on uninhibited S_2 state signals, these centres are magnetically isolated, one comprising the O_2 evolving site and the second a redox intermediate site near YZ. Despite this, the pattern of a 'split' resonance centred near $g\sim 2$ indicates a certain consistency between the different inhibition forms of the ' S_3 ' states as noted above. Thus there are similar signal patterns for the Cl^- depletion / F^- exchange and 1M NaCl incubation treatments, even though the specific signals are significantly different. A reasonable hypothesis would be that in both cases, the split signal arises from a spin-spin interaction between an oxidised protein side chain and an odd spin Mn containing centre.

The inferred spin state interconversion to the first excited state in the 1M NaCl treated PSII appears not to have any obviously observable ESR signals associated with it. From the temperature dependence of the uninhibited PSII multiline S_2 state, where the $S=1/2$ ground state is thermally excited to populate the $S=3/2$ state even at temperatures $\sim 10\text{K}$, one might expect the spin-spin exchange to form an $S=2$ excited state in the altered S_3 state, assuming

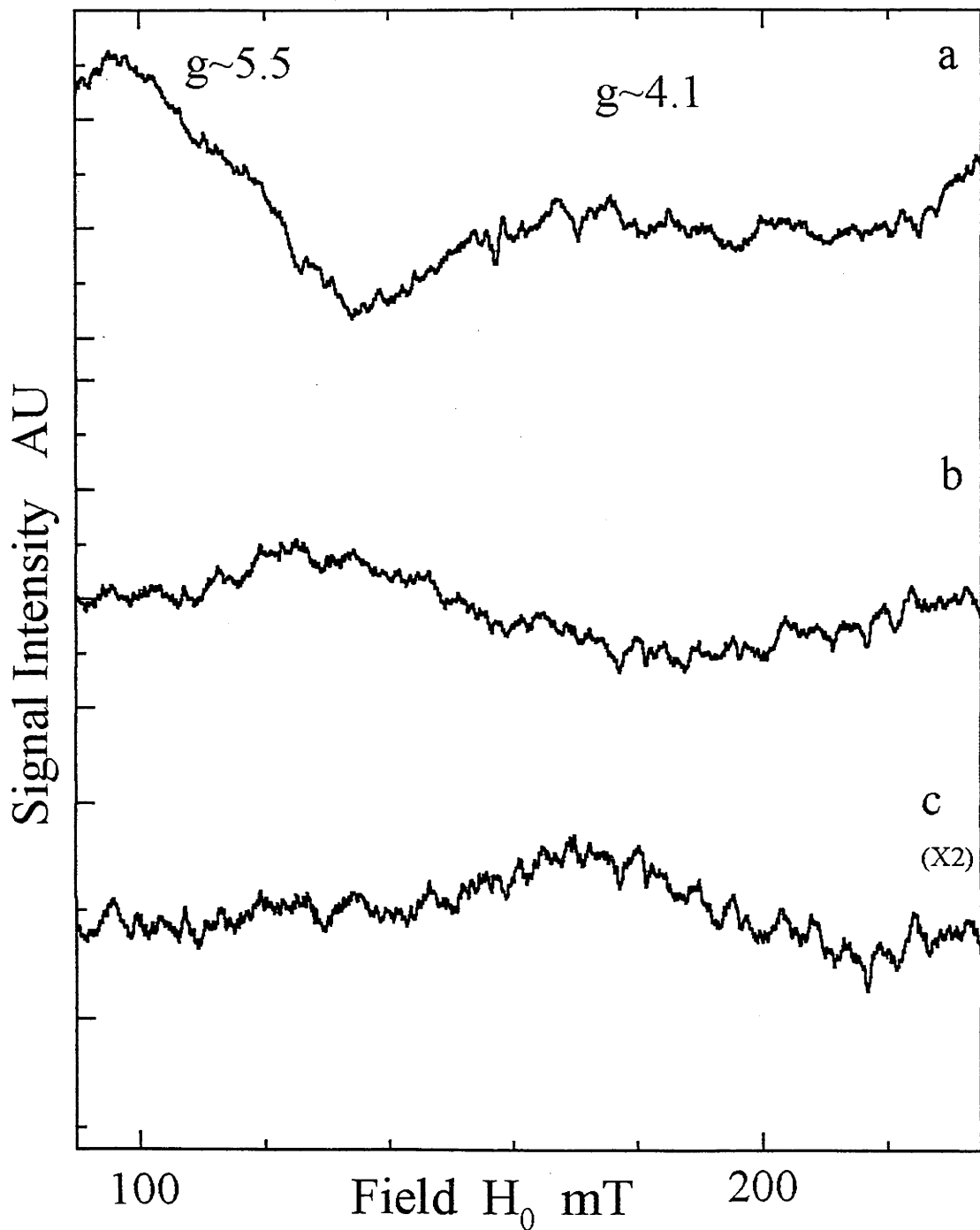


Figure 4.49. S_3^* state signals generated in the $g \sim 4$ to $g \sim 6$ region in PSII incubated in the presence of 1M NaCl, illuminated at 275K. a). Signal line shape for spectrum recorded at 10K, b). signal line shape for spectrum recorded at 15K, and c). signal line shape for spectrum recorded at 25K. Spectrometer conditions as per fig. 4.41.

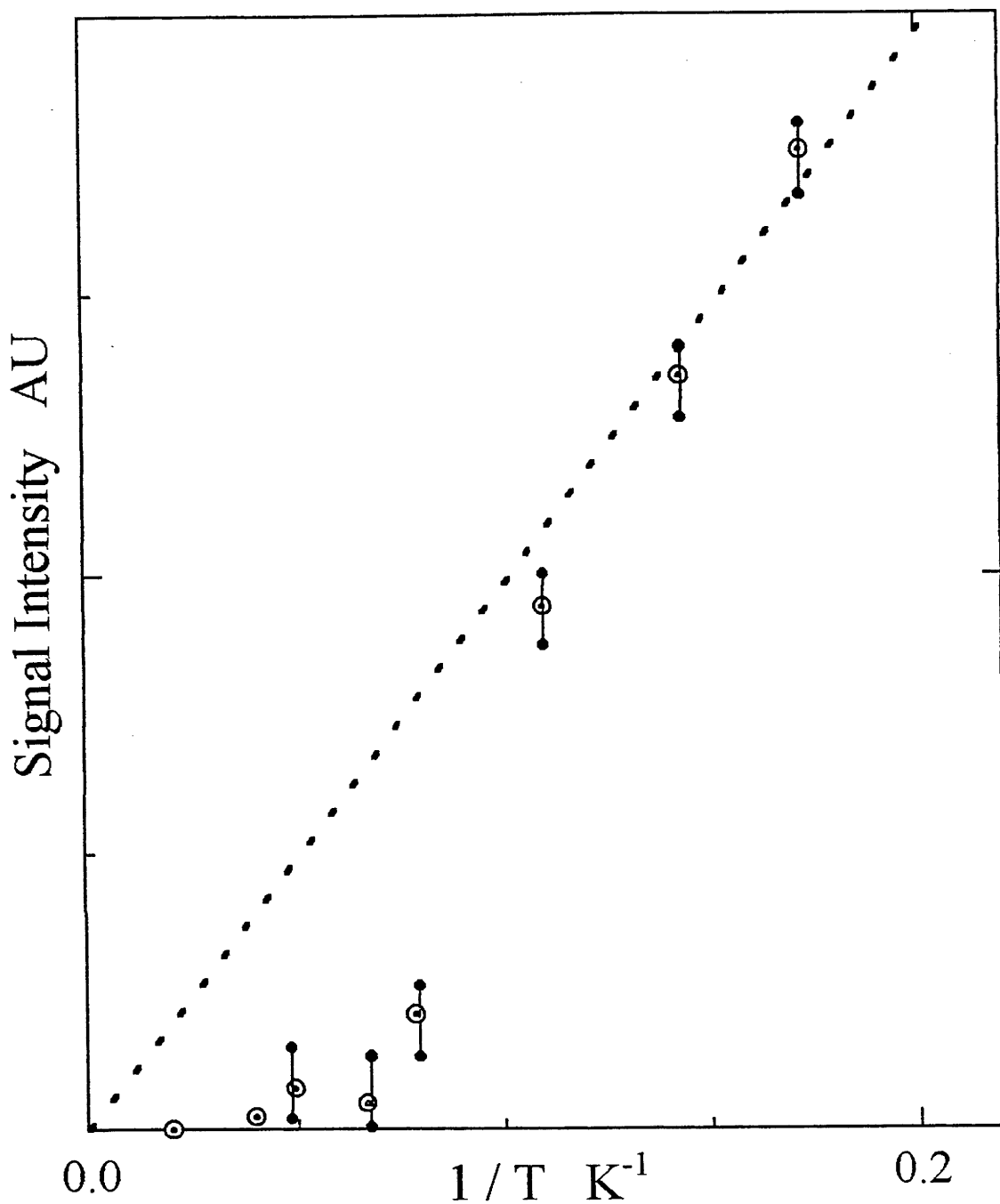


Figure 4.50. Temperature dependence of the S_3^+ state signals generated in the $g \sim 4$ to $g \sim 6$ region in PSII incubated in the presence of 1M NaCl, illuminated at 275K. Signal intensities are derived from the extrapolation of the power saturation to zero microwave power. Signal intensities above ~ 12 K are determined from the signals which have shifted in g value to higher field, see fig. 4.47.

the ferromagnetic exchange behaviour between the $S=1/2$ and thermally populated $S=3/2$ centres is retained. This behaviour does not appear to arise and leads to further speculation over the S_2 to altered S_3 electron withdrawal step. Previous studies on Mn μ -oxo and μ -hydroxo bridged model compounds have indicated two main properties relevant to this study. The exchange coupling between the Mn ions in the compounds is shifted in the antiferromagnetic direction when hydrogen ions are removed from the bridging ligands. That is the μ -oxo bridged compounds have much stronger antiferromagnetic coupling than the μ -hydroxo bridged compounds (Cooper, et al., 1978, Inoue, 1978, Knopp and Wieghardt, 1991, Larson, et al., 1992a, Larson, et al., 1992b, Baldwin, et al., 1994). The second feature of the Mn model compounds concerns the oxidisability of the compounds upon sequential electron withdrawal. The ability to sequentially oxidise a Mn μ -hydroxo bridged compound is enhanced by the deprotonation of one of the bridging ligands upon each oxidation step. As an initial oxidation occurs, the oxidation potential for subsequent oxidations steps is lowered if a proton is released from the bridging ligands (Manchandra, et al., 1991, Thorp and Brudvig, 1990, Thorp, et al., 1989, Baldwin, et al., 1993). These two properties may be playing an important role in the S_2 to S_3 oxidation step within the OEC, with the release of protons from bridging ligands enabling the continued oxidation through the four step process. If a deprotonation occurs upon oxidation from the S_2 to S_3^* stage, the magnitude of the antiferromagnetic coupling between the Mn ions of the dimer will be strengthened, reducing the capability of populating the higher spin states of the exchange coupled dimer system. This may contribute to the inability to observe higher spin state signals in the altered S_3 state, ie. an inability to populate $S=2$ spin state.

Still, the excited state of the S_3 PSII displays no obvious ESR signals, and the loss of the ground state is observed to be dramatic from the temperature dependence. Two possibilities arise. One is that the excited state (probably $S=2$) is simply too broad to see, or is invisible due to large zero field splitting effects. Another possibility is that the spin lattice T_1 relaxation rate for one of the $S=1/2$ centres becomes faster than the effective exchange energy rate (J/h) (see Chapter 2), such that the exchange between the Mn centre and the radical is lost due to one of the centres relaxing at a too higher rate. This breakdown of the exchange interaction leads to the development of signal intensity for one or both of the $S=1/2$ centres individually. No signal intensity is observed for the Mn multiline which would be expected to arise for such a situation. However, such a reduction in T_1 would lead to significant broadening of the signal linewidth, making observation of this signal difficult. The organic radical would generate signal intensity within the Signal II region of the ESR spectrum. Figure 4.51 shows the temperature dependence of the lineshape of Signal II under

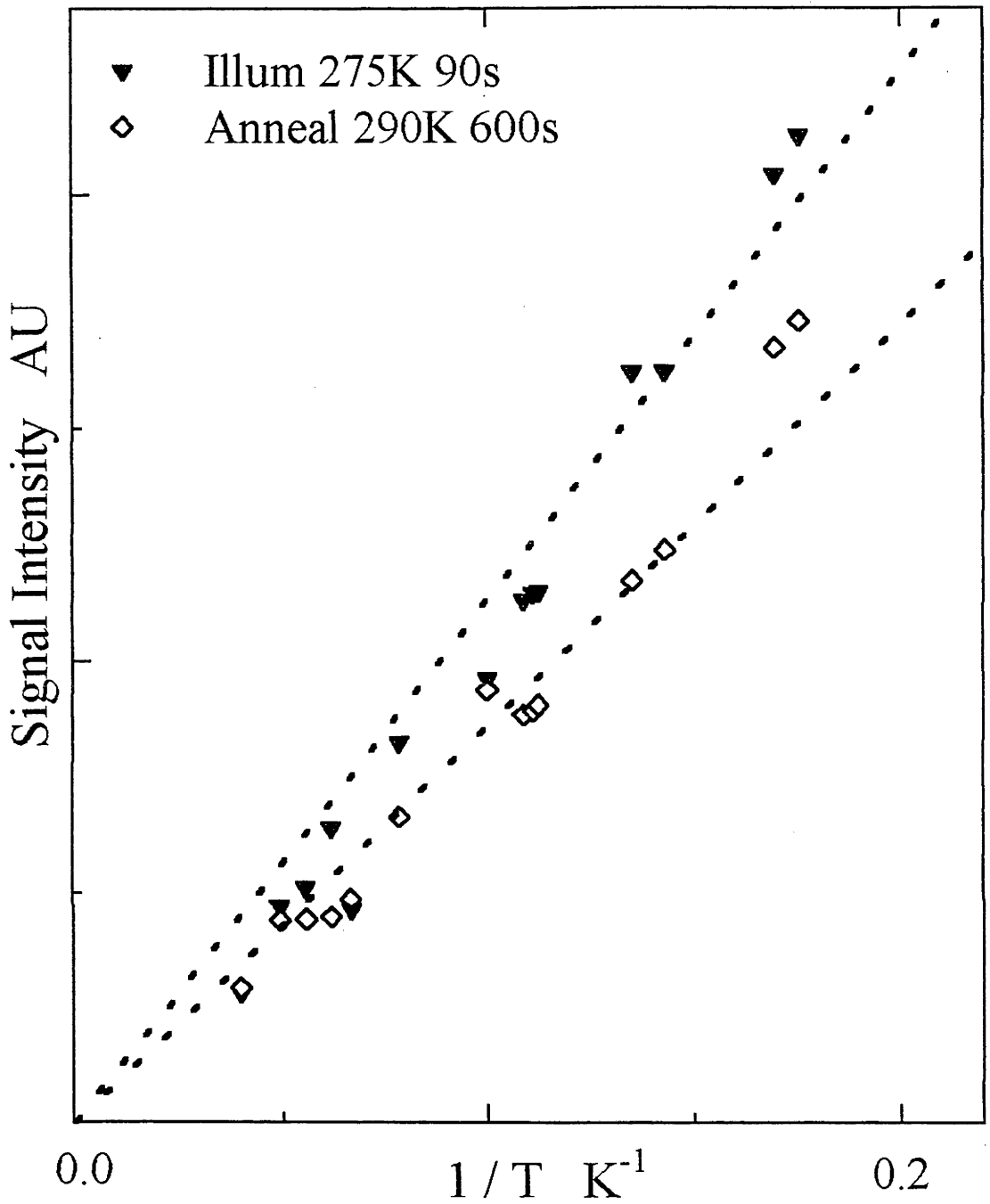


Figure 4.51. Temperature dependence of the total Signal II region intensity generated in PSII incubated in the presence of 1M NaCl, illuminated at 275K, (conditions generating the S_3^* state), and dark annealed at 295K for 10 minutes, (relaxing the PSII back to the S_1 state). Signal intensities determined from the signal line shape amplitude for the spectra recorded at $20\mu\text{W}$, from the data for fig. 4.49.

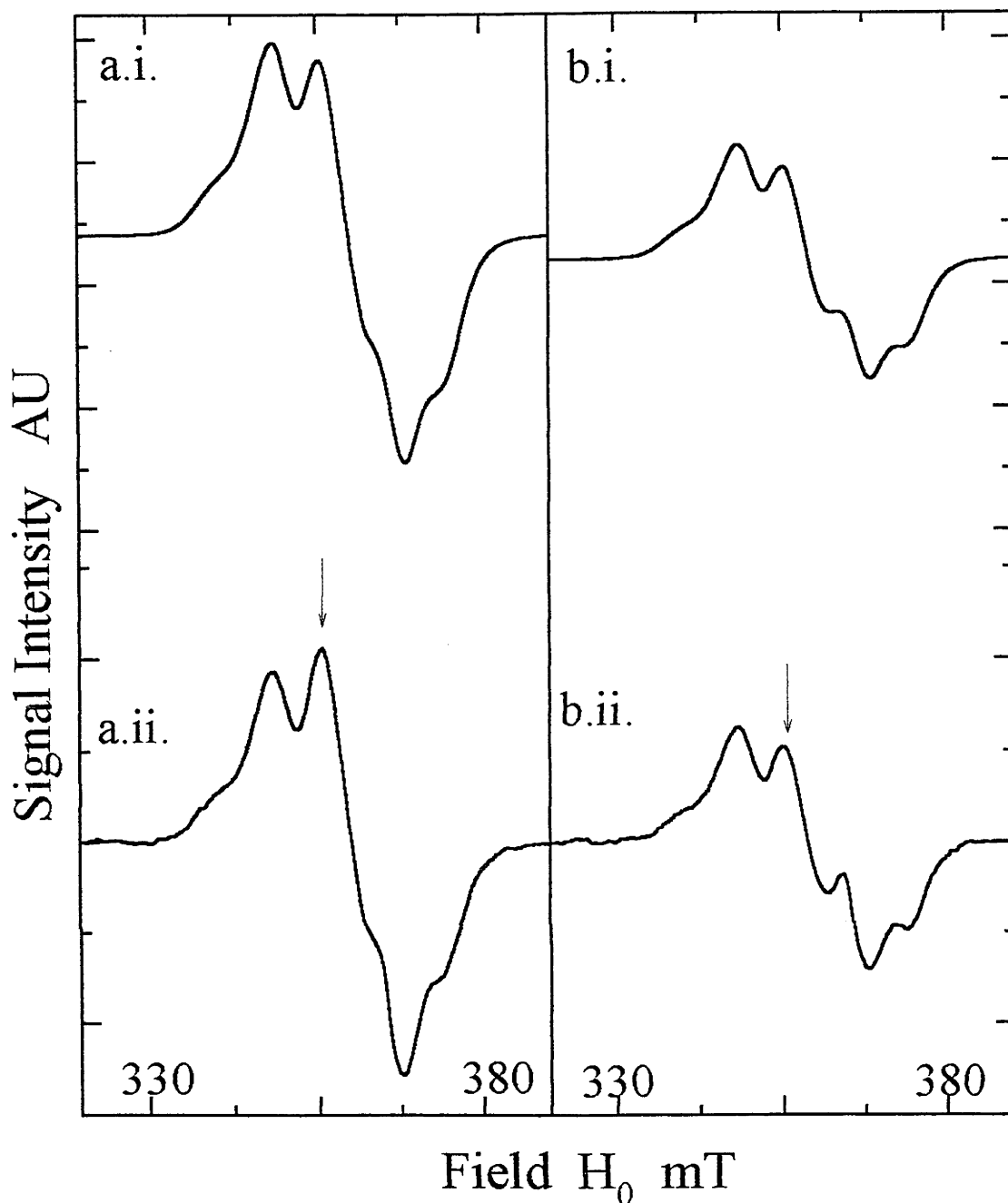


Figure 4.52. Comparison of the Signal II line shapes for spectra recorded from the S_3^* state generated in PSII incubated in the presence of 1M NaCl, illuminated at 275K. Signal II line shapes recorded at a). 6K and b). 25K from (i) illuminated samples (in the presence of the S_3^* state $g\sim 2$ split signal), and (ii) samples subsequently dark annealed at 295K for 10 minutes (in which the PSII is relaxed back to the S_1 state, ie Signal II slow in isolation). Line shapes indicate only minor intensity differences in the hyperfine peaks immediately lower field to the central g value (as indicated). Spectrometer conditions: temperatures as indicated, microwave frequency 9.42 GHz, microwave power $20\mu\text{W}$, modulation frequency 1.56 KHz, modulation amplitude 0.1mT.

1M NaCl incubation conditions, illuminated to the S_3^* state. It is possible that a change in the fine structure of Signal II occurs with increasing temperature, due to the effective 'populating' of the $S=1/2$ radicals spin state leading to $g \sim 2$ signal intensity. However, the temperature dependence of the total Signal II intensity of the illuminated (S_3^* state) and dark annealed (S_1 state) samples indicates no development of additional signal intensity at high temperatures. The curves indicate that the illuminated sample consists of an additional signal overlaying the dark Signal II_s, implying Y_Z^+ formation independent of the $g \sim 2$ split signal in these samples. The lineshapes of the Signal II region recorded at 10K and 25K for each of the 275K illuminated and 290K dark annealed samples, figure 4.52, appears to confirm the conclusion from the temperature dependence. little apparent difference are observed to develop in the Signal II line shape recorded from the illuminated sample. However, the relative signal amplitudes for the Signal II spectra recorded at the different temperatures implicates a constant additional component in the illuminated sample, possibly indicative of oxidation of Y_Z after the formation of the split signal state (Boussac, et al, 1990a, Boussac and Rutherford, 1992b, Boussac, et al, 1992a).

4.8.3. PSII Incubated in the presence of 600mM Acetate

It has been suggested that the inhibitory anion acetate competes with Cl^- for anion binding sites on the donor side of PSII (Bock, et al, 1988, Jursinic and Stemler, 1988, MacLachlan and Nugent, 1993, Ono, et al, 1987, Sinclair, 1984), such that the presence of acetate slows rereduction of Y_Z^+ , ie. limits the electron transfer from the Mn oxygen evolving site (Bock, et al, 1988, MacLachlan and Nugent, 1993). Through Cl^- depletion and exchange of CH_3COO^- for Cl^- , Ono and coworkers observed that acetate restricted the S_2 state to the $g=4.1$ signal form, similar to that observed for the F^- exchange treated PSII, (Ono, et al, 1987 and see earlier). Without the Cl^- depletion step, inhibition of the S_2 state multiline signal generated by 200K illumination of acetate treated PSII was dependent on the initial Cl^- concentration. 200mM acetate was required to inhibit multiline formation in the presence of 1mM Cl^- , while in the presence of 15mM Cl^- an acetate concentration of ≥ 600 mM was required for inhibition of multiline formation (Saygin and Witt, 1986, Sinclair, 1984). The data presented here were recorded with a high level of Cl^- , 35mM, within the storage buffer, while examining the effects of incubation of PSII in the presence of either 600mM $NaCH_3COO$ (NaAcetate) or 300mM $Ca(CH_3COO)_2$ (CaAcetate) at pH ~ 5.5 . The generation

of S_2 state signals by illumination at 200K, and the signals generated by illumination of the acetate treated samples at 275K while cooling under illumination to ~ 100 K were examined.

4.8.3.1 Illumination at 200K

4.8.3.1.1. NaAcetate

Incubation of PSII in the presence of 600mM NaCH_3COO (NaAc) for 20 minutes blocks the generation of the multiline signal when the sample is illuminated at 200K, figure 4.53a. The $g=4.1$ signal is generated in preference to the multiline signal, figure 4.53b, indicating a dysfunction in the electron transfer out of the oxygen evolution Mn site, with the redox equivalent held on YZ. In addition to the $g=4.1$ signal, electron donation to P680^+ from cyt b559 is evident from the observation of the $g\sim 3.0$ and $g\sim 2.2$ turning points of the oxidised centre. The centre field scan for this sample displays two signals on the high field region of $g=2$. These signals both arise from the FeQA centre, at $g\sim 1.82$ and $g\sim 1.74$. The resonance at $g\sim 1.74$ suggests an effect of the acetate on the acceptor side of PSII, as the shift of the FeQA signal has been previously reported to be indicative of an alteration to the environment of the FeQA site (Blubaugh and Govindjee, 1988, Sandusky and Yocum, 1986, Sinclair, 1984, Vermaas, et al., 1984). The presence of the cyt b559^+ and an altered FeQA^- signal suggests effects on both the donor and acceptor regions of PSII. The $g=4.1$ signal generated appears altered, with the lineshape less axial than that for the uninhibited enzyme and for F^- exchange inhibition. This altered $g\sim 4$ signal is centred at $g\approx 4.20\pm 0.05$ with a peak to trough width of 28mT.

4.8.3.1.2. Ca Acetate

Incubation of PSII in the presence of 300mM $\text{Ca}(\text{CH}_3\text{COO})_2$ (CaAc_2), changes the form of the S_2 state generated by 200K illumination such that the multiline signal is now the dominant Mn based ESR signal, figure 4.54. Some cyt b559 signal is generated, evidenced by the presence of signal intensity at the $g\sim 3$ and $g\sim 2.2$ turning points for oxidised cyt b559, and significant FeQA^- signal amplitude is observed, most of which is at $g\sim 1.82$, with less apparent intensity in the $g\sim 1.72$ region. The development of signal intensity in the $g\sim 4$ region by illumination of PSII incubated in the presence of 300mM CaAc_2 at 200K is shown in figure 4.54b. The $g\sim 4$ region signal generated in the presence of CaAc_2 is very similar in form to that observed in the NaAc incubated sample illuminated at 200K. These two $g=4.1$

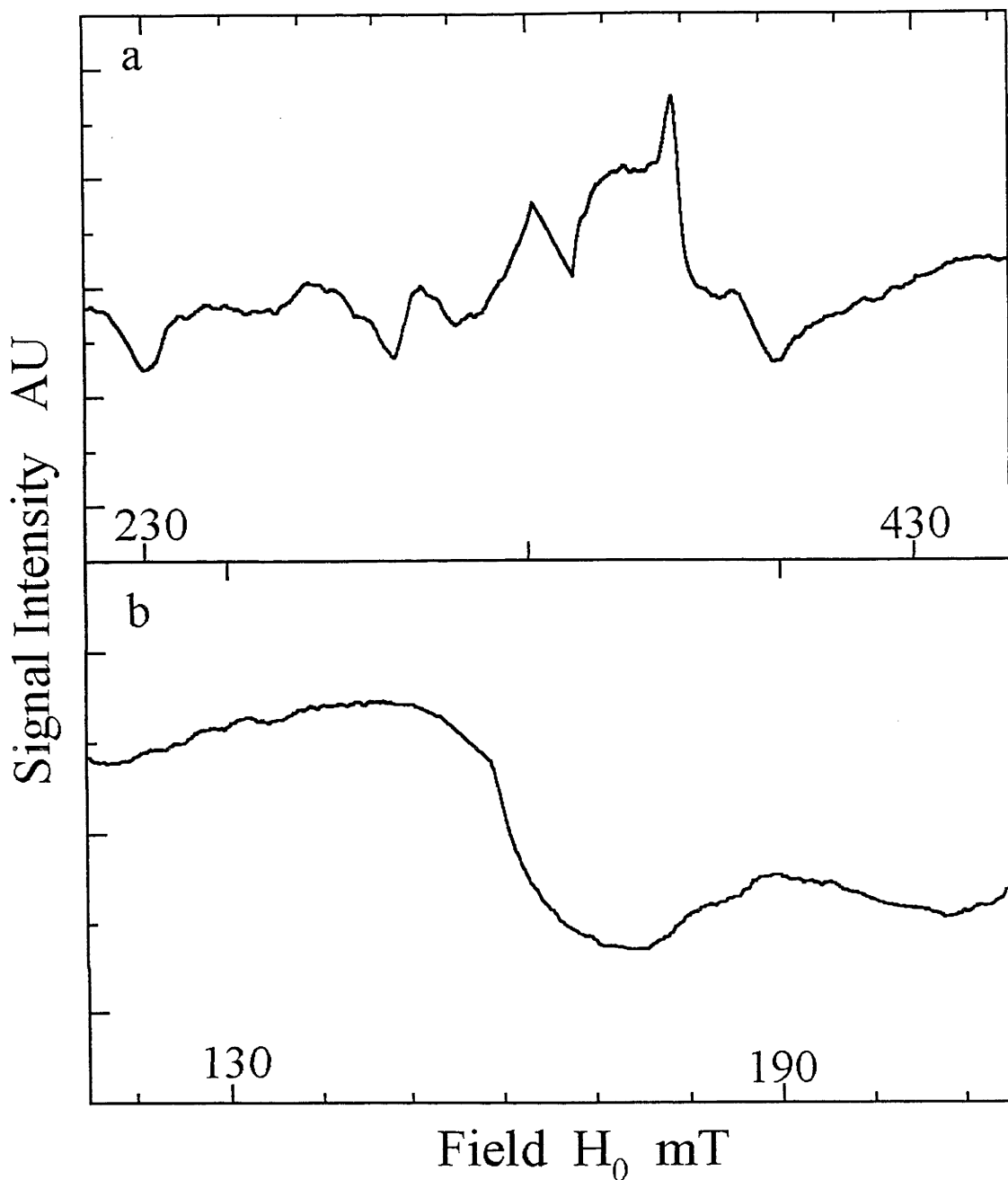


Figure 4.53. S_2 state generated in PSII incubated in the presence of 0.6M NaAcetate, illuminated at 200K. a). $g \sim 2$ region, low field features arise from oxidised cyt b_{559} ($g \sim 2.2$ and $g \sim 3.0$), higher field signals from reduced FeQ_A^- acceptor site ($g \sim 1.78$ and $g \sim 1.82$), b). $g \sim 4$ region. Spectrometer conditions: temperature 6K, microwave frequency 9.42 GHz, microwave power 6.32mW, modulation frequency 100 KHz, modulation amplitude (a) 2mT, (b) 1.4mT.

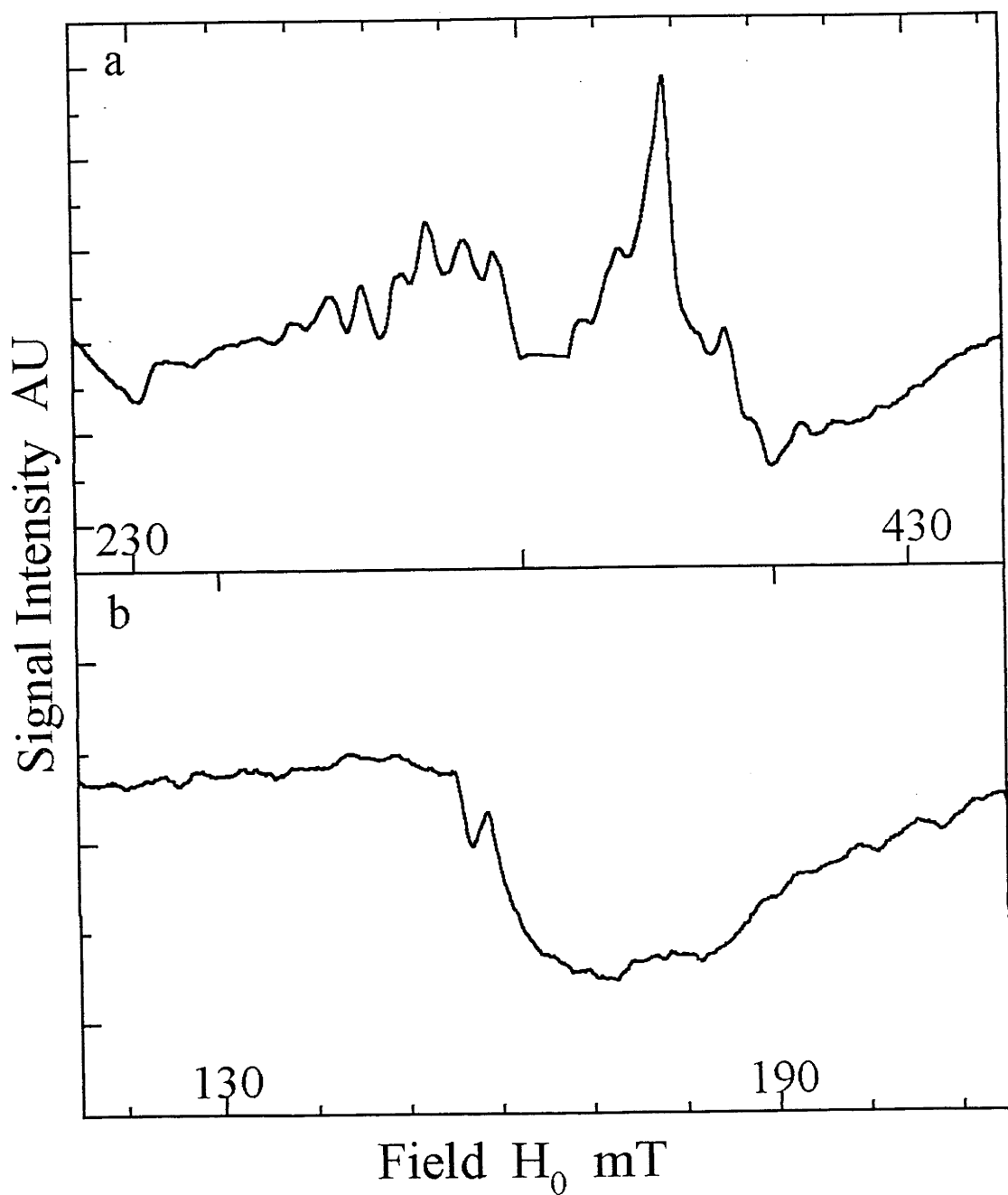


Figure 4.54. S₂ state signals generated in PSII incubated in the presence of 0.3M CaAcetate, illuminated at 200K. a). g~2 region, signals arising near 380mT are from reduced FeQ_A⁻ acceptor site (g~1.78 and g~1.82), b). g~4 region. Spectrometer conditions as per fig. 4.51.

signals are compared for temperatures of 6K and 10K in figure 4.55. Although the signal lineshapes and intensities are similar at 6K, the CaAc_2 treated sample spectrum shows significantly higher relative signal intensity and signal broadening at 10K. This may reflect a higher proportion of ground state $g=4.1$ signal form in the NaAc treated sample spectrum, while the CaAc_2 treated sample consists of a combination of modified ground state and excited state forms of the $g=4.1$ signal. The 10K spectrum for the CaAc_2 treated sample then reflects a greater component of the excited state $g=4.1$ signal, which develops due to spin population changes between 6K and 10K, similar in temperature dependence to that observed for the uninhibited PSII, see previously. This implies that the addition of Ca^{2+} may partially replete electron transfer capability through the donor side of PSII even in the presence of 600mM acetate. The smaller relative intensity of the cyt b559^+ signal observed in the CaAc_2 treated sample compared to the NaAc treated sample supports this, see figs 4.53 and 4.54.

This data for the illumination of PSII, incubated in the presence of 600mM sodium acetate at 200K indicates that the acetate restricts the electron donation from the OEC site, with significant generation of ground state form of the $g=4.1$ signal. The presence of this signal indicates that the electron donation to P680^+ from YZ is only slightly affected. The presence of additional Ca^{2+} , in the form of CaAc_2 , enhances electron donation by the OEC site, with some multiline and excited state $g=4.1$ signal observed. A reasonable hypothesis would be that the acetate interferes with both the Cl^- and Ca^{2+} binding, and that the Ca^{2+} displacement affects mainly the outer, multiline Mn dimer, while Cl^- displacement, which may occur more effectively in the absence of Ca^{2+} , has some perturbing effect on the inner Mn pair, (see next chapter for discussion).

4.8.3.2. Illumination at 275K

Two examples of altered S_3 state signals have been presented here. One where only the ground state form of the $g=4.1$ state signal is generated in the S_2 state, leading to an altered S_3 state signal with a width of $\sim 9\text{mT}$. The second form was where the multiline S_2 state is generated by 200K illumination, leading to a broader altered S_3 state signal of width $\sim 15\text{mT}$ in the presence of NaCl.

The S_2 state generated by illumination of acetate treated PSII at 200K generated a mix of the ground state $g=4.1$ and multiline forms of the S_2 state, dependent on the cation present. The NaAc treated sample appeared to generate the ground state $g=4.1$ signal S_2 state, with

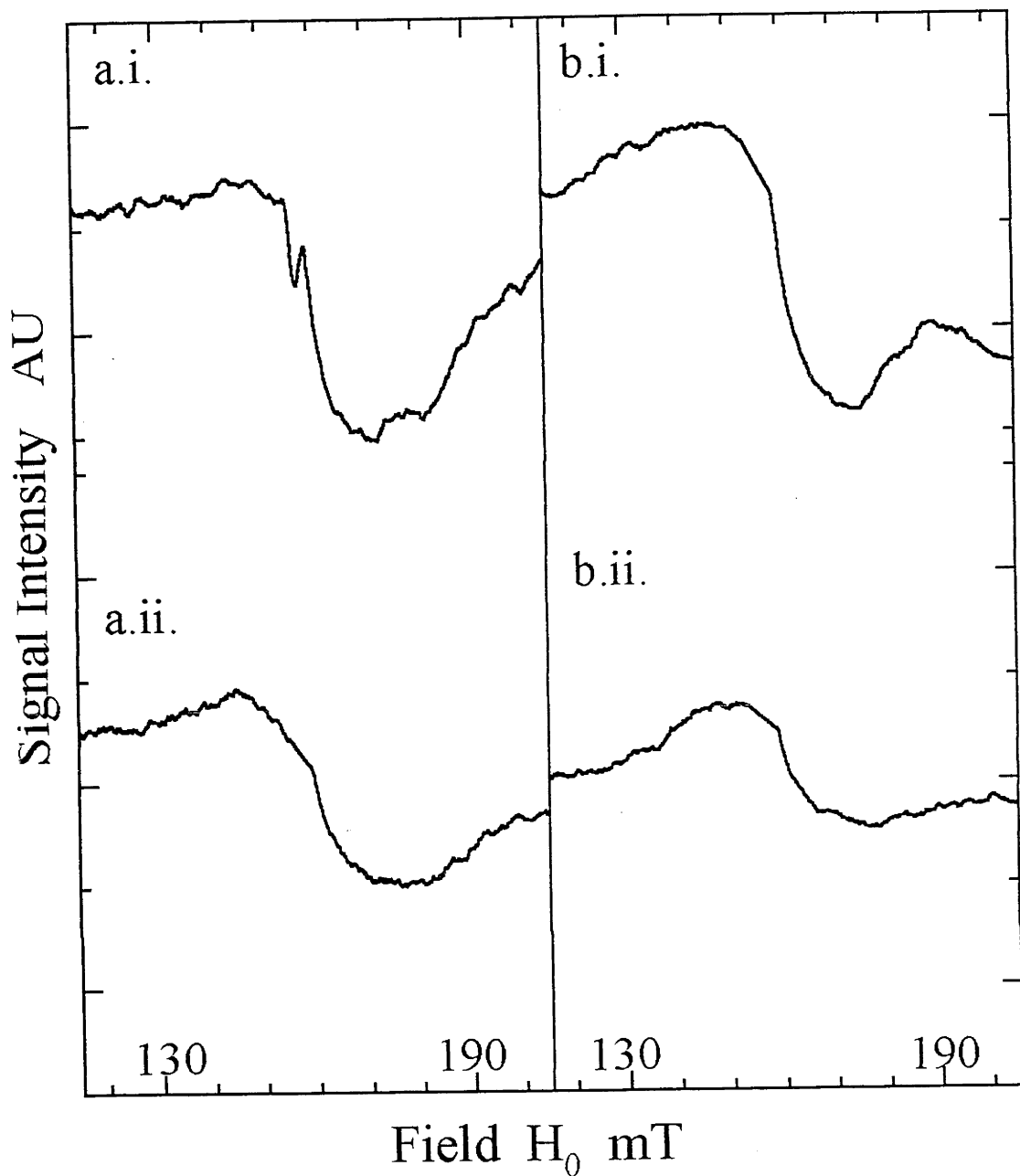


Figure 4.55. S_2 state $g \sim 4$ region signals generated in PSII incubated in the presence of a). 0.3M CaAcetate, b). 0.6M NaAcetate, illuminated at 200K. Shown are comparisons for (i) 6K and (ii) 10K for each PSII treatment. Spectrometer conditions as per fig. 4.51 with modulation amplitude 1.4mT.

significant cyt b559⁺ cogenerated, while the CaAc₂ treated sample appeared to generate a mix of the multiline and ground state g=4.1 forms of the S₂ state. The formation of the multiline S₂ state by illumination of the NaAc treated PSII at 275K in the presence of 100μM DCMU, fig 4.56, indicates that the restriction of the electron transfer through the donor side caused by the presence of acetate is overcome by illumination at higher temperatures. Both multiline and g=4.1 signals are generated, similar to the formation of the S₂ state in CaAc₂ treated PSII samples. This may indicate that the final S₃ state forms generated in the NaAc and CaAc₂ treated samples may be similar. The formation of the altered S₃ in acetate treated PSII samples illuminated at 275K is shown in figure 4.57. The spectral form of the altered S₃ state signal is very similar for the CaAc₂ and NaAc treated samples, with peak to trough widths ~24mT for both the CaAc₂ and NaAc samples. This overall similarity is in contrast to previous reports where the CaAc₂ sample was observed to have a much broader S₃ state signal (MacLachlan and Nugent, 1993). The S₃ state signal for both the NaAc and CaAc₂ treated PSII samples show additional features on the 'wings' of the central signal peak. These wings have been inferred to represent Mn hyperfine features, indicative of involvement of the OEC Mn with this signal. These 'wing' hyperfine features are more pronounced on the CaAc₂ treated sample spectrum, which may be due to increased OEC structural (but not necessarily functional) integrity in the presence of Ca²⁺. No hyperfine features are observed for the F⁻ PSII S₃ state spectrum consistent with the assertion proposed here that the S₂ and S₃ state signals arising in the F⁻ PSII do not arise from the OEC Mn site.

The temperature dependence of the S₃ state signals for PSII treated with CaAc₂ and NaAc are presented in figure 4.58. These curves indicate that the signals arising in the S₃ state are ground state signals, with both the curves for the CaAc₂ and NaAc tending to Curie at low temperatures, below 12K. At higher temperatures, the temperature dependence curves indicate an apparent loss of spin state population, with the signal intensity collapsing to zero at 1/T ~0.03K⁻¹ (T≈30K) for both inhibitory treatments. This temperature dependence behaviour is observed to almost identical to that previously observed for the S₃ state signal generated in PSII treated with 1M NaCl. This implies that the physical spin-spin exchange mechanism giving rise to the formation of the S₃ signal from the interaction of the putative organic radical with the Mn centre of spin 1/2 (Boussac, et al, 1989, Gilchrist, et al., 1995, Hallahan, et al., 1992, Boussac, et al, 1990a) must be similar for all three sample conditions.

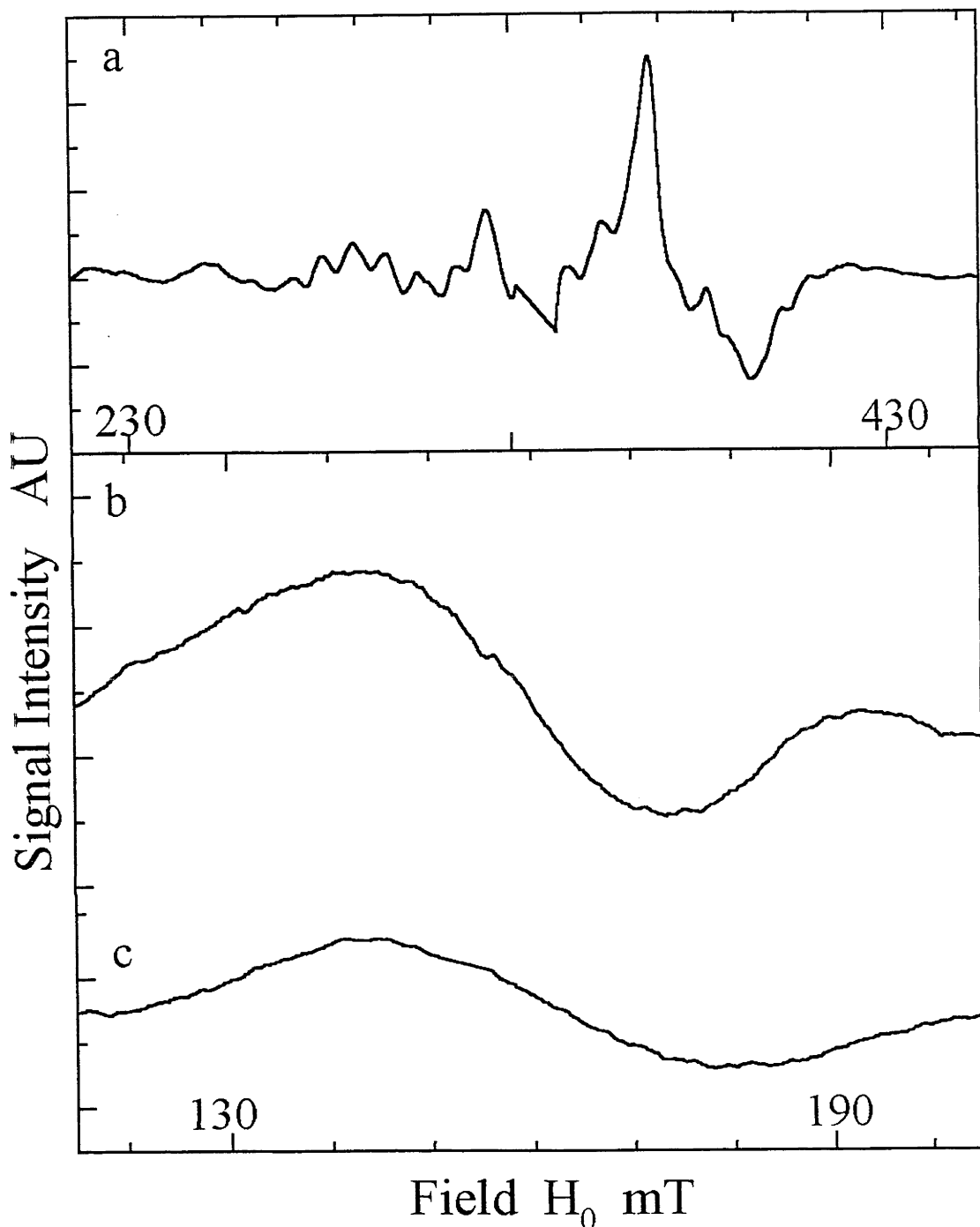


Figure 4.56. S_2 state signals generated in PSII incubated in the presence of 0.6M NaAcetate, illuminated at 275K in the presence of 100 μ M DCMU (in DMSO). a). $g\sim 2$ region multiline signal generated at higher illumination temperatures, b). $g\sim 4$ region recorded at 6K, c). $g\sim 4$ region recorded at 10K. The spectra are a direct comparison to those for the 200K illuminations, fig. 4.51 and fig. 4.53(b). Spectrometer conditions as per fig. 4.51 with modulation amplitude for (c) 1.4mT.

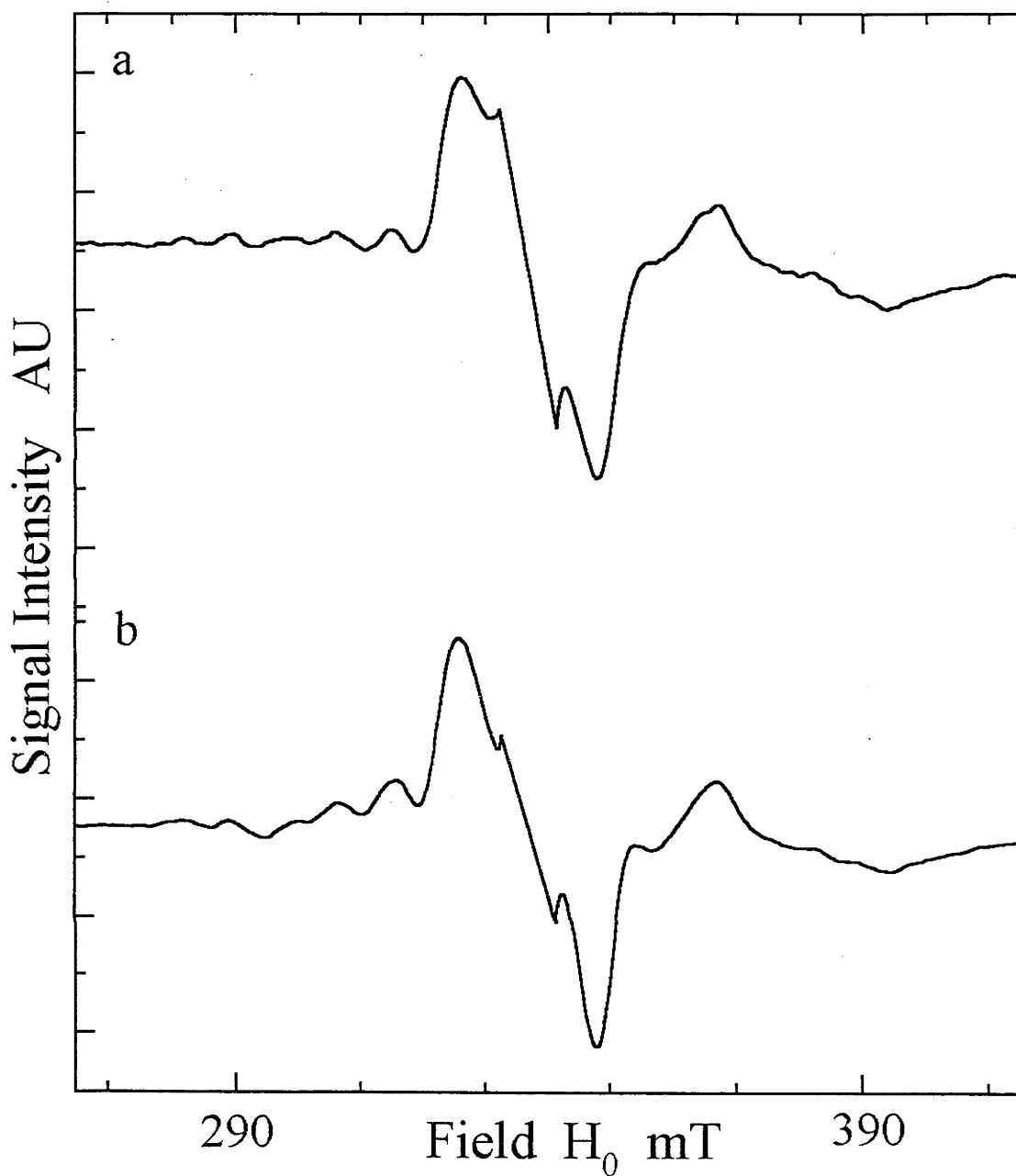


Figure 4.57. S_3^* state $g \sim 2$ signals generated in PSII incubated in the presence of a). 0.6M NaAcetate and b). 0.3M CaAcetate, illuminated at 275K for 90 seconds and cooled under illumination to ~ 120 K. Spectrometer conditions: temperature 10K, microwave frequency 9.42 GHz, microwave power 6.32mW, modulation frequency 100 KHz, modulation amplitude 1mT.

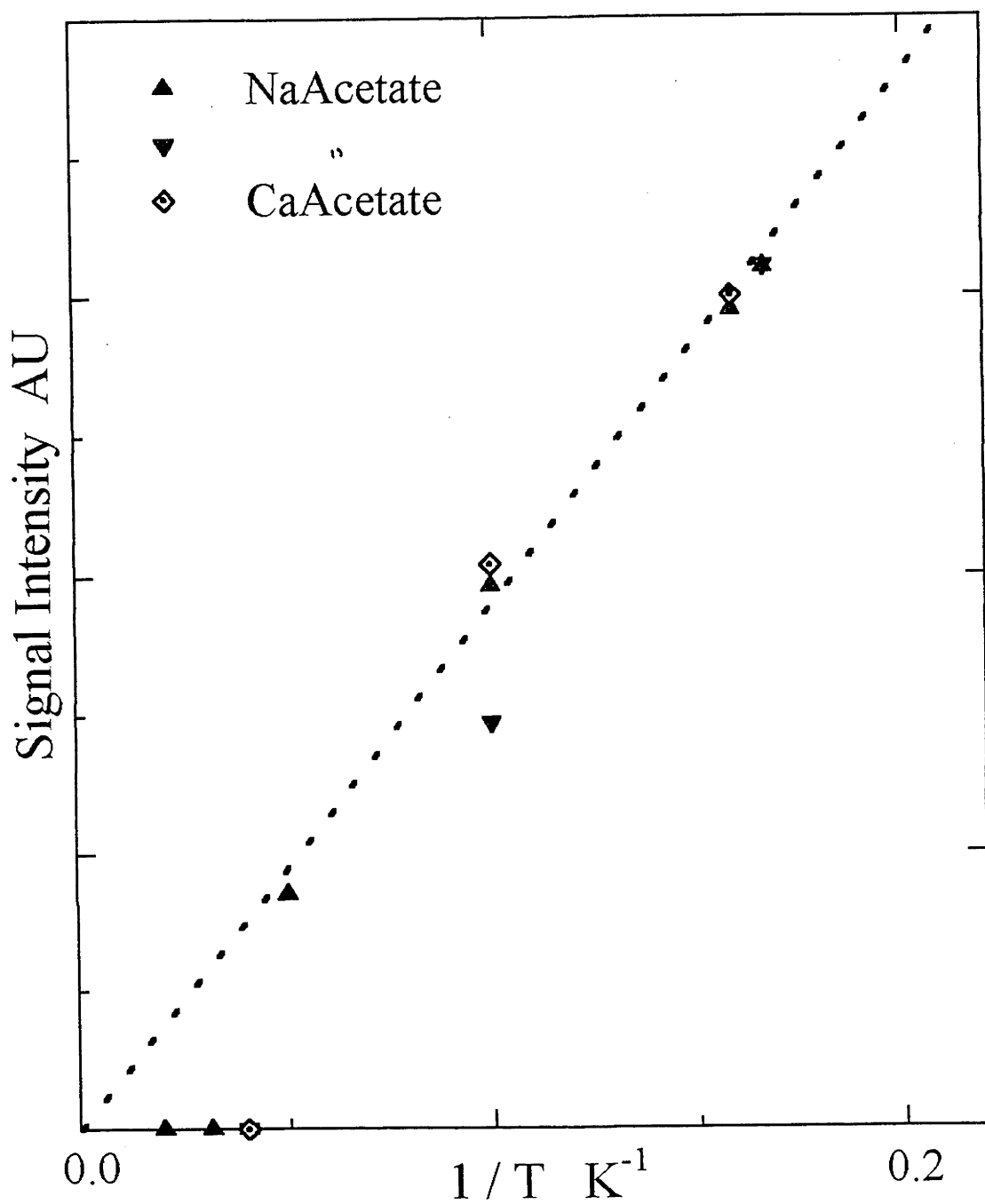


Figure 4.58. Temperature dependence of the S_3^* state $g \sim 2$ signal generated in PSII incubated in the presence of (\blacktriangle and \blacktriangledown) 0.6M NaAcetate, and (\diamond) 0.3M CaAcetate. Signal intensities are determined from the amplitude measures at 6.3mW microwave power. Dotted line represents the intensities expected for Curie behaviour. Temperature for calculation of the exchange coupling (J/k) is estimated from the point for which the curve estimated from the data falls to $1/e$ (0.368) of the Curie curve.

Examining the temperature dependence of the ESR spectra across the $g \sim 2$ region does not indicate the development of an excited state signal arising in this region.

The S_3 states generated in the NaCl inhibited PSII presented earlier indicated cogeneration of signal intensity in the $g \sim 4$ to $g \sim 7$ regions, 4.49. Figure 4.59 shows the low field region, $g \sim 3$ to $g \sim 7$, for the acetate treated PSII illuminated at 275K. Both the CaAc_2 treated and NaAc treated PSII samples generate a signal in this region, these signals showing a high degree of similarity, with peak to trough widths of 28mT for the CaAc_2 and 25mT for the NaAc. This appears to suggest that the S_3 state signals generated in both the CaAc_2 and the NaAc treated samples arise possibly from the same Mn containing centre. These signals would also suggest that this Mn centre is most likely that which gives rise to the multiline form of the S_2 state, indicating that the illumination temperature of 275K overcomes the apparent restriction of the electron flow through the donor side of PSII.

The temperature dependences for these $g \sim 4$ region signals arising in the S_3 state of acetate treated PSII, shown in figure 4.60 for the CaAc_2 and NaAc samples, are very similar in form to those for the $g \sim 2$ 'split' signals. The temperature dependences indicate that the $g \sim 4$ region signals arise from ground state centres, with possible signal state depopulation of this state to some ESR silent or invisible thermally accessible excited state above $\sim 15\text{K}$. Again, these $g \sim 4$ region signals, cogenerated with the split signals, are not excited state signals, but are most likely the $\Delta m_s = 2$ transitions for the minimum $S=1$ state for the S_3 state signals.

The question then arises over the nature of possible excited 'spin' state into which the acetate treated PSII populates, leading to the loss of the 'split' S_3 signal. There are two possible sites for the interaction forming the S_3 signal within the donor side of PSII, where illumination to form the S_2 state generates only the ground state $g=4.1$ signal, with the S_3 state signal being a narrow form, width $\sim 9\text{mT}$, as observed for the F^- PSII, and where illumination to form the S_2 state generates the multiline signal, with the S_3 state signal being much broader, width $\sim 15\text{mT}$, as for the 1M NaCl treatment. It is apparent that the major form of the S_3 state signal observed for the acetate treated PSII samples is that of the broad form, arising from the centre giving rise to the multiline signal in the S_2 state, similar to the 1M NaCl treated PSII. The interaction forming the S_3 state signal has been proposed to be a spin-spin interaction between the multiline centre ($S=1/2$) and an organic radical ($S=1/2$) (Boussac, et al, 1989, Hallahan, et al., 1992, Boussac, et al, 1990a, Tso, et al, 1991a). A second alternative involves dipolar coupling between the two spin centres, with the signal narrowing at higher temperature due to thermal influences overriding the exchange coupling,

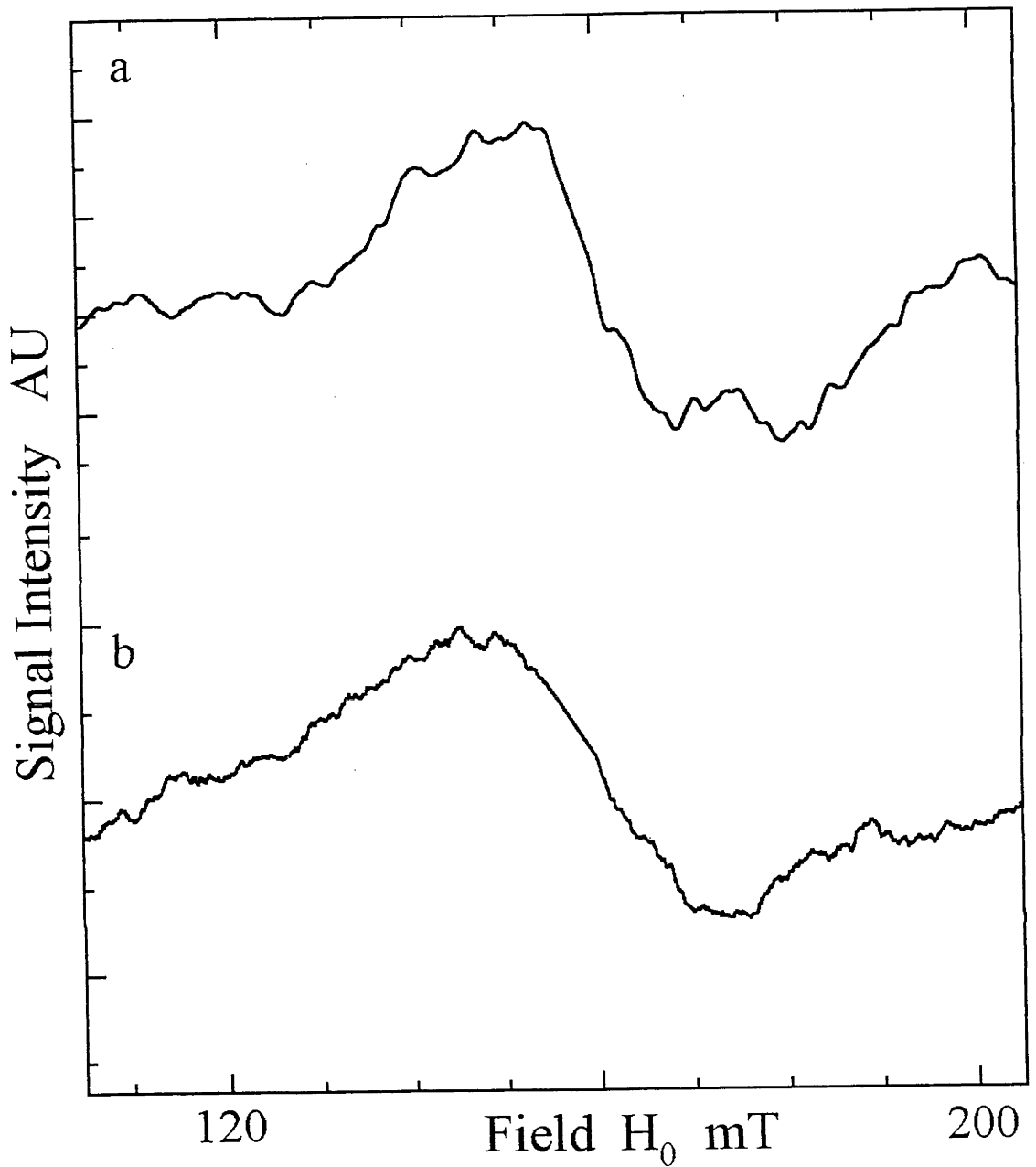


Figure 4.59. S_3^* state $g \sim 4$ signals generated in PSII incubated in the presence of a). 0.6M NaAcetate, and b). 0.3M CaAcetate, illuminated at 275K for 90 seconds and cooled under illumination to ~ 120 K. Spectrometer conditions as per fig. 4.51 with modulation amplitude 1.4mT.

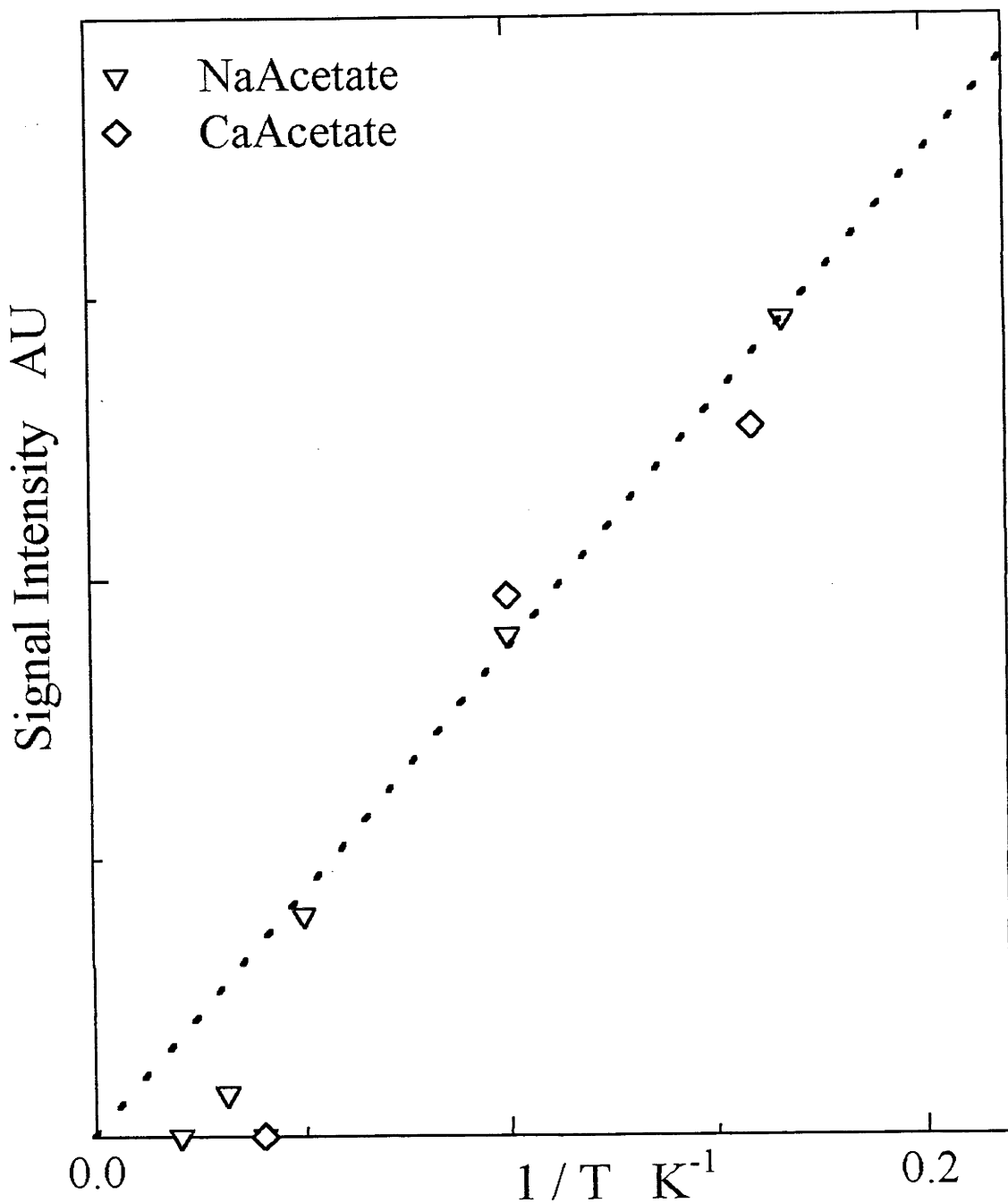


Figure 4.60. Temperature dependence for the S_3^* state $g \sim 4$ signals generated in PSII incubated in the presence of (▽) 0.6M NaAcetate, (◇) 0.3M CaAcetate, illuminated at 275K for 90 seconds and cooled under illumination to ~ 120 K. Signal intensities determined from the amplitudes measured for microwave power of 6.3mW. Dotted line represents intensities expected for Curie behaviour.

leading to observation of the two individual $S=1/2$ states at temperatures where $T_1 < J/h$. Examination of the $g \sim 2$ regions for the two acetate treated PSII sample types at $\sim 25\text{K}$ does not suggest that the S_3 state signal narrows with increasing temperature, but transforms to either another spin state or to an altered spin-spin interaction regime, (see earlier). The spectra recorded at 25K show the presence of additional signals, figure 4.61, but the relationship of these signals to that of the 'split' signal is unsure at this point. Whether this loss of 'split' signal is due to a spin conversion between the two spin $1/2$ centres leading to the interconversion to an $S=0$ excited state (diamagnetic) or a change in T_1 leading to the situation that the spin lattice relaxation occurs at a higher rate (T_1) than the actual effective spin-spin exchange (J/h) is uncertain and prompts further investigation.

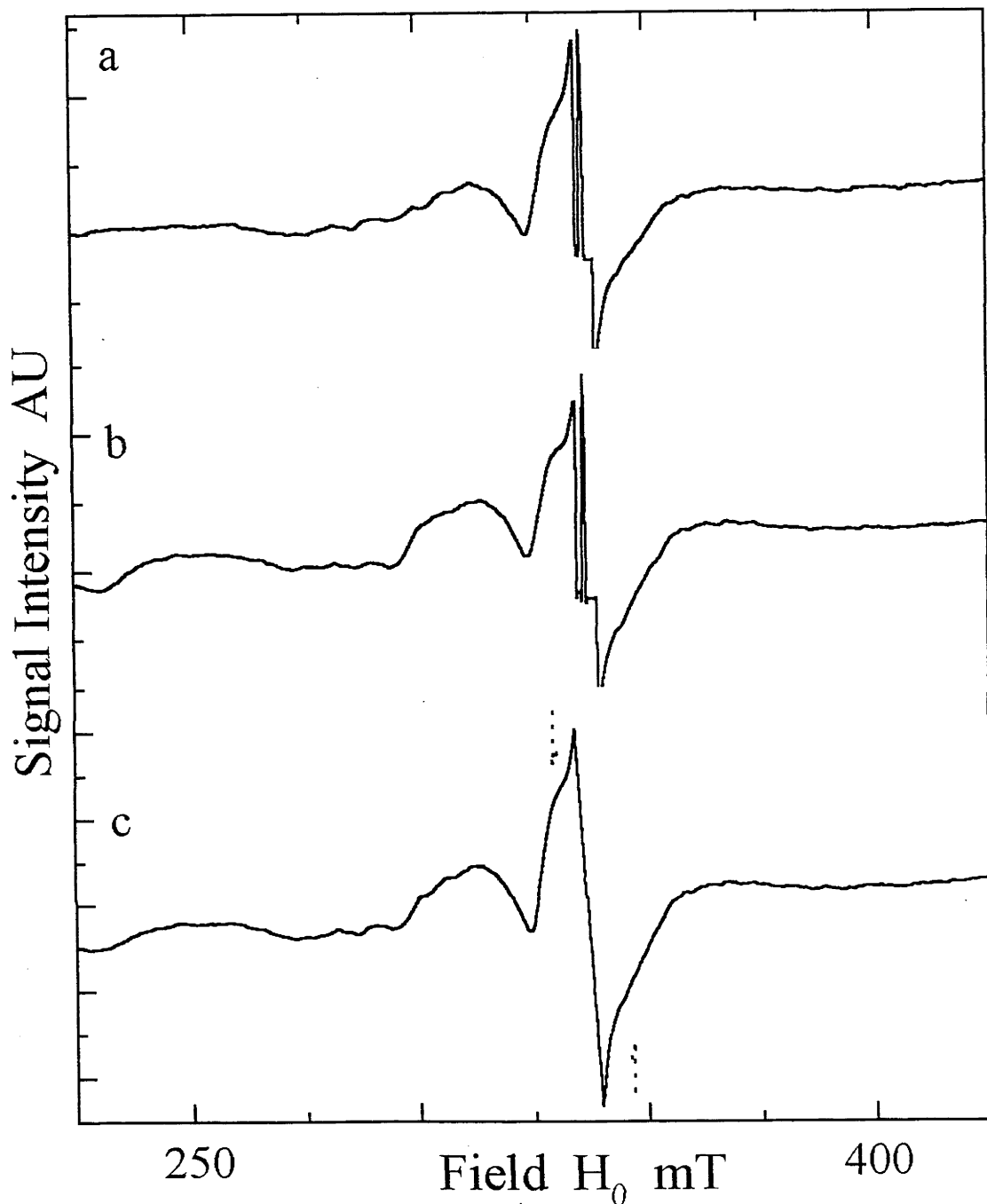


Figure 4.61. S_3^* state $g\sim 2$ signals generated in PSII incubated in the presence of a). 0.6M NaAcetate, b). 0.3M CaAcetate, illuminated at 275K. Spectra recorded at 25K. c). Summation of spectra (a) and (b). Arrows indicate the peak and trough for the narrower $g\sim 2$ signal which underlies the broader split signal, which is the dominant signal form at temperatures below ~ 20 K. Signal intensity of this narrow form of the S_3^* state $g\sim 2$ signal is uncorrelated to the intensity of the broader form of the S_3^* state $g\sim 2$ signal observed below ~ 20 K. Spectrometer conditions as per fig. 4.55.

Chapter 5

Model of Mn in OEC

The data presented in Chapter 4 indicate that the signals generated in the S_2 and S_3^* states may arise from two different Mn containing sites within the donor side of the OEC. This separation of the Mn localisation draws heavily on the established models of Mn ligation to the protein and an electron withdrawal and turnover between the S states. This chapter uses the data presented, analysis of previous models and data based on the properties of Mn model compounds to propose binding sites for Mn to the D1 polypeptide, the state of the Mn within each S state and finally for the processes of functional water cleavage and for the blockage of electron transfer leading to the S_3^* states.

5.1. ESR signals and previous models

The location of Mn within the OEC is still subject to debate. There have been many sets of published line shapes for the S_2 multiline and $g=4.1$ signals, with numerous different attempts at physical analysis and simulation of these S_2 state signals (Dismukes and Siderer, 1981, Dismukes, et al, 1982, Hansson and Andreasson, 1982, de Paula and Brudvig, 1985b, de Paula, et al, 1986c, Haddy, et al, 1989, Haddy, et al, 1992, Vänngård, et al, 1992, Kusunoki, 1992, Åhrling and Pace, 1995). Most of these analyses have assumed the presence of the multiline signal and only one form of the $g=4.1$ signal, the ground state of the $g=4.1$, while neglecting (or being unaware of) the excited state form of the $g=4.1$ signal observed in the presence of the multiline signal (de Paula and Brudvig, 1985b, de Paula, et al, 1986c, Haddy, et al, 1992, Vänngård, et al, 1992, Kim, et al, 1992). From the data presented in this report, any analysis of the Mn structure giving rise to the multiline signal must recognise the existence of this excited state form of the $g=4.1$ signal, as well as the existence and temperature dependence of the new ESR signal at $g\sim 6$, shown to arise as the second excited state of the Mn centre. Analysis of the multiline in isolation disregards the possible nature of the spin exchange interaction between these Mn ions and so is in some measure deficient.

5.1.1 Multiline spectra from SUC PSII and EG PSII

Close comparison of the multiline spectra from these samples indicates only minor differences appear on superhyperfine features between 350mT and 375mT and between 400mT and 425mT. Slight differences are observed for the multiline signal generated in either

$^1\text{H}_2\text{O}$ or $^2\text{H}_2\text{O}$ buffer exchange conditions (Nugent, 1987). The changes in the overall multiline spectrum in the proton/deuterium exchange experiment compared closely with the differences in the multiline observed for the -MeOH and +MeOH PSII measurements (Pace, et al., 1991, Smith, et al, 1993) and for here, comparing the multiline for non alcohol containing sucrose buffer and for the EG buffer. From the interpretation of the signal temperature dependences (see results), the effects of addition of alcohol or changing from "non alcohol" to "alcohol" cryoprotectant was: 1. a modification of the superhyperfine features and; 2. a marked increase of the magnitude of the antiferromagnetic exchange coupling constant J , with $|J/k| \sim 3.5\text{K}$ for the non alcohol containing sucrose buffer and $|J/k| \sim 25\text{K}$ for the EG buffer (see Chapter 4). In model metal oxo bridged dimers, the effect in equivalent metal compounds of the oxo bridges being either protonated, μ -hydroxyl, or deprotonated, strictly μ -oxo, was to observe a stronger antiferromagnetic exchange coupling in the deprotonated μ -oxo, compounds (Larson, et al., 1992a, Knopp and Wieghardt, 1991, Baldwin, et al., 1993). This effect may apply here, with the higher exchange constant in the effective + alcohol samples, either as +MeOH (Pace, et al., 1991, Smith, et al, 1993) or with EG as cryoprotectant (this work) arising from deprotonation of μ -oxo bridging groups in a Mn dimer. It is noted that glycerol (20% V:V) was added to the buffer of the $^1\text{H}/^2\text{H}$ exchange experiment in which the presence of an isotope effect on the multiline indicated protonation of groups intimately in contact with the spin density (Nugent, 1987). This coupled with similar superhyperfine differences between the control ^1H + glycerol and ^1H + EG buffer samples may reflect a dependence of molecular size in the alcohol effect, ie glycerol being too large to access the internal regions of the membrane affected by the small alcohols. This has been previously suggested by the effects of EG and glycerol on proton pools in PSII (Kawamori, et al, 1989). The small chain alcohols may be able to penetrate the luminal surface of the D1-D2 PSII core, increasing the dielectric constant of the protein region containing the Mn OEC. The increase in dielectric constant could then enable deprotonation of the Mn complex resulting in the higher exchange coupling constant and reducing the proton effect on the superhyperfine. The detail in the deprotonated multiline state becomes more apparent due to a loss of hyperfine interaction between the proton and the Mn OEC, reducing the apparent line width of the multiline superhyperfine structure.

5.1.2. One dimer or multi exchange tetramer

The above line shapes and temperature dependences indicate that only a single Mn dimer structure need be invoked for the source of the multiline ESR signal. A third example of the multiline signal has been observed in samples which restrict turnover of the OEC such that the $\text{S}_3 \rightarrow \text{S}_4$ turnover event is blocked. This form of the multiline signal is generated via

illumination of PSII at ~275K (Beck and Brudvig, 1986, Beck, et al, 1986, Boussac, et al, 1990c), or illuminating to generate an altered S₂ and S₃ state, followed by a rapid dark adaptation (approximately 1 min at 275K) (Beck and Brudvig, 1986, Beck and Brudvig, 1988a, Beck and Brudvig, 1988b, Andreasson, et al., 1988, Andreasson and Lindberg, 1992, Britt, 1989, Boussac, et al, 1990c, Gilchrist, et al, 1992, Zimmermann, et al., 1993) allowing a single recombination event. This results in the presence of a dark stable multiline characterised altered S₂ state. This type of multiline signal has been generated in PSII treated with NH₃ (Beck and Brudvig, 1986, Beck, 1986, Beck and Brudvig, 1988a, Beck and Brudvig, 1988b, Britt, et al, 1989, Boussac, et al, 1990c, Andreasson and Lindberg, 1992), acetate (MacLachlan and Nugent, 1993) and in other PSII samples in which the inhibition has resulted from altered Cl⁻ binding and Ca²⁺ depletion (Boussac and Rutherford, 1988c, Boussac, et al, 1989, Boussac, et al, 1990a, Gilchrist, et al, 1992, Zimmermann, et al., 1993, Hallahan, et al., 1992, MacLachlan, et al, 1994a).

It is of note that the illumination of Cl⁻ inhibited PSII at 200K, which allows only a single electron turnover event, generates either little S₂ state signal intensity, as for acetate inhibition (MacLachlan and Nugent, 1993), Cl⁻ depletion (Boussac and Rutherford, 1994a, Boussac and Rutherford, 1994b, van Vliet, et al., 1994, Van Vliet and Rutherford, 1996) or to generate a g=4.1 signal form of the S₂ state as for treatment with NH₃ (Beck and Brudvig, 1986, Beck, et al, 1986, Beck and Brudvig, 1988a, Beck and Brudvig, 1988b, Andreasson, et al., 1988, Boussac, et al, 1990c) or Cl⁻ depletion or addition of acetate (Ono, et al, 1986, Ono, et al, 1987, Damoder, et al, 1986, Baumgarten, 1990). This suggests that in these samples a restriction of Cl⁻ binding to the OEC has occurred such that at 200K an electron is unable to be extracted from the OEC Mn site, either as an altered form of a tetrameric cluster (Beck and Brudvig, 1986, Beck, et al, 1986, Beck and Brudvig, 1988a, Beck and Brudvig, 1988b, deRose, et al., 1995) or as a stalled event from an intermediate electron transfer Mn containing site (this work). At 275K, this restriction is overcome either by an increased effective Cl⁻ activity at the binding site or by increased thermal activation of the electron transfer out of the OEC site, the higher activation energy for the process arising from the restriction in Cl⁻ binding (Ono, et al, 1987).

Whichever the method of overcoming the partial inhibition, the illumination of acetate or NaCl treated (Ca depleted) samples at 273K ultimately generates similar S₃^{*} state signals, characterised by the "split" signal of peak-peak width ~200-240G for acetate treated PS II (MacLachlan and Nugent, 1993, this work) or 13 to 17mT for Ca depleted PS II (Boussac and Rutherford, 1988c, Boussac, et al, 1989, Boussac, et al, 1990a, Hallahan, et al., 1992, this work). These S₃^{*} states are proposed here to arise from an Mn centre interacting with a

oxidised amino acid different to that which gives rise to the narrower form of the S₃ state with p-p width ~9 to 11mT such as generated with Cl⁻ depleted and F⁻ inhibited PSII (Boussac, et al, 1990a, Boussac and Rutherford, 1994a, Boussac and Rutherford, 1994b, Van Vliet and Rutherford, 1996, this work).

The altered, dark stable multiline is characterised in NH₃ treated PSII by a narrower hyperfine spacing (~67G cf ~85G) for "physiological" S₂ state multiline (Beck and Brudvig, 1986, Beck, et al, 1986, Beck and Brudvig, 1988a, Andreasson, et al., 1988, Boussac, et al, 1990c) and an apparent increase in the number of hyperfine peaks in the dark stable multiline, ~26 cf ~22 in physiological S₂ state multiline (Boussac, et al, 1990c, Beck and Brudvig, 1986, Beck and Brudvig, 1988a). This change in hyperfine spacing and increase in hyperfine peaks has been suggested to arise from an alteration of the exchange coupling interactions for a Mn tetramer, due to exchange of O type ligands by N-H type ligands (Beck, et al, 1986, Beck and Brudvig, 1988a, Sandusky and Yocum, 1984, Sandusky and Yocum, 1986) and direct bonding of NH₃ to the OEC Mn site as observed by pulsed ESE spectroscopy (Britt, et al, 1989). The nature of the likely interaction to generate the altered hyperfine pattern is discussed later. The electron donation kinetics, however, suggest that at 275K, illumination allows electron withdrawal from the physiological multiline site, ie the Mn OEC S₂ state site. Illumination at 200K generates a greater proportion of the ground state g=4.1 signal (Beck and Brudvig, 1986, Beck, et al, 1986, Beck and Brudvig, 1988a, de Paula, et al, 1986c, Kim, et al, 1990, Kim, et al, 1992).

The pattern of alternative generation of g=4.1 signal, (ground state form) or multiline signal in these samples, dependent on the illumination temperatures, appears to mimic the g=4.1/multiline formation in ethylene glycol cryoprotected PSII (functional) for the lower illumination temperatures of ~130K and 200K. These patterns of Mn dependent signal formation may be explained in two general ways:

a) as two magnetic states of a single tetrameric Mn containing centre, in which the difference between the lower illumination and higher illumination temperature results arises through changes in magnetic coupling of the Mn ions within the complex (de Paula, et al, 1986c, Yachandra, et al, 1993, Haddy, et al, 1992), or oxidation of the tetramer at different sites under illumination at different temperatures (DeRose, et al, 1994); or

b) two separate Mn containing sites, each containing a Mn dimer liganded to the protein in separate locations with different ligand components and each capable of generating an ESR signal. One is sited at an electron transfer intermediate position within the protein, the other being at the functional Mn OEC site. Illumination at 130K in functional PSII or illumination at 200K in F⁻ PSII (de Paula, et al, 1985a, Thompson, et al, 1988, Casey and Sauer, 1984, Boussac and Rutherford, 1994a, Ono, et al, 1987, Haddy, et al, 1992) in which

Cl⁻ binding is restricted or inhibited outright, gives rise to an oxidation at the electron transfer intermediate site, generating the ground state $g=4.1$ state, while 275K illumination of Cl⁻ binding restricted NH₃ treated (Beck and Brudvig, 1986, Beck, et al, 1986, Andreasson, et al., 1988, Andreasson and Lindberg, 1992, Boussac, et al, 1990c) or acetate (MacLachlan and Nugent, 1993, Szalai and Brudvig, 1996, this work) generates the multiline state from the Mn OEC site.

The first proposal requires that all the properties and spin states of the Mn derived ESR signals may be accounted for by the magnetic interactions of the four Mn ions of the tetramer, arranged nominally as a magnetically coupled dimer of Mn dimers (Haddy, et al, 1992), as from X-Ray data (Klein, et al, 1993, Yachandra, et al, 1993, Mukerji, et al, 1994, Kusunoki, et al, 1989). The second proposal requires that the Mn may be placed within two distinct sites of the PSII polypeptides, as magnetically isolated centres, with the spin states accountable by interactions within the individual Mn dimers (see Dexheimer and Klein, 1992, Smith and Pace, 1996), and with amino acid residues at the two binding regions of the protein (Chu, et al., 1995a, Chu, et al., 1995b, Styring, et al, 1993).

5.1.3. Evidence for and against a Mn tetramer from Multiline data

Support for the Klein and Yachandra model for the Mn structures within the OEC has arisen from the X-ray data, model Mn μ -oxo type structures, and simulations model the multiline and $g=4.1$ signals as arising from a Mn tetramer (Yachandra, et al, 1993, Kusunoki, et al, 1989, Haddy, et al, 1992, Astashkin, et al., 1994b, Kusunoki, 1992). Here, the multiline will be focussed on, with the arguments over the $g=4.1$ signal developed and discussed later.

The main base of support for a Mn tetramer is from simulation of the multiline signal and, more recently, ENDOR/ESE experiments carried out on the multiline signal.

5.1.3.1. Multiline simulations

The multiline signal is observed to differ from synthetic model high valent μ -oxo bridged Mn dimer complexes in two major features:- the overall number of apparent hyperfine features, ~ 22 in the OEC S₂ state multiline compared with ~ 16 for model compounds measured at X band frequencies, and the overall width of the spectrum (Dismukes and Siderer, 1981, Dismukes, et al, 1982, de Paula and Brudvig, 1985b, de Paula, et al, 1986c). These two differences have been inferred to require a Mn tetramer as the functional centre giving rise to the multiline signal (Dismukes, et al, 1982, Haddy, et al, 1989, de Paula and Brudvig, 1985b, de Paula, et al, 1986c).

Many of the simulations have assumed isotropic hyperfine interactions for the individual Mn centres, although studies at varying microwave frequencies and on oriented

samples studied at X, P and S bands have suggested significant hyperfine anisotropy in the multiline signal (Kim, et al, 1992, Haddy, et al, 1989, Vännngård, et al, 1992, Smith, et al, 1993). With simple isotropic exchange and hyperfine interactions, a Mn dimer is expected to generate only 16 hyperfine lines. The complexity of the PSII multiline signal at S Band (~60 "hyperfine" lines (Haddy, et al, 1989, Vännngård, et al, 1992) and X Band (~22 "hyperfine lines") has been taken to require 3 or 4 Mn centres (Dismukes, et al, 1982, de Paula and Brudvig, 1985b, de Paula, et al, 1986c, Haddy, et al, 1989, Vännngård, et al, 1992, Kusunoki, 1992). However, with anisotropic nuclear hyperfine terms, up to 32 lines, double the isotropic number, are theoretically observable (Vännngård, et al, 1992, Haddy, et al, 1992) in a dimer.

The dimeric Mn III-IV complex of bacterial catalase enzymes exhibits a relatively simple hyperfine pattern at X band (Vännngård, et al, 1992, Haddy, et al., 1994, Ivancich, et al., 1995), with the S Band indicating no more than axial anisotropy (Haddy, et al., 1994), and the basic 16 line pattern of the X Band spectrum being observed also at both S Band (3GHz) and P Band (16GHz) (Haddy, et al., 1994).

It is the comparison of this low anisotropy catalase signal to the complexity of the PSII S₂ state multiline which suggested that four Mn must be interacting to generate the PSII multiline (Haddy, et al, 1989, Haddy, et al., 1994, Kim, et al, 1992). Åhrling and Pace considered the consequences of a more highly anisotropic environment for the Mn, which required involvement of anisotropic hyperfine Hamiltonian components, and inclusion of quadrupolar terms. Using a two Mn model and relating all components of the simulation back to an environment for Mn, the simulation of Åhrling et al proposed a Mn III-IV dimer in a low symmetry environment (Åhrling and Pace, 1995). The Mn III was effectively 5 coordinate, in a strong axial environment, with mainly oxygen ligands (Åhrling and Pace, 1995). The Mn IV was also effectively 5 coordinate, the sixth ligand either missing, or at much longer distance. The Mn IV was inferred from the hyperfine and quadrupole parameters of the simulation, to be in a low symmetry environment, with ligation to a histidine involving π backbonding into vacant d orbitals (Åhrling and Pace, 1995). The probability of histidine ligation has been proposed from IR absorption studies (Padhye, et al., 1986, Ono and Inoue, 1991), ESE Experiments (Britt, et al, 1994, DeRose, et al, 1991) and from modelling (Ruffle and Nugent, 1992) and mutational studies (Michel and Deisenhofer, 1988, Roffey, et al., 1994, Chu, et al., 1995b, Nixon and Diner, 1994). The magnitude of the quadrupolar coupling at each Mn implies a highly non spherical ligand environment, as would occur when one ligand is effectively removed from an octahedral co-ordination sphere. This strong quadrupole term is supported by examples of a ligand deficient Technetium complex (Baldas, et al., 1984) using TeCl₅. The Te is observed to be 5 coordinate, with strong axial (square pyramidal) symmetry. The quadrupolar coupling is large, and the inferred value of the nuclear electric field gradient

is comparable to that required for Mn in the Åhrling, Pace simulation (Åhrling and Pace, 1995, Baldas, et al., 1984, Åhrling and Pace pers. comm.).

5.1.3.2. Mn ENDOR studies on Multiline.

Recently, a Mn spin echo ENDOR study at three field positions across the multiline spectra were reported (Britt, et al., 1995). Simulation studies based on a dimeric Mn III-IV model compound, the multiline simulation parameters of Åhrling et al and for a tetrameric Mn model, using a rhombic symmetry Hamiltonian concluded that the Mn tetramer generated the closest spectrum to that observed experimentally. The overall match for any of the three simulations were not good (Britt, et al., 1995, Fig 5). The discussion of such simulation and experimentation is beyond the scope of this report. However, the reported hyperfine parameters appear to be reasonable for Mn complexes, although the quadrupolar couplings; $P_{||}(\text{Mn IV}) \sim +2\text{MHz}$ (0.7G) and $P_{||}(\text{Mn III}) \sim -4.5\text{MHz}$ (-1.6G) suggest a high level of environmental symmetry which does not necessarily reflect the observation for the X, P and S band multiline spectra (Haddy, et al, 1989, Kim, et al, 1992). The simulated spectra using the high magnitude quadrupole parameters of Åhrling et al appeared not to match the experimental spectrum due to broadening of the signal. The results appear inconclusive over whether a tetrameric or dimeric Mn complex is at the source of this ESE ENDOR signal, although a Mn dimer with isotropic environment appears to be ruled out (Britt, et al., 1995). In particular, it is not clear that the Mn ENDOR reported arises only from the multiline signal (or from multiline at all). The shape of the field swept absorption signal for the multiline, reported by Britt et al (Britt, et al., 1995, fig 6) shows it to be substantially asymmetric about $g=2$. The pure multiline spectrum observed in this laboratory (eg see Pace, et al., 1991, fig 1, Åhrling and Pace, 1995, fig 6) is almost symmetric about $g=2$. It appears that the Britt et al signal may contain additional components, possibly related to the broad asymmetric $g \sim 2$ signal reported earlier by Pace et al (Pace, et al., 1991). The origin of this signal is still unclear but it is clearly Mn related, often underlies the multiline signal and is probably an excited state species (Pace, Smith and Åhrling unpublished results).

5.1.3.3. Spin states

A key to the Mn structure, which has appeared to be neglected, is the examination of the temperature dependence (TD) of the multiline in conjunction with the other signals associated with this form of the S_2 state. Until this work, only Pace and coworkers (Pace, et al., 1991) have indicated by examination of the TDs that one form of the $g=4.1$ signal is intimately associated with the Mn species giving rise to the multiline signal. The determination that the 200K illumination sucrose cryoprotected PSII form of the $g=4.1$ signal arises as the

first excited ($S=3/2$) spin state of the multiline ground state ($S=1/2$) centre indicated that the Mn complex is dominated by the interactions of an antiferromagnetically coupled Mn III - Mn IV dimer. Knowing these two spin states points to the Mn dimer model.

However, knowing only these states would not allow one to exclude a tetramer model. For a tetrameric model allowed by the X-Ray absorbance data (deRose, et al., 1995, Kusunoki, et al, 1989, Yachandra, et al, 1993), in which two di- μ -oxo bridged Mn dimers are joined by a μ -oxo or μ -carboxylato flexible bridge, the exchange interactions of the dimers which dominate the spin states are of the form shown in fig. 4.14b. The Histidine ligation is suggested from N \rightarrow ESEEM studies (DeRose, et al, 1991, Britt, et al, 1994, Zimmermann, et al., 1993), the simulation of Åhrling and Pace (Åhrling and Pace, 1995) and from optical studies (Padhye, et al., 1986, Ono and Inoue, 1991). For a spin 1/2 ground state, the model proposes that Mn(3) - Mn(4) are of equal oxidation state, either III-III or IV-IV, and strongly coupled, with net spin = 0. If this were a Mn tetramer, the data from the ground state $g=4.1$ suggests that the Mn(3) - Mn(4) exchange constant would be of the order of $J_{ex}/k \sim 60K$, strongly antiferromagnetic.

From the suggestion of Dexheimer et al that the S_1 state $g=4.8$ signal arises from an even spin (probably $S=1$) excited state (Dexheimer, et al, 1990, Dexheimer and Klein, 1992), and with the TD data for the multiline S_2 state (Pace, et al., 1991, this work), the exchange coupling for the presumed Mn(1)Mn(2) oxidisable dimer (deRose, et al., 1995, Yachandra, et al, 1993) of the Mn tetramer model may still be consistent with the TD data presented here. The multiline ($S=1/2$), $g=4.1$ ($S=3/2$) and $g\sim 6$ ($S=5/2$) states could in principle arise from spin state progression within the weakly coupled dimer, nominally Mn(1)Mn(2) in this picture. With the other Mn dimer, Mn(3)Mn(4), possessing strong antiferromagnetic coupling, significant spin interchange for this dimer into the $S=1$ "excited" state would occur only above 50K. The line shapes for the $g\sim 6$ signal measured at temperatures for 28K and 45K and higher temperatures suggest a change in the overall features, see fig. 4.17. Assuming the tetrameric Mn model, the secondary dimer possibly starts the spin transfer into the $S=1$ state at $\sim 50K$ or higher, which would result in a change of the overall spin state of the tetramer to be $S=7/2$ (assuming a ferromagnetic dimer/dimer exchange coupling (de Paula and Brudvig, 1985b, de Paula, et al, 1986c, Brudvig and Crabtree, 1986, Kusunoki, 1992, Kusunoki, et al, 1989, Yachandra, et al, 1993) based on similar dimer-dimer coupling to that required for a ground state $g=4.1$. If the dimer/dimer coupling was antiferromagnetic, a spin 3/2 state would develop. The quality of the data for the $g\sim 6$ signal is reasonably good, S/N for the $g\sim 6$ at 28K being > 4:1 although somewhat less at higher temperatures. However, the absence of signal intensity reappearing in the $g\sim 4$ region at higher temperatures argues against an antiferromagnetic dimer-dimer coupling. Close examination of the $g\sim 6$ signals suggests, with reasonable

confidence, that the signal changes progressively at the low field edge, possibly indicating the formation of the required $S \sim 7/2$ signal. As a comparison to this model of spin exchange, however, for an isolated Mn dimer with low magnitude exchange constant, $J/k \sim 3.5\text{K}$, the energy gap between the $S=1/2$ and the $S=3/2$ first excited state is $|3J|$ or $\sim 10\text{K}$. The energy gap between this and the $S=5/2$ second excited state is $|5J|$ or $\sim 17\text{K}$. The overall spacing of the ground $S=1/2$ to the second excited $S=5/2$ states is $\sim 27\text{K}$. Continuing the energy gap calculations, the energy gap between the $S=5/2$ and the $7/2$ state, the highest possible spin state for an isolated Mn (III) (spin = 2) Mn (IV) (spin 3/2) exchange coupled dimer, would be $|7J|$ or $\sim 25\text{K}$. This places the energy gap between the ground $S=1/2$ state and the highest spin state $S=7/2$ at $\sim 52\text{K}$. The observed alterations in the $g \sim 6$ signal line shape at temperatures $\sim 45\text{K}$ and above might just as well be due to the populating of the highest energy state of the single magnetically isolated Mn III-IV dimer system in which the exchange coupling is sufficiently low to allow thermal accessibility to the highest spin states of the system.

Based on the spin states of the multiline, excited state $g=4.1$ and $g \sim 6$ signals, the spin state interplay is most simply modelled by the Mn dimer system, although the Mn tetramer model in which most of the spin interchange occurs on one dimer could not be ruled out.

Assuming this tetramer model, however, problems are raised about the spin interactions that occur for the formation of the ground state $g=4.1$ form of the S_2 state. In particular which Mn dimer is oxidised upon the formation of this state. The identity of the Mn dimer which is oxidised is unclear from the Brudvig and Klein discussions (de Paula, et al, 1986c, Yachandra, et al, 1993), although work using EXAFS for the F^- exchanged PSII suggests that the 'multiline' (weakly coupled) Mn dimer is not oxidised in this inhibited state, so that the other dimer becomes oxidised, with a similar oxidation occurring to form the ground state $g=4.1$ state (deRose, et al., 1995). If this were the case, the spin state of the multiline dimer must be either $S=1$ or $S=2$, which would couple ferromagnetically to the $S=1/2$ dimer to form either an $S=3/2$ or $S=5/2$ ground state (de Paula and Brudvig, 1985b, de Paula, et al, 1986c, Brudvig and Crabtree, 1986, Yachandra, et al, 1993). However, the work of Dexheimer et al shows that the spin state and exchange coupling behaviour of the nominal multiline dimer, as revealed by the parallel polarisation $g \sim 4.8$ signal, is unaffected by the presence or absence of the ground $g=4.1$ signal (Dexheimer, et al, 1990, Dexheimer and Klein, 1992). This in itself argues against any coupling of the centres giving rise to these two signals, but in particular means that the multiline dimer (which is even spin in this instance) is unlikely to be the strongly coupled ($J_{\text{ex}}/k \sim 60\text{K}$) pair (de Paula, et al, 1986c, Haddy, et al, 1992) needed to explain the ground $g=4.1$ signal as a spin 3/2 or 5/2 state. The ground state $g=4.1$ signal shows no evidence of any of the Mn derived spin states expected if a weakly coupled

dimer were part of the spin centre giving rise to it (de Paula, et al, 1986c, Haddy, et al, 1992, this work).

At this point, the interaction of all four Mn as a weakly coupled dimer of dimers is strongly argued against by the spin state data at hand for the multiline centre (Pace, et al., 1991 and this work). Based on the multiline state exchange couplings and the measurements of Dexheimer et al (Dexheimer, et al, 1990, Dexheimer and Klein, 1992) the tetramer Mn model can only weakly explain the spin state interchanges observed with the "non alcohol" multiline state.

The data presented for the two different $g=4.1$ signals is also difficult to rationalise within a tetramer model and requires most plausibly that each signal arises from a Mn dimer system essentially magnetically isolated from other Mn containing systems, and so argues for a magnetically isolated dimer of Mn dimers.

5.2. Model for the $g=4.1$ signals

5.2.1. Classification of $g=4.1$ Signals

The results presented in Chapter 4 show conclusively that two types of $g=4.1$ signal are able to be generated in PSII samples. Modelling of the spin states associated with the two types of the $g=4.1$ signal suggest strongly that the two $g=4.1$ signals arise from individual Mn dimers, magnetically and spatially isolated within the D1-D2 PSII complex, although within rapid electron transfer distance. It is the presence of these two Mn dimer sites which requires analysis based on the previous data for the $g=4.1$ signals and proposals for binding of these metal centres in the protein complex.

5.2.1.1. Excited state $g=4.1$ signal

Discussion of the environment and physical characteristics of the multiline have already been made, see above. The excited state form of the $g=4.1$ signal is observed to arise as the ESR signal generated by thermal population of the first excited spin state of the centre giving rise to the multiline signal in the ground state. The present literature consensus on the multiline signal is that it arises from an $S=1/2$ ground state centre (Pace, et al., 1991, Aasa, et al., 1987, Britt, et al, 1992, Hansson, et al, 1987) either from an antiferromagnetically coupled Mn III - IV dimer (Pace, et al., 1991, Smith, et al, 1993, Hansson, et al, 1987, Åhrling and Pace, 1995, Aasa, et al., 1987) or mixed valence magnetically coupled Mn tetramer (Dismukes, et al, 1982, Beck, et al, 1985, Beck and Brudvig, 1986, Beck, et al, 1986, de Paula and Brudvig, 1985b, de Paula, et al, 1986c, Haddy, et al, 1989, Kim, et al, 1992, Kusunoki, 1992). Arguments for the dimer model for the multiline centre have been made, see above.

With a mixed valence Mn III ($S=2$) Mn IV ($S=3/2$) dimer, Heisenberg exchange leads to four possible spin states, $S=1/2$ (observed as the multiline ground state), $S=3/2$, $S=5/2$ and $S=7/2$. This basic argument alone will suggest that, as the first excited state for the exchange is the $3/2$ state and the $g=4.1$ signal observed cogenerated with the multiline exhibits a temperature dependence quantitatively consistent with it arising from a first excited state, this $g=4.1$ signal arises from the $3/2$ state. This argument, based only on the temperature dependence of the expected spin states from Heisenberg exchange of an ($S=3/2$, $S=2$) mixed valence metal dimer, suggests that the next higher spin state should be an $S=5/2$ state. With the ESR signals for the ground and first excited states arising at $g\sim 2$ and $g\sim 4$, respectively (suggesting a strong axially symmetric form of the fine structure interaction), the $S=5/2$ second excited state should arise near $g\sim 6$, which is observed for the measured $g\sim 6$ signal. This signal also exhibits a TD quantitatively consistent with it arising from the second excited state in a coupled dimer. Although line shape modelling for the " $g=4.1$ " signal has been claimed to suggest a rhombic $S=5/2$ state for this signal (Vänngård, et al, 1992, Haddy, et al, 1992, Kim, et al, 1992, Kawamori, et al., 1993, Astashkin, et al., 1994b), the above TD data and the overall axiality of the $g=4.1$ and $g\sim 6$ signals suggest an $S=3/2$ state for the excited state form of the $g=4.1$ signal. The spin states for the model of the exchange coupled dimer and the quantitative agreement of a Boltzmann population analysis with the observed signal temperature dependence seem to provide sufficient evidence that the excited state $g=4.1$ signal arises from a spin $3/2$ thermally accessible state of a mixed valence antiferromagnetically coupled Mn dimer centre.

5.2.1.2. Ground state $g=4.1$ signal.

Based on the TD presented in Chapter 4, the "ground state $g=4.1$ signal" includes the $g=4.1$ signal arising in EG cryoprotected PSII illuminated at 140K (Casey and Sauer, 1984, de Paula, et al, 1985a, de Paula, et al, 1985a), the NH_3 treated PSII illuminated at 200K (Beck and Brudvig, 1986, Beck, et al, 1986, Beck and Brudvig, 1988a, Andreasson, et al., 1988, Boussac, et al, 1990c, Kim, et al, 1990, Kim, et al, 1992, Haddy, et al, 1992) and in Cl^- depleted PSII illuminated at 200K (also with anion exchange similar to F^- exchange, eg SO_4^{2-} CH_3COO^- (Casey and Sauer, 1984, Damoder, et al, 1986, Ono, et al, 1986, Ono, et al, 1987, Beck and Brudvig, 1988a, Baumgarten, 1990, Haddy, et al, 1992, deRose, et al., 1995). This identification of the ground state $g=4.1$ signal as stated is based on a number of lines of evidence:

- the non association of this form of $g=4.1$ to the multiline signal, along with non correlation of the signal intensities of the $g=4.1$ and the multiline generation in the same sample (Cole, et al, 1987);

- . the temperature dependences of the EG cryoprotected, 140K illuminated PSII (Hansson, et al, 1987, de Paula, et al, 1986c, this work), the Cl⁻/F⁻ exchange 200K illuminated PSII (this work), and the NH₃ treated PSII (de Paula, et al, 1986c, Beck and Brudvig, 1986);
- . similarity of the PSII conditions under which the Cl⁻ depleted inhibited PSII illuminated at 200K gives rise to g=4.1 signal in preference to either multiline or Signal II_f intensity (Damoder, et al, 1986, Ono, et al, 1986, Ono, et al, 1987, Baumgarten, 1990);
- . the EXAFS data for the g=4.1 S₂ state under conditions of either anion inhibition (NH₃, F⁻, Cl⁻ depletion) (Dau, et al., 1995, deRose, et al., 1995) or EG cryoprotection 140K illumination PSII (Liang, et al, 1994), suggesting that the Mn- Mn separations under these conditions are very similar, with the Mn - Mn separations split such that one distance remains at ~ 2.72Å, while the other increases to ~2.86Å (Liang, et al, 1994, Dau, et al., 1995, deRose, et al., 1995). This is in comparison to the multiline S₂ state where no obvious changes to the Mn - Mn separations are observed for the generation of the multiline S₂ state (both separations at ~2.72Å in both the S₁ and S₂ states) (Yachandra, et al, 1987, MacLachlan, et al, 1992), although an oxidation event occurs within the Mn environment in both instances of S₂ state formation, evidenced by a shift of the XAS K edge inflection point to higher energy (Yachandra, et al, 1987, Cole, et al, 1987, MacLachlan, et al, 1992, Liang, et al, 1994, Ono, et al, 1994).
- . The absence of the effect of ethanol on this subset of g=4.1 signals is in strict contrast to the effect of alcohols on the excited state g=4.1 signal, in which the presence of alcohols, either by the addition of MeOH or EtOH or as a poly alcohol (EG or glycerol) cryoprotectant or addition to sucrose buffer, precludes the formation of the excited state g=4.1 signal but not the ground state form (Pace, et al., 1991, Smith, et al, 1993, Zimmermann and Rutherford, 1984, Zimmermann and Rutherford, 1986, Rutherford, 1985, Haddy, et al, 1992, Kim, et al, 1990, Kim, et al, 1992, Hansson, et al, 1987, de Paula, et al, 1985a, de Paula, et al, 1986c, Beck and Brudvig, 1988a).

5.2.2. Properties of the Ground State g=4.1 signal

In contrast to the approach taken for the multiline signal, see earlier, the discussion of the ground state g=4.1 signal spin population dynamics is of higher relevance than that of the line shape simulations from ESR and ESEEM, and proceeds this discussions.

5.2.2.1. Spin States

The data here confirm the assignment of this g=4.1 signal, generated by illumination of EG cryoprotected PS II at ~130K, as arising from a ground state centre (de Paula, et al,

1986c, Beck and Brudvig, 1986, Hansson, et al, 1987, Vänngård, et al, 1992, this work). The data also indicated a non Curie curvature at higher temperatures, above ~15K. This non Curie behaviour is indicative of a possible depopulation of the ground state to a low lying excited spin state. This excited state has been shown to be consistent with it arising from a spin 1/2 organic radical, the overall spin system coupling this radical with a Mn III-III or Mn IV-IV dimer, diamagnetic (S=0) in the excited state (this work). The spin state model which most easily describes this temperature dependence data is based on that of Brudvig et al for a cubane Mn tetramer (de Paula, et al, 1986c, Brudvig and Crabtree, 1986), with the organic radical exchanged here for the tightly coupled Mn S=1/2 dimer. The major criterion for the model to generate an S=3/2 ground state from a single oxidation event was for the coupling of the spin 1/2 centre to be equivalent to each of the Mn ions in the second, spin 1 dimer, ie $J'_{1D} = J'_{2D} = J'$, from fig 4.22b. The geometric constraints would require that a Mn tetramer be of Cubane symmetry (Brudvig and Crabtree, 1986). This has shown not to be supported by the Mn-Mn neighbour constraint from X-Ray absorbance studies (Yachandra, et al, 1993, George, et al, 1989, MacLachlan, et al, 1992, Kusunoki, et al, 1989, Penner-Hahn, et al., 1990).

The distorted butterfly coupled dimer of dimers model (Yachandra, et al, 1993, Kusunoki, et al, 1989), satisfied by the X-Ray data, does not appear to satisfy the magnetic exchange coupling requirement ($J'_{1D} \geq J'_{2D} \geq J'_{1D}$). Indeed, the model as proposed places the exchange coupling between the two dimers through a "flexible" μ -oxo- μ -carboxylato bridge between one of each of the Mn ions in each dimer, at a distance of ~3.3Å to ~3.6Å (Yachandra, et al, 1993, Klein, et al, 1993, Kusunoki, et al, 1989). The magnetic exchange coupling between what is essentially a "central" dimer, across the μ -oxo- μ -carboxylato bridge, in this model must be questioned. No absolute coupling scheme has been presented for this model, detailing the spin 3/2 or spin 5/2 ground state arising from such a system. The coupling scheme presented for the generation of the F⁻ PS II, and by inference the other ground state g=4.1 signals (deRose, et al., 1995), assumes an almost cubane like system, the Mn dimers co-parallel (see deRose, et al., 1995, fig 5), although the experimental data precludes this. This scheme has been modelled to require the dominance of coupling from one of the dimers within the system to generate the S=1/2 ground state multiline type signal (Kusunoki, 1992) although the complexity of the X and S band multiline spectra require exchange from all four Mn ions in these schemes (Dismukes, et al, 1982, de Paula and Brudvig, 1985b, de Paula, et al, 1986c, Haddy, et al, 1989).

The exchange coupling scheme of fig.4.22b, in which an S=1/2 organic radical bridges the Mn homodimer, requires little tuning to obtain a sensible spin state model for either a spin 3/2 or 5/2 ground state. With the data for the temperature dependences for the ground and first excited state signals arising from this system, an organic radical bridged Mn dimer is the only

Mn containing structure from which the signals observed could arise. This argues heavily against the Mn tetramer models, although the assignment of the $g=4.1$ signal to either an axially distorted spin $3/2$ (de Paula, et al, 1986c, de Paula and Brudvig, 1985b, Zimmermann and Rutherford, 1986) or rhombically distorted spin $5/2$ (Haddy, et al, 1992, Kawamori, et al., 1993, Astashkin, et al., 1994b) state is still subject to clarification, see later.

The simulation of spin state populations in fig.4.31 ($g=4.1$ and radical $S=1/2$) suggests that the next spin state may be observable within the temperature ranges used. The energy separations between each state are determinable from the exchange coupling scheme, with the energies of the indicated (S_T, S_{12}) states being, for the $(3/2,1)$, $(1/2,0)$ and $(5/2,2)$ configurations, $E(3/2,1) = -5J_{12} + 1/2J'$, $E(1/2,0) = -6J_{12}$, and $E(5/2,2) = -3J_{12} + J'$, respectively. A positive value for J_{12} represents antiferromagnetic coupling in this model, based on the results of de Paula and coworkers (de Paula, et al, 1986c). The simulation for the spin state populations proposed a best reasonable fit for the temperature dependence data of $J_D/k = 65K$ and $J' = -2.6 J_D$. These parameters represent an energy difference between the ground $S=3/2$ and first excited $S=1/2$ states of $\sim 14K$, reflecting to some degree the maximum intensity difference region between the background (annealed, Signal IIS) and illuminated (Signal IIS plus the excited state radical) occurring around 15K in the pure signal intensity temperature dependence graph. The energy difference calculated between the ground $S=3/2$ and proposed second excited $S=5/2$ state is $\sim 50K$. The possible observation of the second excited state signal is hindered by a number of factors:

1. The absolute signal intensity at 50K is very low due to the Curie law,
2. The signal would overlap with remnant ground state $g=4.1$ signal, and would most probably be observable only as a "broadening" of the low field edge on the ground state $g=4.1$ signal, similar to the broadening of the excited state $g=4.1$ signal due to population of the second excited $S=5/2$ state in the sucrose cryoprotected PS II samples illuminated at 200K,
3. The ground state $g=4.1$ signal appears to broaden significantly at temperatures above $\sim 20K$, unlike the excited state form. This might reflect dipolar interaction with thermally populated even spin states of the multiline dimer. Whatever the mechanism, the intrinsic linewidth of the postulated spin $5/2$ state at temperatures above $\sim 50K$ could be so great as to render it virtually undetectable.

The exchange coupling scheme presented as the model for the ground state $g=4.1$ signal precludes the generation of the $S=5/2$ state as the ground state associated with the $g=4.1$ signal and the $S=1/2$ organic radical first excited state. The spin state model for this system, in which an $S=5/2$ ground state is generated for a coupling scheme whereby $J' > -4J_D$, requires that the first excited state must be $S=3/2$, which would certainly not be a radical signal near $g=2$. Indeed, no other ESR signals due to Mn containing structures with spin states of either

5/2, 3/2 or 1/2 are observed to arise as excited state signals (de Paula, et al, 1986c, Haddy, et al, 1992, this work).

In summary, the spin system modelling presented here for the ground state $g=4.1$ signal, indicates that this signal arises from the interaction of an oxidisable amino acid residue bridging a Mn homodimer. The residue is most likely to be Y_Z , observed to be surrounded by a hydrophilic pocket ringed by probable metal ligands, Asp 170, Gln 165, His 190, Glu 189 (Chu, et al., 1995a, Chu, et al., 1995b, Nixon and Diner, 1994, Noren and Barry, 1992, Vermaas, et al, 1993, Svensson, et al, 1991, Styring, et al, 1993). Recently, Britt and coworkers have suggested a close association of Y_Z and a Mn centre in Ca depleted PSII material when advanced to the split signal S_3^* state (Gilchrist, et al., 1995). The spin state modelling indicates that the ground state $g=4.1$ signal arises from an $S=3/2$ signal and is an electron transfer intermediate between the S_1 and the functional S_2 state, represented by the multiline ESR signal.

5.2.2.2. Simulation Studies

The nature of the centre giving rise to the $g=4.1$ signal has been proposed to be a rhombically distorted spin 5/2 centre, with the $g=4.1$ arising from the middle Kramer's transition (Kawamori, et al., 1993, Astashkin, et al., 1994b, Haddy, et al, 1992, Kim, et al, 1992). This designation has been proposed on the basis of simulation studies of the $g=4.1$ lineshape measured at various microwave frequencies on oriented and unoriented samples (Kim, et al, 1992, Haddy, et al, 1992, Vänngård, et al, 1992), and by the simulation of the H_1 field dependence of the $g=4.1$ signal amplitude in ESE experiments (Astashkin, et al., 1994b, Kawamori, et al., 1993).

The measurement of the frequency response of the $g=4.1$ signal line shape was undertaken on a number of different $g=4.1$ signals, including those arising in functional PS II samples illuminated at 200K, NH_3 treated PS II and F^- treated PS II each illuminated at 200K (Kim, et al, 1992, Haddy, et al, 1992, Vänngård, et al, 1992). The $g=4.1$ line shape for the functional PS II measured between X and P bands (9GHz and 16GHz, respectively). developed a separation of the g_{\perp} components with increasing frequency, typical of an anisotropic g tensor (Haddy, et al, 1992). This splitting was similar in form to that observed for the (excited state) $g=4.1$ signal cogenerated with the multiline signal, measured at X and Q bands (Smith, et al, 1993, Vänngård, et al, 1992, this work). The g_{\perp} tensor components for the functional PS II were measured at ~ 4.7 and ~ 3.8 (Haddy, et al, 1992) which differed significantly to the g_{\perp} tensor components measured at Q band, ~ 4.35 and ~ 4.14 (Smith, et al, 1993, this work). In oriented PSII studies, the $g=4.1$ signals observed have indicated that the g tensor has

anisotropy (Kim, et al, 1992, Smith, et al, 1993, Rutherford, 1985), with a shift of the signal to lower field from the $H_{0\perp}$ membrane normal orientation to the $H_{0\parallel}$ membrane normal orientation (Smith, et al, 1993, Haddy, et al, 1992, Kim, et al, 1992, Rutherford, 1985). This orientation dependence is observed for both the "excited state form" of the $g=4.1$ for sucrose cryoprotected PSII illuminated at 200K (Smith, et al, 1993, Rutherford, 1985, Haddy, et al, 1992), and for NH_3 treated PSII, a form of the ground state $g=4.1$ signal, which is not affected by the presence of alcohol (Kim, et al, 1992). In each form measured, the signal line shape was quasi axially symmetric for each of the unoriented $g=4.1$ signals measured at different frequencies (Smith, et al, 1993, Haddy, et al, 1992, Vänngård, et al, 1992) and for the oriented PSII (Smith, et al, 1993, Kim, et al, 1992, Haddy, et al, 1992). The simulations of each signal assumed either a near axial transition of a $S=3/2$ (Smith, et al, 1993, Kim, et al, 1992) system or a middle Kramer's transition in a rhombically distorted $S=5/2$ system (Kim, et al, 1992, Haddy, et al, 1992).

5.2.2.3. Pulsed EPR on the $g=4.1$ signal

To resolve the nature of the spin system giving rise to the $g=4.1$ signal, measurements of the H_1 dependence of the signal intensity in a two pulse experiment were undertaken by Kawamori and coworkers (Kawamori, et al., 1993, Astashkin, et al., 1994b). The measurements were performed on the $g=4.1$ signals from several different preparations:- 1) containing 30% glycerol, possibly a mixture of excited and ground state $g=4.1$ forms (Zimmermann and Rutherford, 1984, Zimmermann and Rutherford, 1986, Smith unpublished data, Kawamori, et al., 1993) 2) sucrose cryoprotected PSII illuminated at 130K, in which no low temperature illuminated $g=4.1$ signal has been previously observed in these samples (Smith and Pace unpublished data) and 3) in Cl^- depleted PSII illuminated at 200K (Astashkin, et al., 1994b), ground state $g=4.1$ form (Ono, et al, 1986, Ono, et al, 1987, Damoder, et al, 1986, Baumgarten, 1990). The H_1 dependence of these $g=4.1$ signals were essentially equivalent, showing a well defined maximum corresponding to $g=4$. Assuming an isotropic g tensor for the effective $1/2 \leftrightarrow -1/2$ transition of the $S=5/2$ state, with $(g_{xx}, g_{yy}, g_{zz}) \approx 4$ (Haddy, et al, 1992) gave a better simulation than for an axial anisotropic g tensor for a $3/2$ spin state, with $g_{xx} = g_{yy} \approx 4.1$ and $g_{zz} \sim 2.05$ (Kawamori, et al., 1993, Astashkin, et al., 1994b) in a randomly oriented sample.

5.2.2.3.1. The $S=5/2$ case

Observance of some anisotropy of the g tensor in the multifrequency studies on the $g=4.1$ signal (Vänngård, et al, 1992, Haddy, et al, 1992, Smith, et al, 1993), the consistent g

value near or above 4 for the oriented PSII samples and simulations of the line shapes for the oriented (Kim, et al, 1992) and unoriented samples (Casey and Sauer, 1984) measured over three microwave frequencies (Haddy, et al, 1992) has led to the proposal of the $g=4.1$ signal arising from the centre transition of a rhombic $S=5/2$ Mn tetrameric structure (Haddy, et al, 1992). The zero field splitting parameters from the simulations were proposed to be $D \approx 0.43\text{cm}^{-1}$ and rhombicity E/D of ~ 0.25 (Haddy, et al, 1992).

At microwave frequencies well below P band (≤ 12 GHz), this model simulates a strong quasi isotropic resonance in the $g\sim 4$ region (Haddy, et al, 1992). At microwave frequencies of P band and above, $g\sim 4$ resonances are observed along only two directions of the fine structure principle axis system (Vänngård, et al, 1992, Haddy, et al, 1992). This Hamiltonian reproduced the experimental P band spectrum of Haddy et al quite reasonably, using an effective gaussian line width of $\sim 35\text{mT}$. The powder pattern simulation assumed an effective spin $1/2$, with anisotropic g tensor, whose principle g components were determined by the exact solution of the zero field splitting Hamiltonian along the principle axis directions (Haddy, et al, 1992). Using a model Hamiltonian simulation program (Gladney, H.M. and Swaten, J.D., Quantum Chemistry Program Exchange, No. 134) the numerically computed field positions and transitions for the above Hamiltonians model, at the Q band frequency used here for the $g=4.1$ measurements ($\sim 34.8\text{GHz}$), indicated strong turning points at $g\sim 4.36$ and $g\sim 3.82$ (Bramley, unpublished results) similar to the situation reported for P band (Haddy, et al, 1992). In addition to these turning points, numerous other transitions of comparable intensity were predicted, from $g\sim 12$ to $g\sim 3$. The angular dependence of the $g\sim 3.82$ transition determined this as the g_x component (Bramley unpublished), the high field edge of the g tensor of an effective spin $1/2$ system, with g_z value below $g\sim 8$. Turning points are predicted for a second group of transitions with a low field edge at $g\sim 3$, extending to $g\sim 1.7$. Neither Q band spectra for the two forms of the $g=4.1$ signal seen here are consistent with turning points at both $g=4.36$ and $g=3.82$.

The pulsed ESR study of Kawamori and coworkers (Kawamori, et al., 1993, Astashkin, et al., 1994b) mentioned above should offer a direct determination of the spin state, based on the microwave field (H_1) dependence of the two pulse experiment signal amplitude. The analysis for this experiment assumed the spin $5/2$ Hamiltonian (Haddy, et al, 1992) with quasi isotropic effective g value $g\sim 4$, which would be applicable to the calculation of the microwave induced transition probabilities for the presumed spin $5/2$ state (in the weak field limit, $D \gg$ microwave quantum). From an exact numerical solution (Gladney, H.M. and Swaten, J.D., Quantum Chemistry Program Exchange, No. 134) of the zero field splitting of a spin $5/2$ Hamiltonian, using the parameters of Haddy (Haddy, et al, 1992) required to simulate the X and P band CW experiment line shapes, the transition probabilities for this system were

observed not to be isotropic (Bramley and Pace unpublished data). The transition probabilities vary by a factor of ~ 2 dependent on the H_1 and H_0 field orientations with reference to the molecular axis system, corresponding to an effective g value range of 3.7 to 5.0. This occurs because D , the axial fine structure parameter, is of the order of the X band microwave quantum (0.3 cm^{-1}), so the weak field limit assumption no longer holds in this system.

The dark annealed sample spectra of Kawamori and coworkers for the $g \sim 4$ region would have a significant contribution from the rhombic iron $g \sim 4.3$ signal always observed in PS II samples (see Rutherford, 1985, Zimmermann and Rutherford, 1984, Zimmermann and Rutherford, 1986). The rhombic Fe $g \sim 4.3$ signal should be a good reference signal for this experiment, with the transition unambiguously arising from a rhombic $5/2$ state centre doublet with $D \sim 0.4 \text{ cm}^{-1}$ and $E/D \sim 0.3$ (Castner, et al., 1960), parameters very similar to those proposed for the $g=4.1$ signal (Haddy, et al, 1992). The H_1 dependence of the ESE echo amplitude measured across the $g \sim 4$ region for this dark sample, in the presence of the rhombic Fe signal only, shows no peak corresponding to $g \sim 4$ but a broad distributed response across $g \sim 5$ to $g \sim 2$ (Kawamori, et al., 1993) fig. 16 II, (Astashkin, et al., 1994b, fig.4). This distributed response is in fact what one would actually expect for a spin $5/2$ system, with parameters similar to those invoked by Haddy and coworkers, when the exact solution of the Hamiltonian is considered, as above. It is not what is observed for any of the $g=4.1$ signal types however. This raises a major doubt over any assignment of the $g=4.1$ signal as a rhombic $5/2$ state.

The spectral shapes of the $g=4.1$ signals observed at Q band (Smith, et al, 1993 and this work) suggest that if the signals arose from a spin $5/2$ state, D should be large enough to allow observation of all three turning points around $g \sim 4$ at the Q band frequency. This would require $|D| \approx 1.2 \text{ cm}^{-1}$ which would make the assumption of an isotropic transition probability at X band more reasonable. The centre doublet for the spin $5/2$ system, from which the $g=4.1$ signal is proposed to arise, is not the ground state. For $|D| \sim 0.43 \text{ cm}^{-1}$ and $E/D \sim 0.3$ (as per Haddy, et al, 1992), this transition is separated from the ground and top energy states by $\pm 1.5 \text{ cm}^{-1}$. Replotting the temperature dependence, fig.5.01, with such a Boltzmann model for the intensity assuming this value for the energy spacing (dotted lines), the curve does not follow the trend of the measured data but probably could not be excluded as the curvature is small. For $|D| \sim 1.2 \text{ cm}^{-1}$, however, the state spacing is over 4 cm^{-1} . Graphing of such an energy state system (solid lines) shows that it is clearly excluded. Thus, a rhombic spin $5/2$ model for the $g=4.1$ signal with low D ($\sim 0.4 \text{ cm}^{-1}$) approximates the X band signal temperature dependence, but is argued against by the shape of the Q band $g=4.1$ spectra and the pulsed ESR data. With D sufficiently large to accommodate the Q band spectral data, the model no longer is compatible with the X band temperature dependence data.

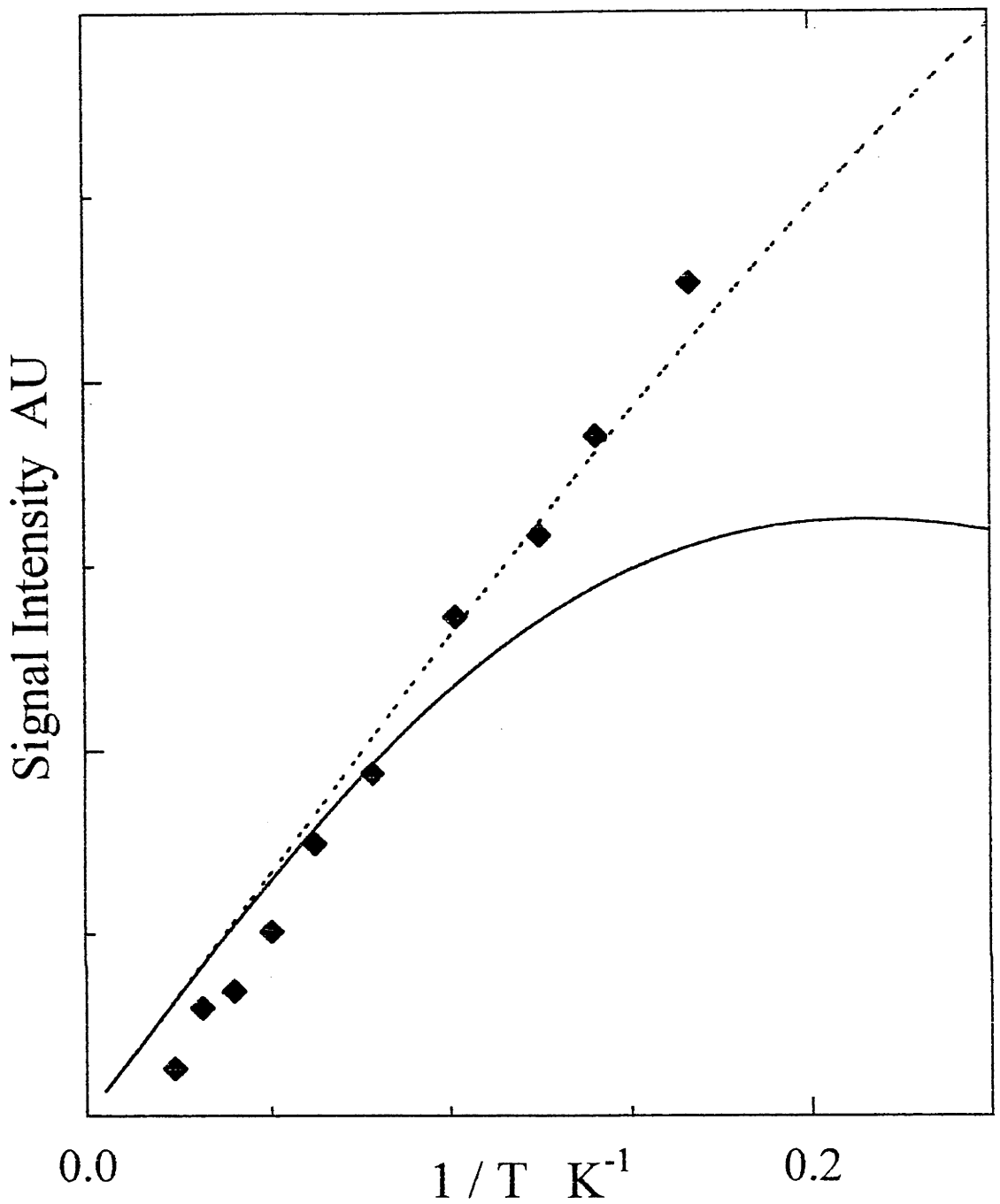


Figure 5.01. Temperature dependence of the S_2 state $g=4.1$ signal generated in PSII cryoprotected with 30% v:v ethylene glycol, illuminated at 130K, ie independent of the S_2 state multiline signal. The data has been modeled as an excited state centre, with the lines indicating the intensities calculated for a Boltzmann spin state for (i) (dotted line) the $g=4.1$ signal state lying $\sim 1.5\text{cm}^{-1}$ above the ground state, and (ii) (solid line) the $g=4.2$ signal lying $\sim 4\text{cm}^{-1}$ above the ground state, see text.

On the basis of this data and arguments presented, any identification of the $g=4.1$ signals arising from a spin $5/2$ centre is difficult to rationalise.

5.2.2.3.2. The $S=3/2$ Case

The analyses for the proposal that the $g=4.1$ arises from an $S=3/2$ state have been based on the data for the $g=4.1$ generated in sucrose cryoprotected PS II illuminated at 200K, the excited state form, (Zimmermann and Rutherford, 1986, Hansson, et al, 1987, Pace, et al., 1991, Smith, et al, 1993). With these samples, the comparison of the Q band and X band data indicates a slightly non axial 'apparent' g tensor. The g_{\perp} tensor components have been reported to be ~ 4.35 and 4.14 (Smith, et al, 1993). At the Q band frequency, these g_{\perp} values result in a crossing point at $g \sim 4.25$, while the X band crossing point, being at lower g value ~ 4.10 , is probably the result of not being able to properly resolve these components at X band microwave frequency (Smith, et al, 1993). This equivalence of the g_{av} at X and Q bands requires a large axial fine structure parameter, D , of the order or higher than the microwave quantum (Hansson, et al, 1987, Smith, et al, 1993). The $|D|$ value was estimated to be of the order of 5cm^{-1} , with E/D of ~ 0.017 , based on the splittings of the g_{\perp} components measured from the Q band spectrum (Smith, et al, 1993). The g_{\parallel} component had been proposed to be near $g \sim 2.0$ (Haddy, et al, 1992). No observations of signals in the $g \sim 2$ region were positively reported (Kim, et al, 1992, Haddy, et al, 1992), although an observation was implied from oriented PS II (see Smith, et al, 1993). From calculations based on the $g_{\perp x}$ and $g_{\perp y}$ components, the true perpendicular component of the g tensor (g'_{\perp}) was calculated to be ~ 2.12 . Such a large value of g'_{\perp} is in fact observed for model Mn dimer compounds, μ -acetato- μ -phenoxy bridged, in which a multiline type signal is observed at low temperatures (ground state) $\leq 30\text{K}$, while at higher temperatures, a resonance is observed at low field, in the $g \sim 4$ region (Diril, et al., 1987, Chang, et al., 1988a, Chang, et al., 1988b). These Mn dimer compounds were antiferromagnetically exchange coupled, with $|J|$ of low magnitude, $|J| \sim 6\text{cm}^{-1}$ (Diril, et al., 1987, Chang, et al., 1988a, Chang, et al., 1988b). The crossing point of the $g \sim 4$ resonance was measured at $g > 4.0$, near $g \sim 4.2$, similar to the g_{av} for the excited state $g=4.1$ signal discussed here. In the model compounds, the axial fine structure parameter was estimated at $|D| \leq 2\text{cm}^{-1}$ (Diril, et al., 1987, Chang, et al, 1988, Chang, et al., 1988b). With $|D|$ of similar magnitude to $|J|$, the zero field parameter may be expected to mix contributions from higher spin states into the g_{\perp} components, but not the g_{\parallel} components, of the g tensor (Chang, et al., 1988a, Chang, et al., 1988b, Smith, et al, 1993), resulting in the $g_{\perp av} > 4.0$.

The shapes of the ground state $g=4.1$ signal, measured at X and Q bands, shown in figs 4.06b and 4.12b resp., are very similar to other proposed forms of this signal, that for NH_3

treated PS II (Beck and Brudvig, 1986, Kim, et al, 1990, Kim, et al, 1992) and F⁻ treated PS II (Damoder, et al, 1986, Ono, et al, 1986, Ono, et al, 1987, Baumgarten, 1990, and see earlier), both measured at X and P bands (Haddy, et al, 1992, Kim, et al, 1992). Neither of these 'ground state' forms of the g=4.1 appeared to develop splitting of g_⊥ tensor components, upon change of microwave frequency from X band to P band, which contrasts to the splitting observed for the excited state form of the g=4.1 (Smith, et al, 1993, Haddy, et al, 1992, Kim, et al, 1992, this work). This lack of splitting of the g_⊥ components led to the proposal that these ground state forms of the g=4.1 signal possessed slightly higher rhombicity and D parameter (~0.5cm⁻¹) in comparison to the excited state g=4.1 signal, denoted as the functional g=4.1 signal (Haddy, et al, 1992, Kim, et al, 1992).

From the data presented here for the ground state g=4.1 signal, the most satisfactory interpretation, consistent with an S=3/2 state, would be for a near axial centre similar to the excited state form. In this case D would be less than for the excited state centre, ($|D| \leq 1 \text{cm}^{-1}$) as the g_{⊥av} value for the signal decreases upon increase of the microwave frequency, g_{⊥av}~4.10 at X band, g_{⊥av}~3.98 at Q band (see earlier). To be consistent with the pulsed ESR results (Astashkin, et al., 1994b) and that this resonance is positioned above g~4.0 at lower microwave frequencies (S, X bands), (Haddy, et al, 1992, Kim, et al, 1992, Casey and Sauer, 1984, Zimmermann and Rutherford, 1986, de Paula, et al, 1986c, Beck and Brudvig, 1986, this work), the true g'_⊥ value of the state would have to be above 2.0 (approximately 2.1 to 2.2), similar to the value for the excited state g=4.1 signal and the Mn dimer model compounds as discussed above. Simulations based on the signal line shapes are beyond the scope of this report, but are being undertaken in the Pace group laboratory (Åhring and Pace unpublished results).

In summary, the temperature dependence and lineshape data presented here for BOTH forms of the g=4.1 signals are best explained by each arising from spin 3/2 states. The two signals are distinct and arise from different Mn dimer centres located within different environments of the PS II complex. The data presented here almost conclusively indicate that these signals can not arise from rhombic S=5/2 centres based on the temperature dependence and implied spin states, and on arguments based on the line shape simulations and measurements for the CW and pulsed ESR experiments.

5.3. The Nature of the Mn Centres

From the data presented and the discussions of the preceding models, based on spin states, temperature dependence data and simulation studies of observed and predicted ESR

transitions, the magnetically isolated dimer of exchange coupled Mn dimers is the model which best explains the available observations.

This magnetically isolated dimer of Mn dimers model requires the arrangement of the minimally four Mn ions within the OEC into two distinct regions of the protein. These regions are most easily labelled based on the dominant ground state ESR signal generated in the S₂ state, either the multiline signal (which incorporates the excited state g=4.1 signal) defining the multiline site, or the ground state g=4.1 signal, defining the g=4.1 site. The distinction in spin nature and generation of the two different forms of the g=4.1 signal is critical for the definitions and arguments within the model. As from before, essentially only two types of g=4.1 signal are observable based on the preparation of the PS II and the illumination regime under which the S₂ state is generated.

5.3.1. Location of the Manganese Sites

From the Temperature Dependence of various EPR signals (de Paula and Brudvig, 1985b, de Paula, et al, 1986c, Aasa, et al., 1987, Hansson, et al, 1987, Vänngård, et al, 1992, Pace, et al., 1991, Britt, et al, 1992) and the X-Ray absorbance data (Yachandra, et al, 1986a, Yachandra, et al, 1987, Yachandra, et al, 1993, George, et al, 1989, Kusunoki, et al, 1989, Penner-Hahn, et al., 1990, MacLachlan, et al, 1992), the Mn ions must be associated with the protein as exchange coupled μ -oxo-bridged dimers. How these dimers associate and the analysis for approximate location is aided by considering the results of studies on amide reduction (Yocum, et al, 1981, Sivaraja and Dismukes, 1988, Messinger and Renger, 1990, Messinger, et al, 1991b, Messinger, et al, 1991a, Mei and Yocum, 1991a, Mei and Yocum, 1992, Rickert, et al, 1991, Riggs, et al, 1992, Kretschmann and Witt, 1993), Mn photo ligation and activation (Cheniae and Martin, 1970, Cheniae, 1980, Tamura and Cheniae, 1987) and Mn removal and reassociation studies (Yocum, et al, 1981, Klimov, et al, 1982, Kulikov, et al, 1983, Allakhverdiyev, et al., 1983; Allakhverdiyev, et al., 1986, Takahashi and Asada, 1986, Isogai, et al, 1988, Dolan, et al, 1990, Mavankal and McCain, 1991, Enami, et al, 1994).

Each set of above experiments gave results leading to the hypothesis that the Mn bound in two regions, which are located close to the luminal surface of the protein. One pair was easier to remove via non physiological conditions, such as high salt, removing the extrinsic polypeptides, with resuspension into low Cl⁻ or low Ca²⁺ media (Isogai, et al, 1988), and washing into Cl⁻ free buffers (Mavankal and McCain, 1991, Dolan, et al, 1990). The conditions which lead to the loss of this more accessible Mn lead to a loss of O₂ evolution activity (Isogai, et al, 1988), although electron transfer through the protein remained intact. Frasche and coworkers have indeed reported an altered g=4.1 signal from samples treated to remove these luminal accessible Mn ions (Dolan, et al, 1990). The other region of Mn binding

is observed to be less accessible to the luminal solution. Small amide reductants are observed not to affect or release these Mn except under extreme conditions, high concentration or with long incubation times (Yocum, et al, 1981, Messinger and Renger, 1990, Messinger, et al, 1991b, Messinger, et al, 1991a, Mei and Yocum, 1991a, Mei and Yocum, 1992, Riggs, et al, 1992). Cl⁻ depletion studies, in which PSII is washed into Cl⁻ free media (in the absence of the extrinsic polypeptides), leads to a loss of two Mn (Mavankal, et al, 1986). The protein requires heating to 60°C, leading to denaturation, for the second group of Mn to be released (Mavankal, et al, 1986). These studies imply that two of the Mn ions are less accessible to reduction and/or removal from the protein, while two Mn ions are close to the lumen and subject to removal by mild treatments.

Mild treatment with NH₂OH may reduce and liberate two of the four Mn, these Mn being accessible from the lumen (Mei and Yocum, 1991a, Mei and Yocum, 1992, Riggs, et al, 1992). Stronger treatment is required to reduce up to four Mn per PS II, with consequent loss of all donor side activity and formation of Y_Z⁺ under illumination (Sivaraja and Dismukes, 1988, Yocum, et al, 1981, Mino and Kawamori, 1994, Diner, et al., 1995, MacDonald, et al, 1993, Kodera, et al, 1992, Koulougliotis, et al., 1995, Takahashi and Asada, 1986, Dolan, et al, 1990, Mavankal and McCain, 1991). Incubation of PS II in the presence of hydroquinone results in the reduction and loosening of two Mn ions, although these "free" Mn are inaccessible to EDTA treatment, remaining within a deeply located region of the membrane bound protein (Mei and Yocum, 1991a, Mei and Yocum, 1992, Riggs, et al, 1992).

5.3.2. Sites for binding

From mutational studies on the D1 and D2 peptides, two regions of metal binding sites are hypothesised.

5.3.2.1. Inner site

Virtually all residues implicated in metal binding to the OEC are located on the D1 polypeptide (Svensson, et al, 1990, Nixon and Diner, 1994, Chu, et al., 1995a, Chu, et al., 1995b). One region consists of amino acid residues located near Y_Z, while the other region is located within the C-terminal region of the D1 protein. The amino acid residues implicated as binding sites are: Asp 170, believed to be the ligand site for initial Mn binding during photoactivation, Glu 165, His 190 and Glu 189 (Nixon and Diner, 1992, Nixon and Diner, 1994, Styring, et al, 1993, Vermaas, et al, 1993, Roffey, et al., 1994, Chu, et al., 1995a). These four amino acid residues are observed to be essential for binding Mn, O₂ evolution activity and photoactivation of the Mn prior to O₂ evolution (Babcock, 1993, Vermaas, et al, 1993,

Chu, et al., 1995a, Nixon and Diner, 1992, Nixon and Diner, 1994, Styring, et al, 1993, Roffey, et al., 1994).

Protein modelling studies indicate that His 190 is located approximately 4.5Å from Y_Z (Svensson, et al, 1990, Svensson, et al, 1991). Modelling of the equivalent site within the D2 polypeptide indicates a D2H189 to D2Y160 (Y_D) distance of ~2.8Å, with a strong Hydrogen bond between these residues aiding in the stability of the D2 polypeptide structure (Svensson, et al, 1992, Vermaas, et al, 1993, Styring, et al, 1993, Debus, et al, 1988). D1H190 and D1Y161 (Y_Z) are postulated to be also H-bonded (Svensson, et al, 1990, Styring, et al, 1993), although see (Nixon and Diner, 1994). However, the large distance between these residues, ~4.5Å (Svensson, et al, 1990, Svensson, et al, 1991), would allow possible Mn binding within this space, with the phenoxy oxygen and imidazole nitrogen at ~2Å from a Mn equidistantly bound to both. This hypothesis is supported by X-Ray absorption data, with O and N ligands at ~1.9 to 2.0Å (Yachandra, et al, 1986a, Yachandra, et al, 1987, George, et al, 1989, Kusunoki, et al, 1989, Penner-Hahn, et al., 1990, MacLachlan, et al, 1992).

The oxidation number to be assigned to these two Mn ions is still unclear, X-Ray data suggesting the oxidation state of Mn to be Mn III-III, Mn IV-IV in the S₁ state (Kusunoki, et al, 1989, MacLachlan, et al, 1992, Yachandra, et al, 1993), whilst strong amino reduction of Mn leading to total loss suggests an S₋₃ formal redox state is attainable, which would imply an oxidation state of Mn (III)₄ in the S₁ state (Mei and Yocum, 1992, Kretschmann and Witt, 1993, Wells, et al, 1993, Rickert, et al, 1991). It is possible these 'deeper' Mn ions are required to be at a Mn IV state for stronger binding, each Mn (II) requiring removal of two oxidative equivalents for binding. This is uncertain although oxidation at both Y_Z and Y_D may well be implicated in the initial stages of photoactivation (Vermaas, et al, 1988, Babcock, 1993, Nixon and Diner, 1994). Either oxidation allows a binding into the ~4.5Å His190 to Y_Z separation. Glu189 is located next to the His 190 and is well positioned to provide either a single or double ligand site to Mn (Chu, et al., 1995a). With these ligands, Mn(IV) or (III) could be stably bound to the protein. The remaining amino acid residues which would contribute to Mn binding in of this group are Gln165 and Asp170 (Nixon and Diner, 1992, Styring, et al, 1993, Chu, et al., 1995a). Further mutation studies on other amino acids have implicated Glu65 as a possible ligand to Ca²⁺ within the D1 polypeptide (Chu, et al., 1995a). This residue appears located near the luminal surface of the α helical region (D1 helix I cf D1 helix III for Gln165 and Asp170) and may coordinate Ca²⁺ along with Asp170 and/or Gln165, with these two amino acids providing one ligand to Mn, one to Ca²⁺ (Chu, et al., 1995a). This would leave ligand binding sites on the Mn ions available, which in the picture of the ground state g=4.1 signal would be taken up by a redox active amino acid residue. Y_Z would easily fit as the

bridging ligand, with the other bridging ligands being of μ -oxo nature, required for consistency with X-Ray data model (Kusunoki, et al, 1989, MacLachlan, et al, 1992, Yachandra, et al, 1993) and for the Mn=Mn separation at $\sim 2.7\text{\AA}$ (see (Dismukes, 1988, George, et al, 1989, Penner-Hahn, et al., 1990, MacLachlan, et al, 1992, Yachandra, et al, 1993, Klein, et al, 1993).

This structure, depicted in figure 5.02, in which the Mn dimer, either Mn III-III or Mn IV-IV is ligated across Y_Z is structurally close to that required by the spin state and exchange coupling model for the ground state $g=4.1$ signal. The possibility that Y_Z bridges the Mn would allow strong exchange coupling to each Mn, a requirement for the formation of the ground state $g=4.1$ signal from a single electron turnover event.

5.3.2.2. Outer site

The other grouping of amino acids observed to be potential ligands for Mn and essential for O_2 evolution, but not necessarily essential for the conformation of the D1 polypeptide and Y_Z redox chemistry are located at the post translational and cleavage C terminus (Nixon, et al, 1992). These include His332, Glu333, His337, Asp342 and the C-terminal Ala344 (Nixon, et al, 1992, Nixon and Diner, 1994, Babcock, 1993, Vermaas, et al, 1993, Chu, et al., 1995b). The nature of the C terminal has been observed by mutation studies to be less dependent on the type of residue, but to require a non sterically hindered free carboxyl group (Nixon, et al, 1992, Nixon and Diner, 1994). This region is in a site that is not analogous to any part of the bacterial anoxygenic photosystem. Little is known of the secondary or tertiary structure of this region of the protein. Recent studies by Wydrzynski and Zheng, using IR spectroscopy of the PS II peptide core complex, have postulated regions of α helical structure associated with functional OEC, which become reversibly disorganised when Mn and Ca are displaced (Zheng and Wydrzynski unpublished).

For the above "outer site" amino acids to come into close approach, a high level of structural clustering is required. The simplest arrangement bringing His 332 and Glu 333 into close approach while siting these residues away from the peptide backbone would be an α helical segment. However, to place Asp 342 and the C terminal carboxyl close to His 332 and Glu 333, a very tight bend must occur. This tight bend may be facilitated by the proline at position 340. Prolines are known to either break or severely kink α helical polypeptide segments. Pro 340 is an important residue as the conformation of the secondary amide bond may allow the twisting to bring the four proceeding C terminal residues away from the helix backbone and along the surface of the helix toward His 332. Modelling of such twisting of the C terminal region back toward His 332 places Asp 342 within $\sim 7\text{\AA}$ of His 332 and Glu 333 (Smith unpublished). With this four residue section approximately linear, Ala 344 may be located between Asp 342 and His 332. Figure 5.03 shows a molecular model construction for

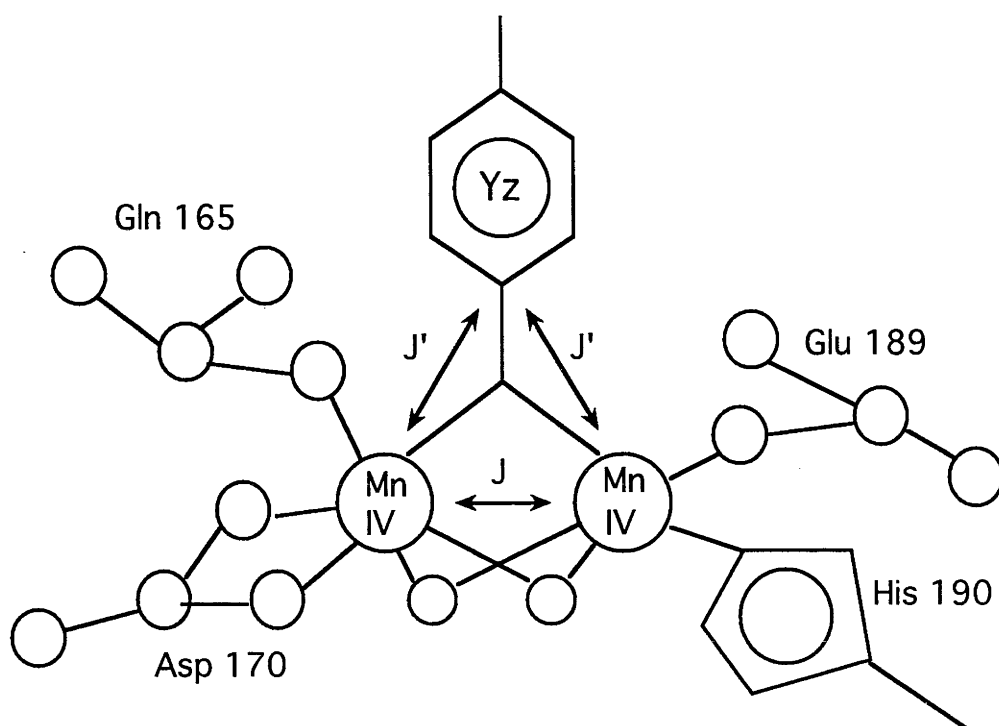


Figure 5.02. Postulated arrangement for the 'Inner site' of manganese binding site. This structure is based on spin states derived for the ground state $g=4.1$ signal determined from the temperature dependence studies. The spin states for this system are an $S=3/2$ ground state, arising from the interaction of oxidised Yz with the Mn dimer ($S=1$). The first excited state for the system gives rise to a radical $g\sim 2.00$ $S=1/2$ signal, expected for an oxidised organic radical. Line shape studies on this excited state signal implicate the involvement of a neutral tyrosyl radical, from the proton hyperfine pattern and the g value (~ 2.0045). It is hypothesised here that Yz, the intermediate electron transfer carrier, bridges two Mn III or Mn IV ions, with ligation within the protein based on mutational and structural simulation studies discussed in the text. The positioning of these ligands is not as yet determined, although the distance between Yz and each of His 190 and Asp 170 is predicted to be ~ 4 to 4.5\AA (Svensson, et al, 1991, Styring, et al, 93), ideal for the location of such a dimer within this pocket.

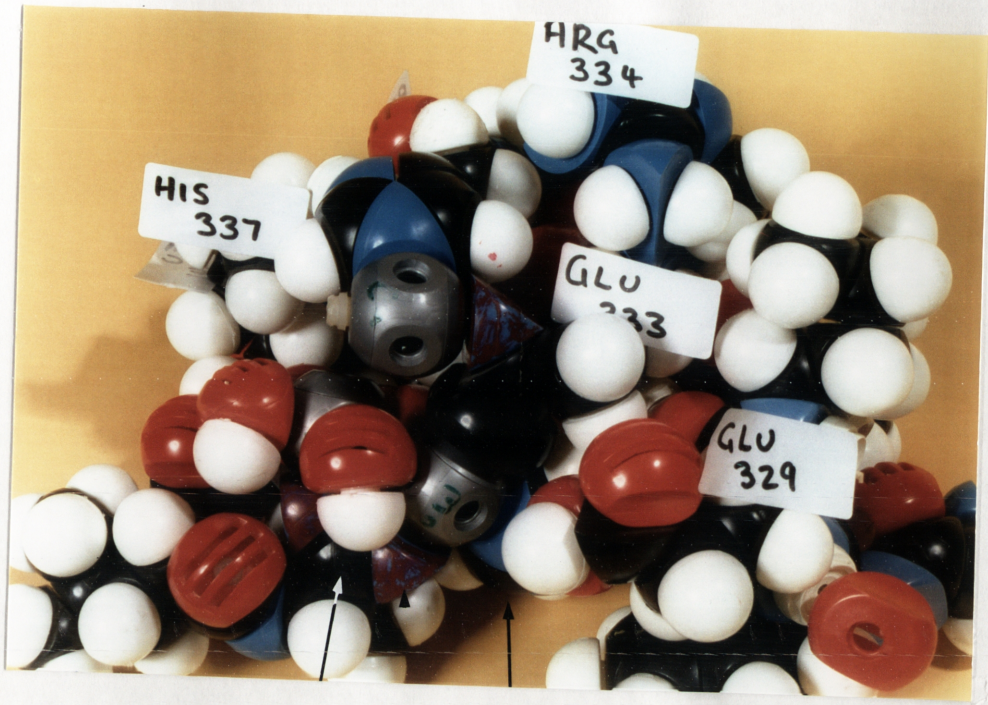


Figure 5.03. Photographic image of a molecular model construction of a possible geometry for the 17 C-terminal amino acid residues of the D1 polypeptide. Mn ligands are His 332, Glu 333, Asp 342 and Ala 344, with the C-terminus carboxyl group modelled as bridging ligand for this dimer.

such a conformation of the 17 C-terminal residues, from Phe 328 through to Ala 344. The two amino acid residues preceding Phe 328, Gly 327 and Ile 326, may form a turn to orient this structured segment. Fig.5.04 shows a triple bridged Mn dimer structure, di- μ -oxo, μ -carboxylato. The site adjacent to which His 332 and Glu 333 ligate one Mn position is apparently ligand deficient. This position is uncertain due to a lack of probable additional ligands, although D2 Glu 65 may be implicated (Vermaas, et al, 1993, Chu, et al., 1995b). The other Mn has an interesting conformation, with Asp 342 contributing the only terminal protein ligand. His 337, which mutation studies suggest is not a direct Mn ligand (Nixon, et al, 1990), may reside traversing one ligand site, ligating a Ca^{2+} which is carboxyl bridged via Glu 333 to the Mn. This Mn-Ca carboxyl bridged structure has been proposed based on IR spectroscopy (Noguchi, et al., 1995). The final ligand position on the Asp 342 Mn may be a substrate binding site. ESEEM studies using NH_3 treated PS II suggest only one terminal ligand position for substrate binding within the Mn complex (Britt, et al, 1989). With the D2 polypeptide in close association to D1 and CPa 43 and three extrinsic peptides, 33KDa, 23KDa and 17KDa, also in close proximity to this site, the overall form of this region suggests limited access for substrate reagents, such as water and amine analogues.

The structure proposed at this site appears, fig. 5.04, to match the dimer structure proposed on the basis of the multiline simulation of Åhrling and Pace (Åhrling and Pace, 1995). The model structure required that one Mn be terminally ligated to Histidine, with one ligand site at this Mn uncertain, this Mn being the Mn IV site in the S_2 state. The other Mn, the Mn III site, was proposed also to be ligand deficient, this vacant ligand position being normal to the plane of the μ -oxygens, ie the z direction. This z direction ligand site is hindered by the plane of His 337 lying almost co-parallel to the plane of the 2 μ -oxygens, the His 337 ring covering this ligand site, blocking binding to the Mn at this position. The conformation of this His 337 ring is held by the Ca^{2+} ligand binding of the imine nitrogen, the Ca^{2+} in turn being held by Glu 333 carboxyl bridging to the Mn IV site.

5.4. Consequences of the Model

5.4.1. Manganese Binding and EPR

The model proposed above maintains an effective octahedral ligand bond geometry for the outer Mn. The ligand deficiency about each of these Mn allows development of a highly oxidative environment (Dismukes, et al, 1994). The model for this outer pair is consistent with nearly all data currently available. The modification to the multiline by the treatment of PS II with NH_3 , whereby the multiline formed displays a reduced hyperfine spacing and additional

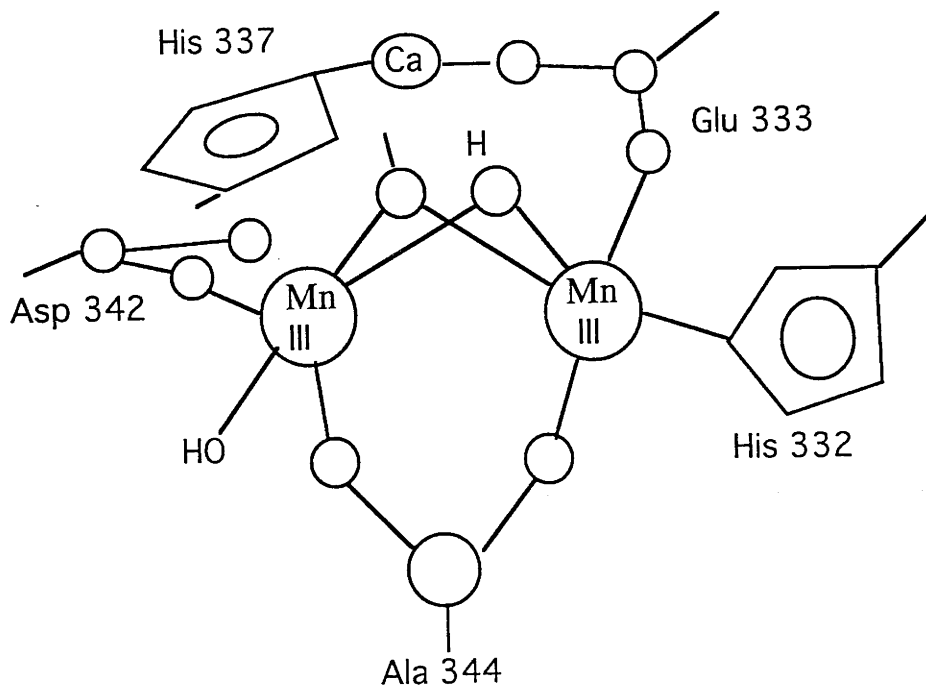
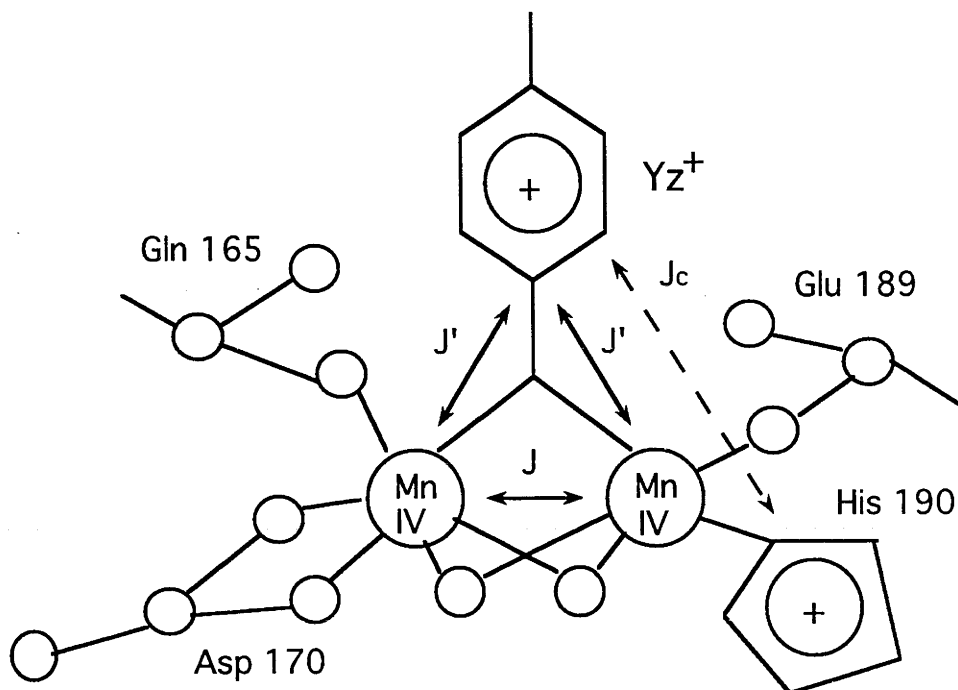


Figure 5.04. Representation of the possible ligand configuration of the multiline Mn dimer. The dimer presented for the model is di- μ -oxo, μ -acetato bridged, consistent with Xray spectroscopic data (eg Yachandra, et al, 93). All storage and functional redox turnover in the process of oxygen evolution is undertaken within the environment of this dimer, see text.

peaks (Beck and Brudvig, 1986, Beck, et al, 1986, Beck and Brudvig, 1988a, Andreasson, et al., 1988, Britt, et al, 1989, Boussac, et al, 1990c) may be consistent with the exchange of NH₃ for H₂O at the Mn substrate binding site. The major concern over the multiline signal arising from an isolated Mn dimer, at present, is the ESE ENDOR study on the multiline signal and on mixed valence Mn complexes (Britt, et al., 1995, Randall, et al., 1995). Simulations based on an isotropic Mn dimer, parameters as per Åhrling and Pace and for a model Mn III-IV dimer complex, with each Mn assumed octahedrally six coordinate, did not appear to match the measured ESE ENDOR signal measured for the multiline (Randall, et al 95, fig.7). The apparent best fit model was for a tetrameric cluster, (as per Randall, et al., 1995) magnetic exchange between all four Mn ions (Randall, et al., 1995). However, this apparent best model did not match the line width and hyperfine pattern of the ESE ENDOR closely (Randall, et al 95, fig.7), and with the previous discussion over possible contamination of the multiline signal in the samples used by Britt et al, a final conclusion on the ESE ENDOR work awaits further simulation on the signal, not a trivial task, and further refinement and definition of the signal measured.

Questions over the proposed second, inner dimer are of greater concern. The lack of significant dipolar broadening and the inability to observe broad hyperfine features on the 'excited state' Y_Z^+ signal require clarification. Both of these observations depend upon the unique consequences that arise when the radical species is equally coupled to two Mn, which are in the same oxidation and spin states. Under these circumstances, the total spin of the Mn pair is a well defined quantum number, S_{12} (Bencini and Gatteschi, 1990). In the state in which the Y_Z^+ signal is visible, $S_{12}=0$, ie the Mn couple strongly to a diamagnetic state. The antiferromagnetic coupling between these Mn has been estimated to be $\sim 60\text{cm}^{-1}$ or more (see earlier). The distance from the midpoint of the dimer to the centre of the tyrosyl ring is $\sim 4\text{\AA}$. Thus the dipolar interaction between the unpaired spin ($S=1/2$) on the tyrosine ring and the Mn centres in the dimer is only a fraction of a wave number (Chapter 2). Thus tyrosine 'sees' only a diamagnetic Mn pair when $S_{12}=0$, to a very good approximation. Similarly the projection of any Mn nuclear hyperfine interaction onto the total (S_T) net spin $1/2$ state represented by the 'excited state' Y_Z^+ signal, depends on terms of the form $S_T.S_{12}$ (Bencini and Gatteschi, 1990, Dismukes and Siderer, 1980, Dismukes and Siderer, 1981). These are rigorously zero when $S_{12}=0$, ie no Mn derived hyperfine appears on the signal. When the symmetry of the spin coupling system is broken or lowered, these diamagnetic 'cancellation' effects are lost. Thus Britt et al have recently reported that a S_3^* signal generated in Ca^{2+} depleted material arises from a Y_Z^+ species massively ($\sim 200\text{G}$) dipolar broadened by close proximity to Mn. This



Dimer is $S=0$ for $J > J' / 2$
 Double turnover may lead to
 increase only in J with effect
 the ground spin state of the Yz
 Mn dimer system. The exchange
 leading to the narrow $S3$ split
 signal is represented by J_c .

Figure 5.05. In Cl depleted PS II, illuminated to form the S_2 state, the oxidative equivalent formed is 'stored' upon Yz . This leads to formation of the ground state $g=4.1$ signal and the Yz radical as the first excited state. Room temperature illumination leads to only two electron step turnovers in these strongly inhibited samples. The two oxidative equivalents, formed by the stalling of turnover at the second event, form oxidised Yz and His 190, which is known to be redox capable from studies on thermoluminescence during back reactions. This forms two organic radicals within 5\AA spacing which, possibly via mutual bonding with the Mn ion ligated between them, forms the centre giving rise to the NARROW form of the $g\sim 2$ split signal. The temperature dependence of this signal suggests strong coupling, as the spin state displays Curie behaviour to at least 50K.

could arise if the disturbance brought by the acetate induced Ca^{2+} depletion disturbs the geometry of the Mn-Y_Z^+ cluster, breaking or diminishing some of the exchange couplings, see figure 5.05.

5.4.2. Amine reduction and binding

The influence of reducing amines is easily explained in terms of the two binding regions within the protein. The addition of NH_2OH to PS II leads to reduction of Mn upon binding in the S_1 state and turnover generated by illumination (Forster and Junge, 1988, Beck and Brudvig, 1988b, Guiles, et al, 1990a). NH_2OH , under mild conditions, is observed to reduce only two Mn (Messinger and Renger, 1990, Messinger, et al, 1991b, Messinger, et al, 1991a, Dolan, et al, 1990, Dismukes, 1986, Kuwabara and Murata, 1982, Sivaraja and Dismukes, 1988, Mei and Yocum, 1992, Yocum, et al, 1981), these being accessible to chelation by EDTA (Mei and Yocum, 1991a, Mei and Yocum, 1992, Takahashi and Asada, 1986). The reduction and release of these outer Mn leads to loss of O_2 evolution (Yocum, et al, 1981, Kuwabara and Murata, 1982, Dismukes, 1986, Sivaraja and Dismukes, 1988, Rickert, et al, 1991) and may lead to unfolding of the lumenal surface of the D1 polypeptide (Isogai, et al, 1988). Generation of the S_0 state by NH_2OH reduction, reduces only one Mn ion to Mn II (Messinger, et al, 1991a, Guiles, et al, 1990a). This results in a one turnover delay in the O_2 release flash pattern (Messinger, et al, 1991a). Treatment of PS II with azide (NH_2NH_2) leads to a net two electron reduction of the OEC (Messinger and Renger, 1990, Messinger, et al, 1991b). With the Mn OEC in the S_1 state, this reduction leads to the S_{-1} state (Messinger and Renger, 1990, Messinger, et al, 1991a), with both outer Mn effectively reduced to Mn II. If the protein is not subjected to denaturation conditions, these Mn may be reactivated by two turnover events, leading back to the S_1 state (Messinger and Renger, 1990, Messinger, et al, 1991a, Messinger, et al, 1991b). Such reactivation leads to the delay of the O_2 release flash pattern by two turnover events.

Treatment of PS II with hydroquinone leads to reduction of two Mn ions in an environment inaccessible to chelators at the lumenal surface (Mei and Yocum, 1992, Riggs, et al, 1992). These Mn ions reduced by HQ would be the inner Mn which, when reduced, remain close to the functional binding within the Y_Z pocket. HQ is too large to be accessible to the outer Mn site (Mei and Yocum, 1992, Riggs, et al, 1992, Beck, et al, 1986). The reduction pathway for the inner Mn must be significantly different to the direct reduction of the outer Mn, and may be via a direct pathway close to Y_Z inaccessible to the outer Mn dimer.

The effects of NH_3 on the OEC observed via ESR, preferential generation of ground state $g=4.1$ signal with illumination at 200K (Beck and Brudvig, 1986, Beck and Brudvig,

1988a, Boussac, et al, 1990c, Britt, et al, 1989, Andreasson, et al., 1988), alteration of the multiline signal generated by illumination and/or rapid annealing at 275K (Beck and Brudvig, 1986, Beck, et al, 1986, Beck and Brudvig, 1988a, Boussac, et al, 1990c, Britt, et al, 1989, Andreasson, et al., 1988), may be due to NH₃ binding at two distinct sites (Sandusky and Yocum, 1984, Sandusky and Yocum, 1986). One site may modify the binding of Cl⁻, allosterically modifying the activation temperature for formation of the multiline state, with the g=4.1 signal preferentially formed with Y_Z oxidation at 200K (Beck, et al, 1986, Beck and Brudvig, 1988a, Andreasson, et al., 1988). ESEEM studies on NH₃ treated PS II have shown binding of one NH₃ directly to the ligand sphere of the OEC (Britt, et al, 1989). This binding is most likely to be at the substrate binding site, on the Asp 342 Mn III. The binding of NH₃ has been suggested to exchange a μ -oxo ligand leading to a bridging amide nitrogen (Beck, et al, 1986, Beck and Brudvig, 1988a, Britt, et al, 1989). Studies on the energetics of ligand exchange in model metal dimer compounds have indicated that the exchange of a bridging ligand required energy sufficient to break the bridging bonds (Tan, et al., 1991, Proserpio, et al, 1992, Gamelin, et al., 1994). The exchange of a terminal ligand was observed to require less energy, and was achievable for the application of stronger Lewis base type ligands (Beck and Brudvig, 1986, Sandusky and Yocum, 1986). These studies imply that the exchange of the ligand may possibly be at a terminal site under the NH₃ treatment regime used. Recent studies have shown that, in the lower S states, the substrate H₂O ligand is highly labile and exchanges on a rapid kinetic scale (Messinger, et al., 1995). Such rapid exchange through all lower S states (Messinger, et al., 1995) implies that bonding of substrates may not be via bridging ligand exchange, but at a terminal ligand site. The addition of NH₃, being a stronger Lewis base than H₂O, may result in exchange at the substrate binding site, a terminal site, in the dark S₁ state. Illumination generating turnover to the S₂ state may result in the deprotonation of this substrate ligand site, leading to either Mn-OH formation or Mn-NH₂ formation. ESEEM studies on NH₃ treated PS II have implicate nitrogen ligation to Mn, although the apparent electron orbital environment of the nitrogen bound was implied to be significantly non spherical, leading to a strong quadrupolar coupling interaction required within the ESEEM simulation (Britt, et al, 1989). The proposed deprotonation at the substrate ligand binding site in the S₁ to S₂ transition may lead to a double bond nature of the substrate-Mn bond. The kinetics of H₂O turnover through the S states requires that such a Mn=O bond be sufficiently labile to allow H₂O exchange on the ~1 second time scale. The deprotonation of the NH₃ treated PS II may result in a stronger Mn=N bond, with the amide species forming an sp² orbital environment. =NH₂ is planar, the electron orbital shell about the amide nitrogen would be significantly non spherical, although may remain axially symmetric. This non spherical

symmetry would result in a strong quadrupole interaction at the amide nitrogen. Such a ligand arrangement for the exchange of NH₃ for H₂O at this substrate binding site would appear to be consistent with the observations from the nitrogen ESEEM experiments (Britt, et al, 1989). The ligand exchange would also be expected to alter the properties of the Asp Mn III ion to which the NH₃ has bound. The hyperfine pattern of the S₂ state multiline is dominated by the interactions of the Mn III ion (Åhrling and Pace, 1995). The binding of NH₃ to this ion would lead to alteration of the hyperfine constant for the Mn, increase the apparent electron shell anisotropy (Beck and Brudvig, 1986, Beck, et al, 1986, Beck and Brudvig, 1988a, Beck and Brudvig, 1988b) and probably alter the Mn nuclear quadrupole interaction. All of these factors would lead to an alteration of the multiline pattern and spacing.

5.4.3. Mn Depletion, Reactivation and Photoactivation

Many studies have reported the ability to partially remove Mn from the OEC. Mild treatment with reductant amines (Beck and Brudvig, 1986, Beck, et al, 1986, Cheniae and Martin, 1970, Kretschmann and Witt, 1993, Mei and Yocum, 1991a, Mei and Yocum, 1992, Riggs, et al, 1992, Sivaraja and Dismukes, 1988, Takahashi and Asada, 1986, Yocum, et al, 1981), removal of the extrinsic polypeptides without satisfying the concomitant increased requirement for Cl⁻ and Ca²⁺ (Boussac, et al, 1989, Coleman and Govindjee., 1987, Homann, 1988a, Isogai, et al, 1988, Kavelaki and Ghanotakis, 1991, Mavankal, et al, 1986, Mavankal and McCain, 1991, Miller, et al, 1987, Sauer, et al, 1988) and Cl⁻ and Ca²⁺ depletion (Homann, 1988a, Mavankal, et al, 1986, Mavankal and McCain, 1991) have been observed to lead to the loss of two to three Mn per PS II. These Mn lost under such conditions have been suggested to be bound at a lumenally accessible site (Isogai, et al, 1988, Mavankal, et al, 1986, Mavankal and McCain, 1991, Mei and Yocum, 1991a, Mei and Yocum, 1992, Riggs, et al, 1992). The other two Mn ions within PSII are reported to be reducible by HQ, but not lost under conditions where the luminal region of the D1D2 reaction core remains essentially intact (Mei and Yocum, 1991a, Mei and Yocum, 1992, Riggs, et al, 1992). Treatment with Tris hydroxy amino methane (TRIS) is reported to be able to reduce and remove two, three, and all four Mn from the protein, dependent on the severity of treatment (Cheniae and Martin, 1970, Rickert, et al, 1991, Shen, et al, 1988, Yocum, et al, 1981). Mild TRIS treatment was observed to differ from the Mn reduction treatment with NH₂OH such that an additional Mn ion was removed with TRIS (Rickert, et al, 1991, Yocum, et al, 1981). These Mn depletion studies indicate a regionality of the Mn binding, as discussed above, consistent with one binding site near the C terminus, close to the lumen, and one near Y_Z, sequestered within the protein framework of the D1 polypeptide.

Complete Mn removal and reactivation studies have shed light on the properties of the protein. Klimov and coworkers have reported that upon removal of all four Mn by TRIS treatment, the metal binding sites may be restored, with restoration of P680⁺ reduction (Allakhverdiyev, et al., 1986) and electron transfer through the donor side (Klimov, et al, 1982, Kulikov, et al, 1983), following the stoichiometric rebinding of four Mn per PS II (Allakhverdiyev, et al., 1983). These experiments indicated two binding sites, at one of which Mn could be replaced by Mg²⁺ or other divalent metal ions (Klimov, et al, 1982, Allakhverdiyev, et al., 1983; Allakhverdiyev, et al., 1986, Kulikov, et al, 1983). At this exchangeable site, the Mn was proposed to play a more structural role, facilitating the turnover of electron transfer (Klimov, et al, 1982, Allakhverdiyev, et al., 1983; Allakhverdiyev, et al., 1986, Kulikov, et al, 1983). This structural Mn site is most likely the inner site, as the redox properties of Y_Z are observed to be altered upon Mn removal (Babcock and Sauer, 1975b, Barry, et al, 1990, Boska, et al., 1983, Britt, et al., 1995, Diner, et al., 1995, Evelo, et al., 1989, Hoganson and Babcock, 1989, Mino and Kawamori, 1994). ESEEM, IR and ENDOR studies on Y_Z⁺ formed in Mn depleted PS II indicate an increased flexibility of the Y_Z site (MacDonald, et al, 1993, Mino and Kawamori, 1994), with the methylene carbon having more rotational freedom resulting in an increased rotational motion of the phenoxyl oxygen (MacDonald, et al, 1993, Mino and Kawamori, 1994). The Mn at this site may play a significant role by "tethering" the Y_Z into an optimal orientation for electron transfer (Barry, et al, 1990, Warncke, et al, 1994), the strong charge density of this region influencing the charge delocalised porphyrin planes of the P680 reaction centre chlorophylls, guiding electron donation from Y_Z to the reaction centre in preference to electron donation from Y_D (Gilchrist, et al., 1995, Mino and Kawamori, 1994).

Frasche and coworkers have reported that under mild reduction conditions, two Mn ions are removed from PS II (Dolan, et al, 1990). Under these conditions, an altered form of g=4.1 signal was observable, the line shape alteration presumably caused by structural changes in the protein caused by the loss of the two Mn ions (Dolan, et al, 1990). The Mn lost are most probably from the outer site, with the g=4.1 formed similar to the ground state form arising from the Y_Z - Mn centre deeper within the protein.

A recent study by Lubitz and coworkers reported that upon complete removal of Mn from PS II, electron transfer activity through the donor side was lost. Upon repletion of two Mn per centre, the ability to generate an altered multiline signal was restored (Fiege, et al., 1995). This treatment seems to be consistent with the experiments by Klimov et al, with the inner site Mn replaced by an alternate divalent metal, possibly Mg²⁺ (Klimov, et al, 1982, Kulikov, et al, 1983, Allakhverdiyev, et al., 1983) (although no detail on divalent metal

content was quoted), with the multiline signal generated at the outer binding site. Further work in this area would be needed to define the situation more closely however.

5.4.4. EXAFS Studies, Mn and Ca.

The structures proposed here are strongly supported by the X-ray absorbance spectroscopy data. The data reported across a number of groups have indicated the dominant structural motif for Mn as μ -oxo bridged dimers, with mainly oxygen type terminal ligands (Yachandra, et al, 1993, MacLachlan, et al, 1992, Kusunoki, et al, 1989, George, et al, 1989, Penner-Hahn, et al., 1990). The two binding structures proposed follow this pattern.

The feature which has caused most discussion over whether the dimeric Mn structures are linked has been the data supporting a Mn-metal distance at 3.3Å to 3.6Å, first reported by Klein and coworkers, and confirmed by all later experiments (Yachandra, et al, 1987, Yachandra, et al, 1993, MacLachlan, et al, 1992, Kusunoki, et al, 1989, George, et al, 1989, Penner-Hahn, et al., 1990). This Mn-metal separation has been modelled to arise from either a Mn-Mn separation, indicating a solely tetrameric Mn structure (Mukerji, et al, 1994, George, et al, 1989, Yachandra, et al, 1987), a Mn-Ca separation (MacLachlan, et al, 1992, MacLachlan, et al, 1994a, Evans, et al, 1994), of which only minor consideration has been made, or a combination of 1 Mn-Mn separation and 1 Mn-Ca separation, indicating an altered open butterfly structure (Yachandra, et al, 1993, Klein, et al, 1993, Liang, et al, 1994, DeRose, et al, 1994, Kusunoki, et al, 1989). The data for the Mn-Mn separation at the 3.3Å distance does not support cubane nor similar butterfly structures, based on the effective nearest Mn neighbour number being only ~0.5 to 1.0 for each Mn ion (Dismukes, 1988, McDermott et al, 1988, Mukerji, et al, 1994, Penner-Hahn, et al., 1990, Sauer, et al, 1988). The effect of replacement of Sr for Ca in PS II has been observed to enhance the ~3.3Å peak intensity (Yachandra, et al, 1993, Klein, et al, 1993), while Ca depletion significantly reduced the peak intensity (Yachandra, et al, 1993, MacLachlan, et al, 1994a). The information content of the longer distance peaks is insufficient to make absolute determination of the Mn-neighbour interactions, with the distance of 3.3Å possibly including contributions from the amino acid ligand atoms such as C or O atoms, in addition to the Mn-metal contributions (Kusunoki, et al, 1989, MacLachlan pers comm). The data for the Ca depletion (Yachandra, et al, 1993, MacLachlan, et al, 1994a) and Sr replacement experiments (Yachandra, et al, 1993) appears to indicate a stronger probability of Mn-Ca being the source for most of the 3.3Å peak. The requirement for magnetic isolation of the dimers, from the S₁ parallel mode experiments (Dexheimer, et al, 1990, Dexheimer and Klein, 1992) and this work, makes the probability of the 3.3Å distance being due to a Mn-Mn separation low. The binding locus proposed for the outer site places a Ca²⁺ ion between Glu 333 and His 337, stabilising both amino acids and the

ligand deficiency of the Asp 342 Mn ion, its "z axis" position blocked by His 337. This proposed binding scheme places the Ca^{2+} within $\sim 4\text{\AA}$ of each of the two Mn ions in this structure and is supported by IR spectroscopic evidence that Mn and Ca are bridged by a carboxylate group (Noguchi, et al., 1995). The binding geometry around the inner dimer is less clear due to the number of intervening amino acids. However, the possibility of Ca^{2+} binding close to this region is supported by mutational studies on residues implicated to be either close to or within this Mn binding region (Chu, et al., 1995a, Styring, et al, 1993, Nixon and Diner, 1992), possibly involving D1 Asp 89, Asp 61, Glu 65 and other residues (Chu, et al., 1995a).

Further data supporting the assignment for the 3.3\AA EXAFS peak as a Mn-Ca peak comes from reduction and turnover studies, in which Ca is observed to limit substrate accessibility to the catalytic site (Mei and Yocum, 1991b, Mei and Yocum, 1992, Riggs, et al, 1992). As the substrate binding site is on the Asp 342 Mn, the Ca may be situated close to this Mn ion. The Ca^{2+} ion(s) sited here is highly likely to play a structural role for the association of the extrinsic polypeptides to the D1D2 core complex.

5.4.5. Inhibited PS II S_2 and Altered S_3 States.

The experiments on inhibited PS II have been performed over only a limited range of inhibitory regimes. The purpose for this has been to examine inhibited PS II samples in which the protein conformation has not been seriously nor deliberately altered. For example, no low pH treatments for the purpose of depletion of essentially all Ca from the protein (Ono and Inoue, 1988) were undertaken.

In terms of the range of inhibition and reports of previous ESR results, as well as the data for functional PS II presented here, the results for the S_2 state and S_3 state generated in inhibited and functional PS II may be grouped into only a few classes. One group involves the depletion of Cl^- from its activation site. Cl^- affects the S_1 to S_2 and the S_3 to S_0 transitions (Damoder, et al, 1986, Sinclair, 1984, Homann, 1988b, Sandusky and Yocum, 1986) with Cl^- depleted PS II able to donate two oxidative equivalents to P680^+ (Theg, et al, 1984, Itoh, et al., 1984, Homann, 1988b, Baumgarten, 1990). From the results for the F^- exchanged PS II, the only form of the S_2 state generable under these Cl^- depleted conditions is the $g=4.1$ signal state (Ono, et al, 1986, Ono, et al, 1987, Baumgarten, 1990, this work). This is an essentially equivalent spin state to the ground state $g=4.1$ S_2 state formed by the illumination of ethylene glycol cryoprotected PS II at 130K (Casey and Sauer, 1984, Haddy, et al, 1992, Kim, et al, 1992, this work). This appears to be the only ESR visible form of the S_2 state generable in these F^- PS II samples. Illumination of these samples at 275K in the presence of DCMU to allow only a single turnover, continues to generate only $g=4.1$ signal. No multiline signal

generation is apparent. This is in contrast to earlier work by Damoder and co-workers, in which saturating pulse flash illumination at 300K followed by rapid quench cooling enabled the formation of multiline (Damoder, et al, 1986), although the level of Cl^- depletion was questioned, with Baumgarten and co-workers unable to generate S_2 state multiline signal in rigorously Cl^- depleted PS II samples (Baumgarten, 1990). This suggests that the role of Cl^- in electron transfer for the S_1 to S_2 state transition is to facilitate the electron withdrawal from the Mn OEC, ie the outer Mn pair.

In samples in which the functional activity of Cl^- is reduced but where Cl^- is not depleted, both multiline and $g=4.1$ signals are formed by illumination at 200K. This is apparent for Ca-acetate and Na-acetate treatments (this work), and for NH_3 treatment (Dau, et al., 1995, Ono, et al, 1987, Boussac, et al, 1990c, Andreasson, et al., 1988, Andreasson and Lindberg, 1992, Beck and Brudvig, 1986, Beck, et al, 1986, Beck and Brudvig, 1988a, Beck and Brudvig, 1988b) and for Cl^- sufficient F^- treated PS II (deRose, et al., 1995). In these samples, binding of Cl^- appears to be restricted, the level of inhibition dependent on the residual concentration of Cl^- and that of the counteracting or competing species (acetate, NH_3 , F^-). Illumination of acetate and NH_3 treated PS II samples at 275K in the presence of DCMU allows the population of the multiline S_2 state (Beck and Brudvig, 1986, Beck, et al, 1986, Beck and Brudvig, 1988a, Beck and Brudvig, 1988b, Britt, et al, 1989). The effect of NH_3 is apparent at two sites in the protein for the S_1 to S_2 transition (Andreasson, et al., 1988, Beck and Brudvig, 1988a, Beck and Brudvig, 1988b). The first is restriction of electron transfer out of the multiline centre for illumination temperatures of ~ 200 K, leading to $g=4.1$ formation (Andreasson, et al., 1988, Beck and Brudvig, 1988a, Beck and Brudvig, 1988b). This appears to arise from an allosteric effect at some Cl^- binding site near to but not within the Mn OEC cluster environment (Andreasson, et al., 1988, Beck and Brudvig, 1988a, Beck and Brudvig, 1988b, Boussac, et al, 1990c). NH_3 is also capable of substrate ligand exchange with water in the S_1 state, leading to an alteration of the hyperfine pattern upon generation of multiline at 275K (Beck and Brudvig, 1986, Beck, et al, 1986, Beck and Brudvig, 1988a, Beck and Brudvig, 1988b, Britt, et al, 1989). Whether acetate may undertake substrate ligand exchange is not at present known. However, it is likely the accessibility of substrates to the Mn OEC site is restricted to small molecules only (Beck and Brudvig, 1986, Beck, et al, 1986, Beck and Brudvig, 1988a, Beck and Brudvig, 1988b). The multiline generated in acetate treated PS II by 275K illumination appears very similar to the control PS II sample multiline generated at 200K. Whether acetate binding as a unidentate terminal ligand to the Asp342 Mn, the probable substrate binding site, would affect the hyperfine and superhyperfine detail of the multiline is uncertain. Whether acetate binds as a bidentate ligand is also uncertain. However, acetate

binding as a bidentate ligand would be observed to alter the symmetry of the electron orbitals about the Asp 342 Mn, which would be predicted to alter the quadrupole and hyperfine interactions at this Mn significantly. This Mn, as Mn III in the S₂ state, would become 6 coordinate with bidentate acetate binding, leading to orthorhombic distorted octahedral symmetry, compared to the inferred axial 5 coordinate symmetry in the functional state (Dismukes, et al, 1994, Åhrling and Pace, 1995).

As to whether F⁻ undertakes ligand exchange is uncertain at present, although experiments using reduced Cl⁻ concentrations (≤5mM) and increased F⁻ concentrations, as NaF or a combination of NaF and CaF₂ (CaF₂ is solubility limited, Aylward and Findlay, 1974b) to generate a system capable of g=4.1 formation at 200K and multiline (possibly altered) at 275K would be instructive, especially as the small ionic radius of F⁻ may provide the capability of binding at two ligand positions on the Asp 342 Mn. These experiments are left for future work. Insufficient hyperfine detail was provided for the low strength Cl⁻ depletion F⁻ exchange samples, capable of multiline formation at 300K (Damoder, et al, 1986), to provide such clarification. Klein and co-workers observed the interchange between the multiline and g=4.1 forms of the S₂ state on samples washed in Cl⁻ free buffer (deRose, et al., 1995). Multiline signal was generable with illumination at 200K, the level of which declined (with increasing g=4.1 signal generation), with higher NaF concentration (deRose, et al., 1995). Again, insufficient detail on the hyperfine and superhyperfine was presented to allow inferences on the status of F⁻ as an exchangeable ligand at the substrate binding site.

The results for the altered S₃ state signals may be interpreted in terms of the S₂ state signals generated under the above inhibitory treatments.

5.4.5.1. S₃ State

The results presented here for the S₃^{*} state signals generated under inhibitory regimes of Cl⁻ depletion / F⁻ exchange, 600mM Na-acetate and 300mM Ca-acetate (in the presence of Cl⁻) and 1M NaCl treatments, may be correlated to the ESR signals generated in the S₂ state.

The development of the S₃^{*} state in the presence of Cl⁻, ie using 600mM acetate (with either Ca or Na as counter ion) and with 1M NaCl, results in a broad form of the S₃^{*} signal, width ~24 mT in the presence of acetate, ~15mT in the presence of 1M NaCl. This is consistent with previous reports for S₃^{*} state ESR signals under similar conditions of inhibition in the presence of Cl⁻, ie with acetate addition or Ca depleted samples (MacLachlan and Nugent, 1993, Tso, et al, 1991a, van Vliet, et al., 1994, Hallahan, et al., 1992, Zimmermann, et al., 1993). Each of these studies reported that such inhibitory treatments led

to the development of an S_3^* state characterised by broad split signals at $g \sim 2.0$, with p-p widths in the range 17mT to 24mT (Szalai and Brudvig, 1996, Boussac, et al, 1989, Boussac, et al, 1990a, Boussac, et al, 1992b, Boussac, et al, 1992a, Boussac and Rutherford, 1994b, MacLachlan and Nugent, 1993, MacLachlan, et al, 1994a) and evident Mn derived structure in the wings in the acetate inhibited PS II spectra (MacLachlan and Nugent, 1993, MacLachlan, et al, 1994a).

The properties of the S_2 and S_3^* states for Cl^- depleted (and F^- exchanged) PS II are somewhat in contrast to the Cl^- "sufficient" data. In the S_2 state, only $g=4.1$ signals are generated with illumination at 200K and at 275K in the presence of DCMU (Baumgarten, 1990, van Vliet, et al., 1994, Van Vliet and Rutherford, 1996, Boussac and Rutherford, 1994a, Ono, et al, 1986, Ono, et al, 1987, this work). The S_3^* state for rigorously Cl^- depleted PS II is characterised by a signal centred near $g \sim 2.0$, with p-p width of 9mT to 11mT (Boussac, et al, 1992a, Boussac and Rutherford, 1994a, Boussac and Rutherford, 1994b, van Vliet, et al., 1994, Van Vliet and Rutherford, 1996, this work), although Baumgarten and co-workers observed a p-p width of 16mT in rigorously Cl^- depleted PS II illuminated at 275K (Baumgarten, 1990). This signal has been proposed to be equivalent in nature to the broader S_3^* state split signal observed for the inhibited (Cl^- sufficient) PS II samples (Boussac and Rutherford, 1988c, Boussac, et al, 1989, Boussac, et al, 1992b, Boussac, et al, 1992a, Boussac and Rutherford, 1994a, Boussac and Rutherford, 1994b, MacLachlan and Nugent, 1993, Nugent, et al, 1993, Hallahan, et al., 1992, Gilchrist, et al, 1992).

The model for the S_3^* state split signal is for a spin-spin interaction between the Mn complex in an $S=1/2$ state, implied to be the multiline state, and an oxidised organic radical centre (Hallahan, et al., 1992, Boussac, et al, 1989, Boussac, et al, 1992b, Boussac, et al, 1992a). This organic radical has been implicated by IR and UV spectroscopy to be a Histidine residue (Boussac, et al, 1990b, Boussac, et al, 1990a, Boussac, et al, 1992b), although Y_Z has also been proposed from room temperature ESR and turnover kinetics which suggest a functional loss of $P680^+$ reduction by Y_Z (Hallahan, et al., 1992). By measurement of the splitting of the S_3^* state signals, with the strength of the interaction dependent on $1/r^3$ (Britt, et al., 1995, Tso, et al, 1991a), the distance between the Mn centre and the radical (r) has been reported to be between $\sim 4\text{\AA}$ and 7.5\AA (Tso, et al, 1991a, Zimmermann, et al., 1993, Boussac, et al, 1990b). Dependent on the protocol for inhibition, the blockage of electron flow at Y_Z has been reported to occur at either the second electron turnover (during S_2 to S_3^*) (Hallahan, et al., 1992, MacLachlan and Nugent, 1993, Baumgarten, 1990), forming the split signal, or the third electron turnover (after formation of S_3^*) (Boussac, et al, 1989, Boussac, et al, 1990c,

Boussac, et al, 1992a, Boussac and Rutherford, 1994b, Boussac and Rutherford, 1995, Tso, et al, 1991a, Ono and Inoue, 1985), with the split signal formed on the second turnover.

Two other inhibitory procedures have been shown to lead to the development of the S_3^* state, displaying an associated $g\sim 2$ split signal, developed by continuous illumination at 275K with illumination continued while freezing to $\sim 77K$. These are treatment with 100mM NH_4Cl at pH7.5 (Andreasson and Lindberg, 1992, Hallahan, et al., 1992, MacLachlan and Nugent, 1993) and the depletion of Ca^{2+} followed by exchange of Sr^{2+} (Boussac and Rutherford, 1988b, Boussac and Rutherford, 1994b). Where these fit into the argument being developed here remains as yet to be fully clarified.

In the above paragraphs the assertion has been that the line width of the S_3 state split signals follow a pattern indicative of the S_2 state signals generable at 275K in the presence of DCMU. For Ca^{2+} depleted or acetate treated PS II, illumination at 275K develops a multiline signal. The linewidth of the S_3^* state split signal is between $\sim 15mT$ (for the Ca depleted PS II) (Boussac, et al, 1989, Boussac, et al, 1990b, Boussac, et al, 1990a, Hallahan, et al., 1992, this work) and $\sim 24mT$ for the acetate treated PS II (MacLachlan and Nugent, 1993, this work). In Cl depleted PS II, illumination at either 200K or 275K in the presence of DCMU leads to generation of the $g=4.1$ S_2 state (Ono, et al, 1986, Ono, et al, 1987, Baumgarten, 1990, this work). The S_3^* state generated by illumination at 275K followed by cooling under illumination to $\approx 100K$ is characterised by a narrow form of the $g\sim 2$ split signal, with p-p width $\sim 9mT$ to $11mT$ (Boussac, et al, 1992a, Boussac and Rutherford, 1994a, Boussac and Rutherford, 1994b, van Vliet, et al., 1994, Van Vliet and Rutherford, 1996, this work).

The data for Sr^{2+} inhibited (Ca^{2+} depleted PS II) appears contrary to the data for the direct Ca^{2+} depleted PS II. The S_2 and S_3^* states generated in the Ca^{2+} depleted PS II are of the multiline S_2 and broad (p-p $\sim 15mT$) signal forms, respectively. The S_3^* state $g\sim 2$ split signal is formed after two photo-oxidation events (Boussac and Rutherford, 1988c, Boussac, et al, 1989).

The addition of Sr^{2+} to Ca^{2+} depleted PS II has been observed to re-establish up to 40% of oxygen evolution activity (Boussac and Rutherford, 1988b). However, the illumination of Sr^{2+} "enhanced" Ca^{2+} depleted PS II leads to the formation of the $g=4.1$ S_2 state, very different to the multiline S_2 state formed in Ca^{2+} depleted PS II. The S_3^* state formed by illumination at 275K is characterised by a narrow (p-p $\sim 10mT$) $g\sim 2$ split signal (Boussac and Rutherford, 1988c, Boussac and Rutherford, 1994b). Although the S_2 and S_3^* forms generated in the Sr^{2+} inhibited- Ca^{2+} depleted PS II are significantly different to the Ca^{2+}

depleted PS II (Boussac and Rutherford, 1994b), the pattern of the lineshape form in the S_3^* state from oxidation of the effective $g=4.1$ form of the S_2 state is consistent with the above argument and model, ie samples which may generate only the $g=4.1$ signal for of the S_2 state are characterised by the narrow form of the S_3^* state, p-p ~ 10 mT signal width. The characterisation of the inhibition of the Sr^{2+} inhibited Ca^{2+} depleted PS II is left for future work, but the data of Boussac and co-workers (Boussac and Rutherford, 1994b) is consistent with the hypothesis developed.

The data for the PS II treated with 100mM NH_4Cl at pH7.5 appears ambiguous in light of the current hypothesis. The S_2 state generable in NH_4Cl treated PS II is characterised by an altered multiline signal, ~ 26 hyperfine lines of average spacing ~ 6.7 mT (Beck and Brudvig, 1986, Beck, et al, 1986, Beck and Brudvig, 1988a, Beck and Brudvig, 1988b, Britt, et al, 1989). This signal has been well characterised and is modelled as an altered form of the functional S_2 state multiline signal in which either a bridging μ -oxo or the terminal water ligand is exchanged for an imido or amide ligand due to the higher Lewis basicity of the NH_3 species over the H_2O species (Beck, et al, 1986, Beck and Brudvig, 1988b, Forster and Junge, 1988). The formation of the S_3^* state in 100mM NH_4Cl treated PS II is characterised by a narrow $g\sim 2$ split signal, p-p ~ 10 mT (Andreasson and Lindberg, 1992, Hallahan, et al., 1992, MacLachlan and Nugent, 1993), similar in form to that observed for Cl^- depleted PS II. As the S_2 state in NH_4Cl treated PS II illuminated at 275K in the presence of DCMU is characterised by an altered form of the multiline signal, the generation of a narrow form of the S_3^* state signal is in disagreement with the model proposed. The S_3 state signal arising in NH_4Cl treated PS II has been generated by continuous illumination of 100mM NH_4Cl treated "functional" and Ca^{2+} depleted PS II, or by flash illumination of 100mM NH_4Cl treated Ca^{2+} depleted PS II, with effectively equivalent S_3^* state signals formed (Andreasson and Lindberg, 1992, Hallahan, et al., 1992, MacLachlan and Nugent, 1993). To determine the nature of the NH_3 inhibition and formation of S_2 and S_3^* states, examination of the precise conditions of formation is warranted. In 100mM NH_4 treated "functional PS II" Boussac and coworkers could not appear to generate significant inhibition of the OEC cycling (Boussac, et al, 1990c). In flash experiments, the OEC appeared to cycle normally, generating the altered multiline S_2 state with a flash period of 4. Under continuous illumination, little inhibition was observed for lower illumination levels (Boussac, et al, 1990c). The arguments proposed were based on the rapid exchange of NH_3 as a substrate analogue ligand to the OEC prevented dysfunctioning of the OEC cycling (Boussac, et al, 1990c). This was supported by both continuous illumination

and flash illumination of NH_4Cl treated Ca^{2+} -sufficient PS II in which the altered multiline S_2 state could be generated was observed by 200K illumination (no spectra for the $g\sim 4$ region were presented) (Andreasson and Lindberg, 1992). No S_3^* state signals were generated by either continuous or flash illumination (Andreasson and Lindberg, 1992).

However, the addition of 100mM NH_4Cl to Ca depleted PS II, with illumination at 275K, generated a narrow form of the S_3^* state signal (Andreasson and Lindberg, 1992). Flash illumination of these inhibited PS II samples indicated a very different turnover pattern to the Ca sufficient NH_4Cl treated PS II. A single saturating flash did NOT generate the multiline signal in the NH_4Cl treated Ca depleted samples (Andreasson and Lindberg, 1992). No mention of signal generation in the $g\sim 4$ region was made. Upon the second flash, the NARROW form of the S_3^* state signal was generated (Andreasson and Lindberg, 1992). Figure 4.46b indicates the generation of S_3^* state signals in 1M NaCl treated PS II, incubated for ~ 20 hours on ice. Illumination at 275K in the presence of DCMU failed to generate either the multiline or the $g=4.1$ signals, while illumination at 275K without DCMU generated a broad (p-p 15mT) S_3^* $g\sim 2$ split signal. The formation of the narrow form of the S_3^* state signal from an S_2 state in which the multiline signal does not form must be due to a cooperative effect of Ca depletion and NH_4Cl treatment. The nature of the cooperative inhibition is left for future work, but may involve multiple NH_3 binding to the OEC Mn dimer. The nature of the signal formation is, however, consistent with the model presented here.

In NH_4Cl treated PS II preilluminated at 250K and subsequently dark annealed, trapping the binding of the amide to the Mn centre (Hallahan, et al., 1992, MacLachlan and Nugent, 1993), illuminating at 275K to generate the S_3^* state, gives either a narrow form of the $g\sim 2$ split signal, p-p width $\sim 10\text{mT}$ (MacLachlan and Nugent, 1993), or a broader form (p-p width not stated, but is of the order of 20mT) (Hallahan, et al., 1992). The result of Hallahan and coworkers is consistent with the (not presented but quoted) S_2 state data, in which an altered multiline is generated. The altered S_2 multiline state is accompanied by a broad signal form of the S_3^* state. The report of MacLachlan and coworkers does not present sufficient data to determine the forms of the S_2 and S_3^* states. The signal presented for the S_3^* state was of a narrow form (p-p not stated, but less than 15mT) (MacLachlan and Nugent, 1993). No indication of the S_2 state was mentioned. This data requires further clarification before any comparison to the model can be made. Without a clarification of the S_2 state and S_3^* state signal forms, the result appears only as an observation, without conclusions being able to be

drawn. It is of note that treatment of the NH_4Cl inhibited PS II with Ca^{2+} prevents the formation of the S_3^* state signals (Nugent, et al, 1993).

Generally, the data of Boussac and coworkers (Boussac, et al, 1990c), Andréasson and coworkers (Andréasson and Lindberg, 1992) and Hallahan and coworkers (Hallahan, et al., 1992) on ammonia treated PS II in the S_2 and S_3^* states indicate a consistency with the pattern presented above.

This apparent correlation between the S_2 ESR signals and the line width form of the S_3^* state split signal has a natural rationalisation within the model proposed here. The centre giving rise to the ground state $g=4.1$ signal (illumination of EG PS II at 130K) appears to be the centre oxidised in Cl^- depleted PS II, with formation of only the $g=4.1$ signal possible in the S_2 state. This centre consists of a Mn dimer bridged by Y_Z (this work), probably liganded to Gln 165, Asp 170, Glu 189 and His 190. Upon advancement from the formal S_1 to S_2 state, Y_Z is oxidised and, coupled to the associated Mn dimer, forms the ground state $g=4.1$ signal. The withdrawal of a second electron from this system will result in the oxidation of an alternate redox site, implicated by IR and thermoluminescence spectroscopy to be a histidine residue (Baumgarten, 1990, Ono and Inoue, 1991, Boussac, et al, 1990b, Boussac, et al, 1992b, Boussac and Rutherford, 1994b). This will result in the interaction of a Mn containing structure and a histidyl radical, the components required to form the S_3^* state split signal (Boussac, et al, 1990b, Boussac, et al, 1992b, Boussac and Rutherford, 1994b). This presents a scheme which satisfies one sequence for formation of an S_3^* signal, in which Y_Z turnover is blocked at the second electron transfer event (Theg, et al, 1984, Hallahan, et al., 1992, Boussac and Rutherford, 1994a, Nugent, et al, 1993), with the involvement of Y_Z^+ in the formation of the S_3^* state signal. Based on a splitting of 9 to 11 mT. the separation of Y_Z^+ , on which the spin resulting from first electron withdrawal resides, and the organic radical would be of the order 5.5Å to 5.9Å (assuming dipolar interaction between two spin 1/2 species) (Tso, et al, 1991a).

The second set of data involves the observation of multiline signal in the S_2 state and a broader split signal in the S_3^* state. In Cl^- inhibited (not Cl^- depleted) samples, illumination at 200K generates a high proportion of $g=4.1$ signal (Beck and Brudvig, 1986, Beck, et al, 1986, Beck and Brudvig, 1988a, Beck and Brudvig, 1988b, deRose, et al., 1995, Ono, et al, 1986). Illumination at 275K in the presence of DCMU generates a high yield of multiline signal (Beck and Brudvig, 1986, Beck, et al, 1986, Beck and Brudvig, 1988a, Beck and Brudvig, 1988b, Andréasson, et al., 1988, Andréasson and Lindberg, 1992, Boussac and Rutherford, 1988c, Boussac, et al, 1989, Boussac, et al, 1990c, Gilchrist, et al, 1992, MacLachlan and

Nugent, 1993, MacLachlan, et al, 1994a, Ono and Inoue, 1990, Zimmermann, et al., 1993, this work). It is this difference which separates the two precursor forms of the S_3^* state split signals. Illumination of these multiline capable inhibited PS II samples at 275K, without DCMU, generates the broader form of the S_3^* state signal (Boussac, et al, 1989, Boussac, et al, 1990c, Boussac, et al, 1990a, Hallahan, et al., 1992, MacLachlan and Nugent, 1993, MacLachlan, et al, 1994a). Histidine is implicated within the ligand environment (Åhrling and Pace, 1995, Boussac, et al, 1990b, Britt, et al, 1994, Tso, et al, 1991a, Zimmermann, et al., 1993). The involvement of an oxidised Histidine ligated to the Mn centre, with the spin pair delocalised across each of the Mn dimer and Histidyl radical moieties, would result in a stronger spin-spin interaction than for the "g=4.1-histidyl centre", where the free spin resides more on Y_Z^+ than the Mn dimer. This smaller unpaired electron separation for the multiline centre S_3 state, should give rise to a broader splitting. From the splitting of this broader S_3^* state, observed in Cl^- inhibited systems to be $\sim 22mT$ to $24mT$ (Hallahan, et al., 1992, MacLachlan and Nugent, 1993), the multiline dimer to radical spin centre distance is estimated $\sim 4.2\text{\AA}$, based on similar considerations to those used for the "g=4.1 centre" S_3^* state. The S_3^* state split signal is observed in this multiline centre - histidyl radical system on the second flash (Boussac and Rutherford, 1988c, Boussac, et al, 1990b, Boussac, et al, 1990a, Boussac, et al, 1992b, Boussac, et al, 1992a, Boussac and Rutherford, 1994b, Tso, et al, 1991a). However, a minimally third turnover event would be required for Y_Z oxidation in this system. Y_Z^+ may not be observed upon formation of the S_3^* state, although continuous illumination at 275K should generate sufficient turnovers to form both the S_3^* state and oxidised Y_Z , allowing EPR observation of both species, and lead to the conclusion that Y_Z^+ turnover is blocked after the formation of the S_3^* state (Boussac, et al, 1990b, Boussac, et al, 1990a, Boussac, et al, 1992b, Boussac, et al, 1992a, Boussac and Rutherford, 1994b, Tso, et al, 1991a) rather than the conclusion that the S_3^* state arises from an $S^*_2-Y_Z^+$ interaction (Hallahan, et al., 1992, MacLachlan and Nugent, 1993).

The temperature dependence of the S_3^* state signals studied in this work indicate a second significant difference between the two proposed forms of this signal. Temperature dependences have been reported for Ca^{2+} depleted PS II S_3^* state split signals (both forms $\sim 16mT$ p-p width) (Boussac, et al, 1989, Tso, et al, 1991a). Each indicated the signals arose from ground state spin centres, with Curie behaviour observed between ~ 6 and $\sim 25K$ (Boussac, et al, 1989) and between ~ 4.2 and $\sim 13K$ (Tso, et al, 1991a).

From the data presented in chapter 4, the temperature dependence of the Cl^- / F^- inhibited S_3^* state split signal indicated Curie behaviour over the temperature range $\sim 5\text{K}$ to 50K . No indication of signal broadening was apparent, as might be expected for a spin-spin coupled system in which the effective exchange rate J/h was of the order of T_1^{-1} , see later. This system must correspond to a tightly coupled centre. The coupling of Y_Z^+ and D1^* His 190 has been proposed for this species (this work). Such a system would need to be strongly exchange coupled to provide an essentially Curie temperature dependence for the $S=1/2$ - $S=1/2$ (net spin 1) coupled centre. Based on the model for the Y_Z environment, inner Mn centre, the exchange coupling of the Mn would be required to be of higher relative magnitude in the S_3^* state, where an $S=1/2$ spin state interacts in the D1H190 , compared to the S_2 state, where the oxidation of this centre generates an $S=3/2$ ground state. The "second oxidation" within this environment may lead to an effective deprotonation of the Mn dimer, where the bridging ligands (apart from Y_Z) are likely to be μ -oxo, which may be proton bridged to residues nearby, contributing to structural integrity. The second oxidation in this environment will increase the effective local charge, which may lengthen any μ -oxo-proton bonds, leading to an increase of the exchange coupling magnitude for the Mn dimer. This would place the coupling of the Y_Z^+ -H190 across a Mn III or Mn IV ion (with a second Mn III or Mn IV ion nearby). The tethering of the tyrosyl ring, via the phenoxyl oxygen, may provide stability for the redox capabilities of Y_Z during functional turnover. The coupling of the Y_Z^+ to H190 in this altered S_3^* state may allow some insight into the recombination pathway, which is predicted, via mutational studies, to be achieved via another coupling of H190 and H195 (Roffey, et al., 1994, Kramer, et al., 1994) consistent with the AT thermoluminescence band (a recombination pathway signal) arising from histidines associated with the Mn binding regimes close to Y_Z and P680 (Kramer, et al., 1994, Ono and Inoue, 1990, Ono and Inoue, 1991, Ono and Inoue, 1992).

The temperature dependences of the broader forms of the S_3^* state, p-p $\sim 15\text{mT}$ for 1M NaCl treated (Ca^{2+} depleted) PS II and p-p $\sim 24\text{mT}$ for 0.6M acetate treated PS II, are significantly different to the smooth temperature dependence of the narrow form in the Cl^- depleted samples studied. As per the reported dependences (Tso, et al, 1991a, Boussac, et al, 1989) the signals display Curie behaviour at low temperatures, consistent with the signals arising from ground state centres (Tso, et al, 1991a, Boussac, et al, 1989). In this study, the TD behaviours have been studied to 50K , higher than that reported previously (Tso and coworkers to $\sim 13\text{K}$, Boussac and coworkers to $\sim 25\text{K}$). The unusual feature of the TD curves, figs 4.49 (NaCl) and 4.59 (Acetate), is that the curve dramatically decreases intensity at temperatures

above ~10K (for the NaCl treated sample) and ~25K (for the acetate treated samples). The possibility of spin state interchange to some diamagnetic first excited state was discussed earlier. Figure 5.06 shows the temperature dependence of the S_3^* state split signal generated in the NaCl treated samples. The dotted curve is calculated from the Boltzmann model for the multiline centre using spin states $S=1, S=2..$, expected for a coupled system consisting of the $S=1/2$ multiline centre and an $S=1/2$ His^+ radical, using equation 4.2, with $|J/k| = 6.5\text{K}$. The curve approximates the apparent intensity decrease of the ground state to ~20K, but does not match the overall dramatic loss of this $S=1$ signal.

A more plausible explanation for the rapidity of the change in behaviour of the two different sets of data for a change in T_1 , which will have itself a strong temperature dependence, to a rate which exceeds the effective exchange rate of the spin couple J/h . An estimate of the T_1 and exchange constant J may be made from the curves of the signal intensity decrease. The temperature dependence of the spin lattice relaxation time T_1 for an Orbach process, the proposed relaxation process for the multiline centre, of which intervals with another organic radical, possibly D1H332, to form the S_3^* signal, is of the form

$$T_1 \propto \exp\Delta/kT = C \exp\Delta/kT$$

where Δ is the activation energy for the relaxation process, T is temperature, k is Boltzmann constant. From previous data, Δ , the effective activation energy, is of the order $\sim 30\text{cm}^{-1}$ for the multiline signal in the presence of alcohol (Hansson, et al, 1987, Pace, et al., 1991, de Paula, et al, 1986c) to -36.5cm^{-1} (Larigon, 94). T_1 has been measured for the multiline signal (in the presence of alcohol) via pulse ESR and was of the order $2.48 \times 10^{-3}\Delta$ at 4K and $8.3 \times 10^{-7}\Delta$ at 10.4K. The above relationship may be re-expressed as

$$1/T_1 = 1.97 \text{ E}8 \exp \left[\frac{-52.523^\circ\text{K}}{T \text{ (in K)}} \right]$$

$$C = 1.97 \text{ E}8\text{s}^{-1}, -\Delta/k = -52.523^\circ\text{K}.$$

From the TD of the split signals, a value for the T_1 at the point where the curve falls to a value of $1/e$ of the Curie curve may be evaluated.

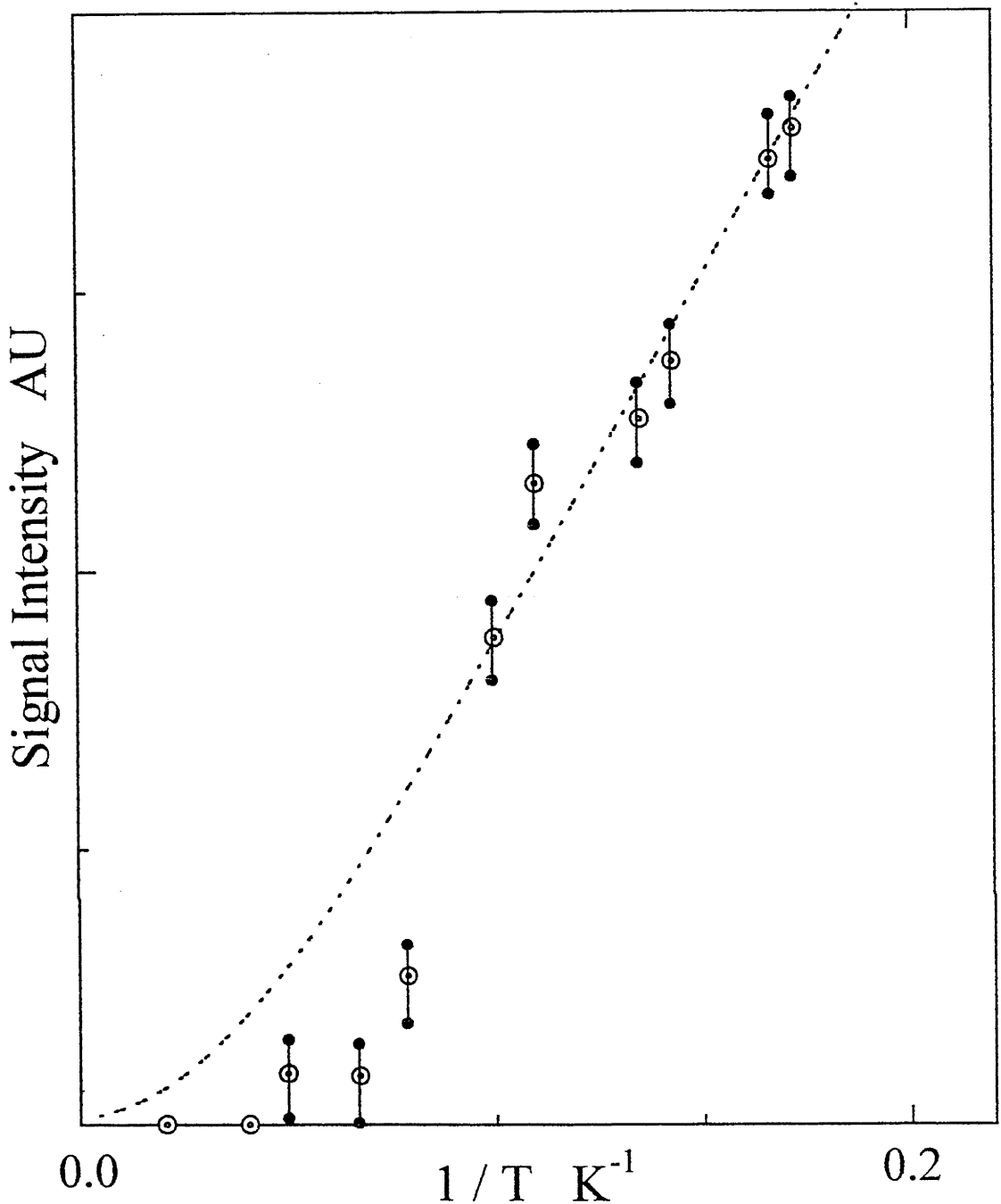


Figure 5.06. Temperature dependence data for the S_3^* state $g \sim 2$ split signal generated in PSII incubated with 1M NaCl, illuminated at 275K. Dotted line indicates the calculated intensity for an $S=1$ ground state according to the Boltzmann model for equation 4.1. The spin state is modeled from the spin-spin interaction of the multiline centre ($S=1/2, 3/2, \dots$) and an oxidised amino acid radical ($S=1/2$), most likely D1His 332. This model generates an $S=2$ excited state, which may be difficult to observe spectroscopically under the operating conditions used.

For the 1M NaCl treated (Ca depleted) PS II, the estimate of the "critical" temperature was $12.2 \pm 0.4\text{K}$, which gives a value of T_1 of $3.7 \pm 0.3 \times 10^{-7}\text{s}$. The TDs of these S_3^* state $g \sim 2$ split signals appear to reflect the proposed differences in the location of their centres. Both of the sets of TD data for samples modelled as arising from the S_2 state multiline centre, the outer site Mn dimer are characterised by a rapid decrease in signal amplitude probably due to changes in T_1 with temperature. In comparison, the TD for the S_3^* state generated in the Cl^- depleted / F^- inhibited samples was a reasonably smooth curve, indicative of strict Curie behaviour over the temperature range $\sim 5\text{K}$ to 50K . This is proposed to arise from the coupling of two spin $1/2$ essentially organic radicals, likely to be Y_Z^+ and D1H^*190 . The influence on the X-ray spectroscopic data arises from the oxidation of centres located close to the Mn pair. The Xanes data reflects an oxidation within the Mn environment for both the S_1 to S_2 and S_2 to S_3^* transitions (Ono, et al, 1993, Ono, et al, 1994, MacLachlan, et al, 1994b, Nugent, et al, 1993). These need not be directly affecting the Mn ions, but may reflect at the oxidation of redox active amino acids directly ligated to the Mn (MacLachlan pers. comm.).

Both forms of the S_3^* state split signal are proposed to involve the interaction of redox active His residues. The TD for Signal II presented for the NaCl treated sample indicates a Curie dependence for both the signal arising in the illuminated sample and the annealed sample. Comparison of the data for the annealed and illuminated samples indicates an additional intensity component overlying the background 295K dark annealed intensity, which reflects only Signal II_s. The lineshapes of the Signal II recorded from S_3^* state illuminated samples and subsequently annealed at 295K indicate this additional intensity is of the same g value and lineshape as Signal II_s. The additional intensity may reflect generation of Y_Z^+ after and in addition to the formation of the S_3^* state signal, indicating the blockage of the OEC turnover in the S_3 to S_0 transition for the samples in which the OEC Mn dimer is accessible to electron donation for the S_1 to S_2 and S_2 to S_3^* transitions. This differs from Cl^- depleted data, which has been prepared to allow only two electron donations to P680 (Theg, et al, 1984, Itoh, et al., 1984, Baumgarten, 1990). Difficulties of measuring Y_Z^+ in the Cl^- depleted S_3 state (Hallahan, et al., 1992, MacLachlan and Nugent, 1993, Boussac, et al, 1992b, Boussac, et al, 1992a) may arise from the possibly of its oxidation and involvement in the narrow form of the S_3^* state $g \sim 2$ split signal, which is proposed here to arise from the interaction of Y_Z and H190, both of which are ligands to the inner Mn site.

In summary, the S_3^* state split signals are observed to fall into line width classes, dependent on the type of S_2 state ESR signal observable in the samples when illuminated at

275K in the presence of DCMU. All forms of the S_3^* state signal are ground state signals arising from the spin-spin interaction between a Mn containing centre and an organic radical, the radical inferred to be histidine via IR and UV spectroscopy (Boussac, et al, 1990b, Boussac, et al, 1992b, Ono and Inoue, 1990, Ono and Inoue, 1991, Ono and Inoue, 1992). The properties of the Mn centres involved with each type of split signal are observed to be changed by the S_2 to S_3 state transition, with a change to stronger antiferromagnetic coupling inferred for each Mn dimer complex in the formation of the S_3^* state from the respective S_2 state form. The properties of the S_3^* state split signal arising from the multiline S_2 state centre, the broader line width form, suggests changes in the OEC centre which may provide insight into the S_2 to S_3 transition in the functional PS II system.

5.5. Functional S state turnover

5.5.1. S_1 state

From the X-ray absorbance data and the spin state data for the S_2 state, the structure of the Mn centre in the S_1 state may be depicted by Fig 5.07. The Mn oxidation state is $Mn(III)_2 Mn(IV)_2$ as per the XAS K edge inflection point data (Kusunoki, et al, 1989, Yachandra, et al, 1993, MacLachlan, et al, 1992, Penner-Hahn, et al., 1990). The outer Mn are both $Mn(III)$, di- μ -oxo- μ -carboxylato bridged with the μ -oxo bridges partially protonated, with the protons creating H bonds to Asp 342 and an amino acid residue possibly from either the 17, 23 or 34 KDa polypeptide or from a D2 residue, possibly D2 E65, implicated as an important residue for the stability of the Mn site (Nixon and Diner, 1994, Chu, et al., 1995b, Vermaas, et al, 1993, Styring, et al, 1993). These protonations are likely to be important for the modulation of the redox potential as the S states cycle through from S_0 to S_4 , as well as the magnetic exchange coupling of the Mn dimer, with protonation of the bridging ligands influencing the magnitude and sign of the exchange model compounds (Larson, et al., 1992a, Larson, et al., 1992b, Knopp and Wieghardt, 1991, Baldwin, et al., 1993; Baldwin, et al., 1994). The low magnitude of the coupling requires that the μ -oxo bridges be protonated.

5.5.2. S_2 state

The nature of the Mn bridging sites is dependent on the nature of the S_2 state ESR signal formed. Under illumination generating the ground state $g=4.1$ form of the S_2 state, Y_Z is oxidised, generating the ground state signal through coupling to the inner Mn (IV-IV) dimer, see fig. 5.02. Illuminating to generate the multiline S_2 state, the functional and terminal site

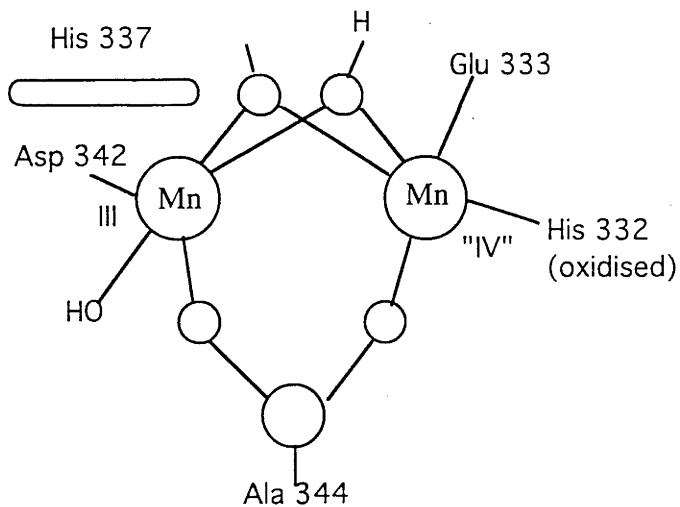
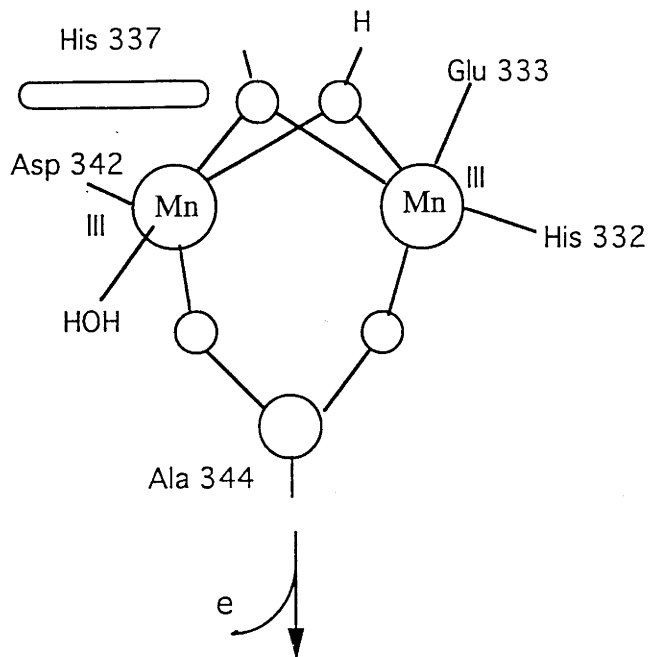


Figure 5.07. a). S1 State: The Mn ions are both in the Mn III state. The μ -oxo bridge oxygens are likely protonated. The exchange constant J between the Mn ions is likely to be of low magnitude antiferromagnetic. The ground state for this dimer is $S=0$. Parallel polarisation ESR has led to the observation of a signal at $g \sim 4.8$ due to the $S=1$ excited state of this dimer. The temperature for this measurement was ~ 10 K (Dexheimer, et al, 1990), inferring $|J/k| \sim 3$ to 4 K which is likely to be irrespective of the presence of added alcohols (EthOH etc).

b). S2 state
The Mn ions are in the Mn III state. However, the oxidation events for the S1 to S2 turnover oxidises His 332. This oxidation coupled with strong exchange between His 332 and the ligated Mn realises an effective Mn III-IV dimer, leading to a net spin $1/2$ ground state. In the absence of alcohol, the exchange coupling of the dimer $|J/k|$ is ~ 3.5 K. With the likelihood of proton release in this state, the maintenance of a low J implicates the loss of protons from the terminal ligands, likely $-OH_2$ to $-OH$

for electron donation, oxidises the His 332-Mn site generating an effective Mn III-His couple, see fig. 5.08, although significant spin density may reside in the amino acid residue without significantly altering the properties of the apparent "Mn IV" formed, the effective backbonding from the histidyl nitrogen to vacant d orbitals on the Mn stabilising the oxidation to the effective Mn (IV) (Åhrling and Pace, 1995). The S₁ - S₂ electron transfer probably does not require a deprotonation step of a bridging ligand, however, a terminal substrate ligand located at the Asp 342 Mn (III) binding site, typically H₂O, may be deprotonated to reduce the overall charge density on the OEC Mn complex, modulating the oxidation potential for the next step.

5.5.3. S₃ state

The data currently available for the S₃ state suggests a number of events upon the withdrawal of an electron from the OEC Mn complex.

Recent K edge XAS spectroscopy has indicated oxidation occurs in the environment of the OEC Mn in the S₂ to S₃ transition (MacLachlan, et al, 1994b, Ono, et al, 1993). The K edge shift for the S₁ to S₂ and the S₂ to S₃ transitions are of similar magnitude, approximately 1.2eV, indicating the oxidation of Mn III to Mn IV on each step. Earlier EXAFS data are not directly supportive of this Mn oxidation, although changes in the Mn environment, with an increase in Mn-Mn separation in one dimer (Guiles, et al, 1990b) appear consistent with Mn oxidation. The report of an amino acid oxidation in the Cl⁻ and Ca²⁺ depleted PSII inhibited samples (Boussac, et al, 1990a) may reflect events leading to blockage of turnover.

In terms of the model for the Mn OEC site, the S₂ to S₃ transition occurs with the Mn (III) ion bound to Asp 342 oxidised to Mn (IV), see fig 5.09. This results in a Mn IV - Mn IV dimer which with antiferromagnetic coupling, leads to a net zero spin ESR silent state. The oxidation potential of an Mn IV- IV dimer for the S₃ to S₄ step, may be modulated by a further deprotonation event around the Mn environment . This is likely to occur at a μ-oxo bridge site. In the altered S₃^{*} state formed in Cl⁻ and Ca²⁺ depleted states, formation of the S₃^{*} state generates an S=1 species. Modelling of the ESR signal has concluded this arises from a spin-spin interaction of an S = 1/2 Mn containing centre and an oxidised amino acid, either His⁺ (Boussac, et al, 1990b, Boussac, et al, 1992b) or Y_Z (Hallahan, et al., 1992). Based on the discussion above for the altered S₃ state, two forms of the ESR signal are generatable. The form which would be closest to the physiological S₃ state is that involving oxidation of His 332 and interaction of this species with the Mn III - IV dimer (outer pair) arising from the S₂ state.

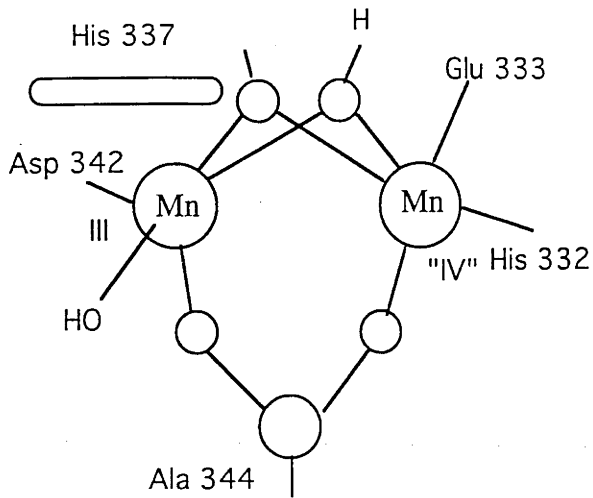
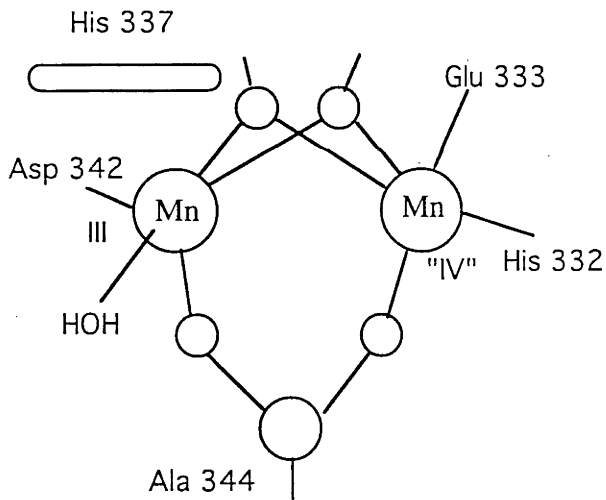


Figure 5.08. a). S2 state
 In samples not treated with alcohols, the exchange constant of the dimer remains effectively unchanged between the S1 and S2 state as evidence by similar signal amplitudes for the S1 $g \sim 4.8$ and S2 $g = 4.1$ signals observed at 8 to 10K (Dexheimer, *et al.*, 1990, Pace, *et al.*, 1991, this work)



b). In the presence of alcohol, the temperature dependence of the multiline is consistent with an increase in the exchange coupling constant due to the presence of the alcohol. This may be most simply modelled by the deprotonation of a bridging rather than terminal ligand.

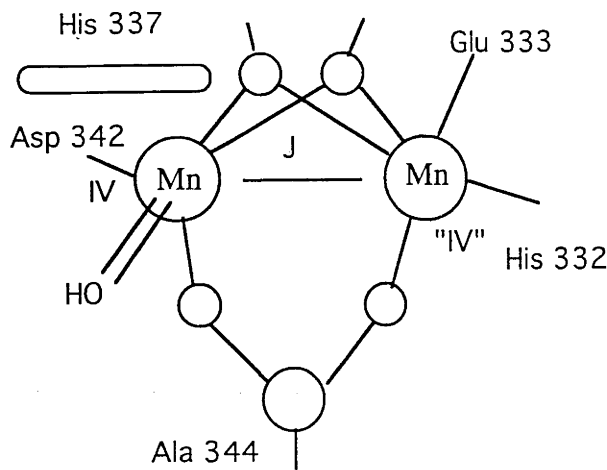
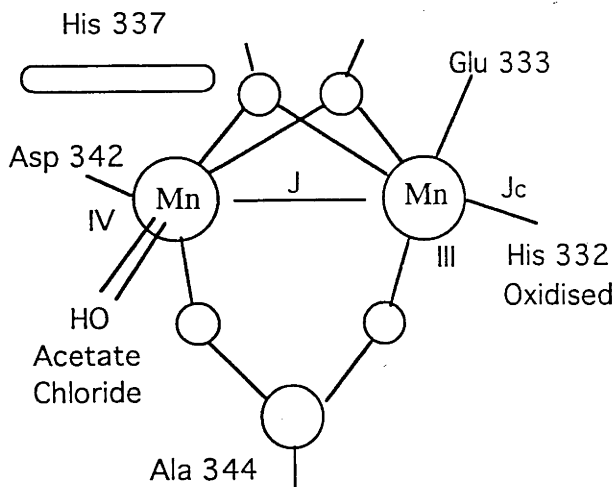


Figure 5.09. S3 state
a). The S3 state in functional PS II

is diamagnetic, evidenced by the loss of the S2 state multiline signal upon advancement by flash illumination (Dismukes and Siderer, 1988). Spin state is $S=0$. It is likely that another deprotonation event occurs in the S2 to S3 transition. From fig. 5.07, showing the oxidation of His 332

on the S1 to S2 step, this centre tightly coupled to the ligated Mn III. The lack of observing an $S=1$ type signal in the S3 state may arise from the J increasing with both S state transition oxidations. The S3 state then forms a Mn IV-IV dimer, which has an $S=0$ ground state.



b). Altered "S3*" state.

With the loss of the proton in the S2 to S3 step, the exchange coupling between the Mn ions becomes stronger. Unlike the functional PS II, one oxidation remains on the His 332 leading to an $S=1/2-S=1/2$ interaction forming an $S=1$ effective state

Deprotonation of a bridge hydroxyl would allow the redox potential of the complex to stay at $\sim 1\text{eV}$, with the terminally bound substrate OH remaining slowly exchangeable (Messinger, et al., 1995). The changes in Mn-Mn separation in one pair observed by EXAFS on the $S_2 \rightarrow S_3$ transition (Guiles, et al, 1990b) may reflect the balance of the Mn oxidation and bridge deprotonation effects. The implied strengthening of the antiferromagnetic coupling in the Mn IV - IV pair (the S_3 state is EPR silent) would be mostly a consequence of the μ -oxo bridge deprotonation.

5.5.4. S_3 to S_4 to S_0 transition - making Dioxygen

Figure 5.10 indicates the proposed functional S_3 state. Recent studies on the S_3 state and the S_3 to S_4 transition indicate that immediately prior to formation of an oxygen oxygen bond, one OH_2 or OH is bound loosely, kinetic exchange time ≥ 10 ms (Messinger, et al., 1995). The strongly bound OH is terminally liganded to the Asp 342 Mn, at the substrate binding site and has an exchange time $\sim 1\text{sec}$ (Messinger, et al., 1995). The major energetic step in the process of O_2 generation is the formation of an O-O bond. To achieve this without the formation of peroxy HO-O^\cdot or superoxide radicals reduces the possibility of damage to the protein. A process by which this might occur, within the context of the present model has been suggested in discussion with Prof. A. Sargesson of the RSC (A. Sargesson pers. comm.). This supposes two stages in O_2 formation, both of which are supported by the restricted water exchange at the Mn binding site. The S_3 to S_4 oxidation step results in a very rapid reorganisation of substrate and reaction intermediates. UV and visible absorbance studies have indicated that indeed two steps occur, one on the time scale of $\sim 40\mu\text{s} - 200\mu\text{s}$, the other on the time scale of 1ms (Rappaport, et al, 1994). The second step was indicative of the reformation of the S_0 state, the initial state of the reaction cycle (Rappaport, et al, 1994). The rapid step probably represents oxidation of some component of the OEC environment, at a site not yet understood, although the formation of a Mn V has not yet been supported by absorbance studies. The oxidation must be close to the Asp 342 - Mn - OH site, leading to further deprotonation of the OH ligand, possibly forming a $\text{Mn}=\text{O}$ double bond. Within the restricted access environment (Tso, et al, 1991b, Mei and Yocum, 1991a, Mei and Yocum, 1992, Riggs, et al, 1992) strong nucleophilic attack by a second (loosely bound) H_2O substrate molecule onto the $\text{Mn}=\text{O}$ double bond could occur. This attack forms the O=O bond, with the high redox potential stored on the Mn site withdrawing four electrons off the $\text{Mn-O}=\text{O}(\text{H})_2$ moiety restoring the dimer to the S_0 state. Release of the O_2 and protons, and rebinding of a fresh substrate OH_2 restarts the cycle. The release of protons within the local environment,

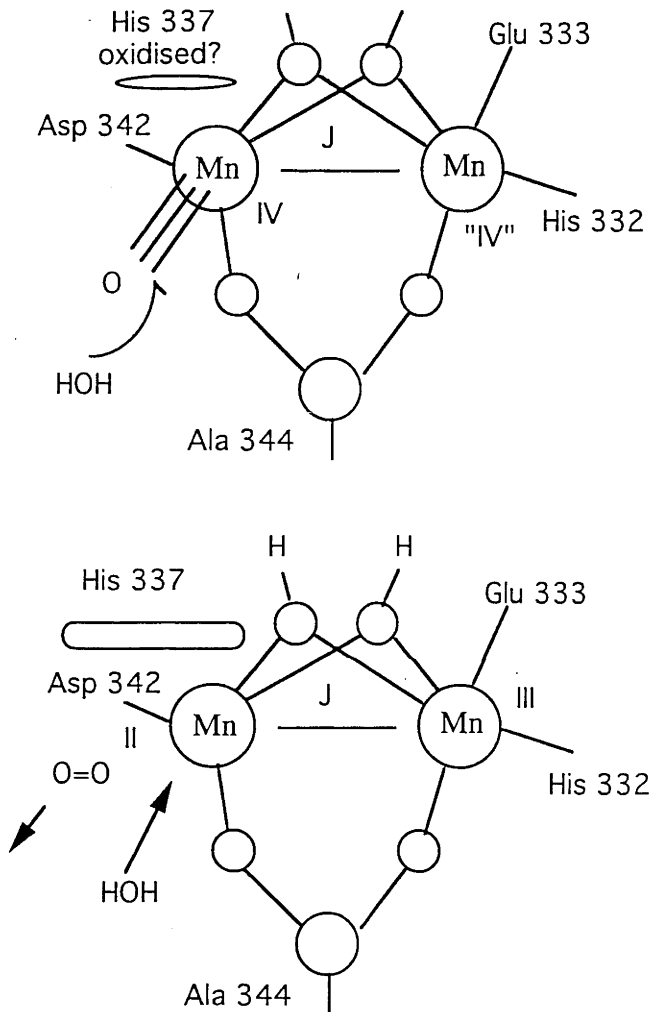


Figure 5.10. S₄ state

The S₃ to S₀ transition is a two stage process. The first stage is observed to be undertaken in $< 40\mu\text{s}$. This is followed by a second slower step of $\sim 1.2\text{ms}$ duration (Rappaport, et al, 1994). The first stage may be oxidation of an amino acid close to the OEC or on the electron transport chain, maybe Yz. The presence of the fourth oxidation equivalent may lead to a final deprotonation event of the terminally located substrate ligand. With HOH as this ligand, this final step may create an Mn-O triple bond, which is highly reactive. To form O₂, this bond may be subject to nucleophilic attack by another water molecule, leading to the formation of an O=O bond, proton redistribution and electron flow out of the newly formed species. O₂ is released and the cycle restarted by the binding of another HOH.

accompanied by the rapid reduction of the Mn centre back to a Mn II - Mn III state may allow reprotonation of the bridging ligands as part of a concerted process.

In this model, most of the electron withdrawal events occur on the Asp 342 Mn, with the S₂ to S₃ transition and the S₃ to S₄ to S₀ catalytic turnover resulting in oxidative and strong reductive events at this site. The reduction of this Mn to Mn II is not supported by ESR evidence, with the S₀ state apparently ESR silent. This implies that one electron of the four liberated in the S₃ to S₄ to S₀ catalytic event may be stored elsewhere within the site. This would lessen the possibility of the loss of an Mn(II) due to its lack of ligand field stability (Dismukes and Siderer, 1981, Dismukes, et al, 1982). In PSII stored in the S₀ state, electron transfer events lead to storage of the electron on Y_D⁺, forming the S₁ state and the Y_D (Styring and Rutherford, 1988). This electron transfer stabilises the Mn environment (Styring and Rutherford, 1988) implying the S₀ state stores the electron close to one of the Mn ions.

5.6. Summary

The four Mn ions within the OEC are arranged as a magnetically isolated pair of antiferromagnetically coupled dimers. One dimer plays a part in stabilising an optimal conformation of the redox active electron transfer intermediate, Y_Z. The other pair are bound in a site with restricted access to water, in the optimally functional state. By storing redox equivalents within the Mn environment and tightly controlling substrate water access, rapid and efficient formation of O=O from two H₂O is enabled.

Appendix One

'Program for calculation of the energy states and relative populations for
' the Manganese dimer structure as per figure 4.14 (a)

```
CLS : SCREEN 0, 0, 0
'
    DIM invt(50), energst(4, 50), sumit(50), E(5)
'
    INPUT "Population Ios"; Ios
    INPUT "Exchange constant"; Jex
    E(1) = 9 * Jex: E(2) = 6 * Jex: E(3) = Jex: E(4) = -6 * Jex
'
    FOR i = 1 TO 50
        FOR j = 1 TO 4
            sumit(i) = sumit(i) + (2 * (CSNG(j) - 1 / 2) + 1) * EXP(-1 * E(j) *
C            .005 * CSNG(i))
            NEXT j
            FOR j = 1 TO 4
                energst(j, i) = (Ios * CSNG(i) * .005) * ((2 * (CSNG(j) - 1 / 2) + 1) *
C                EXP(-.005 * E(j) * CSNG(i))) / sumit(i)
            NEXT j
            invt(i) = CSNG(i) * .005
        NEXT i
'
    INPUT "filename"; name$: NAM$ = name$ + ".dat"
    OPEN NAM$ FOR OUTPUT AS #1
        FOR i = 1 TO 50
            PRINT #1, invt(i), energst(1, i), energst(2, i), energst(3, i),
C            energst(4, i)
            NEXT i
        CLOSE #1
'
END
```

Appendix Two

‘ Program for calculation of the energy states for a three spin centre
‘construct. The structure is depicted in figure 4.22 (b)

```
CLS : SCREEN 0, 0, 0
```

```
‘  
    DIM invt(50), energst(4, 50), sumit(50), E(5)  
    Ios = 2000  
  
    INPUT "J of radical to Mn in dimer"; JR  
    INPUT "Ratio of J' to J"; RJS  
    J12 = JR / RJS  
  
    E(1) = -15 * J12 / 4: E(2) = -11 * J12 / 4 + JR * .5: E(3) = -3 * J12 / 4 + JR:  
    E(4) = 9 * J12 / 4 + 3 * JR / 2  
  
    E(1) = E(1/2,0), E(2) = E(3/2,1), E(3) = E(5/2,2), E(4) = E(7/2,3)  
  
    FOR i = 1 TO 50  
        FOR j = 1 TO 4  
            sumit(i) = sumit(i) + (2 * (CSNG(j) - 1 / 2) + 1) * EXP(-1 * E(j) *  
                .005 * CSNG(i))  
        NEXT j  
  
        FOR j = 1 TO 4  
            energst(j, i) = (Ios * (CSNG(i) * .005)) * (2 * CSNG(j) * EXP(-1 *  
                E(j) * .005 * CSNG(i))) / sumit(i)  
        NEXT j  
        invt(i) = CSNG(i) * .005  
    NEXT I  
  
    INPUT "filename"; name$: NAM$ = name$ + ".dat"  
    OPEN NAM$ FOR OUTPUT AS #1  
  
    FOR i = 1 TO 50  
        PRINT #1, invt(i), energst(1, i), energst(2, i), energst(1, i) * 100 / invt(i),  
            energst(3, i)  
    NEXT i  
    CLOSE #1  
END
```

Appendix Three

Changes made to this Thesis from Referees Reports

Overall

All references checked and reformatted to Journal standard; where single author article referenced, formatted (Name, 19XX (year)); where two author article referenced, formatted (Name1 and Name2, 19XX); where three or more author articles referenced, formatted (Name1, et al, 19XX).

Added a list of Figures to the Contents

Added a list of abbreviations and symbols used in the thesis to the Contents

Added Appendices for additional material.

Chapter1

Text checked for typographical and referencing formatting errors; corrected and reformatted. Some long paragraphs have been altered to be a series of shorter paragraphs, content has not been altered.

Chapter 2

Text checked for typographical errors and corrected. Bibliography list removed and referencing undertaken, references formatted and added to the Reference List after Chapter 5.

Authors note: the length of time for corrections to be made to this Thesis and Thesis return was due to the absence of most of the ESR Bibliography list at the University College London Library. The Referencing of Chapter 2 required the return to the Australian National University Library for completion of the referencing of Chapter 2.

Chapter 3

Text checked for typographical and reference formatting errors, corrected and reformatted. Some abbreviations replaced by full name descriptions, eg SUC by sucrose throughout.

Chapter 4

Text checked for typographical and reference formatting errors, corrected and reformatted. Some abbreviations replaced by full name descriptions, eg SUC by sucrose. Figures checked for typographical errors, scaling and units of axes, corrected and reformatted. The exchange coupling nomenclature for the models proposed have been clarified and standardised throughout. The same names and symbols within the exchange coupling models have been retained, their usage has been clarified.

Chapter 5

Text checked for typographical and reference formatting errors, corrected and reformatted. Figures checked for typographical errors and corrected. Nomenclature for exchange coupling models proposed standardised and clarified as per Chapter 4.

References

Checked Names, spelling, Journals and Publications and Years. Typographical and inaccuracies corrected. Placed the Bibliographically listed journal articles and publications

from the Bibliography List previously following Chapter 2 into the reference list following the above formatting procedures.

Appendices

Added listing of the QuickBasic Programs used for the calculation of the Energy levels and relative spin populations for each of the Mn model structures presented.

Added this list of Corrections.

Authors Note. The content of this thesis was not considered in need of change, only the formatting of the References and the level of typographical errors within the text. These changes have hopefully been completed to satisfaction. A Mars bar will be offered to the person who presents an original typographical or other error to the author. I hope that there are not many, however, there are typographical errors in even the best of texts, so the offer here is made.

Reference List

- Aasa, R., Andréasson, L.-E., Lagenfelt, G. and Vänngård, T. 1987. *FEBS Letters*. **221**:245-248.
- Aasa, R. and Vänngård, T. 1975 *Journal of Magnetic Resonance* **19**, 308-315.
- Abraham, A. and Bleaney, B. 1970 *Electron Paramagnetic Resonance of Transition Ions*, Clarendon Press, Oxford.
- Åhrling, K. A. and Pace, R. J. 1995. *Biophysical Journal*. **68**:2081-2090.
- Åkerlund, H. E., Jansson, C. and Andersson, B. 1982. *Biochimica et Biophysica Acta*. **681**:1-10.
- Allakhverdiyev, S. I., Hayashi, H., Fujimura, Y., Klimov, V. V. and Murata, N. 1993. *Photosynthesis Research*. **35**:345-349.
- Allakhverdiyev, S. I., Klevanik, A. V., Klimov, V. V., Shuvalov, V. A. and Krasnovskii, A. A. 1983. *Biophysics*. **28**:1-5.
- Allakhverdiyev, S. I., Shafiyev, M. A. and Klimov, V. V. 1986. *Biophysics*. **31**:243-247.
- Al'tschuler, S. A. and Kozyrev, B. M. 1964 *Electron Paramagnetic Resonance*, Academic Press, New York.
- Anderson, J. M. 1987. *New Comprehensive Biochemistry*. J. Ames. Elsevier. **15**:273-297.
- Andreasson, L.-E., Hansson, O. and Vänngård, T. 1983. *Chemica Scripta*. **21**:71-74.
- Andreasson, L.-E., Adelroth, P. and Lindberg, K. 1994. *Biochemical Society Transactions*. **22**:347-352.
- Andreasson, L.-E., Hansson, Ö. and von Schenk, K. 1988. *Biochimica et Biophysica Acta*. **936**:351-360.
- Andreasson, L.-E. and Lindberg, K. 1992. *Biochimica et Biophysica Acta*. **1100**:177-183.
- Andreasson, L. E. and Vänngård, T. 1988. *Annual Review of Plant Physiology and Plant Molecular Biology*. **39**:379-411.
- Andreasson, L. E., Vass, I. and Styring, S. 1995. *Biochimica et Biophysica Acta*. **1230**:155-164.
- Andrew, E. R. 1958 *Nuclear Magnetic Resonance*, University Press, Cambridge
- Arnon, D. I. 1949. *Plant Physiology*. **24**:1-15.
- Arnon, D. I. and Tang, G. M. S. 1988. *Proceedings of the National Academy of Science, USA*. **85**:9524-9528.
- Assenheim, H. M. 1965 *Introduction to Electron Spin Resonance*, Hilger and Watts Ltd, London.
- Astashkin, A. V., Kodera, Y. and Kawamori, A. 1994a. *Biochimica et Biophysica Acta*. **1187**:89-93.
- Astashkin, A. V., Kodera, Y. and Kawamori, A. 1994b. *Journal of Magnetic Resonance. Series B* **105**:113-119.

- Aylward, G. H. and Findlay, T. J. V. 1974 *SI Chemical Data*, 3rd Ed. John Wiley and Sons New York.
- Babcock, G. T., Ghanotakis, D. F., Ke, B. and Diner, B. A. 1983. *Biochimica et Biophysica Acta*. **723**:276-286.
- Babcock, G. T. 1987. *New Comprehensive Biochemistry*. J. Ames. Elsevier. **15**:125-158.
- Babcock, G. T. 1993. *Proceedings of the National Academy of Sciences. USA*. **90**:10893-10895.
- Babcock, G. T., Blankenship, R. E. and Sauer, K. 1976. *FEBS Letters*. **61**:286-289.
- Babcock, G. T. and Sauer, K. 1973a. *Biochimica et Biophysica Acta*. **325**:483-503.
- Babcock, G. T. and Sauer, K. 1973b. *Biochimica et Biophysica Acta*. **325**:504-519.
- Babcock, G. T. and Sauer, K. 1975a. *Biochimica et Biophysica Acta*. **376**:329-344.
- Babcock, G. T. and Sauer, K. 1975b. *Biochimica et Biophysica Acta*. **376**:315-528.
- Baldas, J., Boas, J. F., Bonnyman, J. and Williams, G. A. 1984. *Journal of the Chemical Society, Dalton Transactions*. 2395-2400.
- Baldwin, M. J., Gelasco, A. and Pecoraro, V. L. 1993. *Photosynthesis Research*. **38**:303-308.
- Baldwin, M. J., Stemmler, T. L., Riggs-Gelasco, P. J., Kirk, M. L., Penner-Hahn, J. E. and Pecoraro, V. L. 1994. *Journal of the American Chemical Society*. **116**:11349-11356.
- Barber, J. 1994. *Biochemical Society Transactions*. **22**:313-318.
- Baron, M., Arellano, J. B., Schroder, W., Lachica, M. and Chueca, A. 1993. *Photosynthetica*. **28**:195-204.
- Barry, B. A. and Babcock, G. T. 1987. *Proceedings of the National Academy of Science, USA*. **84**:7099-7103.
- Barry, B. A., El-Deeb, M. K., Sandusky, P. O. and Babcock, G. T. 1990. *Journal of Biological Chemistry*. **265**:20139-20143.
- Barry, B. A. and Babcock, G. T. 1988. *Chemica Scripta*. **28A**:117-122.
- Baumgarten, M., Philo, J. S. and Dismukes, G. C. 1990. *Biochemistry*. **29**:10814-10822.
- Beck, W. F., de Paula, J. C. and Brudvig, G. W. 1985. *Biochemistry*. **24**:3035-3043.
- Beck, W. F., de Paula, J. C. and Brudvig, G. W. 1986. *Journal of the American Chemical Society*. **108**:4018-4022.
- Beck, W. F. and Brudvig, G. W. 1986. *Biochemistry*. **25**:6479-6486.
- Beck, W. F. and Brudvig, G. W. 1988a. *Chemica Scripta*. **28A**:93-98.
- Beck, W. F. and Brudvig, G. W. 1988b. *Journal of the American Chemical Society*. **110**:1517-1523.
- Bencini, A. and Gatteschi, D. 1990 *EPR of Exchange Coupled Systems*, Springer-Verlaag, Berlin.

- Bender, C. J., Sahlin, M., Babcock, G. T., Barry, B. A., Chandrashekar, T. K., Salowe, S. P., Stubbe, J., Lindstrom, B., Petersson, L., Ehrenberg, A. and Sjoberg, B.-M. 1989. *Journal of the American Chemical Society*. **111**:8076-8083.
- Berthold, D. A., Babcock, G. T. and Yocum, C. F. 1981. *FEBS Letters*. **134**:231-234.
- Blankenship, R. E., McGuire, A. and Sauer, K. 1977. *Biochimica et Biophysica Acta*. **459**:617-619.
- Blough, N. V. and Sauer, K. 1984. *Biochimica et Biophysica Acta*. **767**:377-381.
- Blubaugh, D. J. and Govindjee. 1988. *Biochimica et Biophysica Acta*. **936**:208-214.
- Blumberg, W. E. and Peisach, J. 1973 *Annals of the New York Academy of Sciences* **222**, 539-560.
- Bock, C. H., Gerken, S., Stehlik, D. and Witt, H. T. 1988. *FEBS Letters*. **227**:141-146.
- Boska, M., Blough, N. V. and Sauer, K. 1985. *Biochimica et Biophysica Acta*. **808**:132-139.
- Boska, M., Yamagishi, A. and Sauer, K. 1986. *Biochimica et Biophysica Acta*. **850**:226-233.
- Boska, M., Sauer, K., Buttner, W. and Babcock, G. T. 1983. *Biochimica et Biophysica Acta*. **722**:327-330.
- Boussac, A., Maison-Peteri, B., Vernotte, C. and Etienne, A.-L. 1985a. *Biochimica et Biophysica Acta*. **808**:225-230.
- Boussac, A., Maison-Peteri, B., Etienne, A.-L. and Vernotte, C. 1985b. *Biochimica et Biophysica Acta*. **808**:231-234.
- Boussac, A., Zimmermann, J.-L. and Rutherford, A. W. 1989. *Biochemistry*. **28**:8984-8989.
- Boussac, A., Zimmermann, J.-L. and Rutherford, A. W. 1990a. *FEBS Letters*. **277**:69-74.
- Boussac, A., Zimmermann, J.-L., Rutherford, A. W. and Lavergne, J. 1990b. *Nature*. **347**:303-306.
- Boussac, A., Rutherford, A. W. and Styring, S. 1990c. *Biochemistry*. **29**:24-32.
- Boussac, A., Setif, P. and Rutherford, A. W. 1992a. *Biochemistry*. **31**:1224-1234.
- Boussac, A. and Rutherford, A. W. 1992b. *Biochemistry*. **31**:7441-7445.
- Boussac, A. 1995. *Chemical Physics*. **194**:409-418.
- Boussac, A. and Rutherford, A. W. 1988a. *FEBS Letters*. **236**:432-436.
- Boussac, A. and Rutherford, A. W. 1988b. *Biochemistry*. **27**:3476-3483.
- Boussac, A. and Rutherford, A. W. 1988c. *Chemica Scripta*. **28A**:123-126.
- Boussac, A. and Rutherford, A. W. 1994a. *Journal of Biological Chemistry*. **269**:12462-12467.
- Boussac, A. and Rutherford, A. W. 1994b. *Biochemical Society Transactions*. **22**:352-358.
- Boussac, A. and Rutherford, A. W. 1995. *Biochimica et Biophysica Acta*. **1230**:195-201.
- Bricker, T. M., Pakrasi, H. B. and Sherman, L. A. 1985. *Archives of Biochemistry and Biophysics*. **237**:170-176.

- Britt, R. D., Zimmermann, J.-L., Sauer, K. and Klein, M. P. 1989. *Journal of the American Chemical Society*. **111**:3522-3532.
- Britt, R. D., Lorigan, G. A., Sauer, K., Klein, M. P. and Zimmermann, J.-L. 1992. *Biochimica et Biophysica Acta*. **1040**:95-101.
- Britt, R. D., Tang, X.-S., Gilchrist, M. L., Lorigan, G. A., Larsen, B. S. and Diner, B. A. 1994. *Biochemical Society Transactions*. **22**:343-347.
- Britt, R. D., Randall, D. W., Ball, J. A., Gilchrist, M. L. J., A., F. D., Sturgeon, B. E., Lorigan, G. A., Tang, X.-S., Diner, B. A., Klein, M. P., Chan, M. K. and Armstrong, W. H. 1995. *Photosynthesis: Light to Biosphere. Proceedings of the Xth Photosynthesis Congress*. P. Mathis Ed Kluwer Dordrecht **2**: 229-234
- Brok, M., Ebskamp, F. C. R. and Hoff, A. J. 1985. *Biochimica et Biophysica Acta*. **809**:421-428.
- Brok, M., Horikx, J. T. G. and Hoff, A. J. 1986. *FEBS Letters*. **203**:36-40.
- Brudvig, G. W., Casey, J. L. and Sauer, K. 1983. *Biochimica et Biophysica Acta*. **723**:366-371.
- Brudvig, G. W. and Crabtree, R. H. 1986. *Proceedings of the National Academy of Sciences USA*. **83**:4586-4588.
- Cammarata, K. V. and Cheniae, G. M. 1987. *Plant Physiology*. **84**:587-595.
- Casey, J. L. and Sauer, K. 1984. *Biochimica et Biophysica Acta*. **767**:21-28.
- Castner, T. J., Newell, G. S., Holton, W. C. and Slichter, C. P. 1960. *Journal of Chemical Physics*. **32**:668-673.
- Chang, H.-R., Larsen, S. K., Boyd, P. D. W., Pierpont, C. G. and Hendrickson, D. N. 1988a. *Journal of the American Chemical Society*. **110**:4565-4576.
- Chang, H. R., Diril, H., Nilges, M. J., Zhang, X., Potenza, J. A., Schugar, H. J., Hendrickson, D. N. and Isied, S. S. 1988b. *Journal of the American Chemical Society*. **110**:625-627.
- Cheniae, G. M. 1980. *Methods in Enzymology*. **69**:349-363.
- Cheniae, G. M. and Martin., M. 1970. *Biochimica et Biophysica Acta*. **197**:219-239.
- Chu, H., Nguyen, A. P. and Debus, R. J. 1995a. *Biochemistry*. **34**:5839-5858.
- Chu, H., Nguyen, A. P. and Debus, R. J. 1995b. *Biochemistry*. **34**:5859-5882.
- Cole, J., Yachandra, V. K., Guiles, R. D., McDermott, A. E., Britt, R. D., Dexheimer, S. L., Sauer, K. and Klein, M. P. 1987. *Biochimica et Biophysica Acta*. **890**:395-398.
- Cole, J. and Sauer, K. 1987. *Biochimica et Biophysica Acta*. **891**:40-48.
- Coleman, W. J., Govindjee and Gutowsky, H. S. 1987a. *Biochimica et Biophysica Acta*. **894**:443-452.
- Coleman, W. J., Govindjee and Gutowsky, H. S. 1987b. *Biochimica et Biophysica Acta*. **894**:453-459.
- Coleman, W. J. 1990. *Photosynthesis Research*. **23**:1-27.
- Coleman, W. J. and Govindjee. 1987. *Photosynthesis Research*. **13**:199-223.

- Cooper, S. R., Dismukes, G. C., Klein, M. P. and Calvin, M. 1978. *Journal of the American Chemical Society*. **100**:7248-7252.
- Critchley, C. 1985. *Biochimica et Biophysica Acta*. **811**:33-46.
- Damoder, R., Klimov, V. V. and Dismukes, G.C. 1986. *Biochimica et Biophysica Acta*. **848**:378-391.
- Danielius, R. V., Satoh, K., van Kan, P. J. M., Plijter, J. J., Nuijs, A. M. and van Gorkom, H. J. 1987. *FEBS Letters*. **213**:241-244.
- Dau, H., Andrews, J. C., Roelofs, T. A., Latimer, M. J., Liang, W., Yachandra, V. K., Sauer, K. and Klein, M. P. 1995. *Biochemistry*. **34**:5274-5287.
- de Paula, J. C., Innes, J. B. and Brudvig, G. W. 1985a. *Biochemistry*. **24**:8114-8120.
- de Paula, J. C. and Brudvig, G. W. 1985b. *Journal of the American Chemical Society*. **107**:2643-2648.
- de Paula, J. C., Li, P. M., Miller, A.-F., Wu, B. W. and Brudvig, G. W. 1986a. *Biochemistry*. **25**:6487-6494.
- de Paula, J. C., Beck, W. F. and Brudvig, G. W. 1986b. *Journal of the American Chemical Society*. **18**:4002-4009.
- Deak, Z., Vass, I. and Styring, S. 1994. *Biochimica et Biophysica Acta*. **1185**:65-74.
- Debus, J. 1992. *Biochimica et Biophysica Acta*. **1102**:269-352.
- Debus, R. J., Barry, B. A., Babcock, G. T. and McIntosh, L. 1988a. *Proceedings of the National Academy of Sciences, USA*. **85**:427-430.
- Debus, R. J., Barry, B. A., Sithole, I., Babcock, G. T. and McIntosh, L. 1988b. *Biochemistry*. **27**:9071-9074.
- Deisenhofer, J., Epp, O., Miki, K., Huber, R. and Michel, H. 1984. *Journal of Molecular Biology*. **180**:385-398.
- Deisenhofer, J., Epp, O., Miki, K., Huber, R. and Michel, H. 1985. *Nature*. **318**:618-624.
- Dekker, J. P., Plijter, J. J., Ouwehand, L. and Van Gorkom, H. J. 1984a. *Biochimica et Biophysica Acta*. **767**:176-179.
- Dekker, J. P., Van Gorkom, H. J., Wensink, J. and Ouwehand, L. 1984b. *Biochimica et Biophysica Acta*. **767**:1-9.
- Dekker, J. P., Van Gorkon, H. J., Brok, M. and Ouwehand, L. 1984c. *Biochimica et Biophysica Acta*. **764**:301-309.
- DeRose, V. J., Yachandra, V. K., McDermott, A. E., Britt, R. D., Sauer, K. and Klein, M. P. 1991. *Biochemistry*. **30**:1335-1341.
- DeRose, V. J., Mukerji, I., Latimer, M. J., Yachandra, V. K., Sauer, K. and Klein, M. P. 1994. *Journal of the American Chemical Society*. **116**:5239-5249.
- DeRose, V. J., Latimer, M. J., Zimmermann, J.-L., Mukerji, I., Yachandra, V. K., Sauer, K. and Klein, M. P. 1995. *Chemical Physics*. **194**:443-459.

- Dexheimer, S. L., Sauer, K. and Klein, M. P. 1990. *Current Research in Photosynthesis*. M. Baltscheffsky. Kluwer Academic Publishers. 1:761-764.
- Dexheimer, S. L. and Klein, M. P. 1992. *Journal of the American Chemical Society*. **114**:2821-2826.
- Diner, B. A., Tang, X.-S., Zheng, M., Dismukes, G. C., Force, D. A., Randall, D. W. and Britt, R. D. 1995. *Photosynthesis: Light to Biosphere. Proceedings of the Xth Photosynthesis Congress*. P. Mathis Ed Kluwer Dordrecht **2**: 229-234.
- Diril, H., Chang, H.-S., Zhang, X., Larsen, S. K., Potenza, J. A., Pierpont, C. G., Schugar, H. J., Isied, S. S. and Hendrickson, D. N. 1987. *Journal of the American Society*. **109**:6207-6208.
- Dismukes, G. C., Ferris, K. and Watnick, P. 1982. *Photobiochemistry and Photobiophysics*. **3**:243-256.
- Dismukes, G. C. 1986. *Photochemistry and Photobiology*. **43**:99-115.
- Dismukes, G. C. 1988. *Chemica Scripta*. **28A**:99-104.
- Dismukes, G. C., Zheng, M., Hutchins, R. and Philo, J. S. 1994. *Biochemical Society Transactions*. **22**:323-327.
- Dismukes, G. C. and Siderer, Y. 1980. *FEBS Letters*. **121**:78-80.
- Dismukes, G. C. and Siderer, Y. 1981. *Proceedings of the National Academy of Science, USA*. **78**:274-278.
- Dolan, E., Green, J. P. and Frasch, W. D. 1990. *Current Research in Photosynthesis*. M. Baltscheffsky. Kluwer Academy Publishers. 1:781-784.
- Durrant, J. R., Klug, D. R., Kwa, S. L., van Grondelle, R., Porter, G. and Dekker, J. P., 1995. *Proceedings of the National Academy of Science, USA*. **92**:4798-4802.
- Enami, I., Tomo, T., Kitamura, M. and Katoh, S. 1994. *Biochimica et Biophysica Acta*. **1185**:75-80.
- Evans, M. C. W., MacLachlan, D. J., Bratt, P. and Nugent, J. H. A. 1994. *Biochemical Society Transactions*. **22**:335-338.
- Evelo, R. G., Hoff, A. J., Dikanov, S. A. and Tyryshkin, A. M. 1989. *Chemical Physics Letters*. **161**:479-484.
- Fiege, R., Zweggart, W., Irrgang, K.-D., Adir, N., Geiken, B., Renger, G. and Lubitz, W. 1995. *Proceedings of the Xth International Photosynthesis Congress*. P. Mathis Ed Kluwer Dordrecht
- Forster, V. and Junge, W. 1985. *Photochemistry and Photobiology*. **41**:183-190.
- Forster, V. and Junge, W. 1988. *Chemica Scripta*. **28A**:111-116.
- Gamelin, D. R., Kirk, M. L., Stemmler, T. L., Pal, S., Armstrong, W. H., Penner-Hahn, J. E. and Solomon, E. I. 1994. *Journal of the American Chemical Society*. **116**:2392-2399.
- Ganago, I. B., Klimov, V. V. and Krasnovskii, A. A. 1985. *Biophysics*. **30**:882-888.
- George, G. N., Prince, R. C. and Cramer, S. P. 1989. *Science*. **243**:789-791:

- Ghanotakis, D. F., Topper, J. N., Babcock, G. T. and Yocum, C. F. 1984. *FEBS Letters*. **170**:169-173.
- Gilchrist, M. L., Lorigan, G. A. and Britt, R. D. 1992. *Research in Photosynthesis*. N. Murata. Kluwer Academic Publishers. **2**:317-320.
- Gilchrist, M. L., Ball, J. A. J., Randall, D. W. and Britt, R. D. 1995. *Proceedings of the National Academy of Science, USA*. **92**:
- Goodin, D. B., Yachandra, V. K., Britt, R. D., Sauer, K. and Klein, M. P. 1984. *Biochimica et Biophysica Acta*. **767**:209-216.
- Goodson, P. A., Glerup, J., Hodgson, D. J., Michelsen, K. and Pedersen, E. 1990. *Inorganic Chemistry*. **29**:503-58.
- Guiles, R. D., Yachandra, V. K., McDermott, A. E., Cole, J. L., Dexheimer, S. L., Britt, R. D., Sauer, K. and Klein, M. P. 1990a. *Biochemistry*. **29**:486-496.
- Guiles, R. D., Zimmermann, J.-L., McDermott, A. E., Yachandra, V. K., Cole, J. L., Dexheimer, S. L., Britt, R. D., Wieghardt, K., Bossek, U., Sauer, K. and Klein, M. P. 1990b. *Biochemistry*. **29**:471-485.
- Haddy, A., Aasa, R. and Andreasson, L.-E. 1989. *Biochemistry*. **28**:6954-6959.
- Haddy, A., Dunham, W. R., Sands, R.H. and Aasa, R. 1992. *Biochimica et Biophysica Acta*. **1099**:25-34.
- Haddy, A., Waldo, G. S., Sands, R. H. and Penner-Hahn, J. E. 1994. *Inorganic Chemistry*. **33**:2677-2682.
- Hallahan, B. J., Nugent, J. H. A., Warden, J. T. and Evans, M. C. W. 1992. *Biochemistry*. **31**:4562-4573.
- Hansson, O., Andreasson, L.-E. and Vänngård, T. 1984. *Advances in Photosynthesis Research*. C. Sybesma. Martinus Nijhoff/ Dr W. Junk. **1**:1.3.307-1.3.310.
- Hansson, O., Aasa, R. and Vänngård, T. 1987. *Biophysical Journal*. **51**:825-832.
- Hansson, O. and Andreasson, L.-E. 1982. *Biochimica et Biophysica Acta*. **679**:261-268.
- Hansson, O., Andreasson, L.-E. and Vänngård, T. 1986. *FEBS Letters*. **195**:151-154.
- Hansson, Ö. and Wydrzynski, T. 1990. *Photosynthesis Research*. **23**:131-162.
- Hoganson, C. W., Ghanotakis, D. F., Babcock, G. T. and Yocum, C. F. 1989. *Photosynthesis Research*. **22**:285-293.
- Hoganson, C. W. and Babcock, G. T. 1988. *Biochemistry*. **27**:5848-5855.
- Hoganson, C. W. and Babcock, G. T. 1989. *Biochemistry*. **28**:1448-1454.
- Hoganson, C. W. and Babcock, G. T. 1992. *Biochemistry*. **31**:11874-11880.
- Homann, P. H. 1988a. *Biochimica et Biophysica Acta*. **934**:1-13.
- Homann, P. H. 1988b. *Plant Physiology*. **88**:194-199.
- Inoue, M. 1978. *Bulletin of the Chemical Society of Japan*. **51**:1400-1403.

- Isogai, Y., Nishimura, M., Iwaki, M. and Itoh, S. 1988. *Biochimica et Biophysica Acta*. **936**:259-268.
- Itoh, M., Yamashita, K., Nishi, T., Konishi, K. and Shibata, K. 1969. *Biochimica et Biophysica Acta*. **180**:509-519.
- Itoh, S., Yerkes, C. T., Koike, H., Robinson, H. H. and Crofts, A. R. 1984. *Biochimica et Biophysica Acta*. **766**:612-622.
- Itoh, S. and Uwano, S. 1986. *Plant and Cell Physiology*. **27**:25-36.
- Ivancich, A., Barynin, V. V. and Zimmermann, J.-L. 1995. *Biochemistry*. **34**:6628-6639.
- Joliot, P., Barber, G. and Chabaud, R. 1969. *Photochemistry and Photobiology*. **10**:309-331.
- Jursinic, P. and Stemler, A. 1988. *Photosynthesis Research*. **15**:41-56.
- Kaminskaya, O. P. and Shuvalov, V. A. 1994. *FEBS Letters*. **355**:301-304.
- Kavelaki, K. a. Ghanotakis, D. F. 1991. *Photosynthesis Research*. **29**:149-155.
- Kawamori, A., Inui, T., Ono, T.-A. and Inoue, Y. 1989. *FEBS Letters*. **254**:291-224.
- Kawamori, A., Kodera, Y., Astashkin, A. V., Dzuba, S. A. and Tsvetkov, Y. D. 1993. *Kwansei Gakuin University Annual Studies*. **62**:105-130.
- Kebekus, U., Messinger, J. and Renger, G. 1995. *Biochemistry*. **34**:6175-6182.
- Kim, D. H., Britt, R. D., Klein, M. P. and Sauer, K. 1990. *Journal of the American Chemical Society*. **112**:9389-9391.
- Kim, D. H., Britt, R. D., Klein, M. P. and Sauer, K. 1992. *Biochemistry*. **31**:541-547.
- Kirby, J. A., Robertson, A. S., Smith, J. P., Thompson, A. C., Cooper, S. R. and Klein, M. P. 1981a. *Journal of the American Chemical Society*. **103**:5529-5537.
- Kirby, J. A., Goodin, D. B., Wydrzynski, T., Robertson, A. S. and Klein, M. P. 1981b. *Journal of the American Chemical Society*. **103**:
- Kittel, C. 1976 *Introduction to Solid State Physics* 5th Ed. , John Wiley and Sons, New York.
- Klein, M. P., Sauer, K. and Yachandra, V. K. 1993. *Photosynthesis Research*. **38**:265-277.
- Klimov, V. V., Allakhverdiev, S.I., Shuvalov, V. A. and Krasnovsky, A. A. 1982. *FEBS Letters*. **148**:307-312.
- Klimov, V. V., Allakhverdiyev, S. I., Shafiev, M. A. and Demeter, S. 1985. *Biochimica et Biophysica Acta*. **809**:414-420.
- Knopp, P. and Wieghardt, K. 1991. *Inorganic Chemistry*. **30**:4061-4066.
- Kodera, Y., Takura, K and Kawamori, A. 1992. *Biochimica et Biophysica Acta*. **1101**:23-32.
- Koike, H. and Inoue, Y. 1987. *Biochimica et Biophysica Acta*. **894**:573-577.
- Kok, B., Forbush, B. and McGloin, M. 1970. *Photochemistry and Photobiology*. **11**:457-475.
- Koulougliotis, D., Hirsch, D. J. and Brudvig, G. W. 1992. *Journal of the American Chemical Society*. **114**:8322-8323.
- Koulougliotis, D., Tang, X.-S., Diner, B. A. and Brudvig, G. W. 1995. *Biochemistry*. **34**:2850-2856.

- Kramer, D. M., Roffey, R. A., Govindjee and Sayre, R. T. 1994. *Biochimica et Biophysica Acta*. **1185**:228-237.
- Kretschmann, H. and Witt, H. T. 1993. *Biochimica et Biophysica Acta*. **1144**:331-345.
- Kulikov, A. V., Bogatyrenko, V. R., Likhtenshtein, G. I., Allakhverdiyev, S. I., Klimov, V. V., Shuvalov, V. A. and Krasnovskii, A. A. 1983. *Biophysics*. **28**:381-388.
- Kusonoki, M., Ono, T.-A., Matsushita, T., Oyanagi, H. and Inoue, Y. 1989. *Memoirs of the Institute of Science and Technology, Meiji University*. **28**:109-154.
- Kusonoki, M. 1992. *Chemical Physical Letters*. **197**:108-116.
- Kusonoki, M., Ono, T., Suzuki, M., Noguchi, T., Uehara, A., Matsushita, T., Oyanagi, H. and Inoue, Y. 1992. *Proceedings of the IXth International Congress on Photosynthesis*. 1-4.
- Kuwabara, T. and Murata, N. 1982. *Plant and Cell Physiology*. **23**:533-539.
- Kwa, S. L. S., Newell, W. R., van Grondelle, R. and Dekker, J. P. 1992. *Biochimica et Biophysica Acta*. **1099**:193-202.
- Larson, E., Haddy, A., Kirk, M. L., Sands, R. H., Hatfield, W. E. and Pecoraro, V. L. 1992a. *Journal of the American Chemical Society*. **114**:6263-6265.
- Larson, E. J., Riggs, P. J., Penner-Hahn, J. E. and Pecoraro, V. L. 1992b. *Journal of the Chemical Society, Chemical Communications*. **1992**:102-103.
- Ley, A. C. and Mauzerall, D. C. 1982. *Biochimica et Biophysica Acta*. **680**:95-106.
- Liang, W., Latimer, M. J., Dau, H., Roelofs, T. A., Yachandra, V. K., Sauer, K. and Klein, M. P. 1994. *Biochemistry*. **33**:4923-4932.
- Lubbers, K., Haumann, M. and Junge, W. 1993. *Biochimica et Biophysica Acta*. **1183**:210-214.
- MacDonald, G. M., Bixby, K. A. and Barry, B. A. 1993. *Proceedings of the National Academy of Sciences. USA*. **90**:11024-11028.
- MacLachlan, D. J., Hallahan, B.J., Ruffle, S.V. and Nugent, J.H.A. 1992. *Biochemistry Journal*. **285**:569-576.
- MacLachlan, D. J., Nugent, J. H. A., Bratt, P. and Evans, M. C. W. 1994a. *Biochimica et Biophysica Acta*. **1186**:186-200.
- MacLachlan, D. J., Nugent, J.H.A. and Evans, M.C.W. 1994b. *Biochimica et Biophysica Acta*. **1185**:103-111.
- MacLachlan, D. J. and Nugent, J. H. A. 1993. *Biochemistry*. **32**:9772-9780.
- Maltempo, M. M. and Moss, T. H. 1976. *Quarterly Reviews of Biophysics*. **9**:181-215.
- Manchandra, R., Thorp, H. H., Brudvig, G. W. and Crabtree, R. H. 1991. *Inorganic Chemistry*. **30**:494-497.
- Mathis, P. and Rutherford, A. W. 1987. *New Comprehensive Biochemistry*. J. Amesz. Elsevier. **15**:63-96.
- Mavankal, G., McCain, D. C. and Bricker, T. M. 1986. *FEBS Letters*. **202**:235-239.

- Mavankal, G. and McCain, D. C. 1991. *Photosynthetica*. **25**:631-638.
- McDermott, A. E., Yachandra, V. K., Guiles, R. D., Cole, J. L., Dexheimer, S. L., Britt, R. D., Sauer, K. and Klein, M. P. 1988. *Biochemistry*. **27**:4021-4031.
- McMillan, J. A. 1968 *Electron Paramagnetism*, Reinhold Book Corp., New York.
- Mei, R., Green, J. P., Sayre, R. T. and Frasch, W. D. 1989. *Biochemistry*. **28**:5560-5567.
- Mei, R. and Yocum, C. F. 1991. *Biochemistry*. **30**:7836-7842.
- Mei, R. and Yocum, C. F. 1992. *Biochemistry*. **31**:8449-8454.
- Merzbacher, E. 1961. *Quantum Mechanics*. John Wiley and Sons. **Chapter 19**:
- Messinger, J., Pauly, S. and Witt, H. T. 1991a. *Zeitschrift für Naturforschung*. **46c**:1033-1038.
- Messinger, J., Wacker, U. and Renger, G. 1991b. *Biochemistry*. **30**:7852-7862.
- Messinger, J., Badger, M. and Wydrzynski, T. 1995. *Proceedings of the National Academy of Science, USA*. **92**:3209-3213.
- Messinger, J. and Renger, G. 1990. *FEBS Letters*. **277**:141-146.
- Metz, J. G., Nixon, P. J., Rogner, M., Brudvig, G. W. and Diner, B. A. 1989. *Biochemistry*. **28**:6960-6969.
- Michel, H. 1982. *Journal of Molecular Biology*. **158**:567-572.
- Michel, H. and Deisenhofer, J. 1988. *Biochemistry*. **27**:1-7.
- Michel, H., Epp, O. and Deisenhofer, J. 1986a. *EMBO Journal*. **5**:2445-2451.
- Michel, H., Weyer, K. A., Gruenberg, H., Dunger, I., Oesterhelt, D. and Lottspeich, F. 1986b. *EMBO Journal*. **5**:1149-1158.
- Miller, A.-F., de Paula, J. C. and Brudvig, G. W. 1987. *Photosynthesis Research*. **12**:205-218.
- Miller, A.-F. and Brudvig, G. W. 1991. *Biochimica et Biophysica Acta*. **1056**:1-18.
- Mino, H., Satoh, J.-I., Kawamori, A., Toriyama, K. and Zimmermann, J.-L. 1993. *Biochimica et Biophysica Acta*. **1144**:426-433.
- Mino, H. and Kawamori, A. 1994. *Biochimica et Biophysica Acta*. **1185**:213-230.
- Montoya, G., Cases, R., Rodríguez, R., Aured, M. and Picorel, R. 1994. *Biochemistry*. **33**:11798-11804.
- Mukerji, I., Andrews, J. C., DeRose, V. J., Latimer, M. J., Yachandra, V. K., Sauer, K. and Klein, M. P. 1994. *Biochemistry*. **33**:9712-9721.
- Nanbah, O. and Satoh, K. 1987 *Proceedings of the National Academy of Sciences USA* **84**: 109-112
- Nixon, P. J., Chisolm, D. A. and Diner, B. A. 1990. *Plant Protein Engineering*. P. Showry and S. Gutteridge. Cambridge University Press.
- Nixon, P. J., Trost, J. T. and Diner, B. A. 1992. *Biochemistry*. **31**:10859-10871.
- Nixon, P. J. and Diner, B. A. 1992. *Biochemistry*. **31**:942-948.
- Nixon, P. J. and Diner, B. A. 1994. *Biochemical Society Transactions*. **22**:338-343.

- Noguchi, T., Ono, T.-A. and Inoue, Y. 1993. *Biochimica et Biophysica Acta*. **1143**:333-336.
- Noguchi, T., Ono, T.-A. and Inoue, Y. 1995. *Biochimica et Biophysica Acta*. **1228**:189-200.
- Noren, G. H. and Barry, B. A. 1992. *Biochemistry*. **31**:3335-3342.
- Nugent, J. H. A. 1987. *Biochimica et Biophysica Acta*. **893**:184-189.
- Nugent, J. H. A., MacLachlan, D. J., Rigby, S. E. J. and Evans, M. C. W. 1993. *Photosynthesis Research*. **38**:341-346.
- Nugent, J. H. A., Bratt, P. J., Evans, M. C. W., MacLachlan, D. J., Rigby, S. E. J., Ruffle, S. V. and Turconi, S. 1994. *Biochemical Society Transactions*. **22**:327-331.
- Nuijs, A. M., van Gorkom, H. J., Plijter, J. J. and Duysens, L. N. M. 1986. *Biochimica et Biophysica Acta*. **848**:167-175.
- Ono, T., Zimmermann, J.-L., Inoue, Y. and Rutherford, A. W. 1986. *Biochimica et Biophysica Acta*. **851**:193-201.
- Ono, T. and Inoue, Y. 1985. *Biochimica et Biophysica Acta*. **806**:331-340.
- Ono, T.-A., Nakayama, H., Gleiter, H., Inoue, Y. and Kawamori, A. 1987. *Archives of Biochemistry and Biophysics*. **256**:618-624.
- Ono, T.-A., Noguchi, T., Inoue, Y., Kusonoki, M., Yamaguchi, H. and Oyanagi, H. 1993. *FEBS Letters*. **330**:28-30.
- Ono, T.-A., Noguchi, T., Inoue, Y., Kusonoki, M., Yamaguchi, H. and Oyanagi, H. 1994. *Biochemical Society Transactions*. **22**:331-335.
- Ono, T.-A. and Inoue, Y. 1988. *FEBS Letters*. **227**:147-152.
- Ono, T.-A. and Inoue, Y. 1990. *Biochimica et Biophysica Acta*. **1015**:373-377.
- Ono, T.-A. and Inoue, Y. 1991. *FEBS Letters*. **278**:183-186.
- Ono, T.-A. and Inoue, Y. 1992. *Biochimica et Biophysica Acta*. **1099**:185-192.
- Orton, J. W. 1968 *Electron Paramagnetic Resonance. An Introduction to Transition Groups in Crystals*. , Iliffe Books Ltd. London.
- Pace, R. J., Smith, P., Bramley, R. and Stehlik, D. 1991. *Biochimica et Biophysica Acta*. **1058**:161-170.
- Padhye, S., Kambara, T., Hendrickson, D. N. and Govindjee. 1986. *Photosynthesis Research*. **9**:103-112.
- Pake, G. E. 1962 *Paramagnetic Resonance. An Introductory Monograph*. , W. A. Benjamin Inc., New York
- Pake, G. E. and Estle, 1973 *The Physical Principles of Electron Paramagnetic Resonance* , 2nd Ed. W. A. Benjamin Inc., Massachusetts.
- Pauly, S. and Witt, H. T. 1992. *Biochimica et Biophysica Acta*. **1099**:211-218.
- Penner-Hahn, J. E., Fronko, R. M., Pecoraro, V. L., Yocum, C. F., Betts, S. D. and Bowlby, N. R. 1990. *Journal of the American Chemical Society*. **112**:2549-2557.

- Peter, G. F., Machold, O. and Thornber, J. P. 1988. *Plant Membranes: Structure, Assembly and Function*. T. J. Walton. The Biochemical Society. 17-31.
- Pilbrow, J. R. 1990 *Transition Ion Electron Paramagnetic Resonance*, Clarendon Press, Oxford.
- Plaksin, P. M., Stoufer, R. C., Mathew, M. and Palenik, G. J. 1972. *Journal of the American Chemical Society*. **94**:2121-2122.
- Poole, C. P. Jr 1967 *Electron Spin Resonance. A Comprehensive Treatise on Experimental Techniques*, Interscience Publications, John Wiley and Sons, New York.
- Preston, C. and Pace, R. J. 1985. *Biochimica et Biophysica Acta*. **810**:388-391.
- Prokorny, A., Wulf, K. and Trissl, H.-W. 1994. *Biochimica et Biophysica Acta*. **1184**:65-70.
- Proserpio, D. M., Hoffmann, R. and Dismukes, G. C. 1992. *Journal of the American Chemical Society*. **114**:4374-4382.
- Powles, J. G. 1958 *Proceedings of the Physical Society* **71**, 497-500.
- Radmer, R. and Ollinger, O. 1986. *FEBS Letters*. **195**:285-289.
- Randall, D. W., Sturgeon, B. E., Ball, J. A., Lorigan, G. A., Chan, M. K., Klein, M. P., Armstrong, Q. H. and Britt, R. D. 1996. *Journal of the American Chemical Society*. **117**: 11780 - 11789.
- Rappaport, F., Blanchard-Desce, M. and Lavergne, J. 1994. *Biochimica et Biophysica Acta*. **1184**:178-192.
- Renger, G. 1987. *Photosynthetica*. **21**:203-224.
- Renger, G. and Weiss, W. 1986. *Biochimica et Biophysica Acta*. **850**:184-196.
- Rickert, K. W., Sears, J., Beck, W. F. and Brudvig, G. W. 1991. *Biochemistry*. **30**:7888-7894.
- Riggs, P. J., Mei, R., Yocum, C. F. and Penner-Hahn, J. E. 1992. *Journal of the American Chemical Society*. **114**:10650-10651.
- Roffey, R. A., Kramer, D. M., Govindjee and Sayre, R. T. 1994. *Biochimica et Biophysica Acta*. **1185**:257-270.
- Ross, R. T., Anderson, R. J. and Hsia, T. L. 1976. *Photochemistry and Photobiology*. **24**:267-
- Ruffle, S. V. and Nugent, J. H. A. 1992. *Research in Photosynthesis*. N. Murata. Kluwer Academic. **II**:191-194.
- Rutherford, A. W. 1985. *Biochimica et Biophysica Acta*. **807**:189-201.
- Rutherford, A. W. 1989. *Trends in Biochemical Sciences*. **14**: 227-232.
- Rutherford, A. W., Boussac, A. and Zimmermann, J.-L. 1991. *Nouveau Journal de Chimie*. **15**: 491-500.
- Sahlin, M., Gräslund, A. and Ehrenberg, A. 1986 *Journal of Magnetic Resonance* **67**, 135-137.
- Sandusky, P. O. and Yocum, C. F. 1984. *Biochimica et Biophysica Acta*. **766**:603-611.
- Sandusky, P. O. and Yocum, C. F. 1986. *Biochimica et Biophysica Acta*. **849**:85-93.

- Sauer, K., Guiles, R. D., McDermott, A. E., Cole, J. L., Yachandra, V. K., Zimmermann, J.-L., Klein, M. P., Dexheimer, S. L. and Britt, R. D. 1988. *Chemica Scripta*. **28A**:87-91.
- Saygin, O. and Witt, H. T. 1987. *Biochimica et Biophysica Acta*. **893**:452-469.
- Saygin, Ö. and Witt, H. T. 1985. *FEBS Letters*. **187**:224-227.
- Schelvis, J. P. M., van Noort, P. I., Aartsma, T. J. and van Gorkom, H. J. 1994. *Biochimica et Biophysica Acta*. **1184**:242-250.
- Schlichter, C. P. 1990 *Principles of Magnetic Resonance* 3rd Ed., Springer-Verlaag, Berlin.
- Shen, J.-R., Satoh, K. and Kato, S. 1988. *Biochimica et Biophysica Acta*. **933**:358-364.
- Sibbald, P. R. and Green, B. R. 1987. *Photosynthesis Research*. **14**:201-209.
- Sinclair, J. 1984. *Biochimica et Biophysica Acta*. **764**:247-252.
- Sinn, E. 1970 *Coordination Chemistry Reviews*. **5**, 313-347.
- Sivaraja, M., Philo, J. S., Lary, J. and Dismukes, G. C. 1989. *Journal of the American Chemical Society*. **111**: 3221-3225.
- Sivaraja, M. and Dismukes, G. C. 1988. *Biochemistry*. **27**: 3467-3475.
- Smith, P. J., Åhrling, K. A. and Pace, R. J. 1993. *Journal of the Chemical Society. Faraday Transcripts*. **89**:2863-2868.
- Smith, P. J. and Pace, R. J. 1996. *Biochimica et Biophysica Acta*. **1275**: 213-220.
- Srinivasan, A. N. and Sharp, R. R. 1986. *Biochimica et Biophysica Acta*. **850**:211-217.
- Styring, S., Davidsson, L., Tommos, C., Vermaas, W., Vass, I. and Svensson, B. 1993. *Photosynthetica*. **28**:225-241.
- Styring, S. and Rutherford, A. W. 1988. *Biochimica et Biophysica Acta*. **933**:378-387.
- Svensson, B., Vass, I., Cedergren, E. and Styring, S. 1990. *The EMBO Journal*. **9**:2051-2059.
- Svensson, B., Vass, I. and Styring, S. 1991. *Zeitschrift Fur Naturforschung*. **46c**:765-776.
- Svensson, B., Etchebest, C., Tuffery, P., Smith, J. and Styring, S. 1992. *Research in Photosynthesis*. N. Murata. Kluwer Academic Publishers. **II**:147-150.
- Szalai, V. A. and Brudvig, G. W. 1996. *Biochemistry*. **35**:1946-1953.
- Takahashi, M. and Asada, K. 1986. *The Journal of Biological Chemistry*. **261**:16923-16926.
- Tamura, N. and Cheniae, G. 1987. *Biochimica et Biophysica Acta*. **890**:179-194.
- Tan, X., Gultneh, Y., Sarneski, J. E. and Scholes, C. P. 1991. *Journal of the American Chemical Society*. **113**:7853-7858.
- Theg, S. M., Jurisnic, P. A. and Homann, P. H. 1984. *Biochimica et Biophysica Acta*. **766**:636-646.
- Thompson, L. K., Miller, A.-F., de Paula, J. C. and Brudvig, G. W. 1988. *Israel journal of Chemistry*. **28**:121-128.
- Thompson, L. K. and Brudvig, G. W. 1988. *Biochemistry*. **27**:6653-6658.
- Thorp, H. H. and Brudvig, G. W. 1990. *Journal of Electroanalytical Chemistry*. **290**:293-301.

- Thorp, H. H., Sarneski, J. E., Brudvig, G. W. and Crabtree, R. H. 1989. *Journal of the American Chemical Society*. **111**:9249-9250.
- Tommos, C., Davidsson, L., Svensson, B., Madsen, C., Vermaas, W. and Styring, S. 1993. *Biochemistry*. **32**:5436-5441.
- Trebst, A. 1986. *Zeitschrift fur Naturforschung C. Biosciences*. **41C**:240-245.
- Tso, J., Sivaraja, M., Philo, J. S. and Dismukes, G. C. 1991a. *Biochemistry*. **30**:4740-4747.
- Tso, J., Sivaraja, M. and Dismukes, G. C. 1991b. *Biochemistry*. **30**:4734-4739.
- van Vliet, P., Boussac, A. and Rutherford, A. W. 1994. *Biochemistry*. **33**:12998-13004.
- Van Vliet, P. and Rutherford, A. W. 1996. *Biochemistry*. **35**:1829-1839.
- Vänngård, T., Hansson, O. and Haddy, A. 1992. *Manganese Redox Enzymes*. V. L. Pecoraro Ed. VCH New York 105-118.
- Vass, I., Deak, S., Jegerschold, C. and Styring, S. 1990. *Biochimica et Biophysica Acta*. **1018**: 41-46.
- Vass, I. And Styring, S. 1991. *Biochemistry*. **30**: 830-839.
- Vermaas, W. F. J., Rutherford, A. W., and Hansson, O. 1988. *Proceedings of the National Academy of Science, USA*. **85**: 8477-8481.
- Vermaas, W. F. J., Styring, S., Schroder, W. P. and Andersson, B. 1993. *Photosynthesis Research*. **38**: 249-263.
- Vermaas, W. F. J., Dohnt, G. and Renger, G. 1984. *Biochimica et Biophysica Acta*. **765**: 74-83.
- Warden, J. T., Blankenship, R. E. and Sauer, K. 1976. *Biochimica et Biophysica Acta*. **423**: 462-478.
- Warncke, K., Babcock, G. T. and McCracken, J. M. 1994. *Journal of the American Chemical Society*. **116**:7332-7340.
- Weiss, W. and Renger, G. 1986. *Biochimica et Biophysica Acta*. **850**:173-183.
- Wells, W., Harton, A and Vincent, J. B. 1993. *Biochimica et Biophysica Acta*. **1144**:346-352.
- Wertz, J. E. and Bolton, J. R. 1972 *Electron Spin Resonance. Elementary Theory and Practical Applications*, McGraw-Hill Book Company, New York.
- Witt, H. T. 1991. *Photosynthesis Research*. **29**:55-77.
- Yachandra, V. K., Guiles, R. D., McDermott, A., Britt, R. D., Dexheimer, S. L., Sauer, K. and Klein, M. P. 1986a. *Biochimica et Biophysica Acta*. **850**:324-332.
- Yachandra, V. K., Guiles, R. D., Sauer, K. and Klein, M. P. 1986b. *Biochimica et Biophysica Acta*. **850**:333-342.
- Yachandra, V. K., Guiles, R. D., McDermott, A. E., Cole, J. L., Britt, R. D., Dexheimer, S. L., Sauer, K. and Klein, M. P. 1987. *Biochemistry*. **26**:5975-59481.
- Yachandra, V. K., DeRose, V. J., Latimer, M. J., Mukerji, I., Sauer, K. and Klein, M. P. 1993. *Science*. **260**:675-679.

- Yachandra, V. K., Guiles, R. D., Sauer, K. and Klein, M. P. 1986. *Biochimica et Biophysica Acta*. **850**:333-342.
- Yim, M. B., Kuo, L. C. and Makinen, M. W. 1982. *Journal of Magnetic Resonance*. **46**:247-256.
- Yocum, C. F., Yerkes, C. T., Blankenship, R. E., Sharp, R. R. and Babcock, G. T. 1981. *Proceedings of the National Academy of Sciences. USA*. **78**:7507-7511.
- Yocum, C. F. 1991. *Biochimica et Biophysica Acta*. **1059**:1-15.
- Zhang, Y. C. and Pilbrow, J. R. 1991 *Journal of Magnetic Resonance*. **93**, 447-457.
- Zimmermann, J. and Rutherford, A. W. 1984. *Biochimica et Biophysica Acta*. **767**:160-167.
- Zimmermann, J.-L., Boussac, A. and Rutherford, A. W. 1993. *Biochemistry*. **32**:4831-4841.
- Zimmermann, J.-L. and Rutherford, A. W. 1986. *Biochemistry*. **25**:4609-4615.
- Zinth, W., Kaiser, W. and Michel, H. 1983. *Biochimica et Biophysica Acta*. **723**:128-131.
- Zuber, H., Brunisholz, R. and Sidler, W. 1987. *Photosynthesis*. J. Amesz Ed. Elsevier. 233-271.